DEVELOPMENT OF CONE TESTING DEVICE FOR IMPROVED DEEP FOUNDATION DESIGN PROTOCOLS

by

HAI MINH NGUYEN

Presented to the Faculty of the Graduate School of

The University of Texas at Arlington in Partial Fulfillment

of the Requirements

for the Degree of

DOCTOR OF PHILOSOPHY

THE UNIVERSITY OF TEXAS AT ARLINGTON

May 2017

Acknowledgements

No one who achieves success does so without acknowledging the help of others. I am very grateful to my research advisor, Dr. Anand J. Puppala, who accompanied me on my journey to earn a Ph.D. in Civil Engineering at the University of Texas at Arlington. His knowledge of and experience with in-situ soil testing technology contributed significantly to my success in developing a novel cone test device for this dissertation. Therefore, the novel cone test device was named “P-cone”.

I will always be grateful to Dr. Laureano Hoyos, who shared with me his advanced knowledge of soil mechanics. Moreover, I would like to thank to Dr. Xinbao Yu, and Dr. Shih- Ho Chao for their valuable comments during examinations related to my research and this dissertation.

Special thanks to Dr. Bengt H. Fellenius and Dr. Masaharu Fukue for their worthy comments on the design of the P-cone device and the research objectives of this dissertation. Special thanks are also extended to Dr. Aravind Pedarla and Ginny Bowers for their help in reviewing some chapters of the dissertation.

Moreover, I would like to thank my friends, Dr. Tejo Vikash Bheemasetti, Dr. Patil Ujwalkumar, Santiago Ricardo, Aritra Banaerjee**,** Ali Shafikhani, Daniel, Jasaswee Das, Sayantan, Anu George, Thomas P. Taylor, Surya Sarat Chandra, Puneet Bhaskar, Rinu Ann Samuel, Jun Lin, Qianmi Yu, Manikanta, and Minh Tran for their support in carrying out the experiments of the P-cone device in the laboratory of the University of Texas at Arlington.

Last but not the least I would like to thank my parents and my beloved wife for their endless love and support throughout my entire life.

March 30, 2017

Abstract

DEVELOPMENT OF CONE TESTING DEVICE FOR IMPROVED DEEP FOUNDATION DESIGN PROTOCOLS

Hai Minh Nguyen, PhD

The University of Texas at Arlington, 2017

Supervising Professor: Anand J. Puppala

A novel cone penetration test device, the P-cone, has been developed to assist in deep foundation design and this P-cone device combines features of CPTU cone sounding technologies with capabilities to perform bidirectional loading at a given soil depth condition. Using two independent systems, the P-cone measures shear stress versus movements of cone shaft and stress versus penetration of the cone tip at desired depths. The P-cone can also improve the penetration depth and offer a potential application for the in situ consolidation test. Laboratory experiments of the P-cone device were successful beyond the expectation.

P-cone Tests performed on three large compaction-unsaturated clayey silt specimens showed that the movements necessary to fully mobilize the shaft shear resistance and tip resistance were close to 0.2 mm and 2.0 mm, respectively. The comparison of the measurements and the equivalent pile-head load-movement curve constructions show an average difference of 15% between the positive and negative shaft resistance of soil when being sheared. An average adjustment coefficient of 1.2 was proposed for the constructed equivalent pile-head load-movement curves.

The investigation of soil failures along the cone shaft and below the cone tip showed that the soil areas sheared surrounding the cone shaft were twice cone

diameters and the shear failures of soil took place at interface between the cone wall and soil. The shear failures of soil below the cone tip did not occur though the movements of the cone tip ranged from 100 through 185% cone diameter. The investigation of soil deformation around the jack indicated that the expansion of the jack did not create tension areas for all tests and thus the effects of the tension areas created by the jack expansion can be ignored for the equivalent pile-head load-movement curve construction from the bidirectional load test results.

The modelling of the axial compression and bidirectional load tests on P-cone showed the influence zones surrounding the P-cone shaft and below the P-cone tip caused by the P-cone installation of about four and thirteen times diameter of P-cone, respectively. It is likely that the dimension of soil chamber used for P-cone tests is not large enough to eliminate completely the effect of the boundary conditions.

Table of Contents

List of Illustrations

List of Tables

Chapter 1

Introduction

1.1 Background

Advances in the design of axially-loaded piles are important in the deep foundation industry because they can save significant amount of money from a reduced factor of safety, which the pile-supported foundations only settle within their tolerate limits. The pile toe movement response to imposed loads plays a key role in the pile foundation design, where settlement of a piled foundation exceeds its tolerable limits (Fellenius, 1999, 2006, 2016, 2017; Vesic, 1967, 1977; Peck, 1967; Hansen, 1967).

For long-term conditions, the development of negative skin friction, induced by settlement of the soil surrounding the pile, significantly reduces the pile capacity, increases the load on the pile, and causes significant settlement of pile. Considerable amount of literature was published on the problem of negative skin friction in the 1960s, some of which was summarized by Fellenius (1998, 2006). Hence, static analysis of piles and pile groups require assessment of long-term conditions for capacity, settlement, drag load, and down-drag forces.

Moreover, sandy soil layers can be subjected to the volumetric compression by liquefaction (Tokimatsu and Seed 1987). This compression leads to the overlying soil layers settled. This settlement may influence significantly the axial load distribution of the pile and increase the foundation costs of projects in seismically active regions (Boulanger and Brandenberg, 2004; Rollins and Strand, 2006; Fellenius et al., 2008; Vijayaruban et al., 2015).

The above mentioned case histories provide compelling evidence that the stress-deformation characteristics of soil below the pile toe play a key role in designing piled foundations. The pile toe response includes aspects of both capacity and settlement patterns. Current methods of pile design assume that the pile toe response is governed by capacity reasoning. Albeit usually safe, this approach is somewhat crude and does not properly account for the soil deformation and settlement.

Full-scale static load tests are usually performed to verify a pile design. In a conventional static load test (head-down test), however, it is difficult to sufficiently mobilize the pile toe resistance to enable an analysis of the pile toe response (Nguyen et al. 2013, 2014, 2016, 2017). It is hard to determine the portion of the applied test load that actually reaches the pile toe, and the potential presence of residual load at the pile toe adds complexity to the analysis. The bidirectional loading test method (Osterberg, 1984 and 1989) eliminates much of the difficulty if the jack can be activated near the pile toe and the shaft resistance is sufficient to supply reaction resistance to the downward push of the cell.

Most piled foundations are designed without the benefit of static loading tests, however, and rely on information received from the site investigation, particularly results of in-situ tests, such as the CPTU. Comprehensive details of CPT and CPTU methods can be found elsewhere (Eslami, et al., 1997).

This research study presents a novel cone penetration test device (P-Cone), which is capable of performing in-situ site investigations, improving the penetration depth, testing consolidation compression, and measuring shear movement above and stress penetration below the cone tip at the desired depths. Laboratory experiments in select compacted soil were performed to evaluate the performance of the P-cone, and test results obtained from the P-cone were used to re-evaluate the equivalent top-down load-movement construction method obtained from the results of the bi-directional load test. The failure modes of soil along the cone shaft and around the cone tip were investigated to provide insight into the pile behavior in practice.

1.2 Problem Statement

The case histories reported in the background section provide compelling evidence that the settlement of a piled foundation is governed by the compressible characteristics of soil below the pile toe for the short term, long term, and liquefied conditions. In practice, full-scale static load tests are usually performed to verify a pile design.

For a conventional static load test (head-down test), however, it is difficult to sufficiently mobilize the pile toe resistance to enable an analysis of the pile toe response and to determine the portion of the applied test load that actually reaches the pile toe. The potential presence of residual load at the pile toe adds complexity to the analysis.

The bi-directional loading test method (Osterberg, 1984 and 1989) eliminates much of the difficulty if the bi-directional cell can be activated near the pile toe and the shaft resistance is sufficient to supply reaction resistance to the downward push of the cell. However, the jacks are often placed above the pile toe due to the balanced requirement of the two resistance components, making it impossible to measure the pile toe load-movement, and the installed jacks are considered expendable and are not recovered after the test is completed. This method cannot be used to test pile sheets or H-piles (Schmertmann et al., 1997).

Most piled foundations are designed without the benefit of static loading tests, and therefore rely on information received from the site investigation, particularly in-situ test results, such as the CPTU, due to similarities between a cone penetrometer and a pile. However, a major difficulty with current CPTU devices is that the limited reaction force prevents the device from reaching into the depths at which the piles are usually installed. Moreover, the current CPTU devices do not measure the shear stresses versus movements of soil along the cone shaft or the penetration stresses versus movements of soil below the cone tip at desired depths in the field condition.

1.3 Research Objectives

The main objective of this dissertation research study is to develop a novel cone penetration test device, the P-cone, to assist in pile design. The P-cone device combines features of CPTU cone sounding and bi-directional loading of the pile in in-situ conditions. The principles of the P-cone, used in combination with a hydraulic jack, facilitate movement-and-force-generating conditions in the field. This combination enables the P-cone device to improve the penetration depth by utilizing the pressure in a cell that uses the cone rods and surface

anchors on the ground surface as a reaction prop to push the cone down. Using two independent systems, the P-cone measures shear stress versus movement above and stress penetration below the cone at desired depths.

The equivalent top load curve construction method from the bi-directional pile load test results, as studied by Osterberg (1998), was re-evaluated, based on the static load test results of the P-cone tests. The influence of the bi-directional load test, where the applied loads were associated with separation of two plates, potentially introducing soil loosening or soil loading in tension mode adjacent to the installed jacks, were investigated. Consolidation test results obtained from the P-cone in the compaction-saturated clay silty soil chamber were studied and correlated with the conventional consolidation test results.

1.4 Scope of Work

The scope of this study consists of design, manufacturing, experiments, and modeling of a novel cone penetration test device (the P-cone). The design and manufacturing of the P-cone were carried out in the civil engineering laboratory of the University of Texas at Arlington. The instruments used to measure the shear resistance and tip resistance during penetration were equipped and supplied by Geokon Inc., USA.

The experimental program of the P-cone consisted of the soil selection, determination of soil properties, setup of the loading system, preparation of the compacted soil chambers, and the P-cone testing. Clayey silt soil was used for the P-cone experiments to minimize the influences of the confining pressure and the boundary conditions on the test results. Moreover, it was convenient for investigating failure modes of soil along the cone shaft and around the cone tip. The soil properties were determined from basic laboratory tests, such as gain-size analysis, liquid and plastic limit tests, compaction tests, direct shear tests, and conventional consolidation tests. A loading system was set up, and three compacted clay silt soil chambers with different water contents and densities were prepared. The experiments of the P-cone consisted of cone penetration tests, conventional static load tests (head-down tests),

bidirectional load tests, end bearing load tests, and consolidation compression tests. The test results were analyzed and evaluated. The P-cone was modeled using finite-element-based PLAXIS 3D FOUNDATION software. The results obtained from the P-cone test modeling were considered to study and validate the experimental results of the P-cone tests. A flow chart summarizing the research activities is depicted in Figure 1-1.

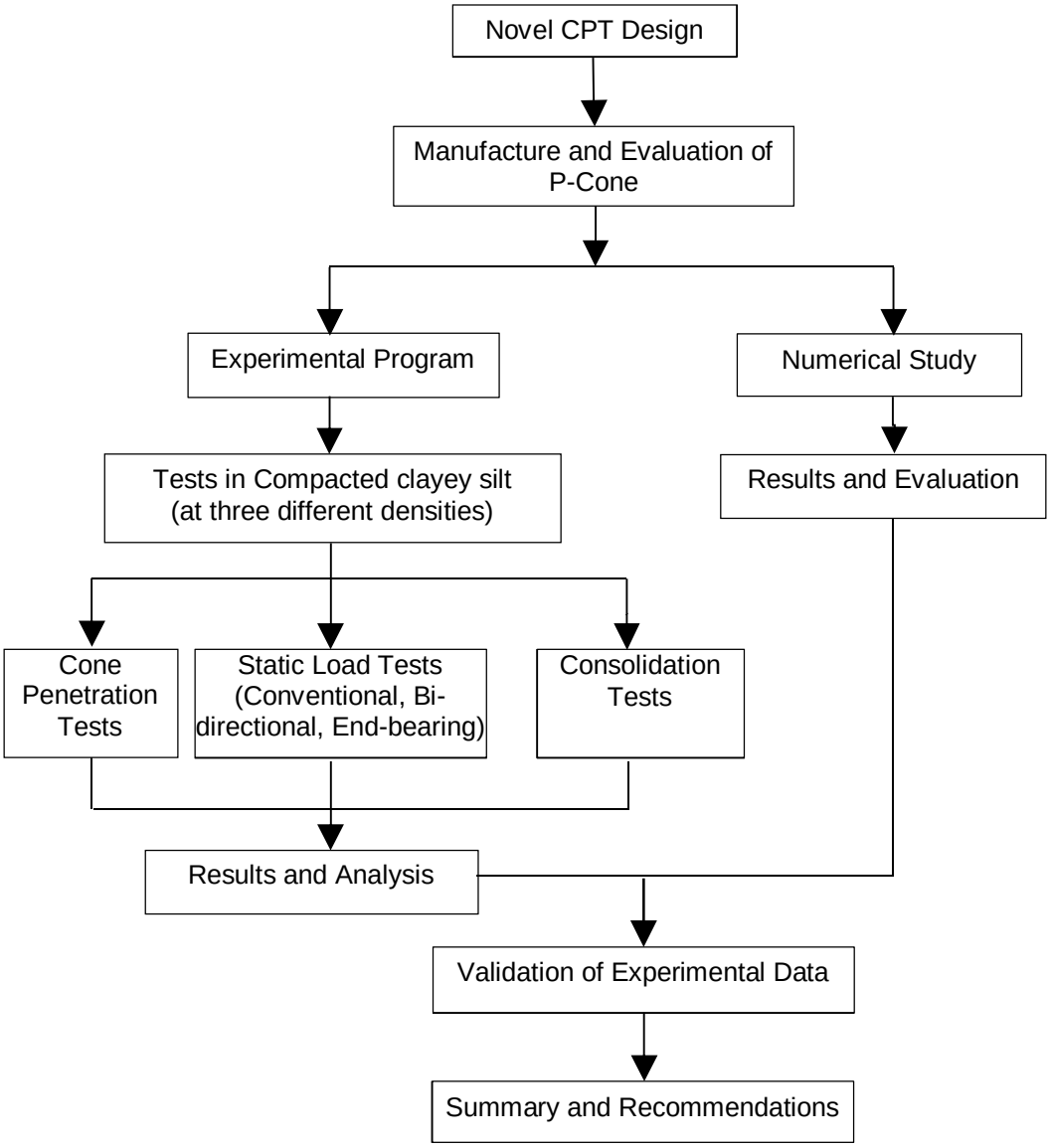

Figure 1-1 Flow chart of novel cone penetration test development for pile design

1.5 Dissertation Outline

This dissertation consists of seven chapters, as follows:

Chapter 1 presents the importance of pile toe for governing the settlement of the piled foundation, the limitations of conventional static load tests and bi-directional loading tests, and the major problems encountered with the current cone penetration devices. A novel solution has been presented by modifying existing cone penetration device.

Chapter 2 provides a comprehensive literature and background to the development of the cone penetration test device and its applications for designing piled foundations. Conventional methods such as static load tests and the bi-directional loading tests on the pile are reviewed, and their limitations are demonstrated.

Chapter 3 provides the design concept and a detailed design of the novel cone penetration test device (P-Cone). Operating principles and details of the instruments used to measure the shaft resistance, cone tip resistance, pore water pressure, and movement are presented.

Chapter 4 presents the experimental program of the novel cone penetration test device. The experimental program consisted of soil tests, setting up the loading system and soil chambers, cone penetration tests, conventional static load tests, bi-directional loading tests, end-bearing tests, and consolidation tests.

Chapter 5 reports and analyzes the results of soil laboratory tests, cone penetration tests, conventional static load tests, bi-directional loading tests, end-bearing tests, and the consolidation compression tests obtained from novel cone penetration test device.

Chapter 6 presents the results of modeling the conventional static load tests and bi-directional load tests of the novel cone penetration test device by software PLAXIS 3D

FOUNDATION. The modeling results were considered to validate the experimental results of the novel cone penetration test device tests.

Chapter 7 summarizes the test results obtained from the novel cone penetration test device and the modeling results of the conventional static load tests and bi-directional load tests. Conclusions are drawn from the test and modeling results, and recommendations are made for future research.

Chapter 2

Literature Review

The three types of in-situ tests related to this dissertation research are reviewed in this chapter. They are: 1) cone penetration testing, 2) conventional static compressive pile load testing, and 3) bidirectional pile load testing.

2.1 Cone Penetration Testing

2.1.1 Evolution of Cone Penetration Testing

The idea of using cone penetration to determine the strength of sub-surface soil is an old one; however, one of the most significant contributions to pile works in the 20th century, the deep sounding apparatus, was only developed recently. Comprehensive reviews on the history of cone penetration testing were reported by Sanglerat (1972), Broms et al. (1988), and Massarsch (2014). Therefore, in this section, only the main contributions to development of the modern cone penetration testing (CPT) are reviewed.

The End of the 19th Century – 1932: Measurement of Total Resistance

At the end of the 19th century, circular or square steel rods, with diameters ranging from 15 to 30 mm, were used to investigate the soft soil in the area in Sweden where railways were to be constructed. The rods, which were later spliced by external couplings, were pressed or rotated into the ground. The penetration resistance, which made it possible to roughly classify the soil as soft or stiff, was often expressed in terms of the number of men required to push the sounding rod into the soil.

In 1900, Wendel presented that the disadvantage of square sounding rods was that when stones were encountered in the clay, the resistance was very uneven because of the outside couplings. He also criticized the method of expressing the penetration

resistance in terms of the ability of the boring crew to push the sounding rod down. Wendel also described a new probe, a needle probe, shown in Figure 2-1a. This tool consisted of a number of short pipes, which were spliced using inside couplings, so that the outside surface of the probe was smooth.

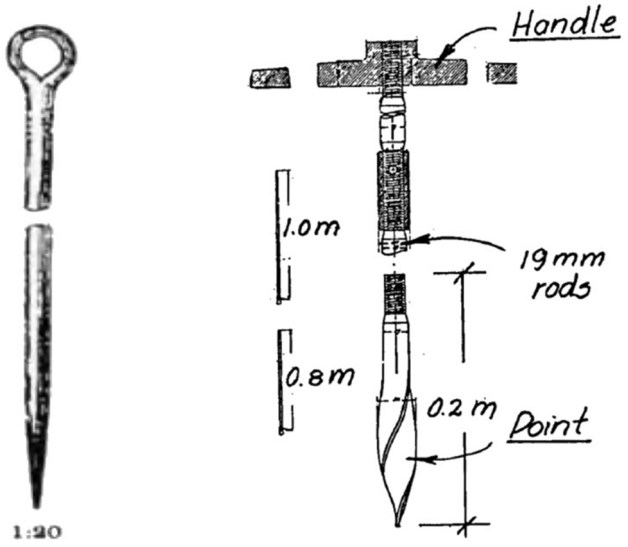

a) b)

Figure 2-1 Needle probe (a) and Swedish sounding tool (b) (After Flodin and Broms, 1981)

A drawing from 1911, signed by Wolmar Fellenius, showed an important link to the development of the Swedish weight sounding method (Figure 2-1b). This device consisted of 1.0 m long solid steel rods, 19 mm in diameter, with outside couplings and an 0.8 m long lower rod which was provided with a twisted screw point, 0.20 m in length. A handle and a clam were also parts of the device.

In 1913, Dahlberg, who was the head of railway construction in Sweden, pointed out the limited knowledge about the stability and settlement of embankments. He presented a relationship, based on experience, between bearing capacity and the results

from soundings made with 25 mm diameter rods (Table 2.1). According to Dahlberg, the bearing capacity could be higher if there was a stiff surface crust. This layer "can, as a rule, not be trusted" if the thickness was less than 4 m or the embankment was not low.

Table 2-1 Relationship between penetration resistance and bearing capacity (after Flodin and Broms, 1981)

Penetration resistance (number of men)	Maximum height of embankment that soil can carry (m)
0.5	0.5
0.5 – 1.0	0.5 – 1.0
1.0 – 2.0	1.0 – 2.0
2.0 – 3.0	2.0 – 5.0
3.0 – 4.0	5.0 – 15.0

In 1915, a weight sounding device, described in John Olson's Handbook of the Swedish State Railways, showed a further development (Figure 2-2). This device consisted of steel rods with a 15-mm diameter and 1.0-m length, and the bottom rod had a twisted point to facilitate the penetration.

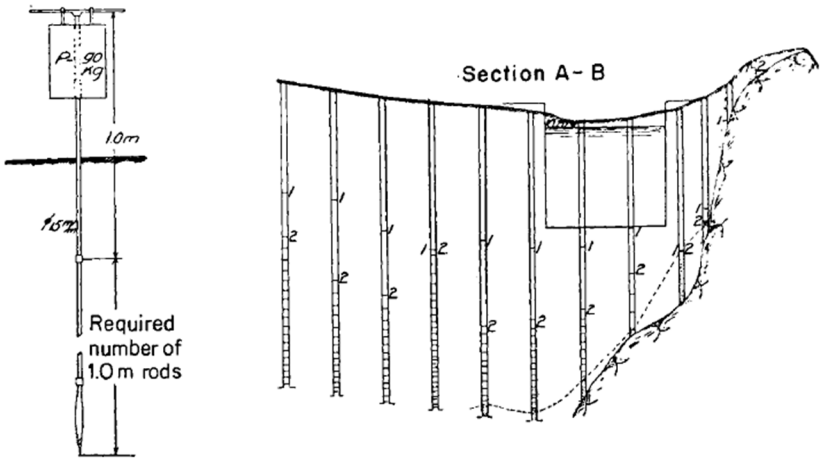

Figure 2-2 Swedish weight-sounding penetrometer in practice (Broms and Flodin, 1988)

When the point penetrated a layer of coarse-grained soil, the noise in the rod was recorded, enabling an experienced foreman to distinguish between sand and gravel. The penetration resistance was expressed as the number of men required to push the penetrometer into the soil. If the penetrometer could not be pushed down by hand, a 90 kg weight was added, the penetrometer was rotated, and the penetration was recorded every 25 turns. The penetration tests were normally supplemented by sampling.

In 1917, the penetration method mentioned in the manual by H. Olsson was developed further by the Swedish Geotechnical Commission. The thrust produced by one or two men was replaced by the number of weights (up to 100 kg) required to push down the penetrometer (Figure 2-3). The penetration resistance when the rod sank under its own weight was recorded. In this way, it was possible to classify the consistency of the various strata. When the penetration resistance exceeded 100 kg, the rod was rotated and the penetration every 25 half-turns was recorded. When the rod diameter was increased to 22 mm, the number of half-turns to drive the rod 200 mm was recorded.

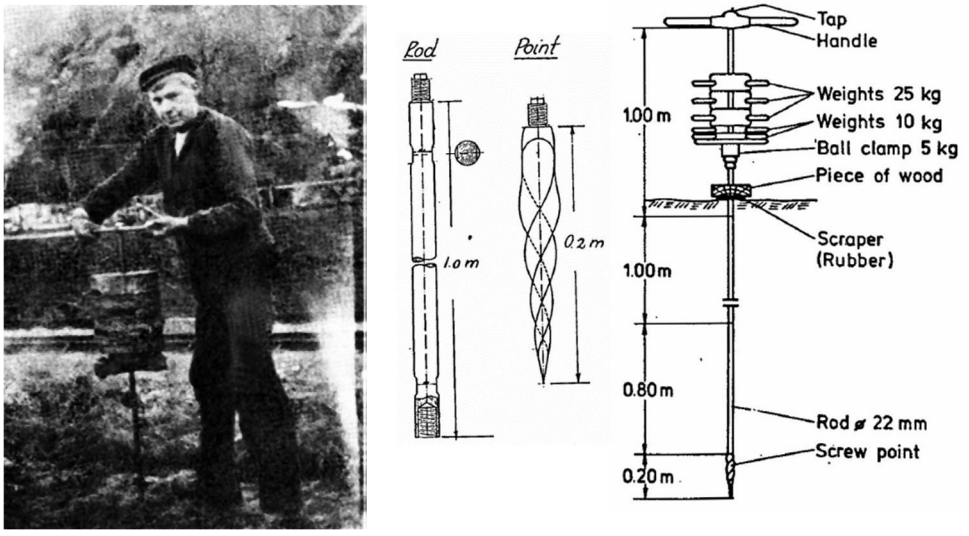

Figure 2-3 Swedish weight-sounding method in 1917 (Broms and Flodin, 1988)

1932 – 1948: Measurement of Total resistance and Point Resistance

In 1932, the first Dutch cone penetrometer was developed by Pieter Barentsen (Figures 2-4 through 2-6). The apparatus consisted essentially of a ¾ inch (19 mm) gas pipe with an internal diameter large enough that a 5/8-inch (15-mm) rod could move freely. At the bottom end of the pipe, a cone with a 60-degree apex angle was attached (Figure 2-5). The cone had a base area of 1.55 square inches (10 $cm^{2,}$), and a collar on the rod attached to the cone prevented it from being pushed out more than 6 in. (150 mm) beyond the pipe.

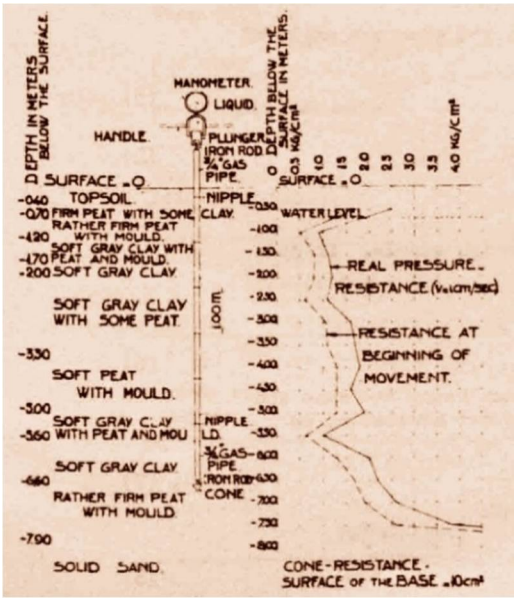

Figure 2-4 Early light-duty Dutch penetrometer (Barentsen, 1936)

In practice, the first gas pipe was pushed, together with rod and cone, into the desired depth in the ground by one or two persons via handles (Figure 2-6). Then, the handles were removed from the gas pipe, and a pressure indicator was affixed to the inner rod that projected outside the gas pipe. Subsequently, only the inner rod with cone tip was pushed downward, while the gas pipe was retained by the skin friction of the soil.

The pressure required to push the cone beyond the gas pipe was measured by a Bourdon gauge. The piston of the Bourdon gauge had a 10 cm^2 area, the same as the base area of cone tip. The point resistance was then obtained from the known area of the cone, the weight of the inner rods, and the pressure exerted. To ensure reliable measurements, the penetration rate into the ground had to remain stable throughout the soil layers. The penetration rate was estimated by observing the movement of the rod for the gas pipe, at a rate of about 1cm/second.

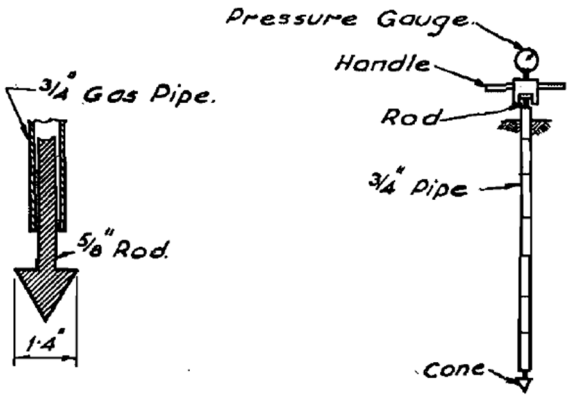

Figure 2-5 Details of the first Dutch static penetrometer (Kantey, 1951)

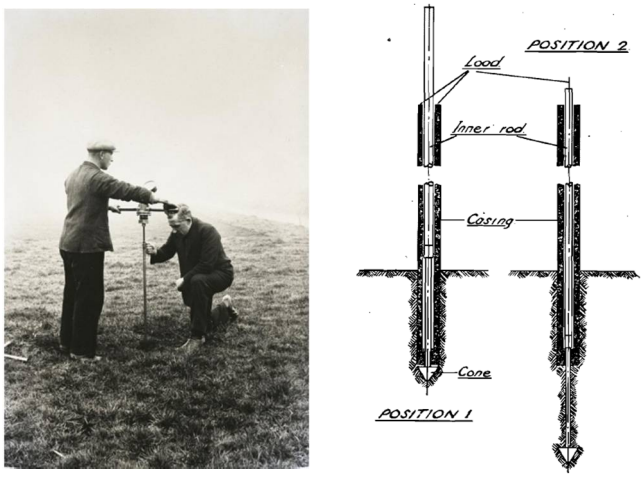

Figure 2-6 Scheme of operating the light-duty Dutch penetrometer (Barentsen, 1936; Kantey, 1951)

After this reading was recorded, the pressure was reapplied to the gas pipe, which moved up and down, caught up with the cone, and continued downward to the depth at which the next sounding was required. By adding lengths of 1 m to the gas pipe and to the inner rods, the apparatus could be used to a depth which depended only on the capacity of the loading device. This procedure was repeated, giving measurements of the point resistance versus depth, and the readings were plotted on a graph with depth as the ordinate (Figure 2-4).

The first Dutch penetrometer was operated by hand, which limited the depth of operation. Further, when passing through a hard crust into soft material, the pressure required to break through the hard crust was frequently so high that control of the apparatus was lost, and the soft layer was penetrated so quickly that the cone might go right through it before a resistance measurement could be taken. This led to further development of the apparatus in 1936, in which the pressure was applied by mechanical means.

In 1936, the Soil Mechanics Laboratory in Delft manufactured the hand-operated machines with a capacity of 2.5 and 10.0 tons, as shown in Figures 2-7 and 2-8, respectively. The reaction was provided by anchoring the machine either with earth-anchors (the left diagram of Figure 2-7) or with a weighted floor (the left diagram of Figure 2-8). The measuring device was arranged so that the total resistance to penetration of the pipe and cone could be measured, while pushing the two down to the required sounding depth, thus also providing a curve of total resistance which facilitated an estimate of the skin friction on the side of the casing. The apparatus could then be used for the complete determination of piled foundations. The 2.5-ton capacity apparatus had a special feature in that the outer tubes had a slightly smaller diameter over 90% of

their length and were all rigidly fixed to the jack so that the casing moved along with the point, thus enabling investigations at greater depths.

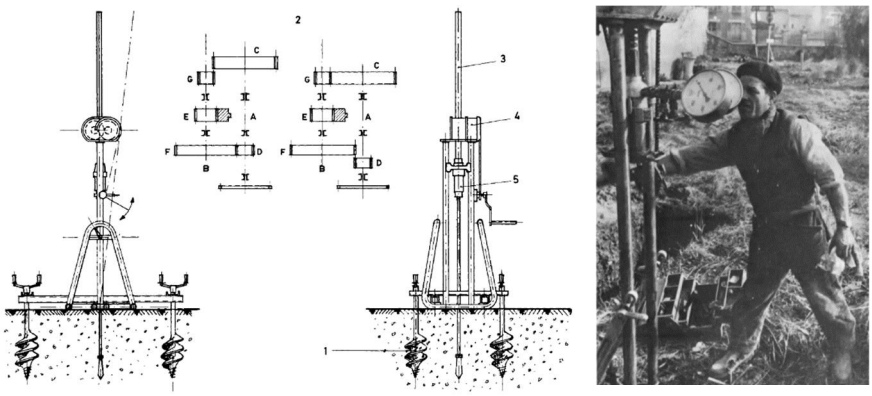

Figure 2-7 Dutch penetrometer with 2.5-ton capacity (Sanglerat, 1972)

The reaction force for this 10-ton CPT apparatus was acquired by digging a hole that was 2 x 3 m wide and 1 m deep. A wooden floor, with threaded ends attached to it that reached above the ground level, was laid on the bottom of this hole. The hole was subsequently filled with six cubic meters of sand. These preparations for the CPT test took up to three working days.

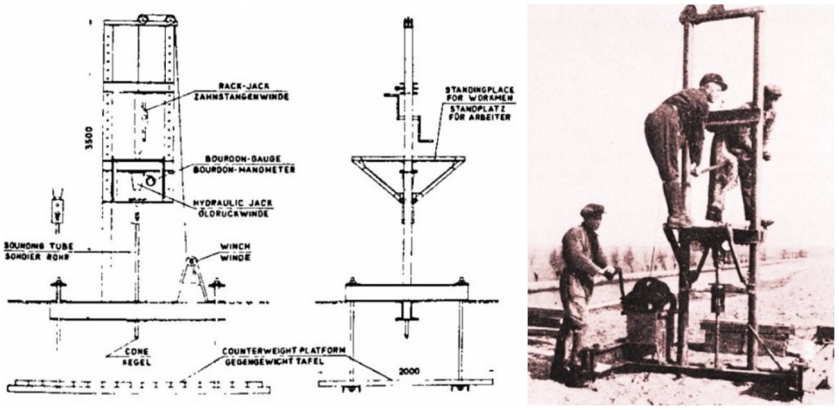

Figure 2-8 Dutch penetrometer with 10-ton capacity (Delft Soil Mechanics Laboratory, 1936)

The final refinement covered the cone itself. When the cone was pushed beyond the casing, a gap was created above the cone (Figure 2-12 b), which might or might not be immediately filled, depending on the type of soil penetrated. This would therefore influence the shape of the sliding surface of failure and hence the shearing resistance. Moreover, when pushing the tube down, there always existed the possibility that fine grains of soil might enter the cone equipment (Figure 2-12 c), causing friction between the lower end of the tube and the rod, thus giving results that were too high.

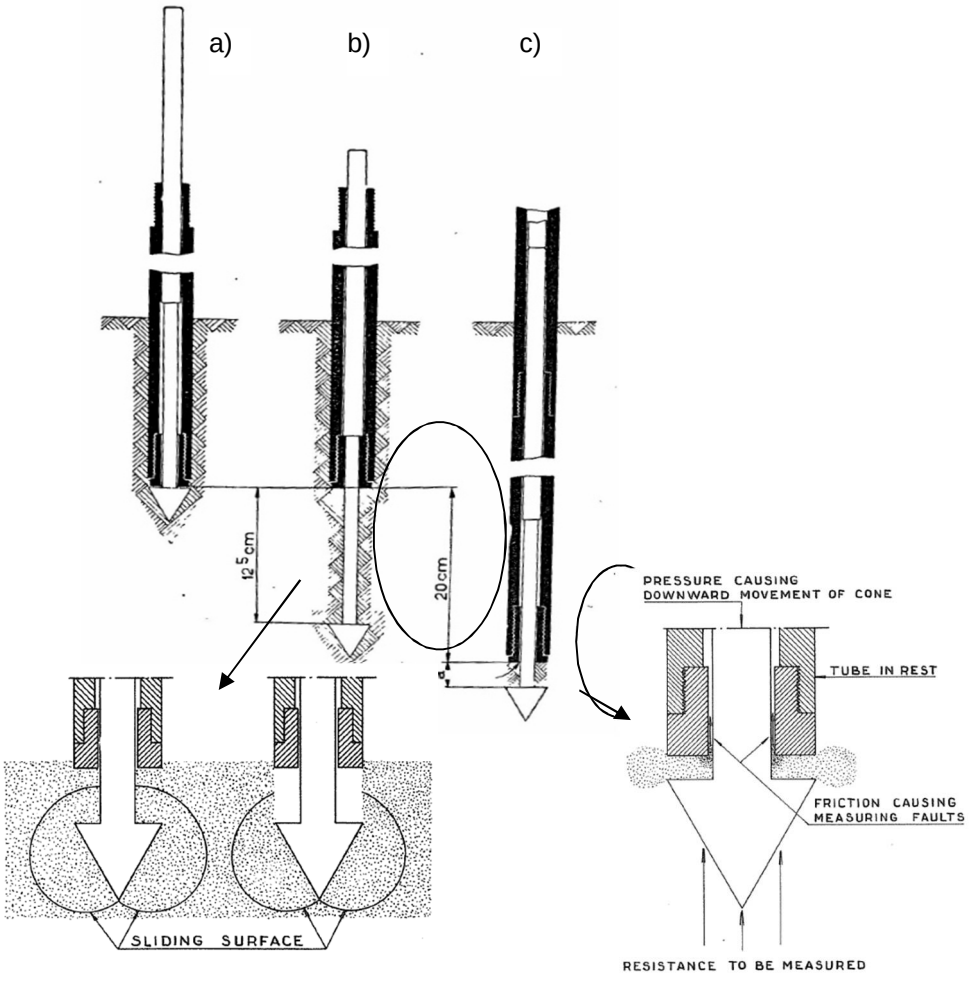

Figure 2-9 Frictional component influence on the measured results of mechanical penetrometer (Vermeiden, 1948; Plantema, 1948)

1948 – 1953: Eliminating Friction between Tube and Inner Rod

In 1948, a mantle type of cone was designed by Delft Soil Mechanics Laboratory (Vermeiden, 1948; Plantema, 1948) to eliminate the friction between the tube and the inner rod (Figure 2-10). The mantle effectively prevented the intrusion of soil grains, thus eliminating the possibility of friction error. The very slight taper on the side of the mantle eliminated the creation of the gap above the cone.

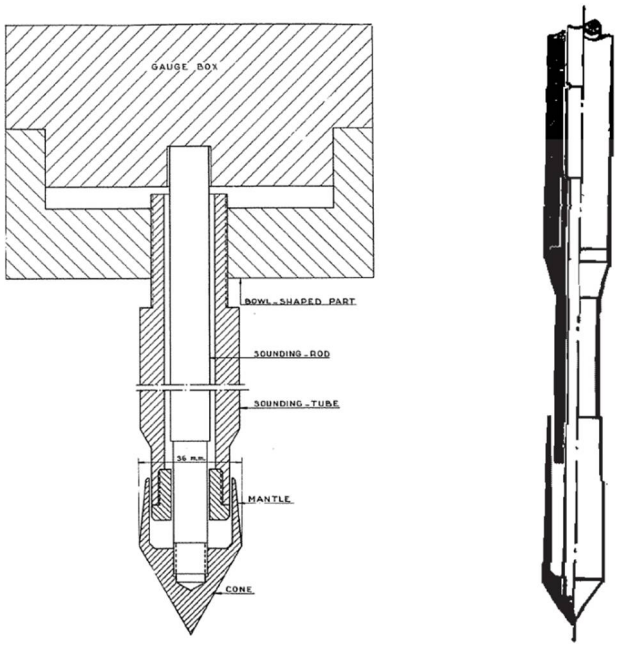

Figure 2-10 Point of the Delft mantle cone (Vermeiden, 1948; Plantema, 1948)

It is of prime importance to know the nature and properties of the soil layers in order to successfully interpret the results of a sounding. To this end, the soil mechanics laboratory of Delft constructed a light soil sampler, which was forced into the soil by means of the sounding apparatus (Figure 2-11). With the aid of this sampler, 100 cm^3 of undisturbed soil samples could be obtained from any desired depth, without a casing.

In position 1 of Figure 2-11, the sampler is ready to be forced into the soil. The lower end of the sampling tube has a plug that is attached to a rod, which bears, by means of the notches, up against two similar notches on the inside of the extension tube, while the sampler is forced down. The turning of the plug itself is prevented by the wings on the plug (position 2). Then, the sampler is lowered again, the plug disappears into the sampler, and the latter is filled with soil (position 3).

The inner rod remains stable during withdrawal by its self-weight seating on the soil sample and balls (position 4). After withdrawal, the samples are pushed out of the sampling tube into zinc cylinders and sent to the laboratory for testing.

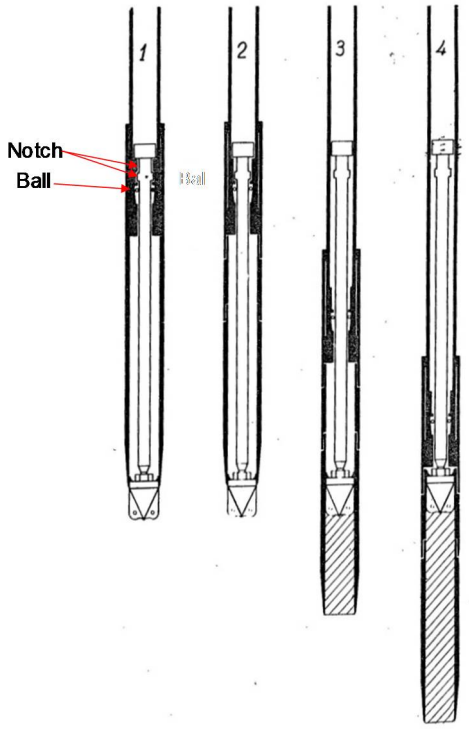

Figure 2-11 Drive sampling apparatus combined with Dutch Penetrometer in 1948 (Vermeiden, 1948)

The improvements made to the deep-sounding apparatus, as shown in Figure 2-12, aimed principally at a more economical working method. This was achieved by using a more efficient pressure appliance and a frame built up from hollow steel beams, which reduced the weight and facilitated dismantling and transport.

An improvement in the measuring cone technique was provided by the invention of a new hydraulic measuring device for reading the penetration resistances. The construction was based on past experience, and special attention was given to preventing leakages and to low piston friction. It appears that the amount of friction was about 4% of the pressure at any moment. The anchoring of this apparatus consisted of an underground weighted floor of screw rods.

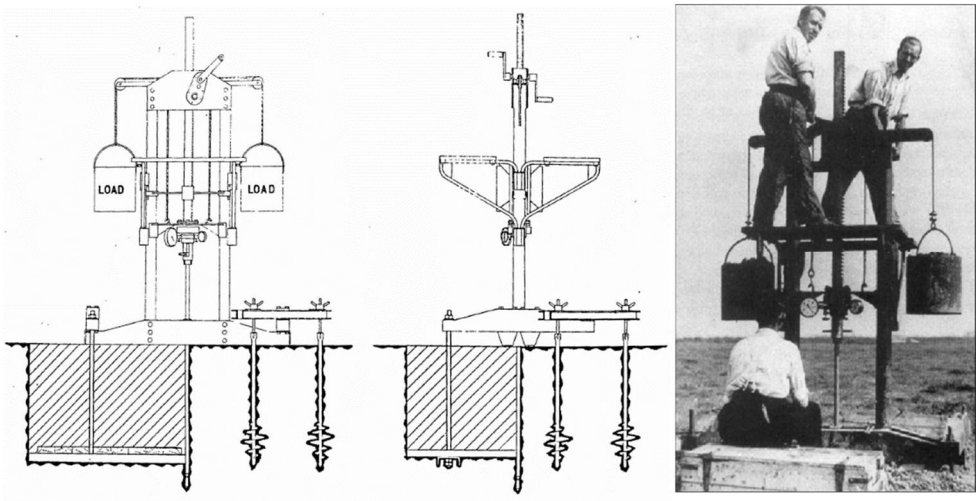

Figure 2-12 Reaction load system of Dutch penetrometer (Vermeiden, 1948)

The measuring apparatus can be applied to the requirements of modern measuring techniques (Plantema, 1948) by replacing the hydraulic measuring method that utilized a Bourdon gauge (with its inherent technical measuring errors) with a gauge box with wire resistance strain gauges so that the pressures could be measured electrically. This measuring method had the advantage of requiring negligible pushing, so

that it was possible for the tube and rod to be pushed down at the same rate. The gauge box was practically invulnerable, and the registering apparatus was easily and safely transportable by unskilled labor. The gauge box and registering apparatus can be seen in Figure 2-13.

In Figure 2-13, an apparatus is shown which was used to perform deep soundings by the City Engineers Department of Rotterdam. By means of a specially designed rack jack, the sounding tubes and rods were pushed down to one meter simultaneously.

Figure 2-13 Point resistance measured by strain gage (Plantema, 1948)

To save time in erecting and dismantling it, the apparatus was designed as shown in Figure 2-14. By means of a winch, the tubes were pressed into the ground one meter at a time and afterwards pulled out. The wagon was anchored into the ground with screw anchors.

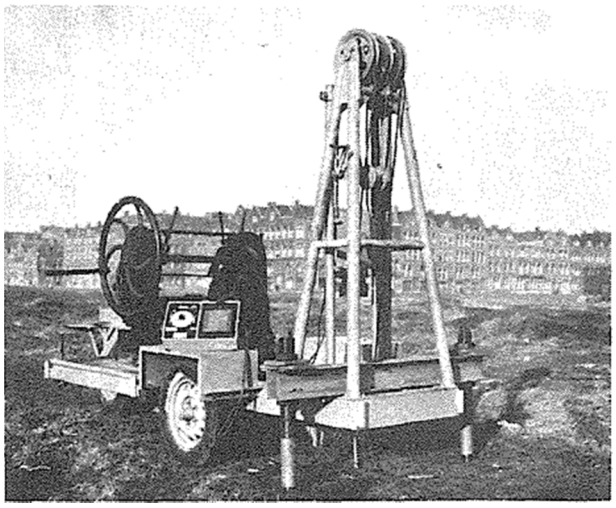

Figure 2-14 Point of the Delft mantle cone (Plantema, 1948)

In 1949, Andina was awarded first prize in a competition organized by Kerisel for the design of penetrometers in France. In 1950, both Andina and Bauer of the Jangot-Bonneton Company patented a fixed-cone penetrometer (90°). The first apparatus developed had a point of 110 mm diameter and was mounted on a 45-ton trailer. It soon proved impractical for field testing. In 1952, modifications were made to the Jangot-Bonneton penetrometer, and a 60-mm diameter cone was developed and operated from a 4-ton truck capable of being anchored and loaded (Figure 2-15). In 1955, the truck weight was increased to 10 tons.

This device was classified as a penetrometer of large diameter. The penetration was automatic and was made with a power take-off from the truck motor. Recovery was achieved with a speed-controlled cable. An exterior casing of 60 mm consisted of two concentric tubes welded together. The interior rods had a 35-mm diameter. Continuous recordings of the point resistance and the total resistance were made with calibrated proving rings. The capacity was 10 tons, and it was capable of investigating great depths (20 - 3 0 m).

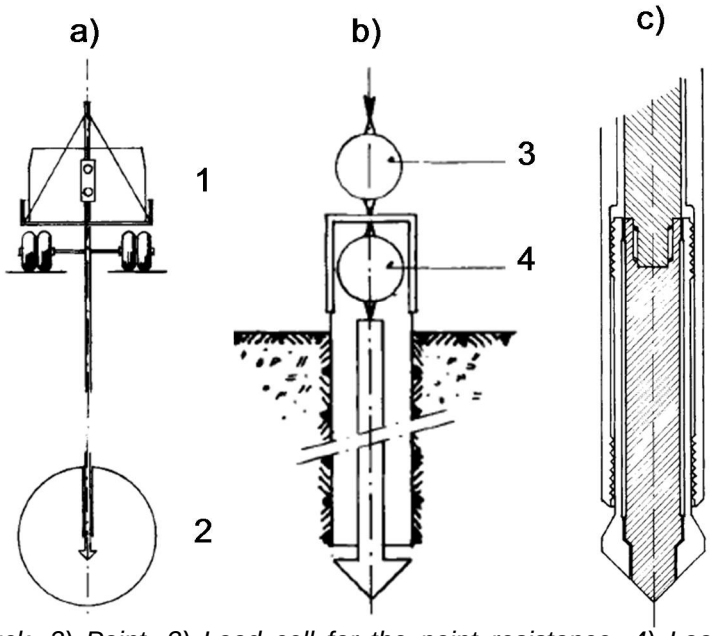

1) Truck, 2) Point, 3) Load cell for the point resistance, 4) Load cell for total resistance

Figure 2-15 Jangot-Bonneton penetrometer: a) General view; b) and c) Cross-section of device (Sanglerat, 1972)

In 1950, the Swedish Geotechnical Institute developed a motorized penetration test which consisted of a 60° cone with either a 25 or 40 mm diameter (Dahlberg, 1974). The cone penetrated the ground at a rate of about 50 mm/second (the left diagram of Figure 2-16). As the cone penetrated without rotation, the rods were automatically rotated from the ground surface at the rate of one revolution per 12.5 mm of penetration. In this way, the skin friction and point resistance could be measured separately. The skin frictional resistance was evaluated from the measured torque. The point resistance was obtained from the difference between the frictional resistance and the total penetration resistance. The cone resistance was recorded by a pen recorder (the right diagram of Figure 2-16).

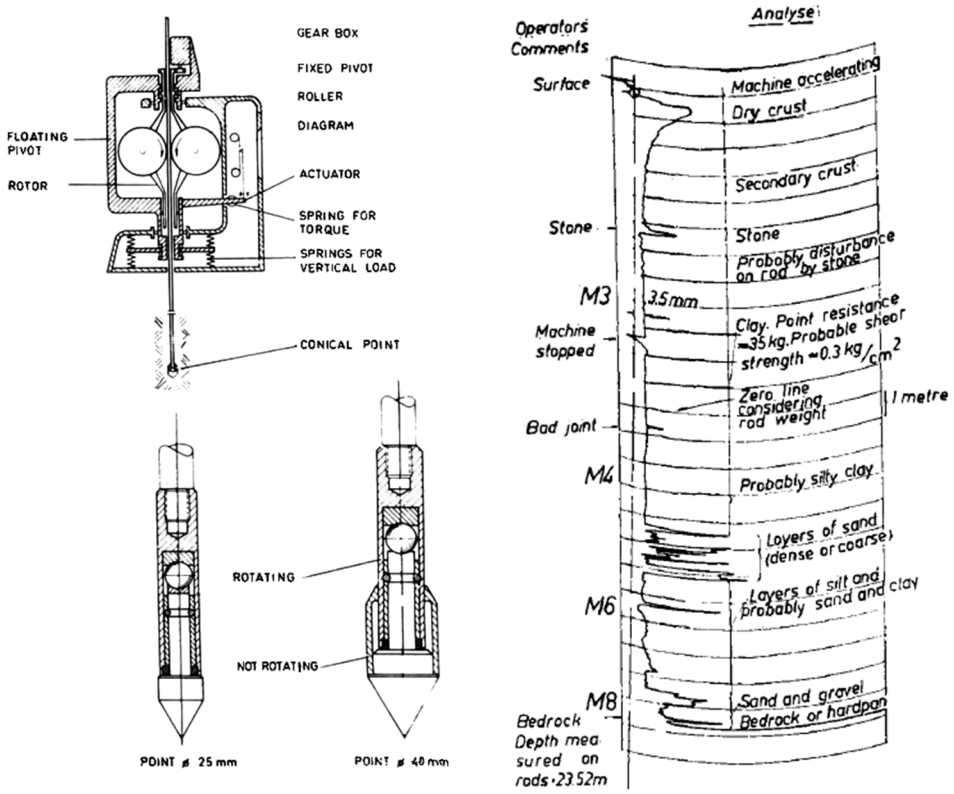

Figure 2-16 Sweden's static sounding equipment and test data (Dahlberg, 1974; Broms, 1974)

In 1953, the SOL-ESS AIS penetrometer (Figure 2- 17) was constructed by L. Parez (1953). This penetrometer included a conical point which was combined with the piston of a small hydraulic jack located at the base of each rod (Figure 2-17b). The pressure was transmitted to manometers at the ground surface by an oil pressure line. Continuous readings were taken of the point resistance. A 15-ton loaded truck provided the reaction for the 45 mm-diameter penetrometer (Figure 2-17a). Small trucks anchored in the soil could be used in the same capacity. A heavily loaded truck (26-30 tons) was required for the large-size penetrometer. Depth recordings were made by an electric lamp which lit up every 10 cm of depth.

The hydraulic feed to the jack was provided by a 2-speed motor. The slow-speed high-pressure feed was used for penetrating the soil and the high speed for lowering and raising the tools in the hole. High pressure was required to pull the tubes out of the ground. The hydraulic system automatically changed speeds.

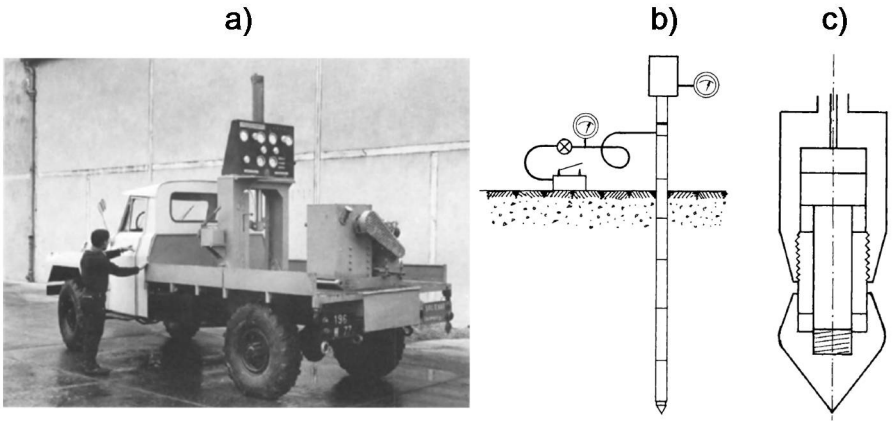

Figure 2-17 The Sol-Essais penetrometer of France: a) General view, b) Sketch of penetrometer, and c) Point of penetrometer (Sanglerat, 1972)

As explained earlier, in a deep-sounding, the total resistance is usually measured with a steel tube and a cone that are pushed down into the ground together. Subsequently, only the inner rod with cone tip is pushed downward to measure the cone tip resistance, while the tube is retained by the skin friction of the soil. The frictional resistance is obtained by deducting the cone tip resistance from the total resistance.

However, in several deep-soundings it was revealed that the total friction measured did not increase after a certain depth had been reached, even though the measured point resistances indicated that the type of soil did not change. This illogical revelation gave rise to measuring the local adhesion.

1953 – 1965: Cone Penetrometer with Measurement of Local Sleeve Resistance

In 1953, a friction sleeve (adhesion-jacket-cone) was designed and added to the back of the cone to measure the local sleeve friction (Begemann, 1953), as indicated in Figure 2-18. The original cone body, "**A,**" was followed by a cylinder, "**B,**" with a length of 10 cm and the same diameter as the base of the cone. The cone side of this cylinder was affixed to an extension of smaller diameter so that the original cone body, "**A,**" could move up and down. The cylinder, "**B,**" fitted very close to body, "**C,**" which, in the original construction, fitted to "**A**".

By exerting pressure on the sounding tubes, the adhesion-jacket-cone could be pushed closed into the ground until the required depth was reached (position 1). Hereinafter, the solid bar present in the sounding tubes was pressed away a length of 1.5 to 2 cm, for measuring the resistance of the cone. Only the cone body, "**A,**" was pushed further into the ground (position 2). However, pushing the bar further down caused the adhesion cover, through the medium of notches, to also go down. This is how the cone resistance, plus the friction of the 10-cm long jacket was measured (position 3). After reading the maximum value, the sounding tube was pushed down again so that body "**C**" slid into body "**B,**" and "**B**" in "**A,**" after which the complete unit could be pushed farther until a greater depth was reached (position 4). With the aid of this adhesion jacket cone, it was possible to obtain a very important extra datum by merely slight pushing through the internal rods.

In 1959, Goudsche Machinefabriek, in cooperation with Delft, introduced a motorized 10-ton capacity penetrometer (Figure 2-19). In 1962 - 1963, they developed a rotating penetrometer which had the added feature of being able to recover samples of cohesive soils. The other two earlier types of penetrometers were also used to recover

samples by first pushing and then rotating the sampling gear. Samples thus recovered had dimensions of 35-mm diameters and were 25 - 30 cm long.

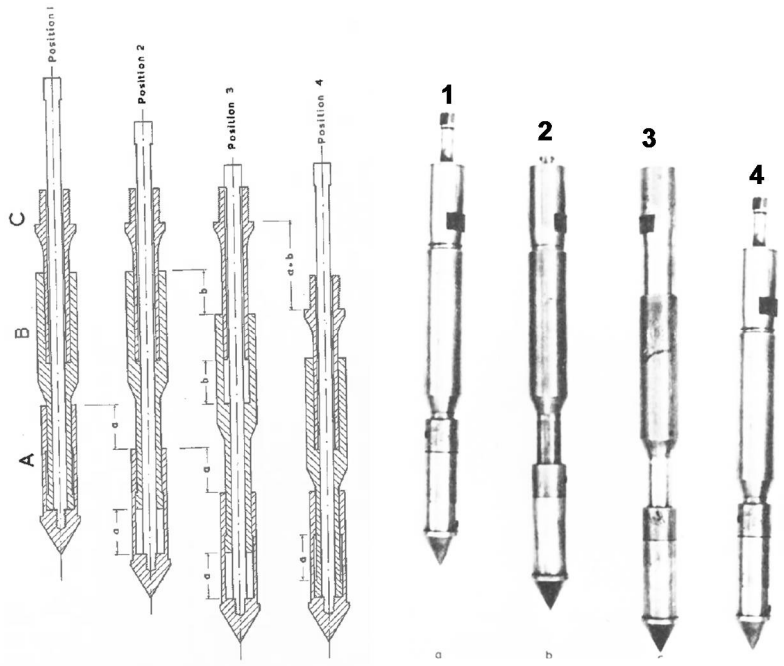

Figure 2-18 four positions of Adhesion-Jacket-Cone (Begenann, 1953)

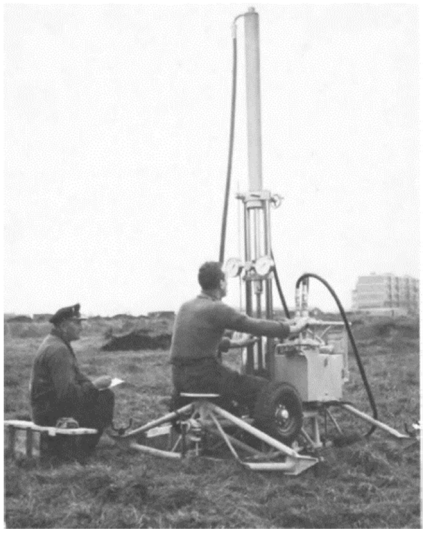

Figure 2-19 Motorized Dutch penetrometer with 10-ton capacity (Sanglerat, 1972)

1965 – 1973: Electric Cone Penetrometer

In 1965, Fugro, consulting foundation engineers in The Netherlands, developed an electric penetrometer (Figure 2-20). The diameter of the point was the same as that of the classical Delft cone penetrometer, but the shape was slightly different from that made by Goudsche Machinefabriek in the Delft Laboratory. The point resistance was measured by an electrically-operated cell during the penetration.

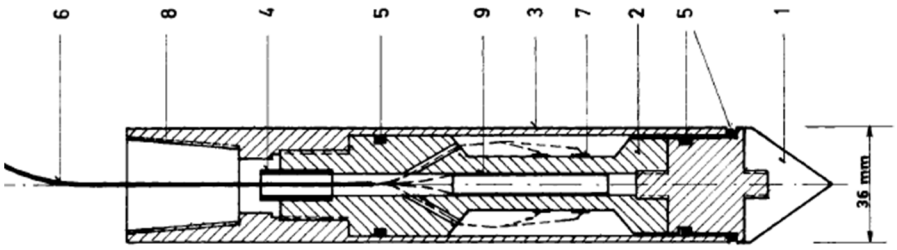

1) Conical tip (10 cm^2), 2) Load cell, 3) Protective mantle, 4) Waterproof bushing, 5) O-rings, 6) Cable, 7) Strain gage, 8) Connection with rods, and 9) Inclinometer.

Figure 2-20 Fugro's electrical strain gage cone (Sanglerat, 1972)

The design was such that there was no direct contact between the cone and the rods other than through the cell. The pressure cell contained a number of strain gages which were arranged so that only axial stresses were recorded. Automatic compensations were made for bending stresses. The cell was surrounded by a thin steel mantle of the same diameter as that of the outside diameter of the cone and the rods. The tip and the mantle were expendable and could be replaced when they became worn. The pressure variations were measured by a Wheatstone bridge and recorded directly on a continuous graph. This cone was preferred in soft clays and gave a higher degree of accuracy than was obtainable with the other points. Details of the electric cone and strain gage are shown in Figure 2-21.

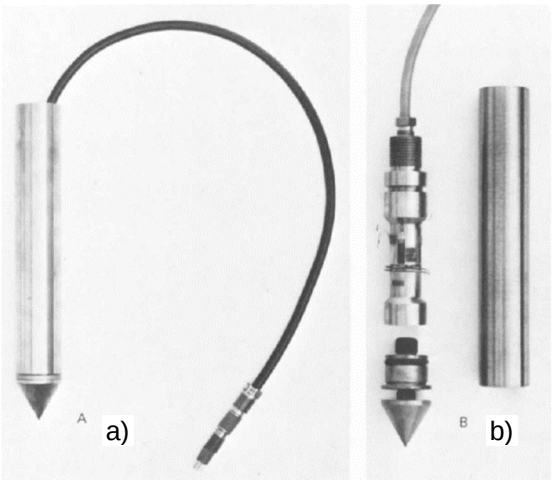

Figure 2-21 Fugro's electrical strain gage cone: a) assembled and b) dismantled (Sanglerat, 1972)

A sleeve, which had the same surface area as the Begemann-type sleeve, was used to measure side friction (Figure 2-22). The surface area of the frictional sleeve was 150 cm^2. The Fugro penetrometer could also be equipped with an inclinometer. For deep soundings, it was therefore possible to know the deviation from the vertical and the bending of the rods due to eccentricity which could cause erroneous readings of the point resistance.

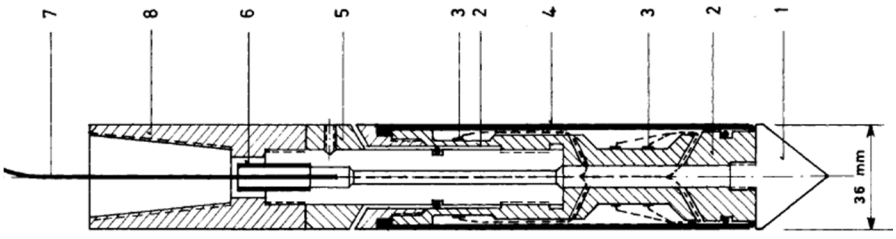

1) Conical tip; 2) load cells; 3) strain gage; 4) friction mantle;
5) adjustment ring; 6) waterproof bushing; 7) cable; 8) connection with rods.

Figure 2-22 Fugro's electrical friction cone (Sanglerat, 1972)

In 1966, the Centre Experimental du Bâtiment et des Travaux Publics (CEBTP) in Paris developed an electric static penetrometer. Many improvements were incorporated, and different penetrometers were ultimately developed for use in the field and in the laboratory.

The point-resistance device consisted of two coaxial proving rings. The more sensitive dynamometer was used for loads not exceeding 1/10 of the capacity. For larger loads, both dynamometers were operated in parallel (Figure 2-23). The total capacity was 20,000 kg, which was equal to that of the hydraulic jacks used to advance the point.

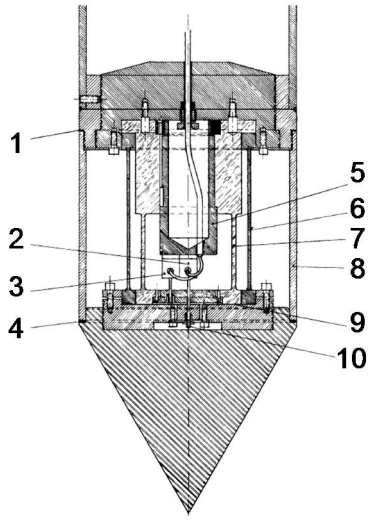

1&4) Flexible joint, 2) Principal deflection recorder, 3) Secondary deflection recorder, 5) Recorder support, 6) 20-ton dynamometer, 7) 160-ton dynamometer, 8) friction sleeve, 9) clearance: 0.2 mm, and 10) zero setting control for recorder.

Figure 2-23 Point of the 320-mm static penetrometer CEBTP, (Sanglerat, 1972)

At the same time, the regional laboratory of the Ponts et Chaussées at Saint-Brieuc developed an electrically-instrumented point for increasing the performance of the 10-ton capacity Gouda static penetrometer. The point resistance was recorded directly and involved no relative motion between the point resistance and the sleeve resistance.

The point resistance consisted of a cone affixed to a guide rod sliding in a casing and provided with a ball joint at the upper end (Figure 2-24). During penetration into the soil, the stresses were transmitted to a special nickel-chrome steel alloy plate onto which four strain gages were placed at opposite ends. The special steel alloy plate was submitted to loading and unloading cycles to remove its hysteresis characteristics prior to its use in the penetrometer. Therefore, the stress-measuring device consisted of the instrumented plate, the strain gages, a Wheatstone bridge, and a galvanometer.

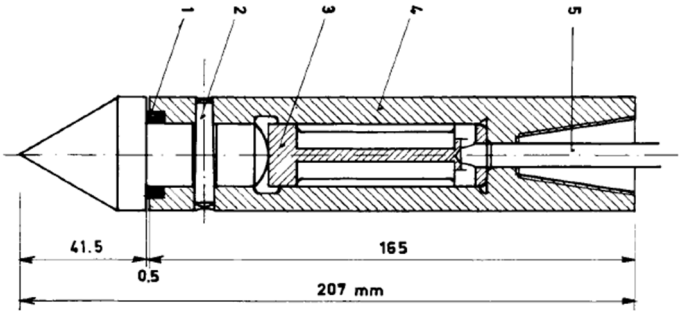

1) Joint; 2) Cotter pin; 3) Extensometer; 4) Sheath; 5) Connecting cable.

Figure 2-24 Electric penetrometer of the Ponts et Chaussees' laboratory at Saint-Brieuc, (after Sanglerat, 1972)

1973 – 1982: Measurement of Pore Water Pressure (Piezocone)

The influence of pore pressures on cone tip resistance has been the focus of many researchers. In 1973, a pore pressure sounding, shown in the diagram on the right side of Figure 2-26, was developed at the Norwegian Geotechnical Institute (Janbu and Senneset, 1974) by using an electric piezometer with the same outer dimensions as the cone penetrometer and constructing the pore pressure measurements at the shoulder of the cone tip. The porous filter was placed 1 cm above the cone tip, followed by a water-saturated chamber. The outer pore pressure was measured by a vibrating wire device, placed in contact with the chamber. This pore pressure sounding was pushed down at

the same rate of penetration as in the penetration test. During penetration, the cone resistance, the sleeve friction, and the pore pressure were measured simultaneously. Figure 2-25 shows the cone resistance and pore pressure measured in moraine clay and sand deposits (Senneset 1974). The rate of dissipation of the measured excess pore pressure is illustrated in Figure 2-26.

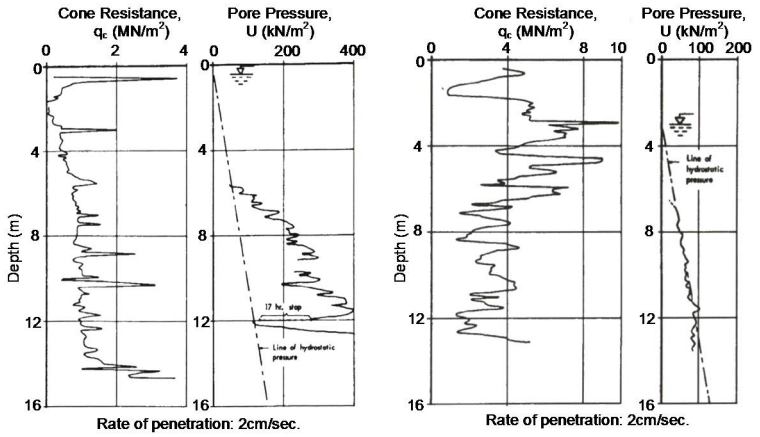

Figure 2-25 Penetration test with pore pressure measurement: a) Cone penetration test in clay, and b) Cone penetration test in sand (Senneset, 1974)

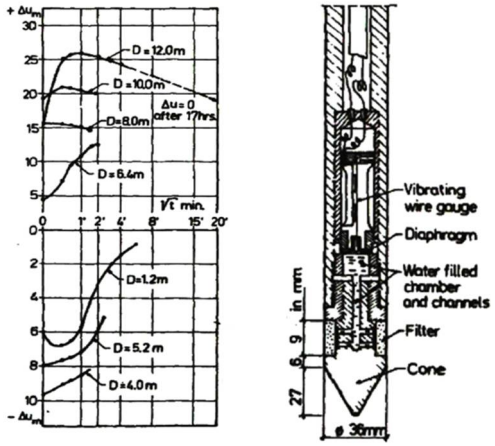

Figure 2-26 Excess pore pressure dissipation test (Janbu and Senneset, 1974)

The first piezocone was developed by Fugro in 1973 (Figure 2-27a). Its basis was an eclectic cone penetrometer with a capacity of 5 tons (no friction sleeve). The porous element was located in the cylindrical part of the base of an extended cone. A pressure transducer was placed immediately above it, in the center of the load cell. In 1980, the piezocone penetrometer was further developed. The first prototype of a cone penetrometer (Figure 2-27a) was built with a conical tip and a porous stone at mid-height (Figure 2-27b). Based on the satisfactory results with this prototype, a new friction cone penetrometer with a piezometer was built (Figure 2-27c), combining the required sensitivity for testing soft soils and the rigidity for the piezometric system.

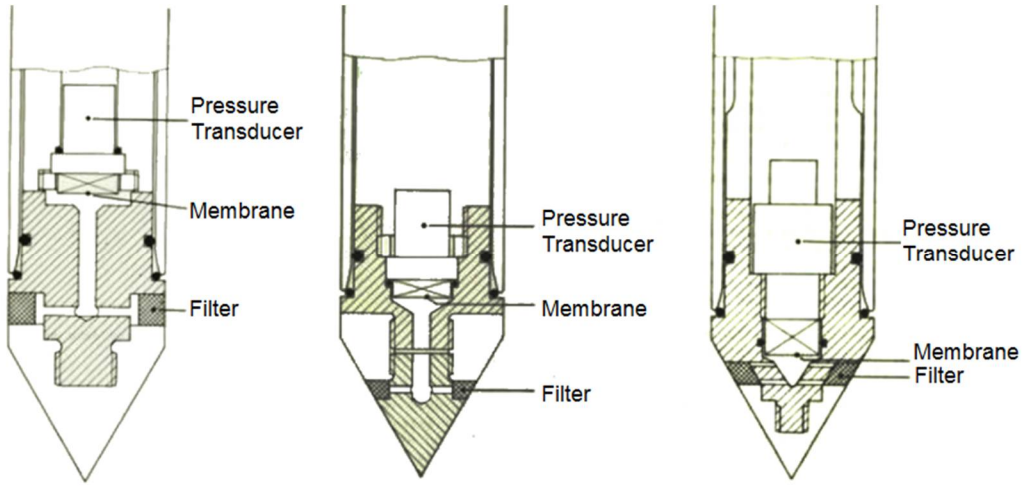

a) b) c)

Figure 2-27 Types of Fugro's Piezocone: a) Piezocone in 1973, b) Piezocone in 1980, and c) Piezocone in 1981 (Zuidberg et al., 1982)

In 1974, Schmertmann studied the influence of pore pressures on the cone tip resistance and concluded that negative pore pressures can add significantly cone tip resistance for some sands, and the positive pore pressures can significantly reduce the cone tip resistance in some cohesive soils. Early versions of the pore pressure cone in

the United States of America contained only a piezometer element, so that q_c and f_s had to be measured in separate adjacent tests (Wissa et al. 1975, Torstensson 1975, Baligh et al. 1978), as shown in Figure 2-28. Subsequently, this type of pore pressure transducer became incorporated into a standard electric penetrometer (Baligh et al. 1981; Gary et al., 1981; Campanella et al., 1981; Muromachi, 1981; De Ruiter 1981; Tumay et al., 1981), so that the direct correlation between q_c, f_s and pore pressure, u, could be studied (Figure 2-29). The excess pore pressure, Δu, was found by stopping the penetration and allowing the pore pressure to dissipate to the equilibrium pressure U_0.

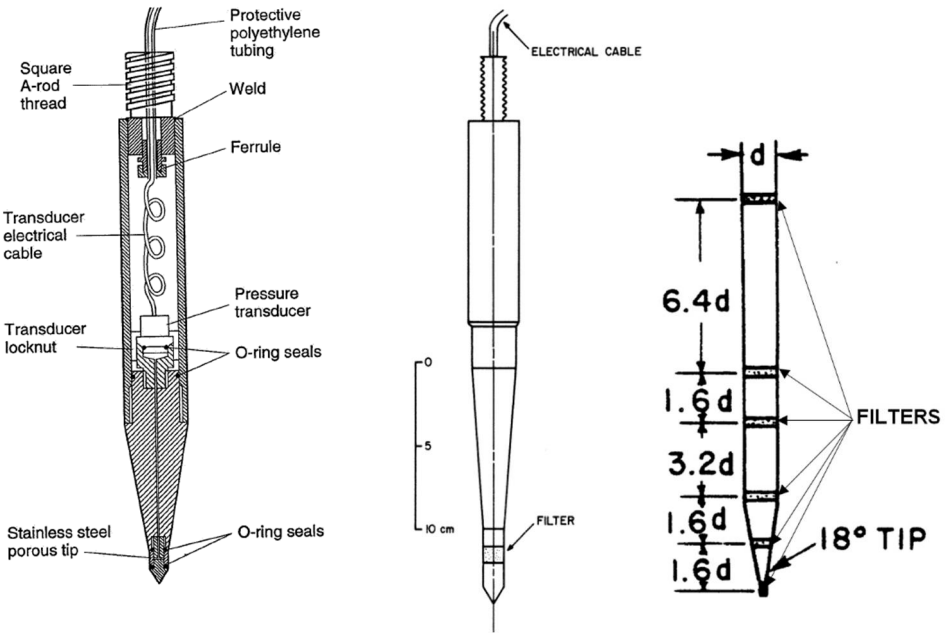

Figure 2-28 Schematic of Piezometer probes: a) Wissa et al. (1975), b) Torstensson (1975), and c) Baligh et al. (1978)

Excess pore pressure is a function of soil type, strength, and deformability characteristics. Its measurement opens the way for an effective stress analysis of the cone resistance and for an improved determination of soil parameters from CPT data.

The obvious advantage of a simultaneous measurement of q_c, f_s, and u leads automatically to adopting the standard penetrometer geometry for the piezocone. Because of these reasons, a10 cm^2, 60^0 apex angle cylindrical penetrometer is now generally accepted.

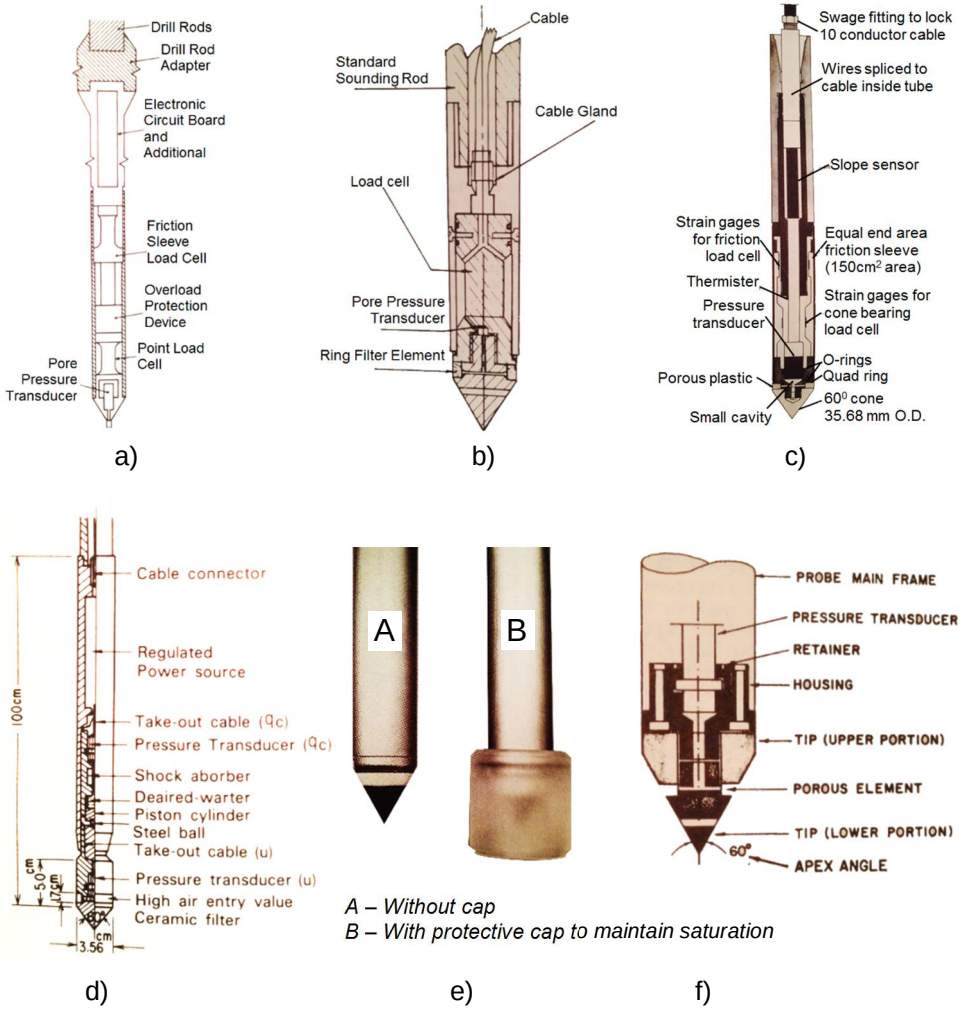

Figure 2-29 Types of pore pressure transducer incorporated in the electric penetrometer: a) Baligh et al.(1981), b) Gary et al. (1981), c) Campanella et al. (1981), d) Muromachi (1981), e) De Ruiter (1981), and f) Tumay et al. (1981)

In 1982, at the Building Research Station in the UK, standard Fugro-type cones were mounted directly to the front of low-volume-change-diaphragm type transducers that were fitted with a silicon strain gauge diaphragm (Figure 2-30).

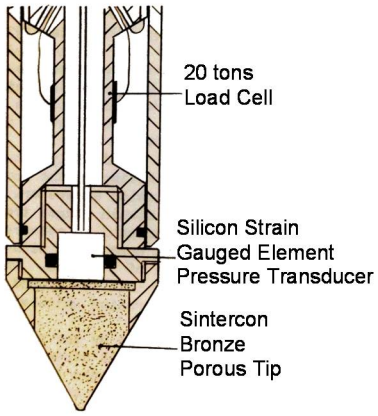

Figure 2-30 Piezometer in cone tip (Marsland and Quarterman, 1982)

In general, the main difference in piezometers is the location of the installed porous filter element. It is an important aspect of the piezocone and it has not been standardized yet. Piezocones have often three common locations for porous filter elements: 1) on the cone face/tip (u_1 or u_t), 2) just behind the tip (u_2 or u_{bt}), or 3) behind the friction sleeve (u_3 or u_{bs}), as shown in Figure 2-31.

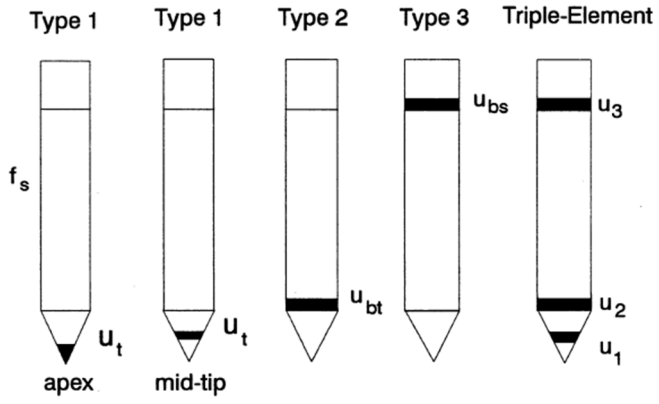

Figure 2-31 Locations of piezocone porous filters (Chen, 1994)

Measurements taken with piezometer probes that have a shaft with the same diameter as the cone show that the magnitude of the pore pressure is greatest at the very tip (Torstensson 1975, Baligh and Levadoux 1980, Tymay et al. 1981, Battaglio et al. 1981) and remains more or less constant along the conical part of the penetrometer. This is illustrated in Figure 2-32. A sharp decrease in pore pressure is observed immediately above the cone along the friction sleeve of the penetrometer. This pressure distribution agrees with the expected behavior, because the zone of maximum stress and strain on the face of the cone should exhibit the highest dynamic pore pressures.

To measure the peak pore pressure, the porous element should be placed in the conical tip (Type 1 of Figure 2-31). In view of the vulnerability of the point, the element is often situated in the conical face (Tumay et al. 1981, De Ruiter 1981, Zuidberg et al. 1982). It is believed that with this filter location, the piezocone will have the greatest sensitivity to changes in stratification and soil properties.

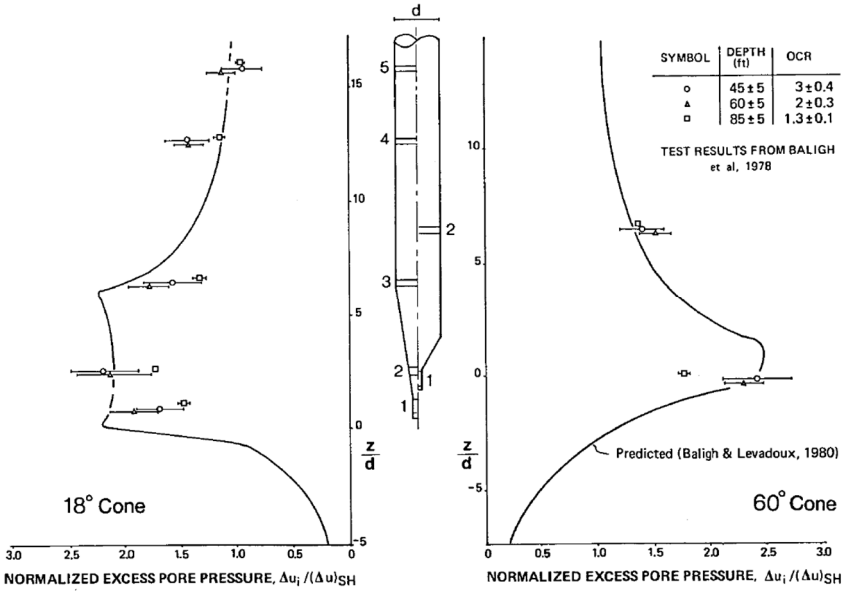

Figure 2-32 Distribution of pore pressures along face and shaft of 18^0 and 60^0 cones during penetration (Baligh et al., 1980)

An alternative place for the porous element is directly above the cone tip (Type 2 of Figure 2-31). The advantages of this filter position are better protection against damage and abrasion during penetration, and an easier saturation procedure (Senneset 1974, Campanella et al. 1982, Tavenas et al. 1982). However, it is likely that the stress conditions at this point are less stable, which could reduce the repeatability of the measurements.

1982 – Present: Penetrometers Combined with a Variety of Sensors and Modules

A variety of sensors and modules can be combined with the electric penetrometer for other measuring purposes, and data from the combined sensors can be recorded simultaneously with tip resistance and friction, if desired. Some common types are reviewed below.

Seismic Cone

Geophones and/or accelerometers have been added to cone penetrometers to measure compression and shear waves. In situ seismic measurements have traditionally been made with two or more boreholes. The modern seismic cone device was developed at the University of British Columbia (UBC) to facilitate more economical downhole measurements (Campanella et al., 1986; Robetson et al., 1986). It consists of a piezocone unit with a receiver above it (the left diagram of Figure 2-33). A schematic diagram of a seismic cone is shown in the right diagram of Figure 2-33.

The memory oscilloscope and impulse source with the trigger for the oscilloscope are additional equipment. The source consists of a steel or aluminum beam for generating shear waves, or a flat plate for generating compression waves. The shear wave is created by hitting the beam ends with a hammer in the long axis direction. The

seismic cone device is pushed often into the ground and stopped at 1 m intervals. Then, the shear wave is created at the ground surface and the time that the shear wave reaches the seismometer will be recorded.

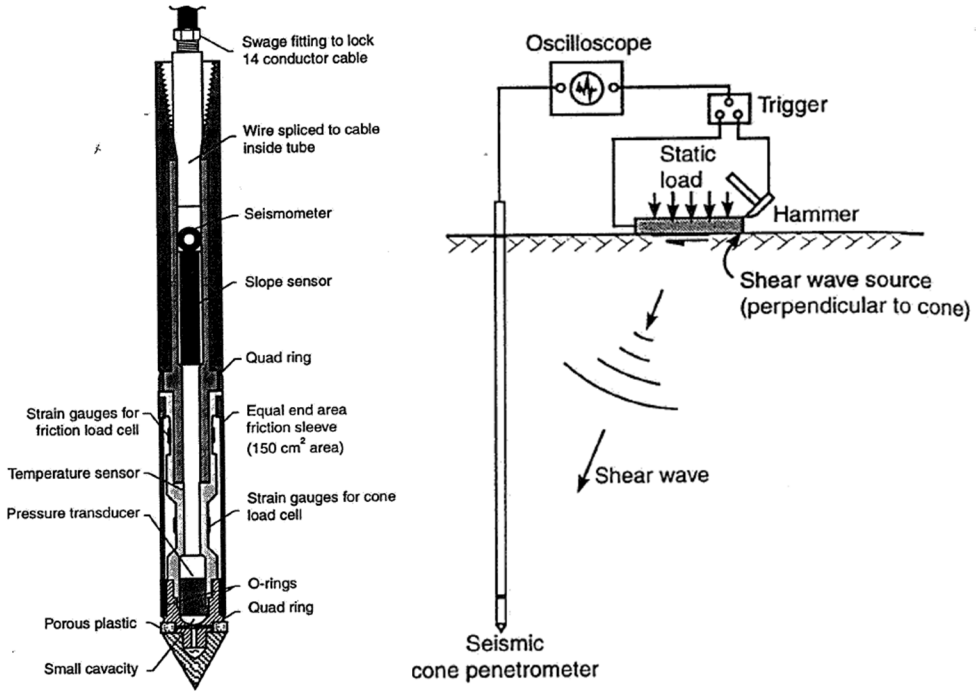

Figure 2-33 The UBC seismic cone and survey technique (Campanella et al., 1986)

Acoustic Penetrometer

Friction cone penetrometers are equipped with a microphone and a data acquisition system to monitor the acoustic response of the soil during penetration of the probe, as shown in Figure 2-34 (Muromachi, 1981; Villet and Mitchell, 1981). Noise level, spectrum, and frequency are functions of soil type and density. Results obtained so far indicate that the acoustic response provides reliable information on soil type and profile

conditions; however, the technique is in a research state and needs further development before it can be used for normal site investigations.

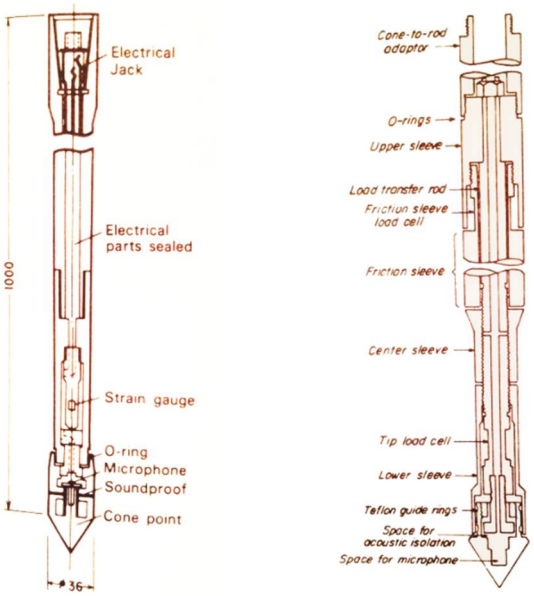

a) b)

Figure 2-34 Acoustic penetrometer: a) Phono-sounding apparatus, b) Penetrometer (Muromachi, 1981; Villet et al., 1981)

Pressuremeter

A pressiopenetrometer with an 89-mm diameter (Figure 2-35a) was developed by Jezequel et al., (1982) and was often installed by using a vibrating hammer. Due to the large diameter, it was difficult to install and thus was replaced by a device with a smaller diameter, which was known as a cone pressuremeter (a pressuremeter module mounted behind a standard electrical cone penetrometer). This device enables the performance of pressuremeter tests as part of the CPT operations, and can be installed by standard CPT jacking equipment.

The first cone pressuremeter (Figure 2-35b) was designed and built in situ by Cambridge, originally to Fugro's specifications, which are described by Withers et al.

(1986). The pressuremeter module, with a 43.7-mm diameter and 437-mm length is operated behind a standard 15-cm^2 CPTU. The pressuermeter cell is comprised of a cylindrical rubber membrane inflated by nitrogen gas. Protection of this membrane during insertion is provided by an additional steel-reinforced rubber membrane in the form of a "Chinese lantern." Measurements of inflation pressure and cavity strain are recorded at mid-height of the module by instrumentation at three locations, 120^0 apart. The maximum radial strain is 50%. Other cone pressuremeters have been developed by the University of British Columbia, UBC, (Campanella and Robertson, 1986), ISMES (Ghionna et al, 1995) and Fugo (Zuidberg and Post, 1995).

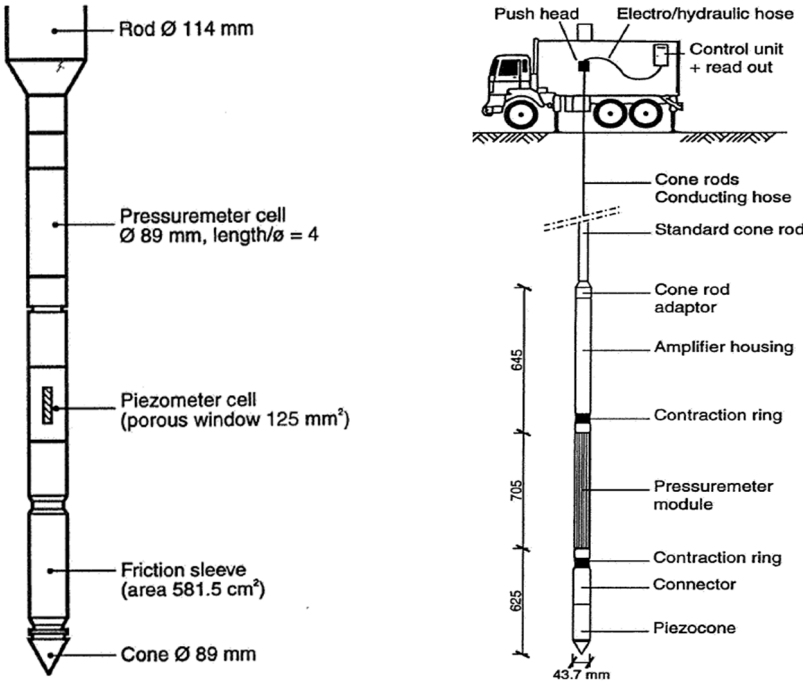

a) b)

Figure 2-35 Types of electric penetrometers combined with pressuremeter: a) the LPC pressionpenetrometer, and b) the Fugo-McClelland cone pressuremeter (Lunne et al., 1997)

2.1.2 Direct CPT-based Methods Used to Estimate Axial Pile Capacity

CPT data may be applied to pile design by either direct or indirect methods (Eslami and Fellenius 1997; Fellenius, 2017). The indirect methods calculate the pile capacity based on the employed soil parameters estimated from the cone data. The dramatic uncertainties are inherent in the indirect methods. They ignore horizontal stress, strain softening, and compressibility of soil. The indirect methods are not suitable for use in engineering practice and, therefore, will not be reviewed.

The direct CPT-based methods consider the cone as a model pile, in which the measured cone tip and sleeve resistances correspond to the pile toe and shaft resistance. For this approach, the soil compressibility, rigidity, and mean effective stress influence the pile and the cone in a similar way. Thus it can eliminate the need to calculate intermediate values, such as the bearing capacity coefficient, N_q, and the earth pressure coefficient, K_s. Niazi and Mayne (2013) reported 36 pile design methods based on CPT data, which consisted of both the purely empirical and semi-empirical direct methods. Within the scope of this study, the six direct methods usually used are considered.

Schmertmann and Nottingham

The method of Schmertmann and Nottingham was developed basing on the work of the full-scale and model piles (Nottingham, 1975; Schmertmann, 1978). The unit pile toe resistance (r_t) is computed basing on the average cone resistance over an influence zone of 8d above the pile toe and 0.7d to 4d below the pile toe (Figure 2-36). The upper limit of the unit toe resistance is 15 MPa. The pile toe resistance is determined as:

$$r_t = Cq_{ca} \tag{2.1}$$

Where r_t is the unit pile toe resistance, C is the correlation coefficient depended on the overconsolidation ratio of the soil, and q_{ca} is the arithmetic average of q_c in an influence zone.

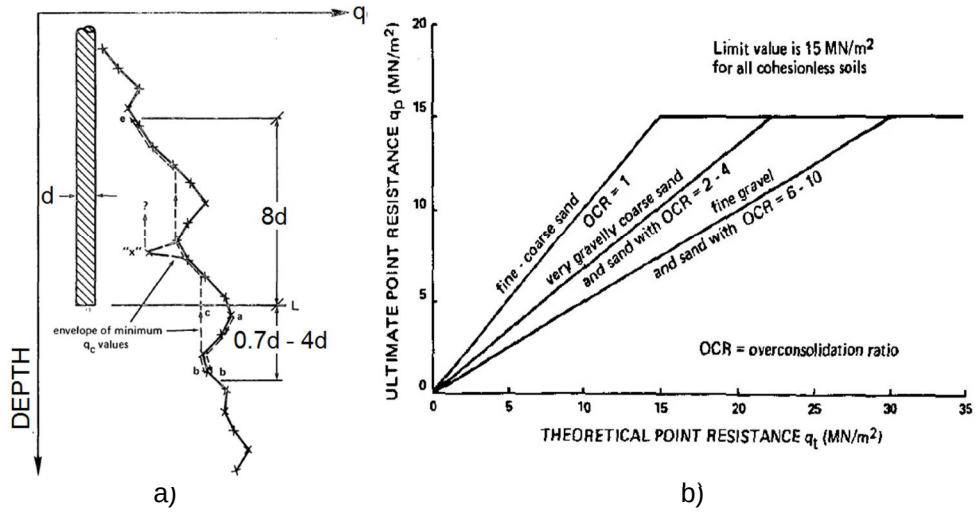

Figure 2-36 Influence zone to determine toe resistance: a) Calculation of average cone resistance (Schmertmann, 1978), and b) Limiting unit toe resistance for overconsolidated sand (After De Ruiter, 1982)

The unit pile shaft resistance, r_s, may be calculated from the sleeve friction as:

$$r_s = K_f f_s \tag{2.2}$$

Where K_f is dimensionless coefficient and f_s is the cone sleeve friction. The K_f coefficient depends on the embedment ratio, cone type, and pile shape. The K_f coefficient ranges from 0.8 to 2.0 for sand and from 0.2 to 1.25 for clay. The unit pile shaft resistance is interpolated linearly from zero at the elevation of the ground surface to the value obtained by (2.2) at the eight pile diameters depth below the ground surface.

De Ruiter and Beringen

De Ruiter's and Beringen's method (1979) was developed basing on the experiences of the offshore construction in the North Sea. In sand, the unit pile toe resistance of this method is similar to the method of Schmertmann and Nottingham. For clay, the unit pile toe resistance is computed following the analysis of the total stress, as presented in (2.3) and (2.4)

$$r_t = N_c S_u \tag{2.3}$$

$$S_u = \frac{q_c}{N_k} \tag{2.4}$$

Where N_c is the factor of the bearing capacity; S_u is the undrained shear strength; and N_k is dimensionless factor, ranging from 15 to 20. The upper limit of the unit toe resistance is 15 MPa.

The unit shaft resistance in sand is the smallest of $q_c/300$ and the sleeve friction (f_s). The unit shaft resistance in clay may is calculated basing on the undrained shear strength, S_u, as given in (2.5):

$$r_s = \alpha S_u \tag{2.5}$$

Where α is the adhesion factor equal to 0.5 and 1.0 for overconsolidated clays and normally consolidated, respectively. The upper limit of the unit shaft resistance is 120 kPa.

Bustanmante and Gianselli

The Bustanmante and Gianselli method (1982) was developed basing on the full-scale static load test results of 197 piles performed by Laboratoire Central des Ponts et Chausees (LCPC). The sleeve friction, f_s, was not considered. The unit toe and shaft resistances were calculated from the average con resistance, q_c. The filtering rules to compute the average cone resistance are shown in Figure 2-37.

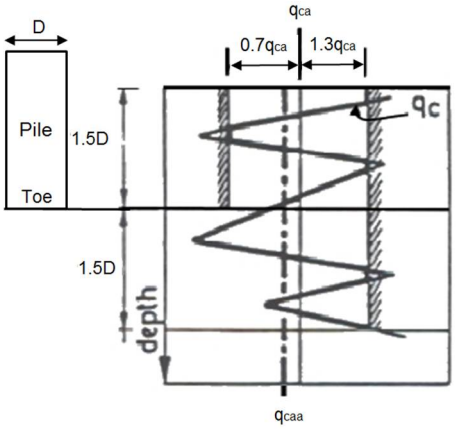

Figure 2-37 Determining the average cone resistance (Bustamante and Gianselli, 1982)

The unit toe resistance, r_t, is estimated from 40 to 55% of the average value of q_c over a zone of 1.5 times pile diameter above and 1.5 times pile diameter below the pile toe.

$$r_t = C_{LCPC} q_{caa} \tag{2.6}$$

Where r_t is unit toe resistance and the upper limit of the unit toe resistance is 15 MPa, C_{LCPC} is correlation coefficient, and q_{caa} is average of the average cone resistance in the influence zone. The correlation factor, C_{LCPC}, ranges from 0.45 to 0.55 for clay and from 0.40 to 0.50 for sand to apply into the driven steel piles and driven precast piles. The values are about 20 % smaller for the bored piles.

The unit shaft resistance, r_s, is computed from Equation (2.7). The K_{LCPC}-coefficient depends on type of soil, type of pile, and the magnitude of the cone resistance. The upper limits of the unit shaft resistance range from 15 through 120 KPa, depending on pile type, pile installation method, and soil type.

$$r_s = K_{LCPC} q_c \leq J \tag{2.7}$$

Where r_s is unit shaft resistance, K_{LCPC} is a dimensionless coefficient (Table 2), J is upper limit value of unit shaft resistance (Table 2), and q_c is cone resistance.

Table 2-2 Coefficients and Limits of Unit Shaft Resistance Quoted from the CFEM (1992) (After Fellenius, 2016)

Soil type	Cone Stress	Concrete Piles & Bored Piles	Steel Piles	Maximum r_s
	(MPa)	K_{LCPC}	K_{LCPC}	J (KPa)
CLAY	$q_c < 1$	0.011	0.033	15
	$1 < q_c < 5$	0.025	0.011	35
	$5 < q_c$	0.017	0.008	35
SAND	$q_c < 5$	0.017	0.008	35
	$5 < q_c < 12$	0.010	0.005	80
	$12 < q_c$	0.007	0.005	120

Mayerhof

The Mayerhof method (Mayerhof, 1951, 1976, 1983) was developed basing on theoretical and experimental studies of the driven piles in sand. The unit toe resistance of driven piles in sand is calculated following equation (2.8). The influence of shadow penetration and scale effect of piles in dense sand is considered by two modification coefficients, $C_1$and C_2, to the q_c average. For bored pile, the unit toe resistance is reduced to 30% of that calculated from (2.8):

$$r_t = q_{ca} C_1 C_2 \tag{2.8}$$

Where r_t is unit toe resistance; q_{ca} is the arithmetic average of q_c in a zone from 4b above through 1b below the pile toe; $C_1 = [(b + 0.5)/2b]^n$ is a modification coefficient of scale effect for b > 0.5 m, otherwise $C_1 = 1$; $C_2 = D_b/10b$, otherwise $C_2 = 1$; n is an exponent (n = 1 for loose sand, n = 2 for medium dense sand, and n = 3 for dense sand); and D_b is the pile embedment in dense sand strata (in m).

The unit shaft resistance for driven piles is computed following Eq. (2.9), with $K_f = 1$, or Eq. (2.10) with $K_c = 0.5\%$. The reduction factors of 70 and 50% are used to calculate the shaft resistance of bored piles.

$$r_s = K_f f_s \qquad K_f = 1 \tag{2.9}$$

$$r_s = K_c q_c \quad K_c = 0.5 \tag{2.10}$$

Where r_s is unit shaft resistance, K_f is modification factor of sleeve resistance, and K_c is modification coefficient of cone resistance.

Tumay and Fakhroo

The method of Tumay and Fakhroo (1981) is developed basing on an experimental study of the piles installed in clay in Louisiana. The unit toe resistance is calculated the same as the method of Schmertmann and Nottingham (Eq.2.1). The unit shaft resistance is computed following Eq. (2.11) and the K factor calculated following (2.12):

$$r_s = K_f f_s \tag{2.11}$$

$$K_f = 0.5 + 9.5e^{-0.09 f_S} \tag{2.12}$$

Where r_s is unit shaft resistance; f_s is the sleeve friction (in kPa). The upper limit of the unit shaft resistance is 60 kPa.

Eslami and Fellenius

The method of Eslami and Fellenius (Eslami, 1996; Eslami and Fellenius, 1995, 1996, 1997) was developed basing on the piezocone. The effective cone resistance (q_E) cone resistance is obtained from difference between the cone resistance (q_t) and the pore pressure (U_2). The unit pile toe resistance is determined as

$$r_t = C_t q_{Eg} \tag{2.13}$$

Where r_t is unit toe resistance, C_t is the toe correlation coefficient, and q_{Eg} is the effective cone resistance.

For pile installed through a weak soil into a dense soil, the unit pile toe resistance is calculated basing on the average effective cone stress over the influence zone of 8b above through 4b below the pile toe. For pile installed from dense soil layer into weak soil layer, the unit pile toe resistance is computed basing on the average effective cone stress over the influence zone of 2b above through 4b below the pile toe.

The pile unit shaft resistance is determined from equation (2.14).

$$r_s = C_s q_E \tag{2.14}$$

Where C_s is a function of soil type and determined from the soil profiling chart, and q_E is the cone point resistance after adjustment to effective stress and correction for pore pressure.

2.2 The Static Compressive Load Test

The economical design of a piled foundation depends on the use of rational procedures to calculate the axial bearing capacity of the pile. The static compressive load tests provide the best means of determining the axial bearing capacity of pile. Depending on availability of time and cost considerations, the static load testing program of pile may be performed either in the design phase or in the construction phase. Details of the static load test are presented below.

2.2.1 Early Development of Static Compressive Load Test

The static compressive load test for pile was developed very early, but more significant development started after the concrete pile became a factor in the foundation industry. For driven concrete piles, it is possible to calculate the bearing capacity of the pile from its resistance to the last hammer blows of driving, basing on empirical formulas. When unusual soil conditions are encountered, the static load tests are performed on one or more piles to make sure that the unusual soil conditions have not influenced the general application of the rule.

Testing loading piles requires simple equipment. A platform is set up for loading test piles with weights (Figure 2-38). The concrete cap cast on top of the pile provides bearing for the 12x12 inch timber beams to take levels is embedded in the cap. Wedges or jacks are placed at the outer ends to prevent the platform from tipping during loading (Figure 2-38b). After the loads have been placed, the platform is balanced and the blocking is lowered slightly so that the entire weight rests on the pile. If sand or other loose loading material is used, the platform must be provided with sides (Figure 2-38a). The head of the 3/4 inch bolt should be accessible for taking level readings. A static load test was performed on the pedestal pile in 1910, as indicated in Figure 2-39. The

pedestal test pile was about 10 feet long, and the pedestal foot was about 3 feet high and 3 feet wide. The maximum test load was about 45 tons, without any recorded settlement.

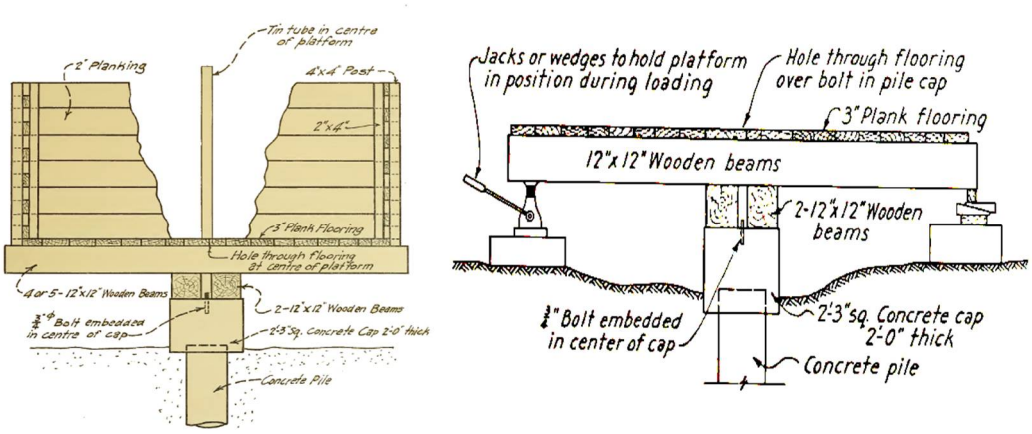

a) b)

Figure 2-38 Method of testing load for concrete pile: a) Platform with sides and b) Platform with jack at the outer ends (Henley Abbot, 1915; Portland Cement Association, 1951)

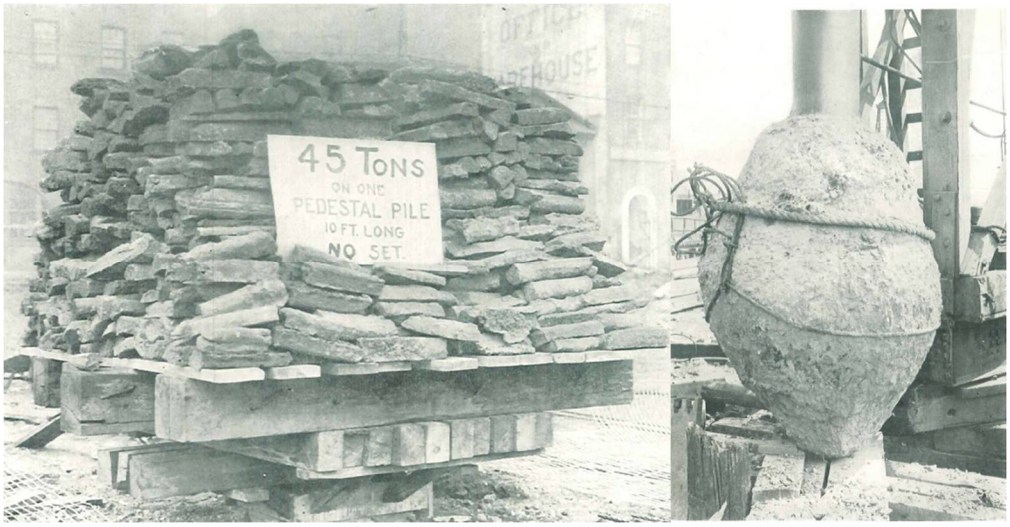

Figure 2-39 Load test on pedestal pile (Mac Arthur, 1910)

Figure 2-40 shows a 60-ton load test on composite pile performed at Warners, N. J. in 1916. The ground was very soft “marsh” mud to a depth of 33 feet, below which hardpan was found. The composite pile consisted of 20 feet long wood and 15 feet long concrete, making a total pile length of 35 feet. The maximum test load and settlement were about 120,000 pounds and 0.015 feet, respectively.

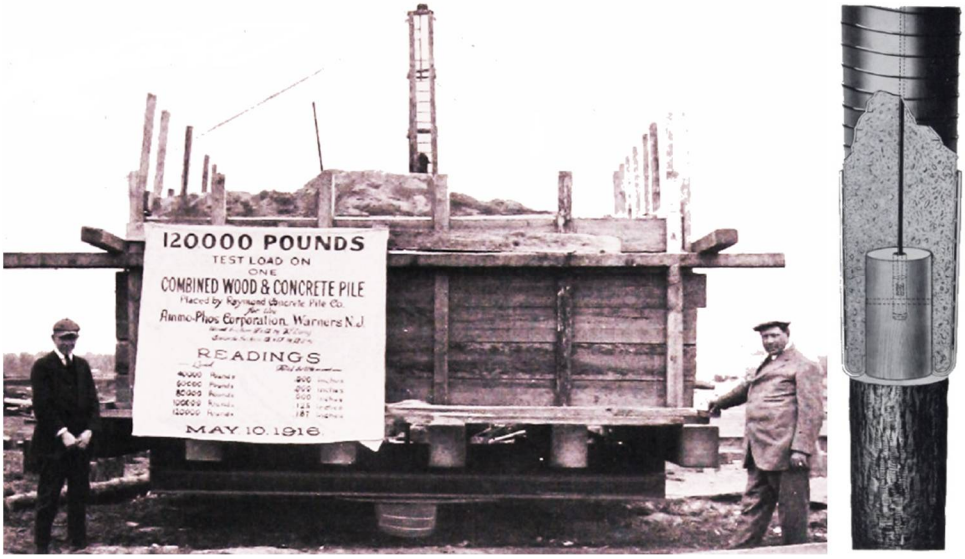

Figure 2-40 Load test on composite pile at Warners, N. J. in 1916 (Raymond concrete pile company, 1926)

2.2.2 Modern Static Compressive Load Test

The Reaction Load Arrangement

The reaction load arrangement for the modern static pile load test depends on the required test load and the conditions at the site. In general, there are four ways to arrange the reaction load for the static load test, as shown in Figure 2-41.

Figures 2-41a and 2-41b show the static pile load test with the kentledge system and with the kentledge system combined with the anchored screw piles, respectively. Cast concrete blocks are often used as reaction load, and the anchored screw piles (Figure 2-38b) may be used to increase the test load or reduce the height of the concrete blocks.

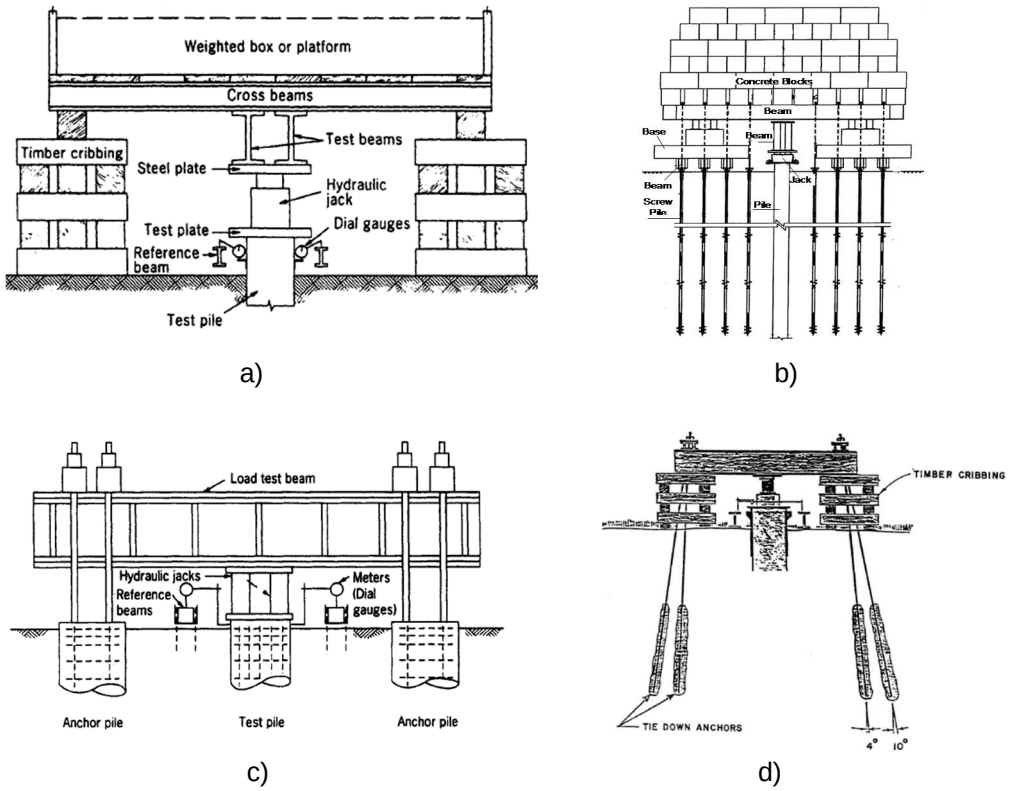

Figure 2-41 Types of the reaction load arrangements for the modern static pile load tests: a) Kentledge system, b) Kentledge combined with anchored piles, c) System of anchored piles and d) System of tie-down anchors (Prakash and Sharma, 1990)

The important criterion is that the reaction load remains stable during the static load test. The kentledge is often placed on a deck of steel beams. The area of the

cribbage platform should be adequate to avoid the bearing failure of soil below platform. The cribbage should be spaced at least 3 or 4 diameters from the test pile to reduce the influence of the interaction between the pile and the surrounding soil during loading.

Anchored piles and tie-down anchors may be utilized to provide a satisfactory reaction, as shown in Figure 2-41c and 2-41d, respectively. It is most convenient if the adjacent permanent piles are used. If only two adjacent piles are suitable, they would often have to be lengthened to provide adequate pull-out resistance, sometimes leading to severe problems of lateral instability under load. It is important that the spacing of the piles is as large as practical, as significant interaction between them can occur at spacing of less than 5 pile diameters. In practice, spacing of 3 to 4 diameters between the centers of the test pile and the reaction piles is commonly adopted. The pile interaction reduces the observed settlement of the pile, and it may be necessary to make corrections for this where close spacing is unavoidable. It is suggested that the pile layout be arranged to limit the effect of pile interaction to an absolute maximum of 20% of the settlement of the test pile.

The reaction steel beam is often subjected to buckling stresses and high bending. Therefore, it should be designed safely for the maximum load. The whole system should be firmly wedged or bolted together to prevent any member from slipping. The reaction load is usually provided 20% above the maximum test load of the pile.

Instrumentation and Measurements

A key element in the design of a load test program is that of instrumentation. Failure of the pile instrumentation to function properly results in unusable data or, even worse, the interpretation of “bad” information that could potentially lead to an unsafe design.

Figure 2-42 indicates the typical arrangement for applying load and measuring movements in an axial compressive test. The application of the load to the test pile is performed by the hydraulic jacks placed directly on the pile head or steel plates. The applied loads are measured by the load cells placed directly on the jack heads or via the steel plates and Bourdon gages. During loading and unloading, the movements at the pile head are measured by dial gages, linear displacement transducers, wire gages, and an optical levelling system. It is noted that an optical levelling system is often set up outside the pile load test area to directly measure the movement of the pile head, movement of reference beam, and movement of the reaction system (cross beams, main beams, and timber cribbing).

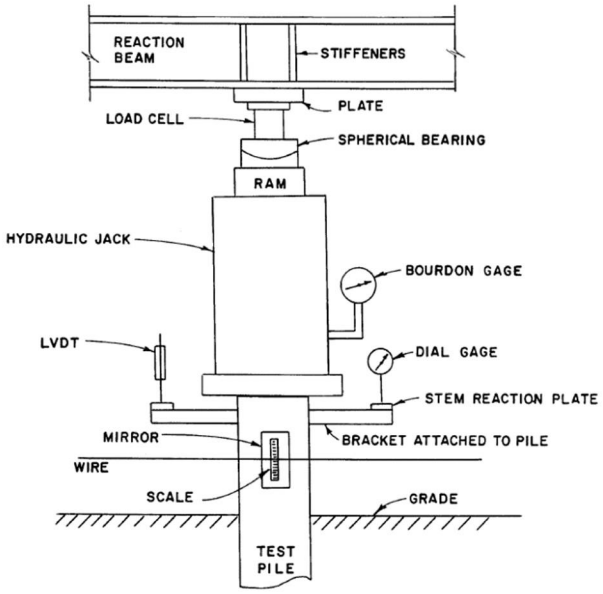

Figure 2-42 Instruments for measuring the applied load and movements (Zenon et al., 1992)

Figure 2-43 depicts the instruments used to measure strain along the pile shaft and the load distribution diagram obtained from the strain measuring instruments. The

instruments usually used for measuring strain along the pile shaft are strain gages, telltales, and load cells. The strain measured during the load test can be converted into the load by the equation: P = E.A.ε. Where P is the load, E is the elastic modulus of the pile material, A is the cross-section area of pile, and ε is the measured strain.

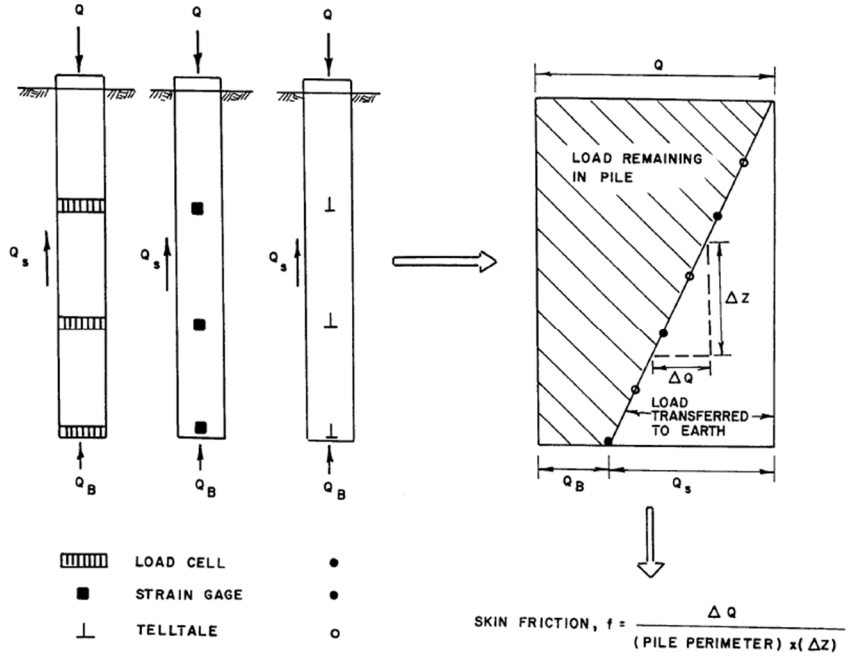

Figure 2-43 Instruments to determine load transfer and skin friction (Zenon et al., 1992)

Figure 2-44 and 2-45 show modern notebook computers loaded with suitable data acquisition software to record all data during the pile load test. Indeed, it is practical to automate the whole test procedure, recognizing perhaps the need for human intervention in specific circumstances. The degree of sophistication of the data-logging equipment depends to some extent on the volume of data to be recorded and on the number of piles to be tested. The quality of the output can be significantly better than that achieved with conventional test methods.

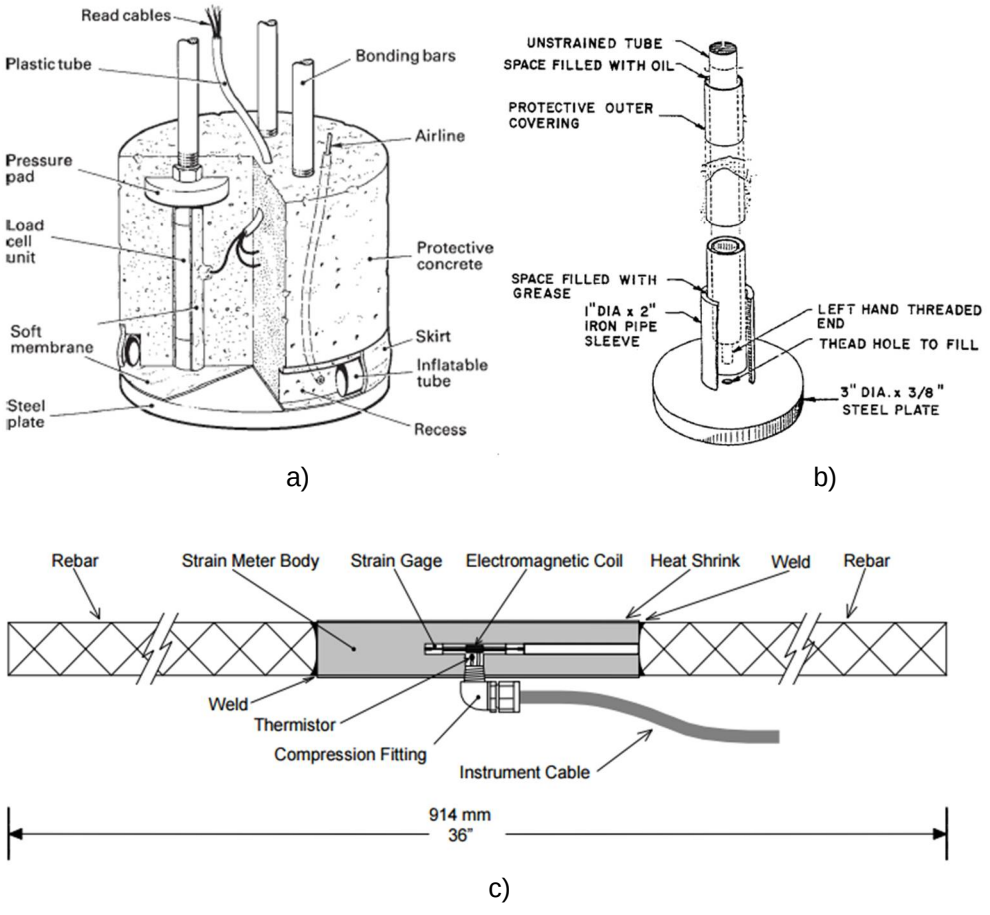

Figure 2-44 Instruments to measure strain along the pile shaft: a) Modular pile load cell (Fleming et al., 2009), b) Mechanical telltale (Zenon et al., 1992), and c) Vibrating wire strain gage (Model 4911A, Geokon)

Loading Procedures

Many loading procedures for the static pile load test were presented in several publications (ASTM D1143-81; Whitaker, 1976Butler and Hoy, 1977; Fellenius, 1975, 1980; Mohan et al., 1967; New York State DDT, 1974; Prakash, 1990). The following load test methods are considered as the basic load test methods.

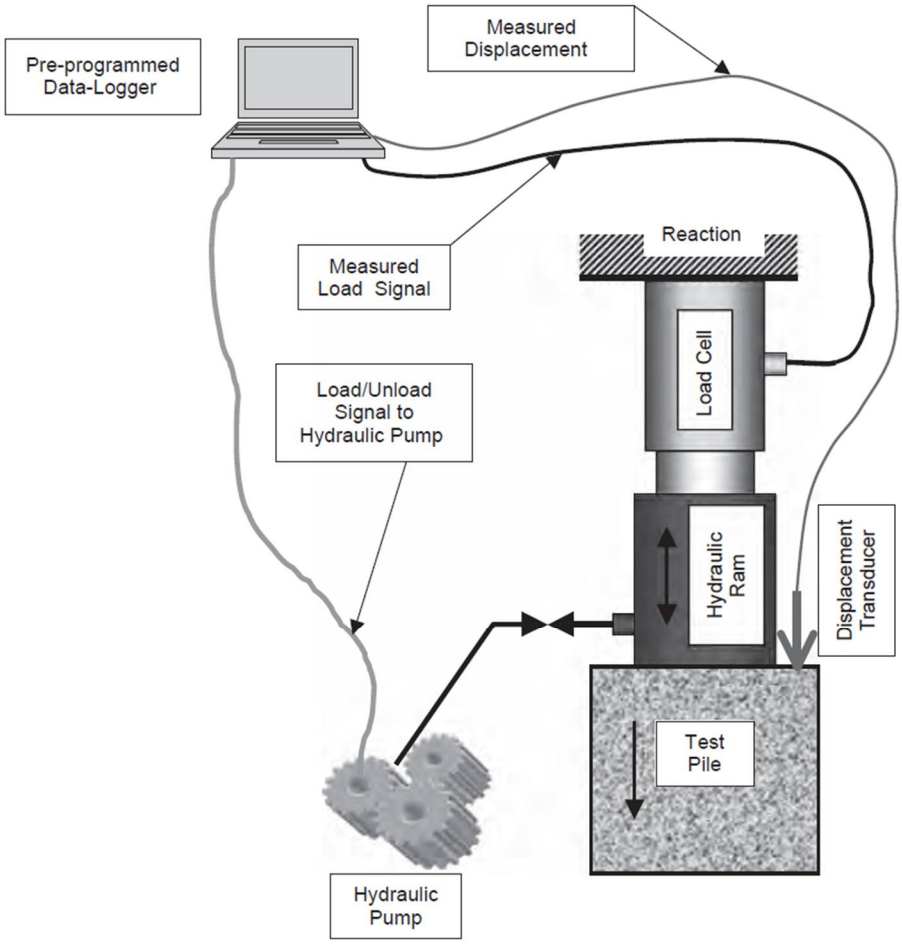

Figure 2-45 Schematic diagram of basic method of computer control of a maintained load pile test (Fleming et al., 2009)

Slow Maintained Load Test Method: The ASTM Designation D1143-81 (89) recommends a slow test, where the pile is loaded in eight equal increments to the 200% design load of the pile. Each successive load increment is held until the settlement rate has reduced to 0.25mm/h, but not longer than 2 hours. The load is held for 24 hours at the load increment of 200% design load, then the unloading is performed in four equal

increments, with 1 hour between them. This test method is commonly regarded as the ASTM Standard Test Method. The disadvantage of this test method is time-consuming.

Quick Maintained Load Test Method: This test method is recommended by the Federal Highway Administration, the New York State Department of Transportation, and ASTM 1143-81 (89). It may eliminate the influence of time-dependent settlements of the pile. The test pile is loaded in 20 increments to 300% of the design load. Each successive load increment is held for 5 minutes and the readings are taken every 2.5 min. Then, the unloading is performed in four equal increments, with 5 minutes between them. This test method is economical and fast, and can usually be completed in three to five hours.

Constant Rate of Penetration Test Method: This method is proposed by New York State Department of Transportation, the Swedish Pile Commission, and ASTM D1143-81 (89). The pile head is forced to settle at 1.25mm/min, and the force required to obtain the penetration rate is recorded. The test is performed to a total penetration of 50 to 75 mm. The main advantages of this test method are fast (2 to 3 hours) and economical.

Swedish Cyclic Test Method: This method is recommended by the Swedish Pile Commission. The pile is loaded to one-third of the design load, and the unloading is performed to one-sixth of the design load. The reloading and unloading are repeated, then the load increment is performed up to 50% higher than the previous load increment and repeated until failure. The disadvantage of this test method is time-consuming.

2.2.3 Interpretation of the test results

The pile load test results are plotted as load versus settlement, and the failure load is determined based on several interpretation techniques if the plunging failure does not take place during pile load testing. (Plunging failure is the excessive movement under

small or no load increase.) In such cases, the failure load is defined as “the load that produces an increase in settlement disproportional to the increase in pile load,” which was used prevalently before 1942.

Terzaghi (1942) presented the results of two different load tests, (a) and (b), on 35-foot long wood piles to discuss the above definition of “the failure load,” as shown in Figures 2-46 and 2-47. In Figure 2-47, each of the two load-settlement diagrams shown in Figure 2-46 was plotted to a different settlement scale.

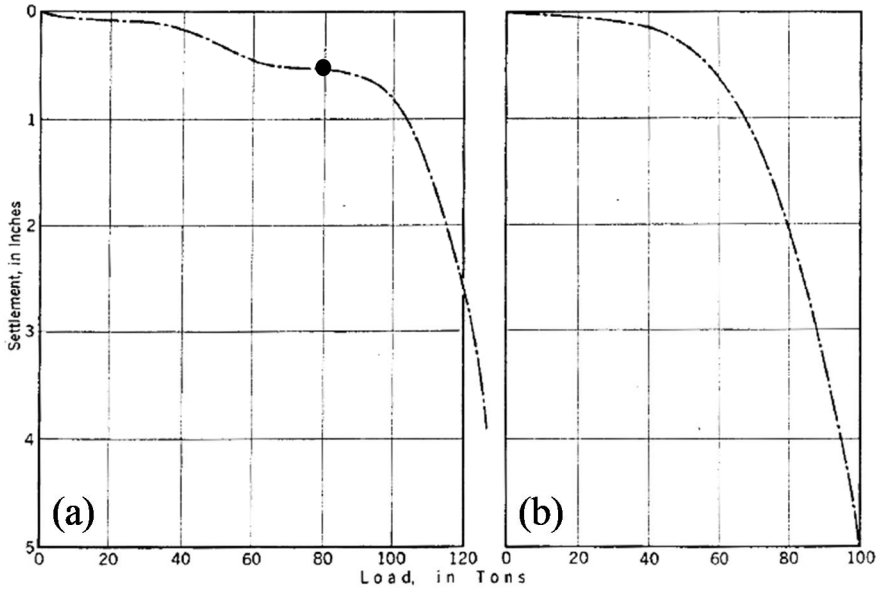

Figure 2-46 Load settlement curves for the 35-foot long wood piles (Terzaghi, 1942)

When applying the foregoing definition of “the failure load” without taking the first steep descent of the curves into consideration, the failure loads obtained the values of 80 and 95 tons for the pile (a), from Figure 2-46(a) and 2-47(a), respectively. They were at least of the same order of magnitude, but Terzaghi wondered what the failure load of the pile (b) in Figures 2-46(b) and 2-46(b) would be, following the foregoing definition. He would not even dare to make a guess. Then, he stated that “*The Manual should specify*

somewhere that the failure load is not reached unless the penetration of the pile is at least equal to 10% of the diameter of the tip of the pile. At smaller penetrations, not more than a fraction of the ultimate point resistance of the pile has been mobilized."

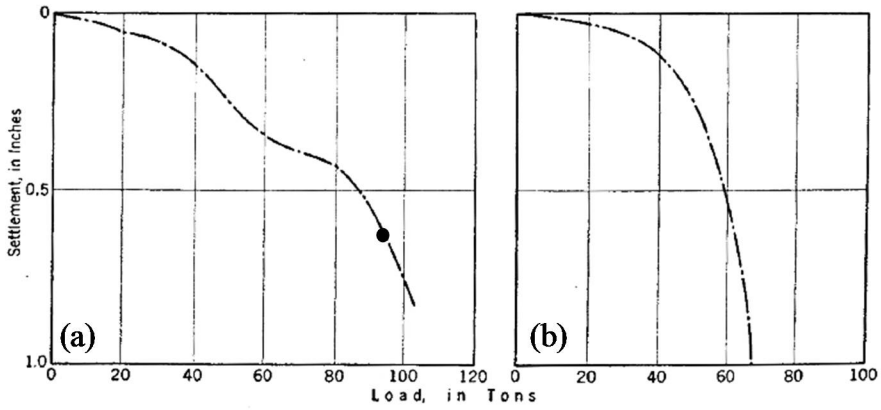

Figure 2-47 Load settlement curves with different vertical scale (Terzaghi, 1942)

It should be noted that his statement did not claim that the bearing capacity of pile was a function of pile diameter, but that the bearing capacity of a tested pile requires the pile toe to penetrate the soil with a reasonable length. This reflects that "*the definition of the failure load is the load that the movement measured at the pile head is 10% of the diameter of the pile*" is a misinterpretation of Terzaghi's statement.

Another definition of the pile capacity, mentioned in the "Concrete Pile Manual" of the Portland Cement Association (1951), is that "*the load-movement curve of pile may resemble a stress-strain curve having a yield point. If so, the load at the yield point may be considered as the load capacity of the pile. If there is no break in the curve, an arbitrary limiting value of the settlement, such as 0.25 inch, may be selected.*"

Such definitions have not considered the elastic shortening of the pile. To be useful, the bearing capacity definition of pile from the plunging non-failure test results should be based on the mathematical rules and create a repeatable value, which is

independent of scale relations and the visual ability of the individual interpreter. Fellenius (1975; 1980; 2016) reported the different definitions of pile capacity based on the load-displacement curves of the non-failure static loading tests. These interpretation techniques are reviewed in the following.

Vander Veen Method

Based on the load-settlement curves of the toe of a concrete pile in the harbor area of Amsterdam (Figure 2-48a), which did not show a sharp break (no tendency toward an ultimate value), Vander Veen (1953) used a well-known function in the branch of biology which represents a growth of a living individual as a function of time (Eq.2.15) to propose a method for determining the pile capacity (Figure 2-48b).

$$P = P_{\max}\left(1 - e^{\alpha z}\right) \tag{2.15}$$

Where P is the load on the pile toe; Z is the settlement of the pile toe caused by the load P; P_{max} is the ultimate resistance of the pile; and α is a coefficient, which influences the shape of the load-settlement curve.

If this formula is valid, the load-settlement curve has to become a straight line – if the settlement z is plotted against $\ln\left(1 - \frac{P}{P_{\max}}\right)$. In this way, a method seems to be found to determine the ultimate bearing resistance of a pile (Figure 2-46b). For various supposed values of P_{max}, the ultimate resistance $\ln\left(1 - \frac{P}{P_{\max}}\right)$ is plotted against the settlement z. Only for P_{max} approximately equal to 140 tons, the curve appears to consist of the straight line, that is, to comply with the formula (16).

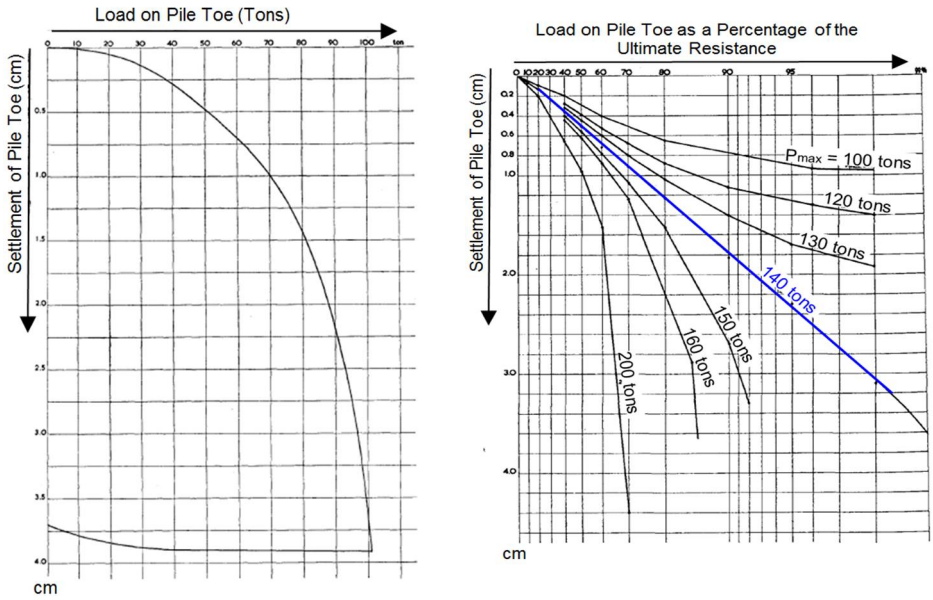

a) b)

Figure 2-48 Pile capacity determined based on the load-settlement curve with the various supposed ultimate resistances: a) The test result of the concrete pile No.2 and b) The proposed method of Vander Veen, Vander Veen (1953)

Brinch Hansen Criteria Method

Hansen (1963) developed two methods (90% and 80% criteria) to determine the failure load from the load-movement curves of the static pile load tests (Fellenius, 1975; 1989; 2016). The first defines the failure load as the load that is associated with twice the movement measured at the pile head, as obtained for 90% of the load (the $0.90Q_u/0.5\delta_u$ point lies on the curve). The 80% criterion defines the failure load as the load that is associated with four times displacement measured at the pile head, as gained for 80% of the load (the $0.80Q_u/0.25\delta_u$ point lies on the curve). The criterion provides the following simple relationship when used for estimating the pile capacity.

$$Q = \frac{\sqrt{\delta}}{C_1\delta + C_2} \tag{2.16}$$

$$Q_u = \frac{1}{2\sqrt{C_1 C_2}} \tag{2.17}$$

$$\delta_u = \frac{C_2}{C_1} \tag{2.18}$$

Where Q is any applied load, δ is the movement associated with Load Q, Q_u is ultimate load, δ_u is movement measured at the ultimate load, C1 is slope of the straight line in the $\sqrt{\delta}/Q$ against movement diagram, and C2 is y-intercept of the straight line in the $\sqrt{\delta}/Q$ against movement diagram.

These methods apply to the piles tested in a strain-softening soil and determine the peak resistance. The 90% criterion is applicable to the constant rate of penetration tests regardless of the soil type. The 80% criterion assumes that the load-displacement curve is nearly parabolic. This method is appropriate for both the fast and slow maintained load tests. The failure criteria show a good agreement with the plunging failure load; nevertheless, the calculations and plot cannot be performed before the test loading. This method of interpretation is not applicable to the cyclical and plunging non-failure load tests.

DeBeer Intersection Load

DeBeer (1968) used logarithmic linearity to plot the load-displacement data in a double-logarithmic diagram (Figure 2-49). The ultimate load was obtained from the intersection of the two lines, where a change would occur in the response of the piles to the applied load. The load at the intersection was called the "yield load." Figure 2-49

points out that the intersection occurred at a load of 360 kip for the example test (Fellenius, 2016).

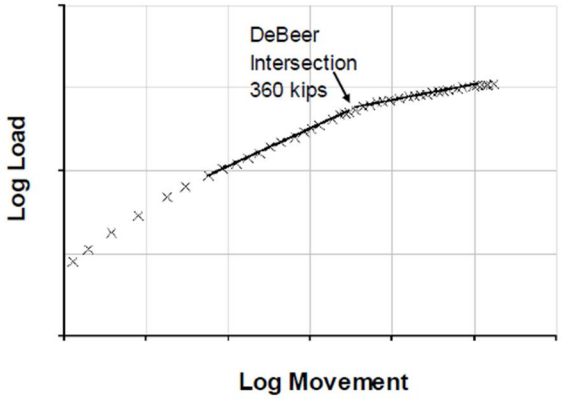

Figure 2-49 DeBeer's double-logarithmic plot of load-movement data (Fellenius, 2016)

Chin-Kondner Extrapolation Method

Konder (1963) presented the framework of a hyperbolic stress-strain relationship for a remolded cohesive soil tested in consolidated-undrained triaxial compression (Figure 2-50). Figure 2-50a is a rectangular hyperbola passing through the origin of coordinates in two-dimensionl stress-strain space, with the lines as asymptotes.

$$\left.\begin{array}{l} \varepsilon + \alpha = 0 \\ \\ \sigma - \beta = 0 \end{array}\right\} \qquad (2.19)$$

In which σ is deviator stress $\sigma_1 - \sigma_3$ and ε is the axial strain. The equation of the hyperbola can be written as

$$\varepsilon\sigma - \beta\varepsilon + \alpha\sigma = 0 \qquad (2.20)$$

Diving Eq. 20 by σ and rearranging terms yields

$$\frac{\varepsilon}{\sigma} = a + b\varepsilon \qquad \text{Or} \qquad \sigma = \frac{\varepsilon}{a + b\varepsilon} \tag{2.21}$$

In which $a = \frac{\alpha}{\beta}$ and $b = \frac{1}{\beta}$

The ultimate value of the stress can be obtained by taking the limit of Eq. 21 as ε becomes very large, or

$$\sigma_{ultmate} = \lim_{\varepsilon \to \infty} = \frac{1}{b} \tag{2.22}$$

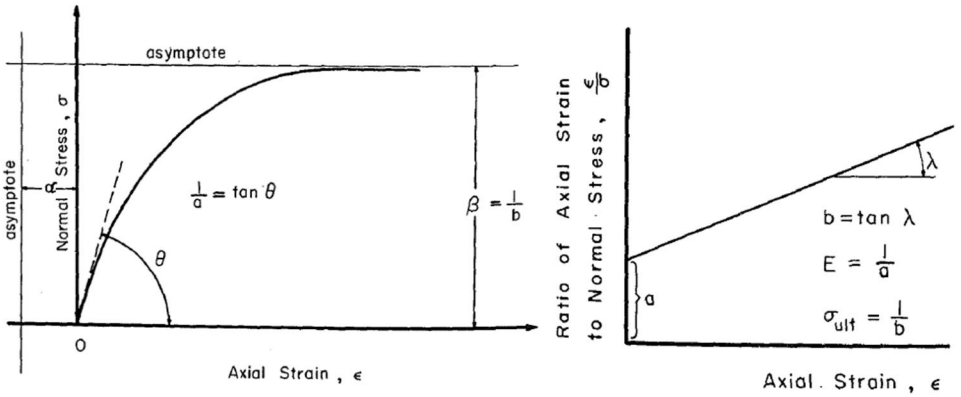

a) b)

Figure 2-50 Hyperbolic representations of stress-strain: a) Rectangular hyperbolic representation, and b) Transformed hyperbolic representation (Konder, 1963)

Therefore, the ultimate strength is measured by the inverse of the slope of the straight line, as shown in Figure 2-48b.

Chin (1970) proposed applying Konder's (1963) work to piles. This method assumes that the load-movement relationship is hyperbolic, a plot of movement/load

(δ/Q) versus movement (δ) is linear, and the inverse slope of this linear relationship is then the ultimate value of load (Figure 2-49). Similar to Brinch Hansen's method, this method can be used, through mathematical relationships, to extrapolate the load-movement values beyond the maximum applied load.

$$Q_u = \frac{1}{C_1} \tag{2.23}$$

Where Q_u is capacity or ultimate load (i.e., load at infinite movement; $\delta \rightarrow \infty$), and C_1 is slope of the straight line in the δ/Q versus movement diagram.

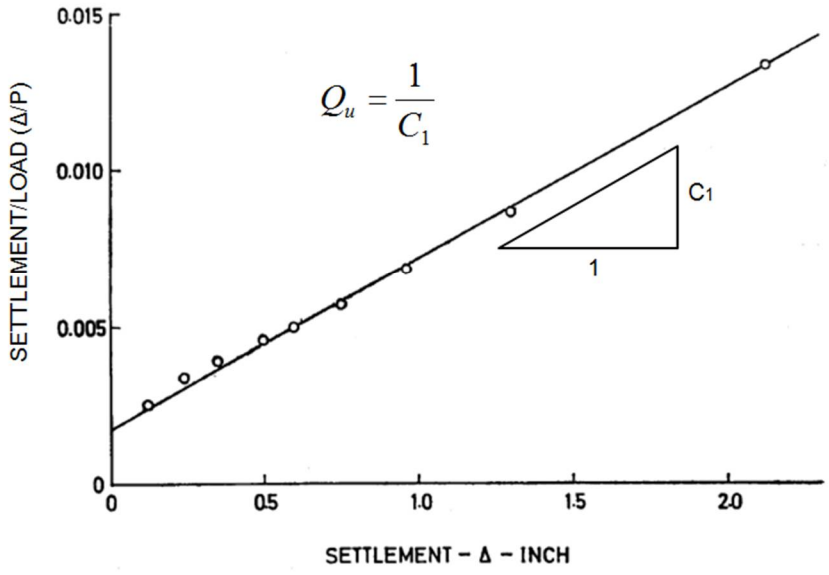

Figure 2-51 Chin extrapolation method (Chin, 1970)

The Chin-Kondner method has an ultimate load, which is reached asymptotically with infinitely large movement. However, in practice, no capacity is used for a larger movement than the maximum measured movement of the tested pile; therefore the Chin-Kondner method applied is limited.

Fuller and Hoy Method

Fuller and Hoy (1970) proposed a simple method to determine the failure load for non-failure load tests by employing a maximum slope of the load-settlement curve. As shown in Figure 2-52, the failure was defined as the load that results in a slope greater than 0.05 in. per ton on the gross load-settlement curve, or a slope greater than 0.03 in. per ton on the plastic load-settlement curve, whichever is smaller. This is a general approach and an arbitrary definition of failure. The total criterion would include a maximum allowable gross settlement under the design load, with consideration given to elastic shortening of the pile and to safety. This method is applicable for the Quick Maintained Load test. The main disadvantage of this method is not applicable to the long piles because of the large elastic shortening of the pile, which makes the 0.05 inch/ton slope occur sooner.

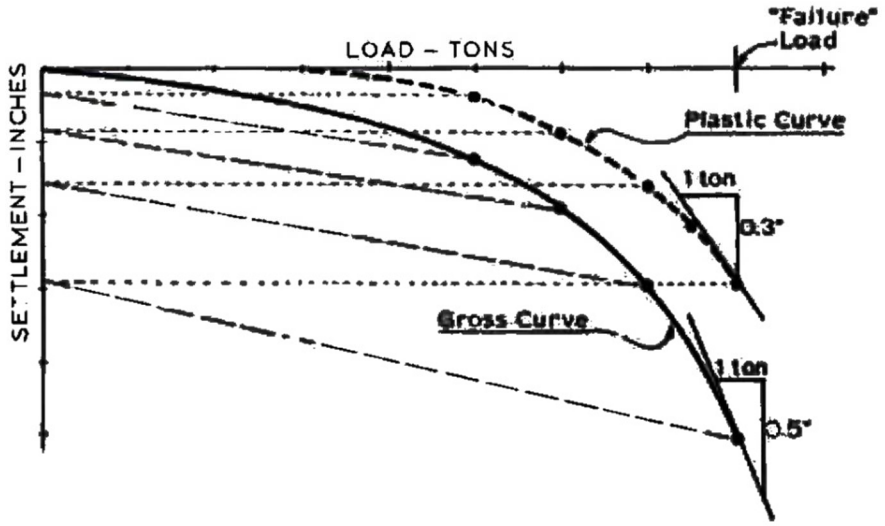

Figure 2-52 Slope criteria for determining "failure" load from load-settlement curves (Fuller and Hoy, 1970)

Davisson Method

The Offset Limit Method was suggested by Davisson (1972). The ultimate load was determined from the movement that exceeds the elastic shortening of the pile by a value of 0.15 inch plus the pile diameter divided by 120. Figure 2-53 presents an example of a load-displacement diagram obtained from the static loading test on the precast concrete pile with a 12-inch diameter. For an offset value of 0.25 inch (0.15 inch + 12 inches/120 = 0.25 inch), the Davisson limit load added to the curve was about 181 tons. This method is suitable for the driven piles in small diameter tested following quick methods, and it has been used widely the increasing popularity of dynamic load testing and wave equation analysis of driven piles (Fellenius, 2016).

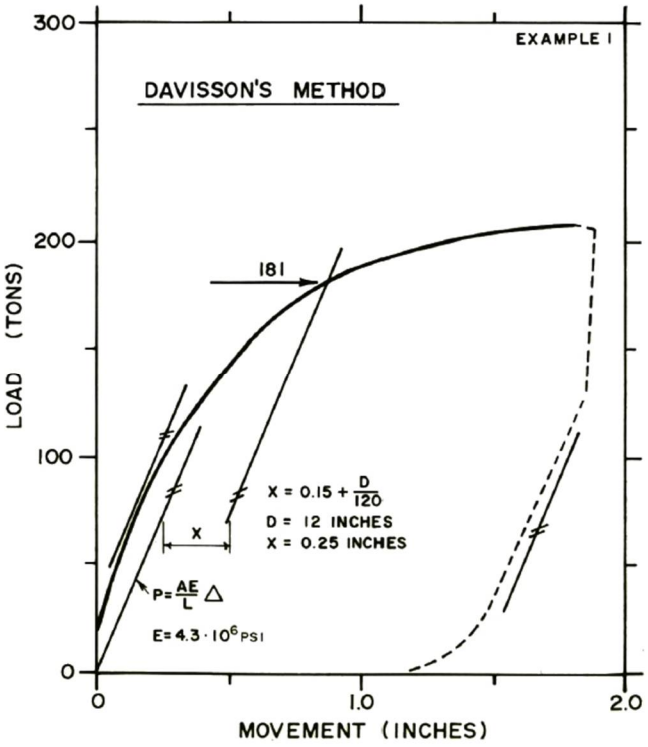

Figure 2-53 Construction of Davisson's limit (Fellenius, 1980)

Mazurkiewicz Method

Mazurkiewicz (1972) proposed a method that allows the failure load to be extrapolated, even if the maximum test load is smaller than the failure load. Figure 2-54 shows how the equal pile-head movement lines are arbitrarily chosen, and the corresponding load lines are built from the intersections of the load-movement curve and the movement lines. For the intersection of each load line with the load axis, a 45^0 line is drawn to intersect with the next load line. These intersections lie approximately on a straight line; the failure load is determined from the intersection with the load axis.

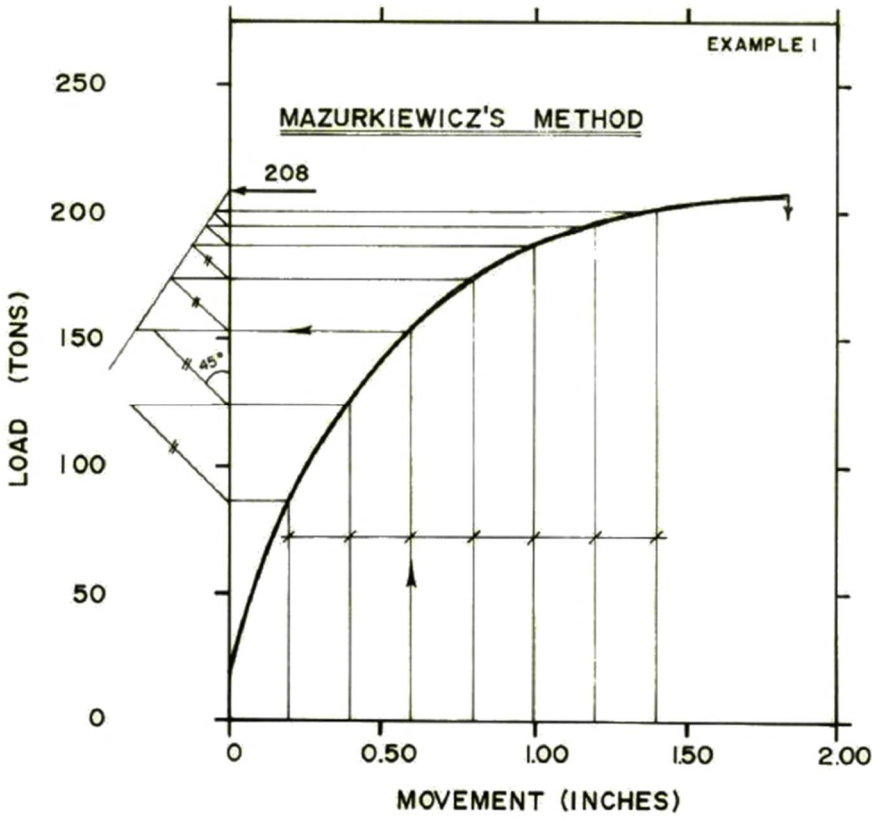

Figure 2-54 Mazurkiewicz parabola method to determine the ultimate failure load (Fellenius, 1980)

Butler and Hoy Method

Butler and Hoy (1977) proposed a "double tangent" method to interpret the load-settlement data obtained from the Quick-Load Test, which could provide reproducible and independent values of the judgment of the interpreter (Figure 2-55).

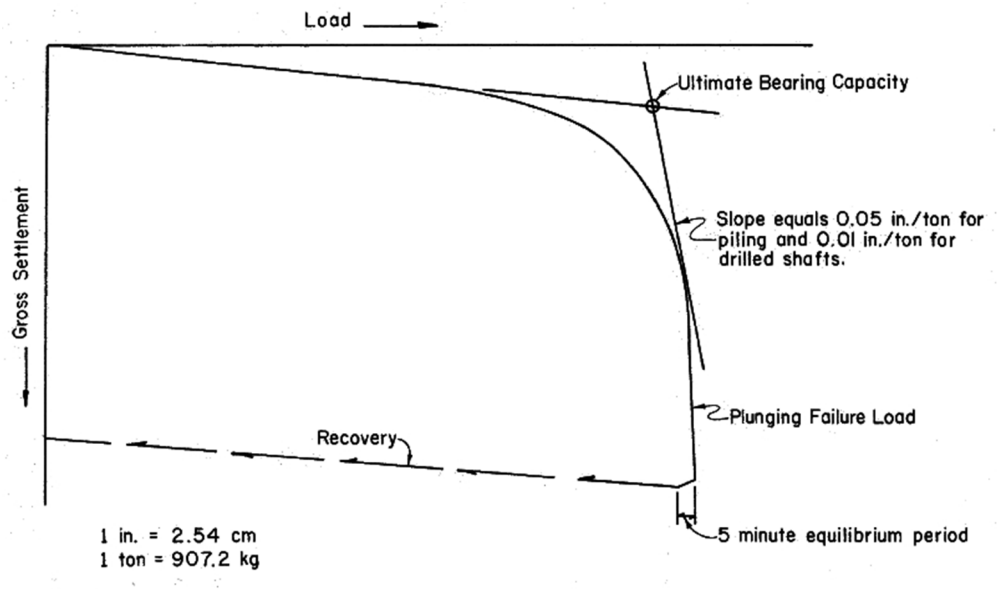

Figure 2-55 Slope criteria for determining the failure load (Butler and Hoy, 1977)

The failure load is defined as the load at the intersection of the two tangent lines. The first line is drawn from the point of zero load tangent to the initial flat portion of the gross settlement curve. The slope of this line will be approximately the same as the slope of the recovery line. The second line was drawn tangent to the steep portion of the gross settlement curve, with a slope 0.05 inch/ton of load for a driven pile load test and a slope of 0.01 inch/ ton of load for a drilled shaft load test.

Decourt Extrapolation Method

Décourt (1999, 2008) suggested a method to extrapolate load test results (Figure 2-56). From the load test results, the stiffness (the load or stress divided by the corresponding movement) is computed and plotted versus the applied load. The failure load, (Qs)u, is defined as the load corresponding to zero stiffness. For the example in Figure 2-56, the failure load, (Qs)u, was estimated about 164.81 MN at stiffness of zero. However, zero stiffness corresponds to infinite deformation and cannot be used in practice.

The Decourt and Chin-Kondner methods are similar in that they both assume the load-movement to be hyperbolic. Therefore, the limitations of the Decourt method are similar to those of the Chin-Kondner method.

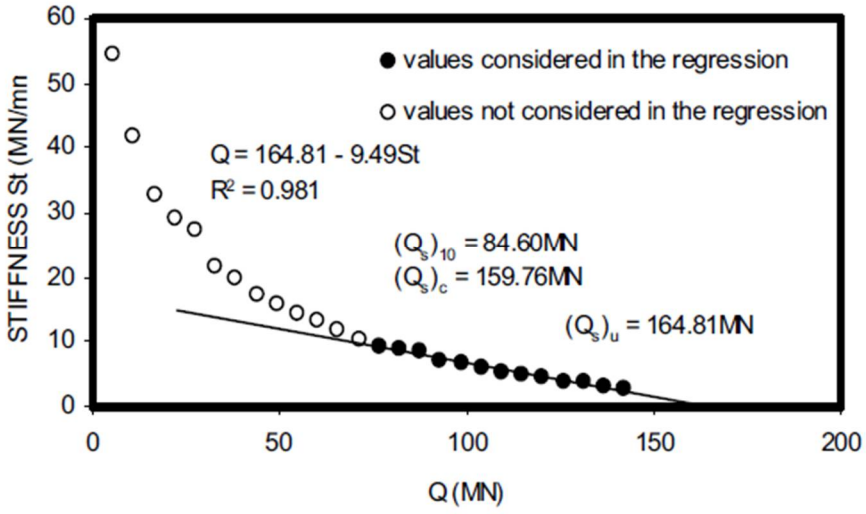

Figure 2-56 Stiffness method to determine the failure load (Decourt, 2008)

2.3 Bidirectional Load Test

Conventional load tests require a reaction load system, (kentledge, anchored piles, or both), that is greater, at a minimum, than 10% of the required test load. Since the load capacity of the piles ranges from hundreds to thousands of tons, it is expensive and time consuming to build a reaction load system and later remove the reaction load. Also, if the required test load is too great or the test piles are performed under water or in narrow urban areas, the conventional load test is difficult to perform. To eliminate the above mentioned difficulties, the bidirectional load test method has been selected as an optimum solution. It is simple to install the jacks at or above the pile toe, which balances the resistance above and below the jacks. Figure 2-57 shows the position of the jacks, as well as a comparison between the conventional load test and the bidirectional load test.

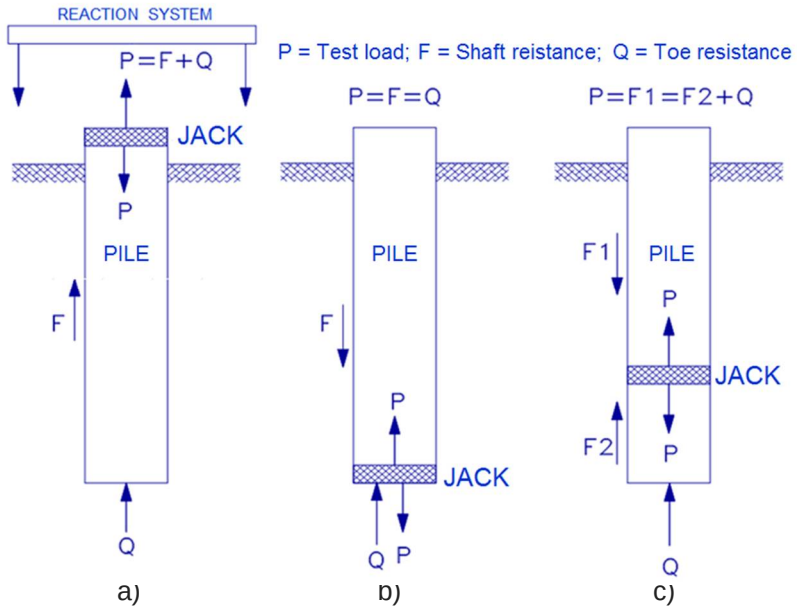

Figure 2-57 Comparison between conventional load test and bidirectional load test: a) Conventional load test, b) Bidirectional load test with jack placed at pile toe, and c) Bidirectional load test with jack placed above pile toe

2.3.1 History of Bidirectional Load Test

In 1973, an in situ load testing method for the bond between concrete and bedrock was proposed to eliminate the need for a reaction system and to save such system costs as shown in Figure 2-58 (Gibson et al., 1973). The test could be carried out in the bore holes, as part of the site investigation. A hydraulic jack was installed at the bottom of the bore hole and the concrete plug was placed above it. Then, the load test was performed by pressurizing inside jack until the plunging failure occurred. The load test method gave the bond stress values for designing the rock sockets.

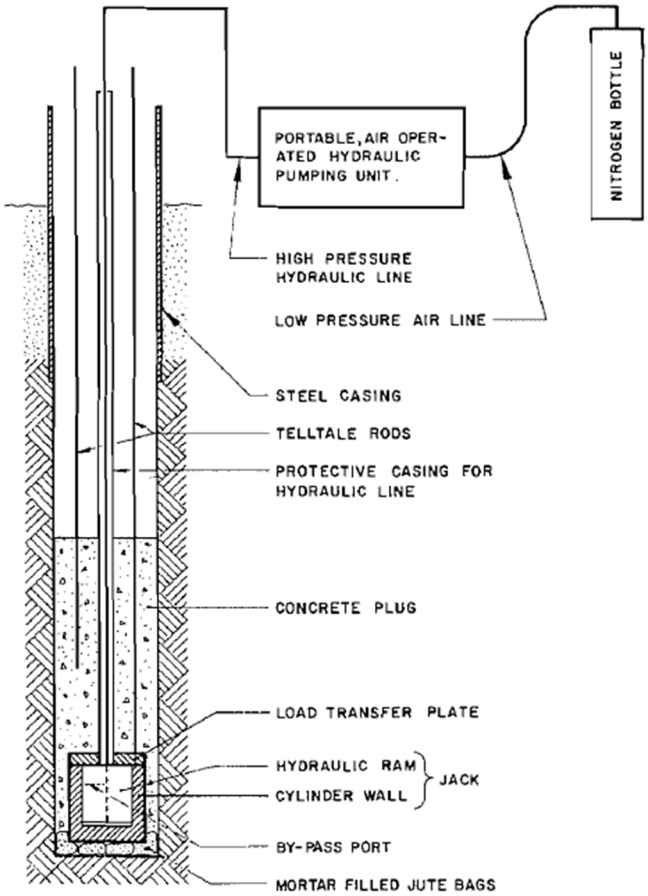

Figure 2-58 Schematic of bond test installation (Gibson et al., 1973)

In 1981, a load test system for piles in rock, using an internal hydraulic jack, was offered by Amir (1981; 1983). This jack is steel and is embedded in the pile at a designed depth. A steel plate is placed at the bottom, with tell-tales going through the jack up to the pile head. After the concrete develops enough strength, the jack becomes pressurized, and then upward and downward movements are measured (Figure 2-59).

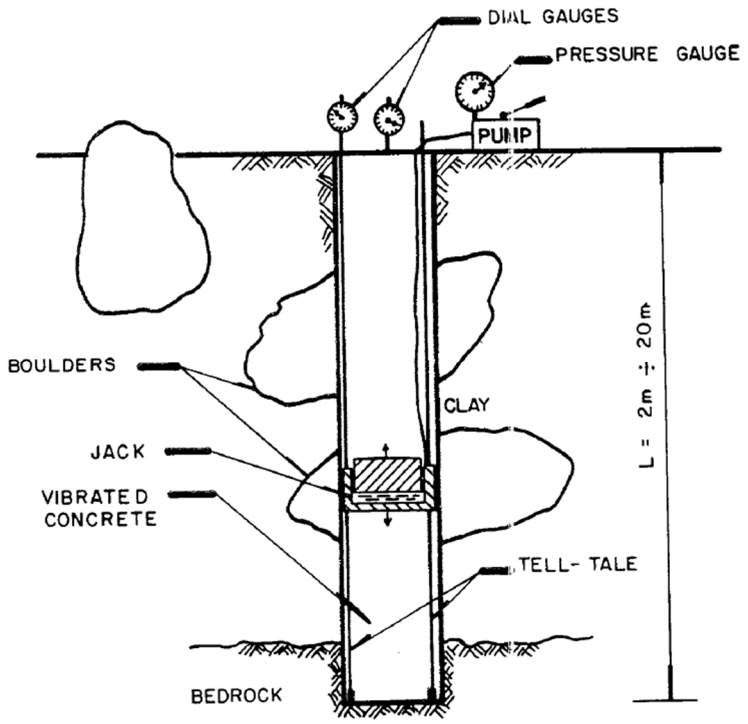

Figure 2-59 Load testing system for pile in rock (Amir, 1981)

In 1983, the method of preloading the socket base to improve the performance of drilled piers in weak rock was introduced by Horvath et al. (1983). Load tests were performed on the full-scale concrete piers socketed into weak shale to investigate the load distribution between end bearing and shaft resistance. Figure 2-60 shows the instruments installed for a load test of pier in weak rock. The results of load test showed

that preloading the socket base leaded to stiffer load-displacement behavior of the pier-socket system.

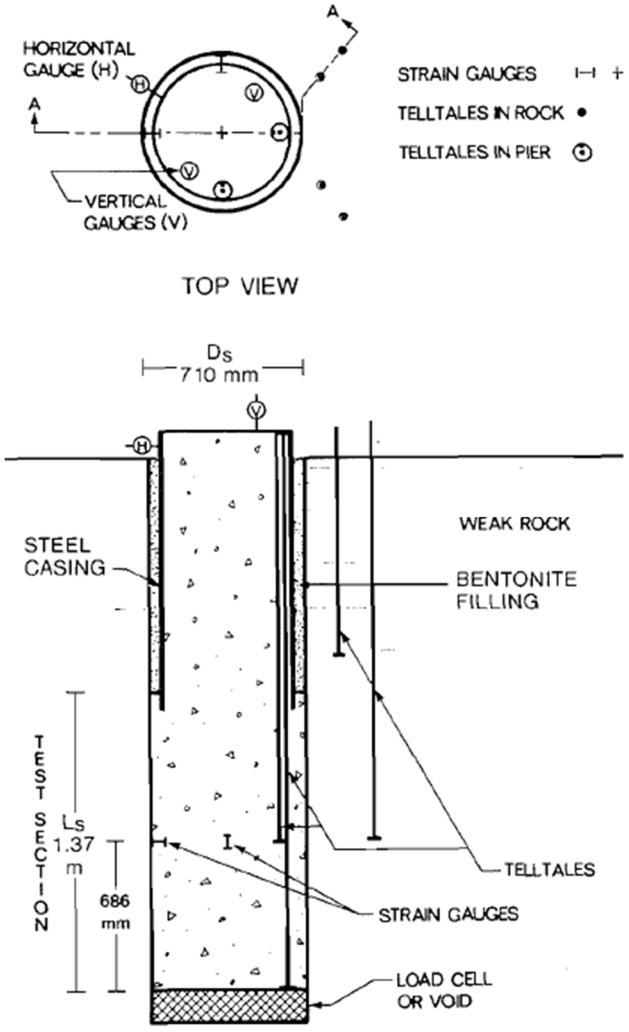

Figure 2-60 Installed instruments for a bidirectional load test (Horvath et al., 1983)

At the same time (1983), the bidirectional pile load method was developed in Brazil (Elisio; 1983, 1986). Figure 2-61 presents the bidirectional test results performed by Elisio (1983). The test pile, with a 0.52 m diameter and 13 m length, was drilled

through 7 m sandy silty clay and 6 m sandy clay silt. The bidirectional cell was placed 2.0 m above the pile toe (Fellenius, 2015).

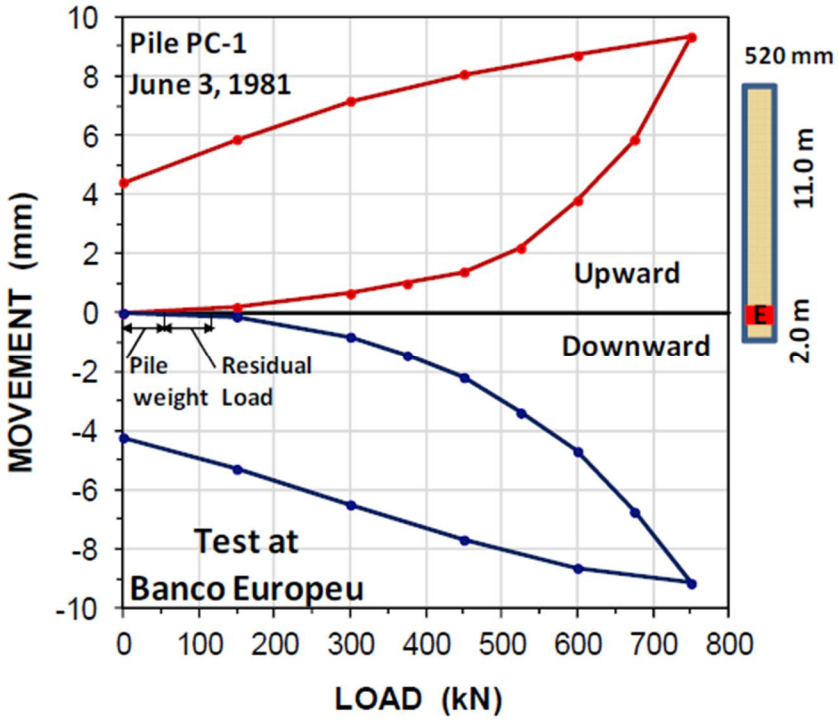

Figure 2-61 Bidirectional cell test results of Elisio (Fellenius, 2015)

In 1986, Dr. Jorj Osterberg applied for a patent for a bidirectional load test device entitled “Device for Testing the Load-Bearing Capacity of Concrete-Celled Earth Shafts” (U.S. Pat. No.4, 614,110). The patented device measures the shaft resistance and the end bearing resistance of soil separately (Figure 2-62). An expansion is placed at the hole bottom and a shaft resting above it. The loading is performed by pressurizing fluid via a coaxial pipe and rod. The upward movement of the shaft and downward movement of the earth below the bottom of the expansion device are recoded. The ultimate shaft resistance is determined from the load-upward movement curve and the ultimate end bearing capacity is determined from the load-downward movement curve.

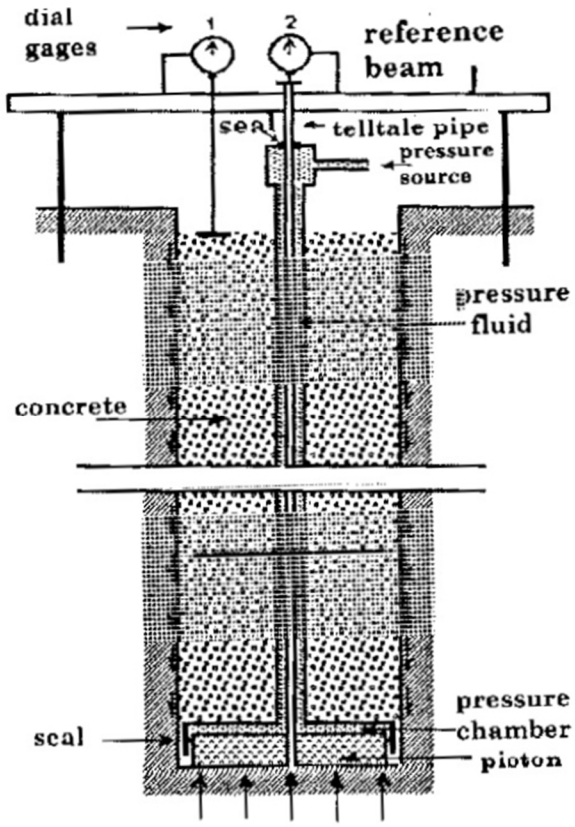

Figure 2-62 Device for testing the load-bearing capacity of concrete-celled earth shafts (Osterberg, 1996)

Later, in 1996, Dr. Osterberg applied for a patent for a new version of the bidirectional load test device (Figure 2-63) entitled “Method and Apparatus for Subterranean Load-Cell Testing” (U.S. Pat. No. 5,576,494). The test apparatus included an expansion chamber placed at the bottom of the hole, hose and return lines so that the entrapped air and fluid are displaced when the fluid and the grout are pumped into the chamber, respectively. Telltale rods are also installed to measure movement of chamber when chamber is pressurized. The testing can be applied in the cyclical loading as conventional static load test.

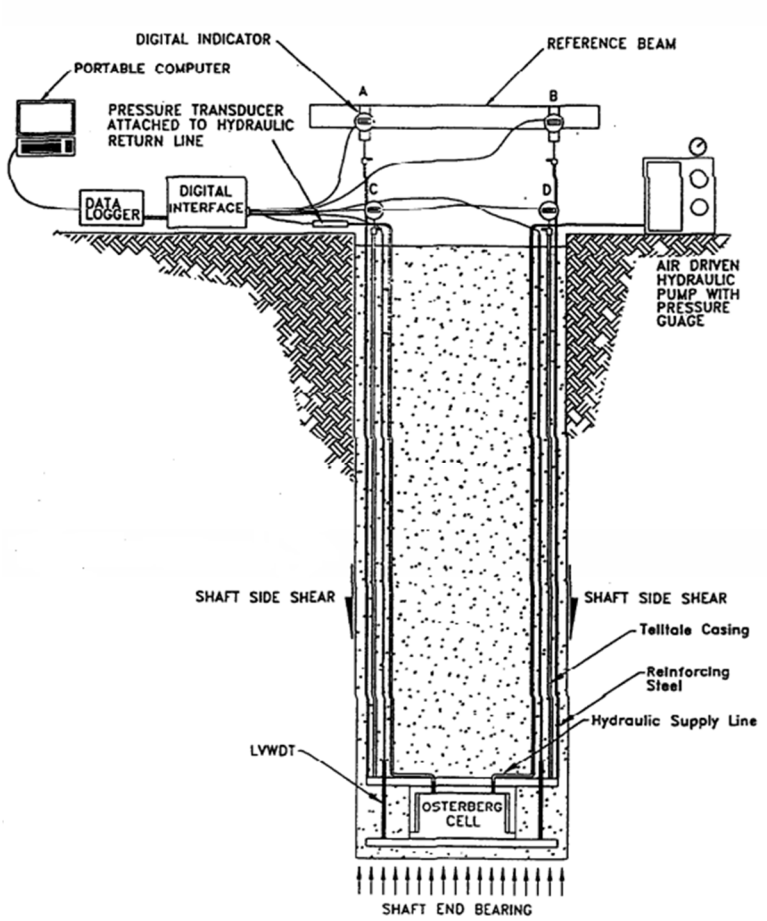

Figure 2-63 Method and apparatus for subterranean load-cell testing (Osterberg, 1996)

2.3.2 Instrumentation, Arrangement and Loading Procedure

The instruments and arrangement often used for a bidirectional load test are shown in Figure 2-64. The instruments include: 1) the jacks and hydraulic control system to apply load onto the test pile, 2) the linear displacement transducers and telltales to measure the opening (movement upward and downward) of the jacks, 3) the strain gages to measure the shaft resistances, 4) the dial gauges (or linear displacement transducers and pressure transducers) to measure the applied load and movements, and 5) the data

logger, software and computer to record the data during testing. Details of the instruments are similar to those of the instruments described in the conventional static load test.

Loading procedures are usually applied according to ASTM Standard D1143-81 (89), which consists of both the quick and slow maintained load test methods. These loading procedures have been described clearly in the section 2.2.2 pertaining to the conventional static load test.

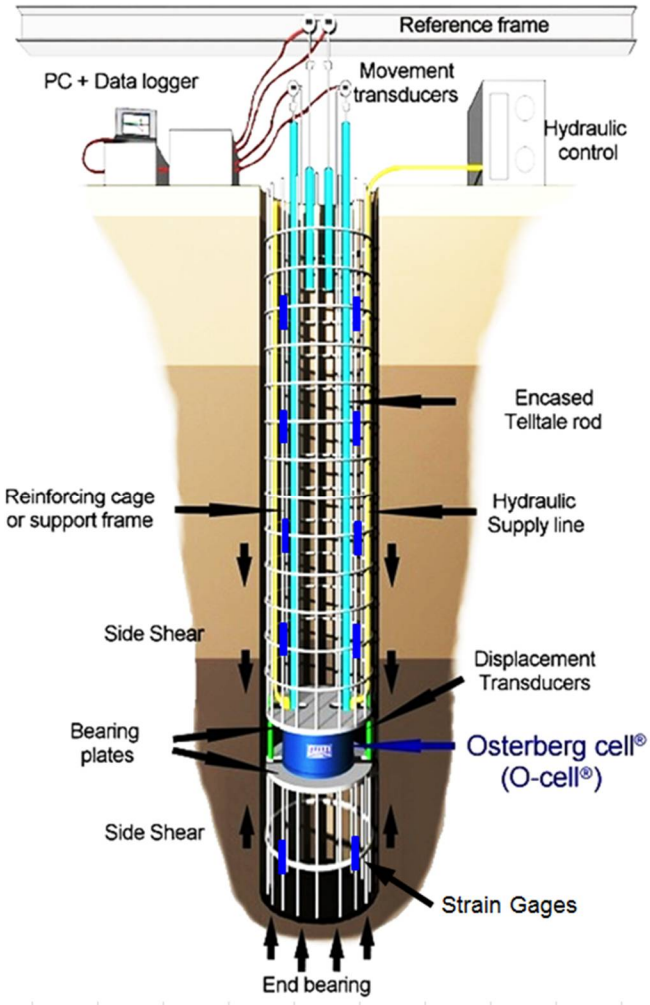

Figure 2-64 Instrument scheme for a bidirectional load test (www.Loadtest.com)

2.3.3 Interpretation of Test Results

Equivalent Pile Head Load-Movement Construction

The results obtained from bidirectional load tests are the pile shaft shear resistance from the installed jacks versus movement; the pile toe compressive resistance versus movement for the case of the jacks placed at the pile toe (Figure 2-65b); the pile shaft shear resistance above the jacks versus movement; and the pile shaft shear resistance below the jacks, plus the pile toe compressive resistance versus movement for the case of the jacks placed above the pile toe (Figure 265c). It should be noted that the test results obtained from a bidirectional load test cannot provide a value of movement at the pile head under the design load. Therefore, Osterberg (1996) proposed a method to convert the load-movement curves obtained from the bidirectional load test (Figures 2-65b and 2-65c) into an equivalent pile head load-movement curve of the conventional load test (Figure 2-65a). This method was termed the “Equivalent Top-Down Curve Construction Method” or the “Equivalent Pile Head Load-Movement Construction Method.”

The proposed method was developed on the basis of three assumptions: 1) the upward load-movement curve of the pile shaft in bidirectional load test is similar to the downward load-movement curve of the pile shaft in a conventional load test, 2) the pile toe load-movement curve obtained from an bidirectional test is similar to the pile toe load-movement curve of the conventional head-down test, and 3) the pile is considered rigid. This method is performed by determining the same movement points on the upward and downward load-movement curve of the pile shaft and toe, respectively. At each similar movement point, the load on both curves is summed. An equivalent pile head load-movement curve is obtained by repeating this process.

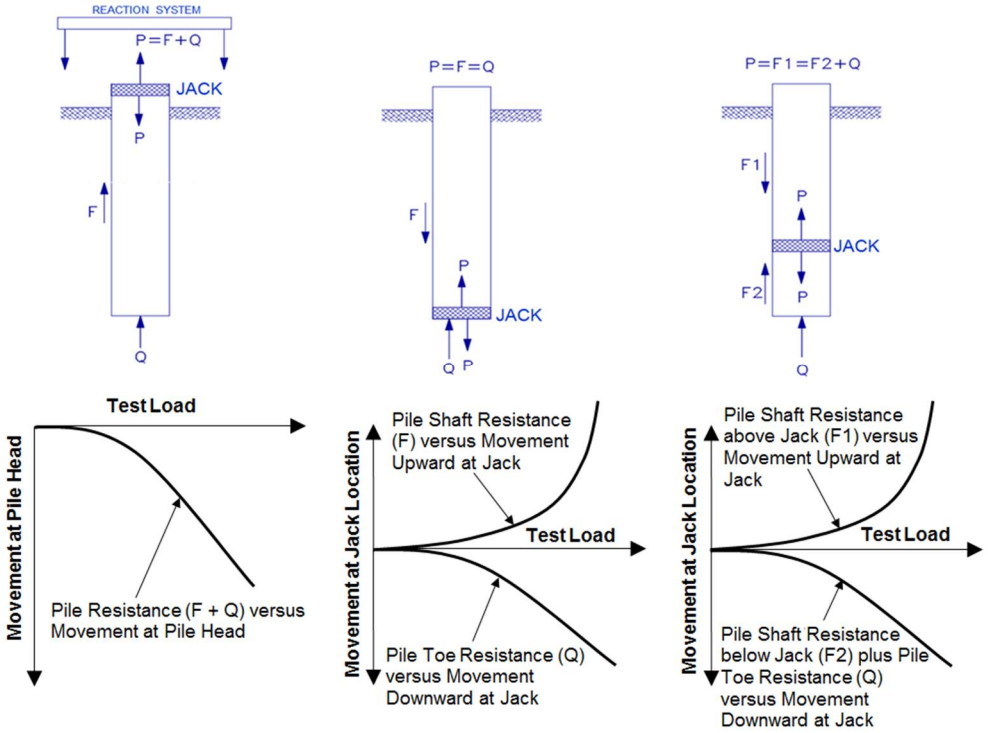

Figure 2-65 Comparison of the pile test results: a) Conventional load test, b) Bidirectional load test with jack placed at pile toe, and c) Bidirectional load test with jack placed above pile toe

Figure 2-66 details the process of constructing an equivalent pile head load-movement curve from a bidirectional load test. Each of the curves shown in Figure 2-66 has points numbered from 1 to 12, so that the same point number of each curve has the same movement. An arbitrary point is selected, such as point 4, on the measured side shear load-movement curve (Figure 2-66a). That point (point 4 in this example), is then found on the measured end bearing load-movement curve which has the same movement of 10 mm (Figure 2-66a). Because the pile is assumed rigid, the movement at the pile head is similar to the movement at the pile toe in a load-movement curve of a

conventional load test. Since the movements at both points (4 in this case) are the same, the load for a conventional load test having the same movement is the sum of the side shear (18.6 MN) and the end bearing at point 4 (9.4 MN,) which is shown at point 4 in Figure 2-66b (28.0 MN).

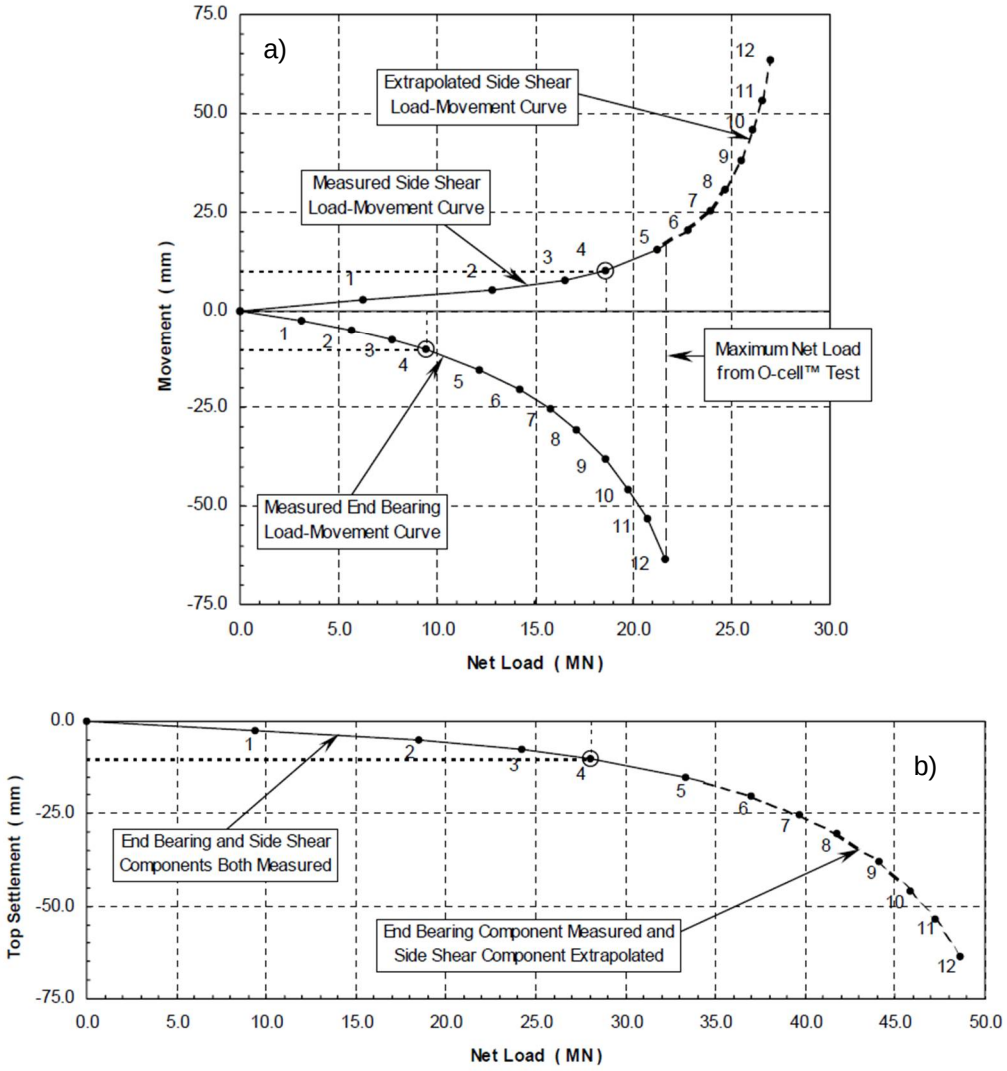

Figure 2-66 Example of constructing the equivalent pile head load-movement curve: a) Load-movement curves of a bidirectional load test, and b) The equivalent pile head load-movement curve (Loadtest International Pte. Ltd., 2013)

By repeating the process shown in points 1-5, the pile head load-movement curve equal to the measured side shear and end bearing curves of the bidirectional load test is determined, as shown in Figure 2-66b. It is recognized that point 5 is the last point on the side shear curve. Thus, the side shears need to be extrapolated to the same maximum movement of the end bearing (point 12). Points 6 to 12 on the side shear curve are obtained by using a hyperbolic extrapolation.

The process is then continued to obtain points 6 to12 on the equivalent pile head load-movement curve, for which the portion of the equivalent curve for the end bearing component has been measured and the side shear component has been extrapolated. The same procedure can be used if the ultimate end bearing is greater than the side shear.

Adding the Elastic Shortening of Pile Material

In practice, the elastic shortening of pile material is relatively significant for long pile. It is not reasonable to assume that the pile material is incompressible (assumption no.3). Therefore, the elastic shortening of pile material has been considered to add into the equivalent pile head load-movement curve. The following method is often used to calculate the elastic shortening of pile material for the bidirectional and conventional load tests (Khoo, 2007).

For a bidirectional load test, the elastic shortening of pile material is computed as.

$$\delta_{BLT} = C\frac{(Q - W_{L1} - W_{L0})L_1}{AE} \tag{2.24}$$

Where δ_{BLT} is the elastic shortening of pile material for the bidirectional load test, C is centroid factor (C = 1/3 for the shaft resistance distribution shown in Figure 2-67a and C = 1/2 for the shaft resistance distribution shown in Figure 2-67c), Q is load imposed on the pile by jack, W_{L0} and W_{L1} are weight of pile segments L_0 and L_1, L_1 is length of the pile segment from the location of the jack to the ground surface, A is cross-section area of pile, and E is the elastic modulus of the pile material.

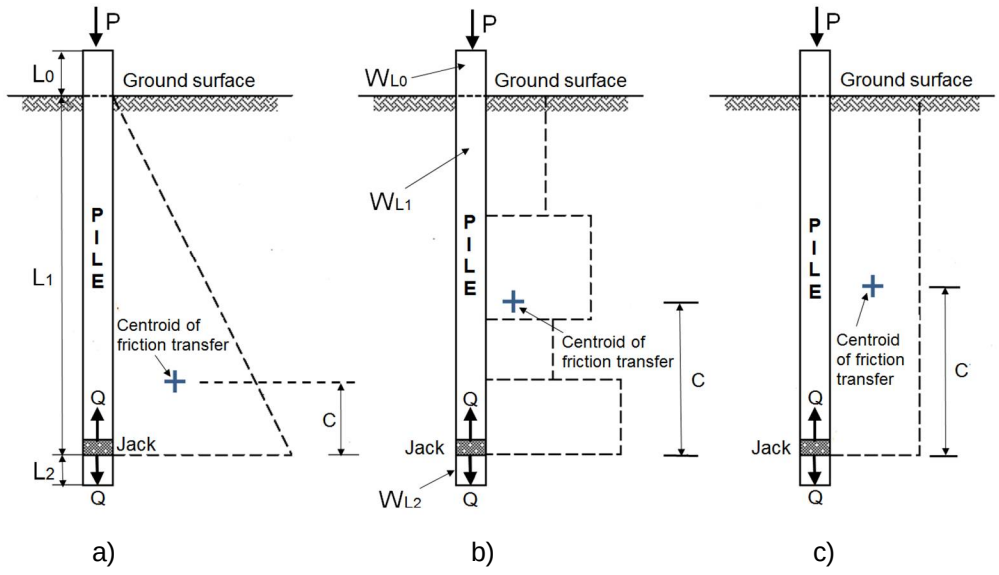

Figure 2-67 Calculation of the elastic shortening of pile material: a) Pile in cohesionless soil, b) Pile in layered soil, and c) Pile in cohesive soil (Loadtest International Pte. Ltd., 2013)

For a conventional load test, the elastic shortening of pile material is computed as:

$$\delta_{CLT} = \frac{PL_0}{AE} + (1-C)\frac{PL_1}{AE} + C\frac{(Q+W_{L2})L_1}{AE} \tag{2.25}$$

$$P = 2Q - W_{L0} - W_{L1} + W_{L2} \tag{2.26}$$

Where δ_{CLT} is the elastic shortening of pile material for the conventional load test, C is centroid factor (C = 1/3 for the shaft resistance distribution shown in Figure 2-67a and C = 1/2 for the shaft resistance distribution shown in Figure 2-67c), Q is load imposed on the pile by jack, W_{L0}, W_{L1} and W_{L2} are weight of pile segments L_0, L_1 and L_2, respectively (Figure 2-67), L_1 is length of the pile segment from the location of the jack to the ground surface,; A is cross-section area of pile, and E is the elastic modulus of the pile material.

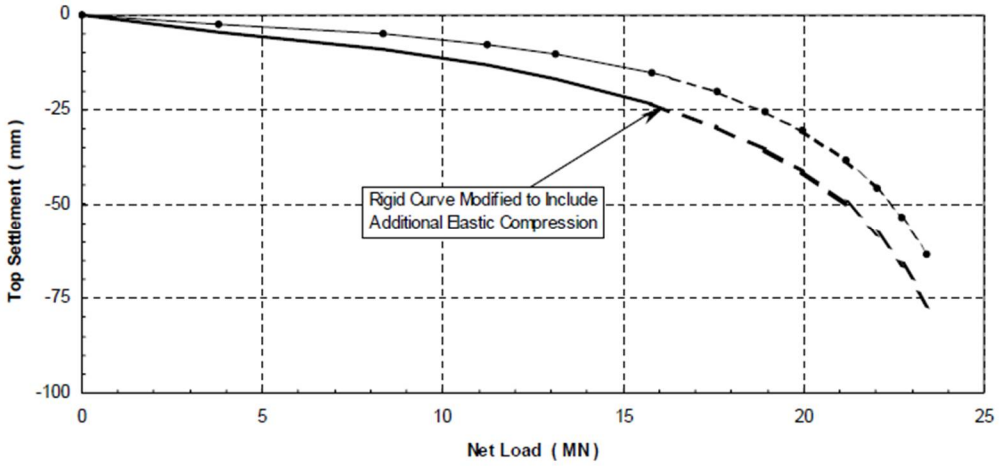

Figure 2-68 Equivalent pile head load-movement curve adjusted by the elastic shortening of pile material (Loadtest International Pte. Ltd., 2013)

Therefore, the elastic shortening of the pile material added into the equivalent pile head load-movement curve is calculated as:

$$\delta_{Adjusted} = \delta_{Equivalent} + \left(\delta_{CLT} - \delta_{BLT}\right) \tag{2.27}$$

Where $\delta_{Adjusted}$ is the movement of the rigid curve adjusted by the elastic shortening of the pile material; $\delta_{Equivalent}$ is the movement of the equivalent pile head load-

movement curve shown in Figure 2-63, assumed as rigid; δ_{CLT} is the elastic shortening of pile material calculated theoretically from the conventional load test; and δ_{BLT} is the elastic shortening of pile material calculated theoretically from the bidirectional load test.

Figure 2-68 shows the equivalent pile head load-movement curve before and after adjusting the elastic shortening of pile material.

2.4 Summary

The Cone Penetration Testing

1) Mechanical penetrometers have a sleeve that can move independent of the cone tip. They provide a discontinuous measurement of cone tip resistance and sleeve friction resistance, with the depth intervals for the measurements normally from approximately 10 to 20 cm. The measurements of tip resistance and sleeve friction are not taken at the same level, which can lead to serious errors in calculating friction ration (f_s/q_c). For soft soils, the obtained results are insufficient accuracy for the quantitative analysis of soil properties. For highly stratified soils, the satisfactory qualitative interpretation is impossible. The effect of pore water pressure on cone tip resistance and sleeve friction is not considered. The main advantages of the mechanical penetrometers are their simple operation and low cost.

2) Electric penetrometers are built-in load cells that can measure continuously the cone tip resistance and sleeve friction. Calibration and zero load errors are often encountered for this device. During penetration testing, calibration and zero load errors change due to mechanical influence, and the zero load error has to be corrected after each penetration test. During field use, the electric penetrometers have to be returned periodically to the workshop for maintenance and calibration. The electrical system is

complicated and requires a well-equipped workshop with trained personnel for the calibration and maintenance of the instruments. It also demands more operators in the field, since they must understand the equipment they are using and must be able to check the proper performance of the electric penetrometer and the other instruments. The effect of pore water pressure for cone tip resistance and sleeve friction is not considered, and the cost of electric penetrometers is relatively high. The main advantages of the electric penetrometers are their high accuracy and repeatability of results, precision in soft soils, high degree of resolution in stratified soils, and accurate determination of friction ratio (f_s/q_c).

3) Piezocones provide a simultaneous measurement of the cone tip resistance, the sleeve friction, and pore water pressure during penetration testing. The pore water pressure measurement of the piezocone has opened the way for an effective stress analysis of the cone resistances and for an improved determination of soil parameters from CPT data. The main difference of the current piezocones is that the porous filter is installed at or above the conical tip. The location of the porous element has not yet been standardized. The limitations of the piezocone are the same as those of the electric penetrometers.

4) The penetration depth of all of the current CPT devices depends on the reaction load system that pushes the cone downward. The normal capacity of the current reaction load systems is about 22 tons; therefore, the penetration depth is limited to 22 tons for both the cone shaft and tip resistance of soil. In some cases, when the competent soil layers have a total soil resistance of just over 22 tons for cone, the current CPTU devices cannot overcome such soil layers to reach into the depth at which the piles need to be installed.

5) None of the current CPT devices can establish the relationship between shear stress versus movement above and stress penetration below the tip cone at desired depths of soil layers, which is important for determining the pile capacity, predicting the long-term pile settlement, and estimating the pile settlement caused by seismic loads.

6) The direct CPT-based methods employ the values of total stress, while the long-term behavior of piles is governed by the effective stress. The upper limits of the unit shaft and toe resistance are not reasonable because the unit shaft and toe resistance of the pile are frequently greater than the recommended limits.

7) For the European method and the Schmertmann and Nottingham method, the over-consolidation ratio is used to relate the cone tip resistance to the unit toe resistance. However, for sand, the overconsolidation ratio is difficult to determine. The European method uses the undrained shear strength converted from the cone tip resistance to estimate the pile toe capacity. However, the pile capacity in long-term condition for cohesive soils is governed by the drained soil characteristics. Thus, the undrained strength used to calculate the pile capacity in long-term condition is not justified.

8) The Bustanmante and Gianselli method does not use of sleeve friction, which ignores an important component to determine soil characterization from the CPT results. Moreover, the influence zone above and below the pile toe (1.5 times of pile diameter) is relatively short. The influence zone below the pile toe is very important because the resistance of soil for the pile toe penetration is reduced if a weaker layer exists below the pile toe.

The Conventional Static Compressive load Testing

The purpose of the static pile load test is to examine the response of a pile under load applied at the pile head. The static pile load test may be performed during the

design or construction phase of a project, depending on whether foundation design parameters are desired or the pile accuracy is to be verified. The often-used reaction load system is kentledge, anchored piles, and a combination of kentledge and anchored piles. The instruments usually installed for the test piles are strain gage, load cell, telltales, dial gauges, hydraulic jacks, and linear displacement transducers. The four commonly-used loading procedures are slow maintained loading, quick maintained loading, constant rate of penetration, and Swedish cyclic loading. The usually-applied methods to interpret the test results for the non-failure test are Vander Veen, Brinch Hansen, DeBeer, Chin-Kondner, Fuller and Hoy, Davisson, Mazurkiewicz, Butler and Hoy, and Decourt.

The conventional static pile load tests are limited by the cost and time required to perform them. Safety considerations present serious limitations for the large load tests. Many static load tests are not carried to failure, and the test results only represent a lower bound on the pile capacity. It is almost impossible to perform static load tests offshore, in deep and strong river waters, or congested areas. It is a difficult problem even when the reaction system is anchored.

It is difficult to sufficiently mobilize the pile toe resistance to enable an analysis of the pile toe response when performing the conventional loading test. It is also hard to determine what portions of the applied test loads actually reach the pile toe. Moreover, the potential presence of the residual load at the pile toe adds complexity to the analysis.

The Bidirectional Load Test

The bidirectional load test method incorporates a sacrificial hydraulic jack placed at or near the pile toe, which uses the shaft friction to react the toe force during the load application by jack. The test is performed by increasing the pressure in the jack to push the pile shaft upward and the pile toe downward. The measurements recorded are the

jack pressure (the load), the upward and downward movements, and the expansion of the jack.

The advantages of the bidirectional load test are the amount of time and money required for obtaining piles performance; the end bearing and skin friction are measured separately; and testing can be performed on piles over water, in congested areas, or on piles installed a batter. In addition, the safety problems are significantly less than those associated with the conventional static load test, and the test load capacity is high.

The disadvantages of the bidirectional load test are that the load cell is expendable and cannot be retrieved, and the total pile capacity in both friction and end bearing cannot be obtained since only one of the two resistance components reaches the ultimate value. The construction of the equivalent pile head load-movement curve requires many assumptions and one of the two resistance components to be extrapolated. Thus, the reliability of this curve is limited. Moreover, the jack expansion creates a tension in the soil outside the cell location and thus the influence of the tension zone should be addressed in the analysis of the test results.

Chapter 3

P-Cone: A Novel Cone Penetration Test Device for Deep Foundation Design

3.1 Introduction

The cases of piled foundations cited in Chapter 1 provide compelling evidence that the settlement of a piled foundation is governed by the characteristics of the soil properties below the installed pile toe.

Full-scale conventional static load tests are usually performed to verify a pile or pier foundation design. The pile load tests are classified into two categories: the failure load test and the proof load test. The failure load test is performed until the plunging failure of the pile takes place, which is when the pile experiences excessive movements under small or no load increases. Load tests to failure are necessary to determine the ultimate bearing capacity of the pile; however, they are not administered often because they are costly and time-consuming. Moreover, it is nearly impossible to perform the test for large-diameter long bored piles because of the limitations of the reaction load system and the load-applied equipment, as well as problems related to safety. A proof load test is used to ascertain whether the pile will sustain a specified service load. It is important to note that the proof test does not provide the ultimate bearing capacity of the pile and thus does not contribute to reducing the foundation costs. The failure load is usually estimated based on the interpretation of techniques described in Chapter 2. The cost of performing the proof test is less than that of the failure load test; hence it is frequently performed.

It is difficult, in a conventional static load test, to mobilize the pile toe resistance sufficiently to enable an analysis of the pile toe response, especially since it is hard to determine the portion of the applied test loads that actually reaches the pile toe. Even if a load cell is placed at the pile toe, the potential presence of residual load at the pile toe will add complexity to the analysis (Hunter and Davision, 1969; Gregersen et al., 1973; Cook

and Price, 1973; Veisic, 1977; Holloway et al., 1978; Cook, 1979; O'Neill et al., 1982; Briaud, 1984; Poulos, 1987; Randolph, 1991; Maiorano et al., 1996; Costa et al., 2001; Fellenius, 2000, 2002, 2006, 2009, 2015, and 2017).

The bidirectional loading test method eliminates much of the difficulty, provided that the bidirectional cell can be activated near the pile toe and that the shaft resistance is sufficient to supply reaction resistance to the downward push of the cell. However, the bidirectional load test only reaches one of the two resistances of pile (either the pile toe resistance or the pile shaft resistance). Thus, the actual bearing capacity of the pile is not determined (Schmertmann and Hayes, 1997). The determination of the shaft resistance component is not simple, even when many jacks are installed at different levels along the pile length, due to the unknown cross-section area of the bored piles.

Most designs of piled foundations have to be carried out without the benefit of static loading tests. Most rely on information received from the site investigation; in particular, results of in-situ tests, such as the cone penetration test with measured pore pressure (CPTU). Over the last 100 years, the development of a CPTU device focused only on measuring the sleeve friction, the cone tip resistance, and the pore pressure around the cone tip during penetration. One question that needs to be answered is how movements are required to mobilize the measured values of the sleeve frictions and cone tip resistances. Most types of soil tests (both in laboratory and in situ) can provide the values of movement to mobilize fully the resistance components of soil, but the CTU devices do not.

This chapter presents a novel cone penetration test device with the ability to measure pile foundation capacities (the P-Cone). This P-cone is capable of performing site investigations and measuring shear-movement above and stress-penetration below a

cone at the desired depths in the ground. The P-cone can also improve the penetration depth and offer a potential application for the in situ consolidation test.

3.2 Concept of Design

A major difficulty with current CPTU devices is that the limited reaction force prevents the sounding from reaching into the depth at which the piles are usually installed. To assist in pile design, a novel cone penetration test device, the P-cone, was developed by combining the features of CPTU cone sounding and bidirectional loading (Figure 3-1). The P-cone device can improve the penetration depth by utilizing the pressure in a cell that uses the cone rods and surface anchors on the ground surface as a reaction to push the cone down. This is clearly illustrated in Figure 3-1.

As can be seen from the left diagram of Figure 3-1, the required reaction load, P, of the current CPT devices is equal to the shaft resistance, P1, plus the cone resistance, P2. The reaction load of the newly designed P-cone (right side of Figure 3-1) is equal to the reaction load of the current CPT device, plus the shaft resistance, P1.

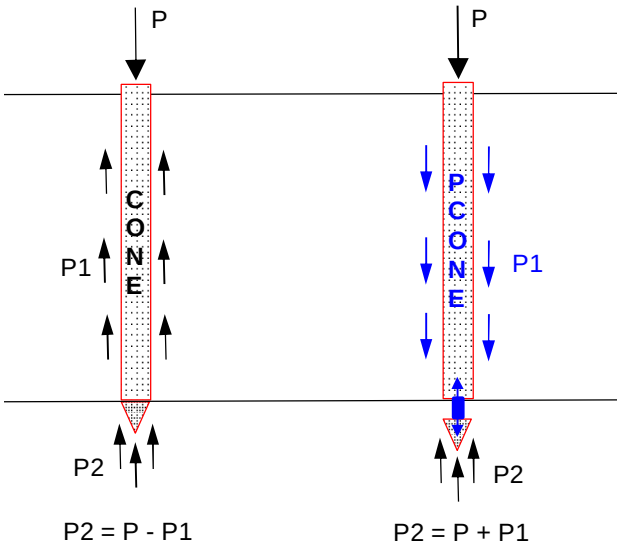

Figure 3-1 Illustration of the penetrating depth information of the P-Cone.

Figure 3-2 illustrates the principles of the P-cone used in combination with a hydraulic jack that serves as the movement-and-force-generating essential feature. The cone resistance is measured by a separate load cell. The other necessary measurements are similar to those of a conventional cone sounding device: the downward and upward movements measured by rod extensometers, the force in the shaft measured by means of strain-gages, and the pore pressure acting on the cone shoulder measured by a pressure transducer.

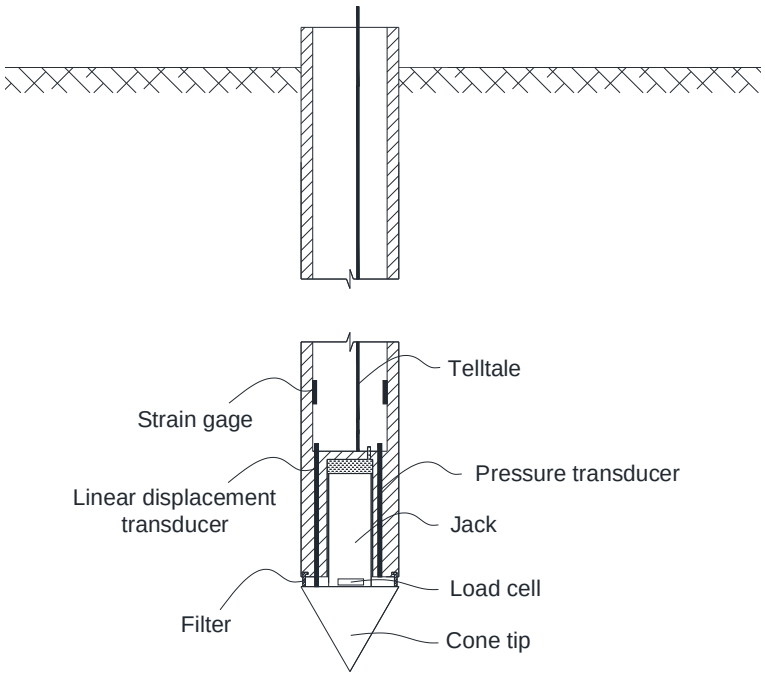

Figure 3-2 Scheme of the P-Cone device.

3.3 Detailed Design of the P-Cone Probe

Figure 3-3 depicts the detailed design of the P-cone. The hydraulic jack has a 65-mm outer diameter (O.D.), 35-mm inner diameter (I.D.), and a 160-mm height. The piston diameter of the jack is 30 mm, with a 120 mm travel. The capacity of the jack considered in this study is about 20 kN. The pressure inside the jack and piston movements are

measured with instruments installed from the jack's upper surface. The cone tip has a 60^0 apex angle with a 66 cm^2 base area. In addition, another cone tip of 120^0 apex angle and a 38 cm^2 base area was also designed to serve the consolidation-compressive test. It is presented in Figure 3-5.

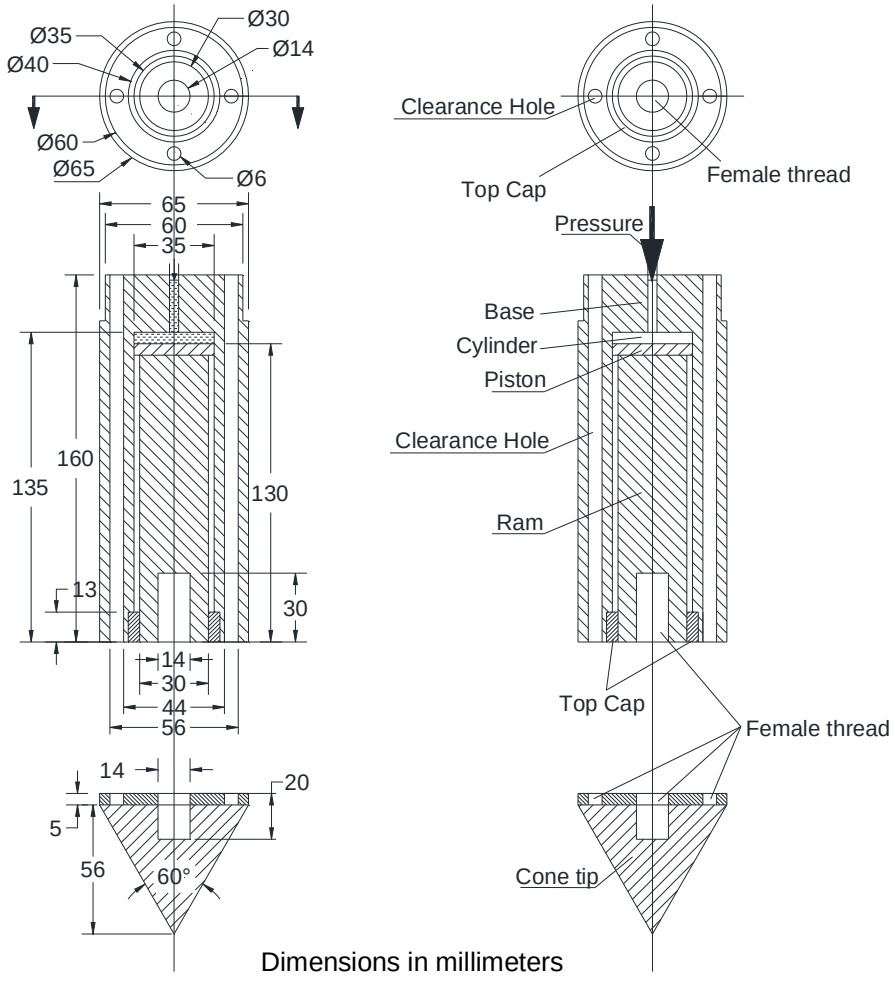

Figure 3-3 Detailed design of the P-Cone probe

Figure 3-4 shows the dimensions of the steel tubes designed for the P-Cone. The steel tubes of 5-mm thickness were designed with a 65-mm outer diameter, the same as

the diameter of the jack, and 500-mm length. The effective thread length of the steel tubes and the jack bottom designed are 25 mm; the male thread diameter of the tubes is 60 mm. The steel tube attached by strain gages is connected with the jack.

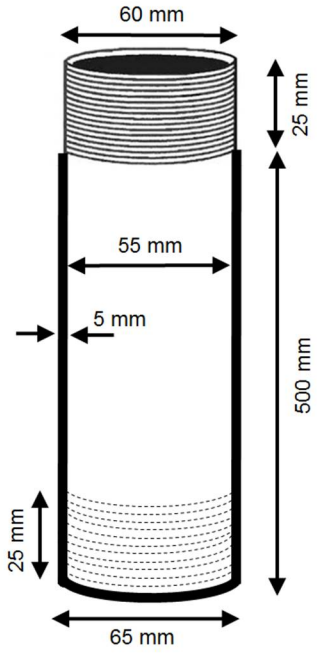

Figure 3-4 Detailed design of steel tube

3.4 Manufacture and Assembly of the P-Cone Probe

The main cone devices (jack, cone tip, and shaft) were manufactured in Vietnam, and the attached instruments were supplied by Geokon, Inc., USA. Figure 3-5 shows the prototype of the P-cone. In order to measure the shaft resistance, the vibrating wire sensors (model 4150) with measureable ranges of 3,000 micro strains (με) were installed 200 mm above the cone tip. The cone stress was measured by a pressure transducer (model 4500HH) with a measureable range of 5 MPa and pressure gauge of 4 MPa (600 PSI). Telltales were used to measure the upward and downward movements during testing in a laboratory chamber, instead of the linear displacement transducers designed originally and depicted in Figure 3-2.

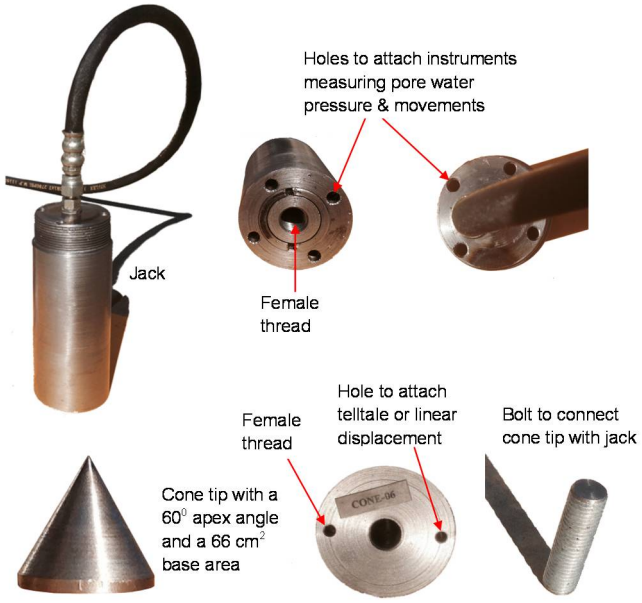

Figure 3-5 Manufacture of the P-Cone probe

Figure 3-6 shows the assembled P-Cone probe, the manufactured steel tubes, and a cone tip with a 120^0 apex angle and a 38 cm^2 base area. This cone tip was manufactured to serve the consolidation compressive test so that the vertical stress distribution difference between the conventional consolidation compressive test and the consolidation compressive test performed by the P-Cone is narrowed. Cone tips with a greater apex angle can be used; however, they are less practical for the in situ conditions.

Figure 3-6 Assembled P-Cone probe and the 120^0 cone tip

Figure 3-7 displays the trial operation of the P-Cone. The P-Cone was assembled completely (Figure 3-7a). The trial operation of the P-Cone was performed by pressurizing the fluid inside the jack via a small hand pump system (Figure 3-7b). After increasing the fluid pressure inside the jack, the jack was expanded to separate the cone from the cone shaft. The trial operation of the P-Cone was regarded as complete.

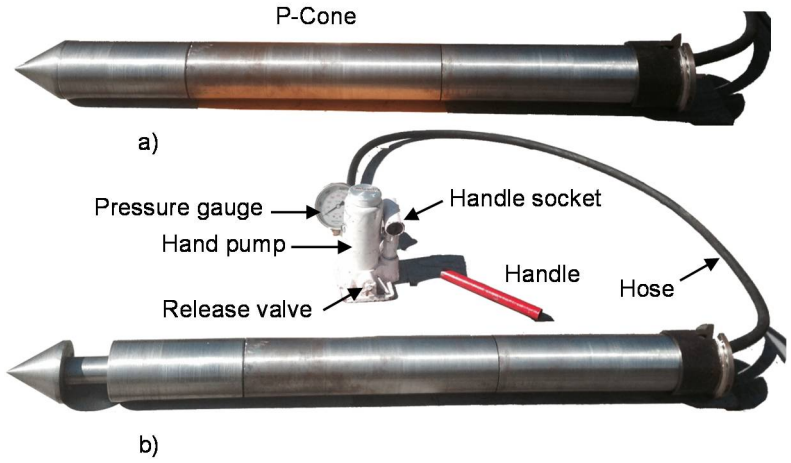

Figure 3-7 Trial operation of the P-Cone: a) Completely assembled P-Cone and b) Pressurized P-Cone.

The following sections depict the instruments that were used to measure the cone tip and shaft resistance while pushing the P-Cone into the ground. The instruments used to measure movements are also depicted.

3.5 Instruments and Installation

3.5.1 Vibrating Wire Strain Gage

The Model 4151 Vibrating Wire Strain Gage, manufactured by Geokon Inc., was used to measure strains on the surface of steel structures; therefore, it was used to measure the sleeve friction of the P-cone during penetration. The strain gage contains a

steel wire tensioned between two end blocks (Figure 3-8). The pins are welded to the end blocks to be grouted into two short holes of the drilled materials.

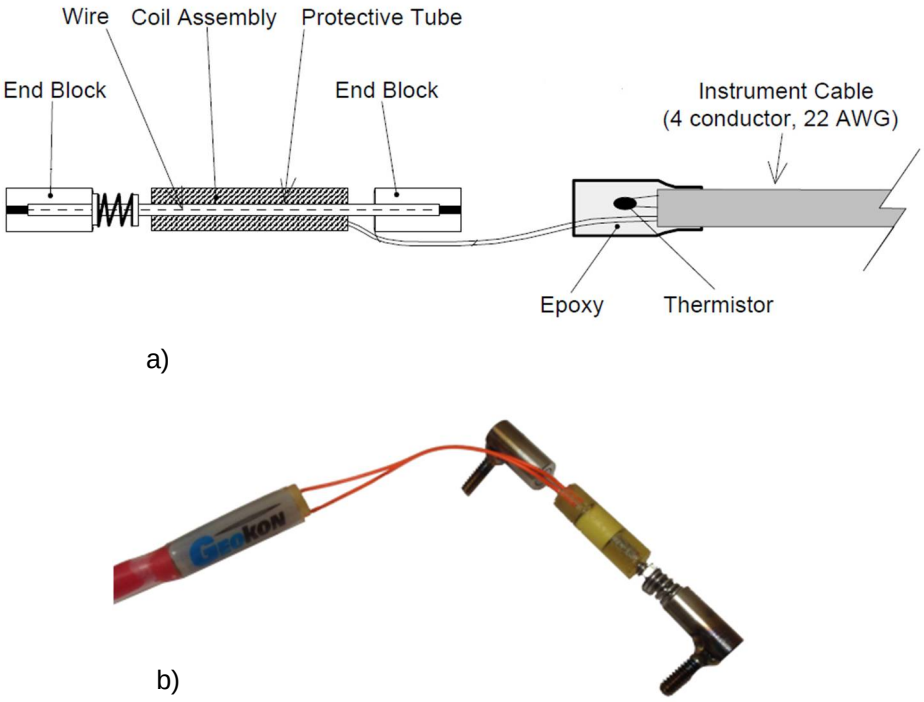

Figure 3-8 The Model 4151 Vibrating Wire Strain Gage: a) Components of strain gage, and b) Manufactured strain gage (Geokon Inc.)

For the applied load, the deformation of structures makes the end blocks to displace relative to one another, leading to a change of the wire tension and the resonant frequency of the wire vibration. The wire is plucked by the electronic coil and the permanent magnet to send voltage pulses to the coil, and then transmitted into data logger and computer via signal cable. The wire vibration causes an alternating current in the coil; the frequency of which is similar to the wire vibrating frequency and is measured by the same electronic coil and data logger. The squared frequency value is multiplied by

a constant so that the values the data logger are displayed directly in microstrain (Equation 3-1).

$$\mu\varepsilon = 0.391\left(f^2 x10^{-3}\right) \tag{3-1}$$

Where με is the strain of the vibrating wire in microstrain and f is the resonant frequency of the vibrating wire.

Figure 3-9 shows the dimensions of the Model 4151 Vibrating Wire Strain Gage. The length of the vibrating wire is 51 mm, which corresponds to the 51 mm length segment of the P-Cone to calculate the sleeve friction after installation. The strain of the steel tube induced by the sleeve friction during penetration into the ground is computed as

$$\mu\varepsilon_{Apparent} = \left(R_1 - R_0\right)B \tag{3-2}$$

Where $\mu\varepsilon_{Apparent}$ is strain of the steel tube induced by the sleeve friction, R_0 is the initial reading, R_1 is a subsequent reading, and B is a batch gage factor supplied with each gage (Appendix A). It should be noted that when (R_1 - R_0) is positive, the strain is tensile; when (R_1 - R_0) is negative, the strain is compressive. Table 3.1 shows the technical specifications of the Vibrating Wire Strain Gages – Model 4151.

In order to convert strain into load, it is necessary to know the values of the elastic modulus and the cross-section area of the steel tube. The elastic modulus and the cross-section area of the used steel tube are about 200 GPa and 942 mm^2, respectively. These values will be used to calculate the sleeve friction while pushing the P-Cone into the ground.

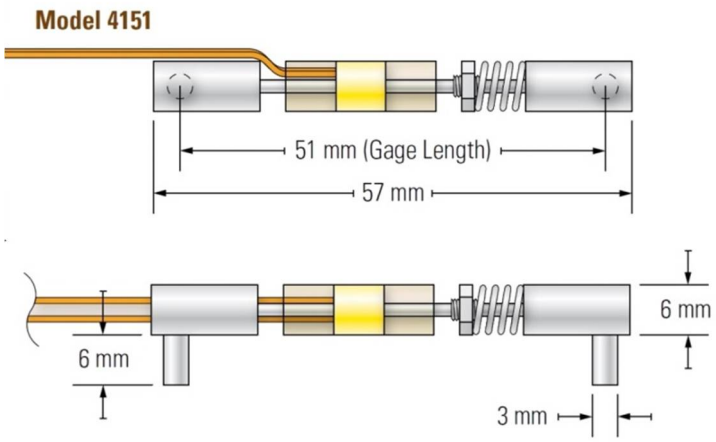

Figure 3-9 Dimension of the Model 4151 Vibrating Wire Strain Gage (Geokon Inc.)

Table 3-1 Technical Specifications of Strain gage - Model 4151

Items	**Parameters**
Standard Range	3000 με
Resolution	0.4 με
Calibration Accuracy	0.1%FS
System Accuracy	2.0% FS
Stability	0.1%FS/yr
Linearity	± 2.0% FSR
Thermal Coefficient	12.2 με /^{0}C
Frequency Range	1400 – 3500 Hz
Temperature Range	-20^{0}C to +80^{0}C
Active Gage Length	51 mm

Figure 3-10 indicates the position of the strain gages attached to the P-Cone. The two diametrically opposed strain gages (Model 4151) were installed into the steel tube at 200 mm above the cone tip. The installation of the strain gages was performed by

drilling holes into the steel tube to attach the spins of the strain gages, and then using glue to fill the spaces between the drilled holes and the pins. The strain gage installation was done carefully to ensure that the strain of the steel tube was similar to the strain measured by the strain gages.

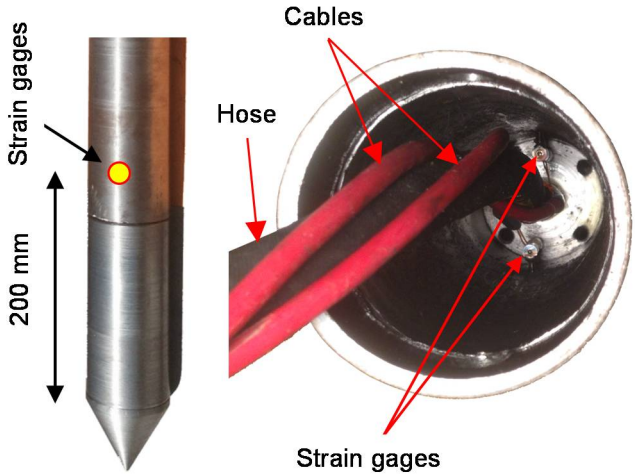

Figure 3-10 Locations of the strain gages installed into the P-Cone

3.5.2 Vibrating Wire Pressure Transducer

The model 4500H Vibrating Wire Pressure Transducer manufactured by Geokon Inc. was designed for high fluid pressure measurement (Figure 3-11). The transducer uses a pressure-sensitive diaphragm attached a vibrating wire element. The pressure-sensitive diaphragm is welded to a capsule and hermetically sealed. Fluid pressures cause the deformations of the pressure-sensitive diaphragm and make changes of the vibrating wire frequency. The changes of the vibrating wire frequency is transmitted to the datalogger device by the electrical coil acting through the capsule walls. Table 3-2 shows the technical specifications of the model 4500H Vibrating Wire Pressure Transducer.

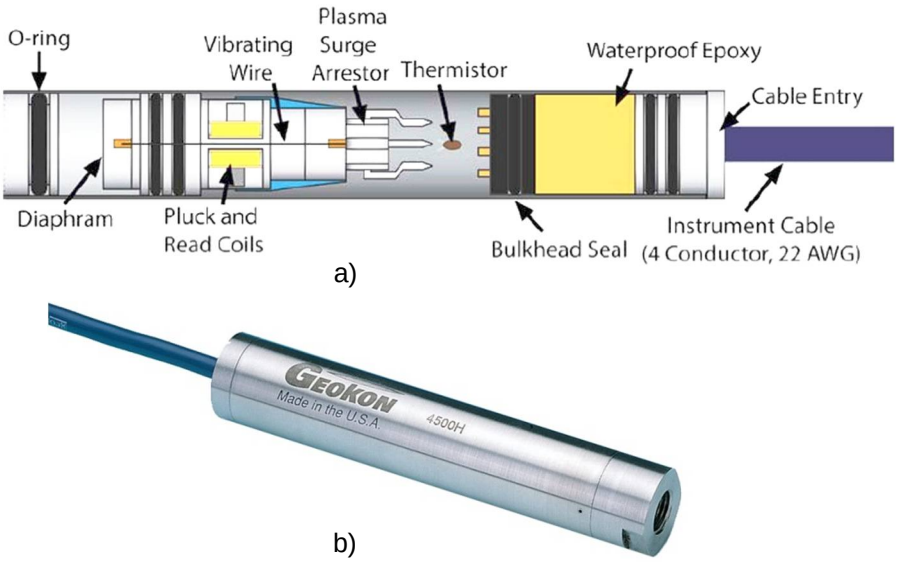

Figure 3-11 The Model 4500H Vibrating Wire Pressure Transducer: a) Components of Pressure Transducer, and b) Manufactured Pressure Transducer (Geokon Inc.).

Table 3-2 Technical Specifications of Pressure Transducer - Model 4500H

Items	**Parameters**
Standard Range	5 MPa
Over Range	1.5 × rated pressure
Resolution	0.025% F.S.
Accuracy	0.1% F.S.
Linearity	< 0.5% F.S.
Temperature Range	-20^0C to $+80^0$C
Thermal Zero Shift	< 0.05% F.S./°C
Diaphragm Displacement	< 0.001 cm^3 at F.S.
Length x Diameter	143 × 25.4 mm
Mass	0.30 kg

The pressure is computed as

$$P = (R_1 - R_0)G \quad (3\text{-}3)$$

Where P is pressure induced by the sleeve friction, R_0 is the initial reading, R_1 is a subsequent reading, and G is linear calibration factor (Appendix A).

Figure 3-12 presents the installation of a pressure transducer to measure the fluid pressure change inside the jack during penetration of the P-Cone into the ground. In addition, the two pressure gauges are also installed to measure and control the loading of the pump system for the load tests performed following the P-Cone penetration test.

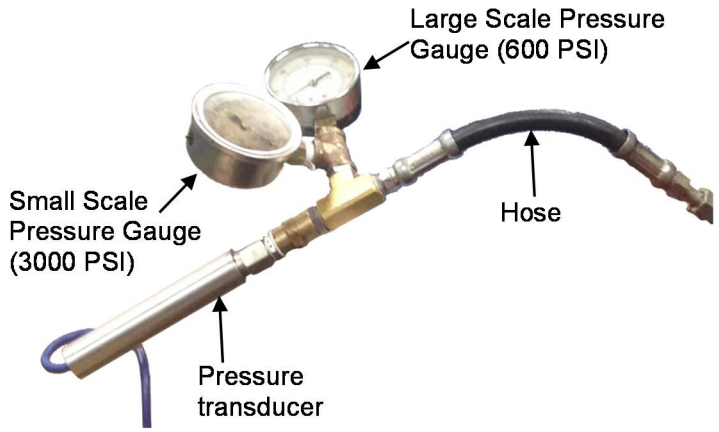

Figure 3-12 Pressure transducer installation to measure the fluid pressure

3.5.3 Pressure Gauge

The liquid-filled pressure gauge (Figure 3-13) is used to measure the fluid pressure changes inside the jack while pushing the P-Cone into the ground. The main purpose of this pressure gauge installation is to measure and control the loading of the pump system for the bidirectional load test, the end bearing load test, and the consolidation compressive test. It should be noted that it is nearly impossible to control the load application of the pump system with a pressure transducer.

Table 3-3 Technical Specifications of Glycerin-Filled Pressure Gauge

Items	Parameters
Standard Range	600 PSI
Weight	1.0 lbs.
Gauge Diameter	4 inches
Accuracy	2%
Bourdon Tube	C-shaped
Pointer	Black enameled aluminum
Dial	White aluminum
Movement	Brass
Mount Type	Back
Fill Material	Glycerin
Connection Size	1/4 Male NPT (Inches)

Figure 3-13 Glycerin-filled pressure gauge with measuring range of 600 PSI

(www.northerntool.com)

The used pressure gauge has the measuring range of 600 psi, which is suitable for measuring the small load increments during the experiments of the P-cone. If the resistance of the compacted soil exceeds 600 psi (use smaller case letters), it will be measured by the pressure gauge, with the measuring range of 3000 PSI, as shown in Figure 3-12. Table 3-3 gives the technical specifications of the used pressure gauge.

3.5.4 Hand Pump and Jack

The portable hydraulic hand pump manufactured by Strongway Inc. is designed to work with the single-acting portable ram. The pump has a maximum operating pressure of 8,939 PSI and it can be optimized by an internal pressure relief valve to protect overload, where ram is rated to 10 tons. This portable hand pump is used to pressurize the fluid inside the jack to push the cone tip down into the deeper soil layers. Figure 3-14 shows the components of the hand pump and the completely manufactured hand pump. The main components of the hand pump consist of a handle, release valve, oil filler screw, hose, hose coupler, and dust cover.

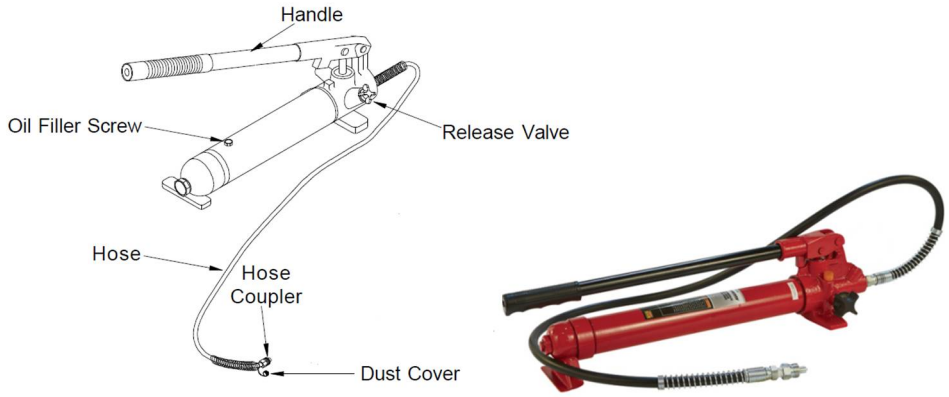

Figure 3-14 Portable hydraulic hand pump with capacity of 10 tons

(www.northerntool.com)

The components inside the hand pump are not reported because the pump is not the study object of this dissertation. The technical specifications of this hand pump are shown in Table 3-3. Before pressurizing the fluid inside the jack of the P-Cone, the pump has to be filled with oil via the oil filler screw. Then, the hand pump system is connected with the P-Cone and the instruments to measure the fluid pressure change inside the jack, as indicated in Figure 3-15. Next, the release valve is closed, and the control valve is opened. After that, the jack is pressurized via the handle.

Table 3-4 Technical Specifications of Hand Pump – 10 tons

Items	**Parameters**
Capacity	10 tons
Rated	8,939 PSI
Dimension L x W x H (in.)	20.4 x 5.2 x 5.5
Weight	17.2 lbs

It is very important to note that the control valve is closed while pushing the P-Cone into the ground so that the fluid pressure changes induced by the cone tip resistance will be measured and recorded by the pressure transducers.

Figure 3-16 shows the jack used for pushing the P-Cone into the ground. This jack is designed for lifting; however, it is also used to push the P-Cone into the ground, to apply load for the conventional static load test, and to use as a reaction load for the end bearing load test. The jack used has a maximum lifting capacity of 8 tons and a maximum lifting height of 1,067 mm, which is suitable for carrying out the experiments of the P-Cone in the laboratory. Table 3-5 provides the technical specifications of the jack.

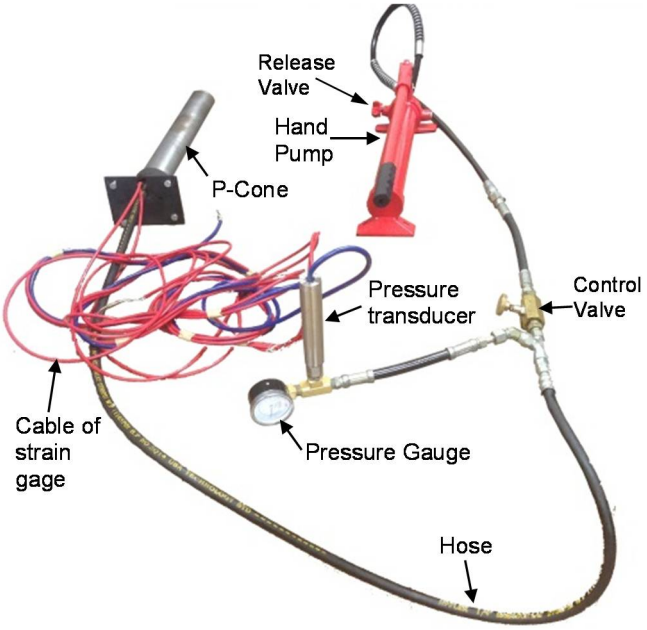

Figure 3-15 Hand pump connected with the P-cone and the measuring instruments.

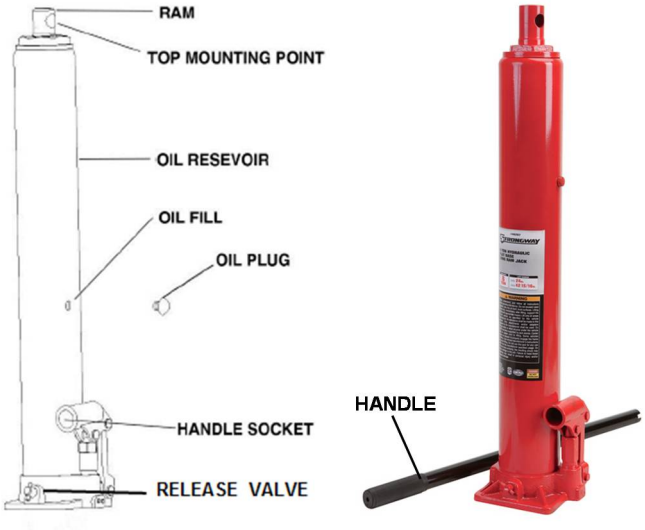

Figure 3-16 8-ton jack used for pushing the P-Cone into the ground

(www.northerntool.com)

Figure 3-17 shows the jack attached to the reaction steel frame. The jack was connected with the reaction steel frame by a 10-mm steel plate welded into the ram of the

jack. Four holes were drilled in the steel plate to join the jack and the reaction steel frame with bolts. The bottom of the jack was also drilled with four holes to connect with the P-Cone to the jack. Details of connecting the jack with the P-Cone are presented in the next chapter.

Table 3-5 Technical Specifications of the Jack – 16,000 PSI (8 tons)

Items	**Parameters**
Lift capacity	16,00 PSI (8 tons)
Minimum lift height	24 inches (610 mm)
Maximum lift height	42 inches (1,067 mm)
Weight	26.0 lbs.
Base L x W (in.)	5.0 x 4.5
Operating temperature	40^0F – 105^0F

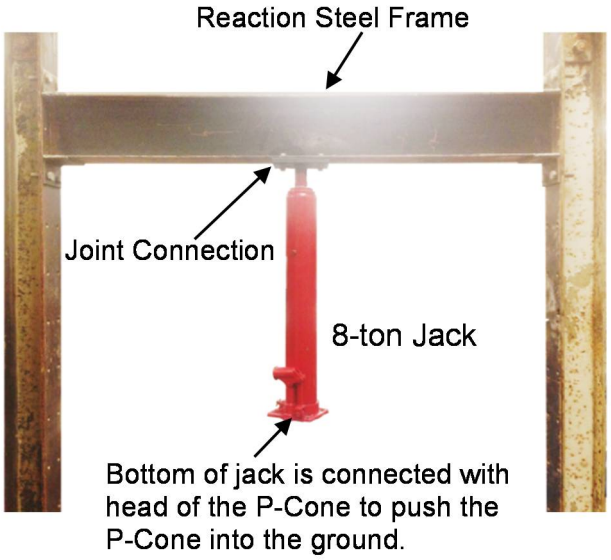

Figure 3-17 Connection of the jack with the reaction steel frame

3.5.5 Telltales and Dial Gauges

In order to measure the downward and upward movements of the P-Cone during the bidirectional load test and the end bearing load test, both telltales and dial gauges were used as as shown in Figures 3-18 and 3-19, respectively.

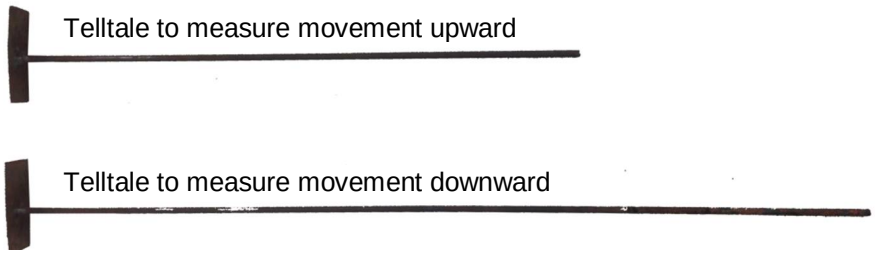

a)

b)

Figure 3-18 Instruments to measure the movements: a) telltales, and b) dial gauges.

Figure 3-18 presents the telltales and dial gauges installed to measure the downward and upward movements of the bidirectional load test. When the jack of the P-Cone is pressurized, the downward movement of the cone tip is measured by Dial Gauge

No. 2, and the upward movement of the cone shaft is measured by Dial Gauge No. 1. It is worth noting that the telltale attached with Dial Gauge No.1 only extended into the bottom of the jack, while the telltale attached with Dial Gauge No.2 extended through the jack and into the cone tip. The dial gauges used have a range of 1 inch and a graduation of 0.001 inch.

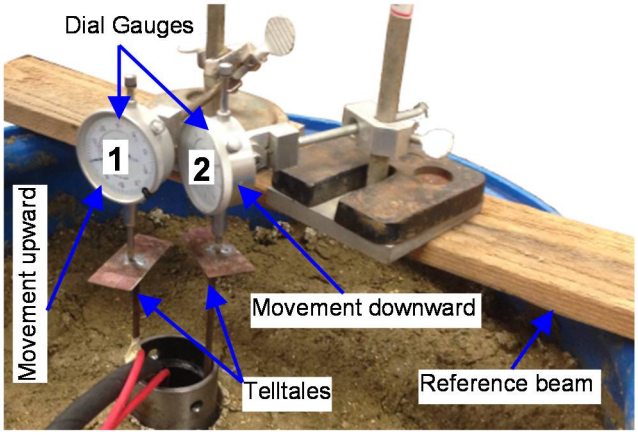

Figure 3-19 Installation of the telltales and dial gauges to measure movements

3.5.6 Datalogger and Software

The Model LC-2x4 4 Channel Datalogger (Figure 3-20) was used to measure and record the data of the strain gages and the pressure transducer during experiments of the P-Cone. This Datalogger can read up to 4 vibrating wire sensors and thermistors. The standard memory of 320K provides storage of 10,666 data arrays.

Each array includes an optional datalogger ID string of 16 characters, a timestamp including the year, date, time, and seconds when the reading was taken. In addition included in the data is the internal battery voltage of 3V, the temperature of datalogger, the readings of vibrating wire, the temperature of transducer, and the array number.

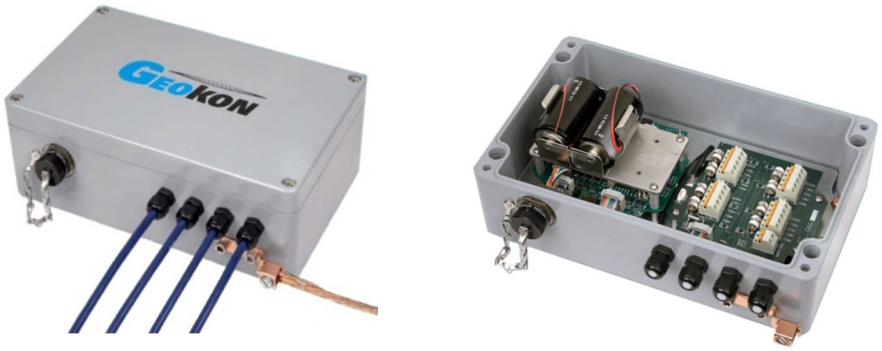

Figure 3-20 Datalogger – Model LC 2x4, (www.geokon.com).

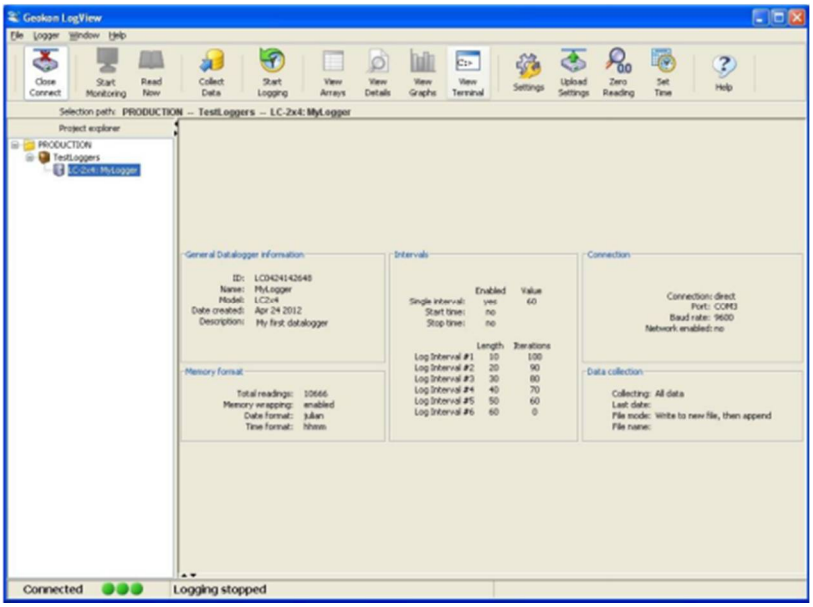

Figure 3-21 LogView main and datalogger connected (www.geokon.com)

Internal math was calculated using a 32 bit floating point notation. Math operations on the instrument readings, such as the gage calibration factors, the application of zero readings, and offsets, provide outputs in engineering units. The

internal configuration of datalogger is defined through communication with a computer using USB interface cable. The datalogger was configured and monitored using LogView (Figure 3-21). Table 3-6 shows the technical specifications of the datalogger used.

Table 3-6 Technical Specifications of Datalogger – LC-2x4

Items	**Parameters**
Accuracy of Measurement	±0.05% F.S. (450-4000 Hz)
Resolution of Measurement	1 part in 20,000
Memory of Program	24K FLASH
Memory of Data	320K EEPROM
Data Connection	RS-232, USB or RS-485
Capacity of Storage (Arrays)	10,666
Range of Temperature	−30˚C to +50˚C
Accuracy of Temperature	Accuracy: 2.0% F.S.; Resolution: 0.1°C.
Speed of Communication	9600 bps
Parameters of Communication	8 data bits, no parity, 1 stop bit
Power Supply	3 VDC (2 Alkaline ‘D’ cells)
Communication Current	< 100 mA
Measurement Current	< 200 mA
Quiescent Current	< 500 μA
Scan Interval	10 - 86,400 seconds (24 hours)
Sensor Connection	Hard wired
Dimension (L × W × H)	260 × 160 × 91 mm

3.6 Operating Principle and Measurement

The operating principle of the P-Cone for the tests is performed according to the following steps:

Step 1: The P-Cone is connected with the jack and the reaction steel frame to be pushed into the compacted soil chamber. Then, the hose of the P-Cone is connected with the hand pump, the pressure gauges and the pressure transducer. Next, the cables of the strain gages and the pressure transducer are connected with the computer via the datalogger (Figure 3-22).

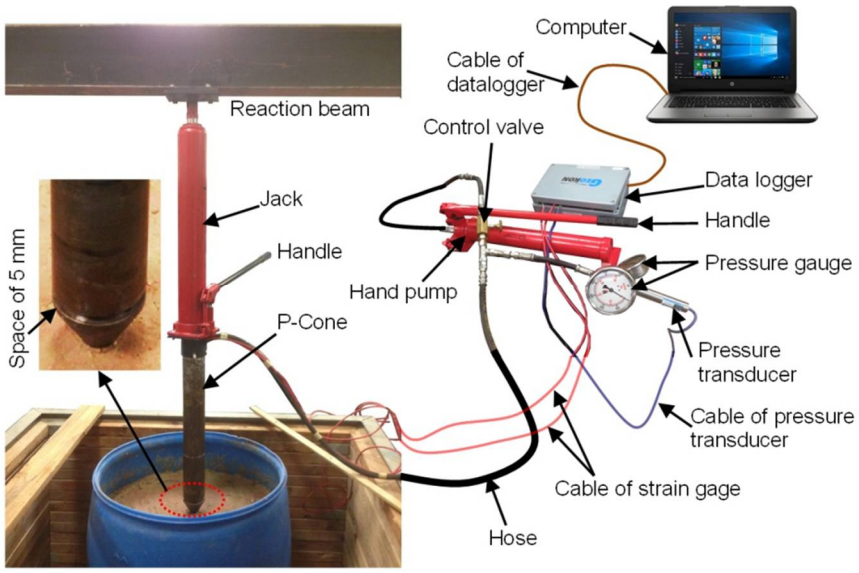

Figure 3-22 Operating principle and the measurement system of the P-Cone.

Step 2: The LogView software installed in the computer communicates with the strain gages and the pressure transducers. Then, the release valve of the hand pump (Figure 3-14) is closed, and the control valve is opened to operate the hand pump via the handle and to push the cone tip open about 5 mm (Figure 3-22). At this time, the values of the fluid pressure and the strain gage of the P-Cone are taken as the initial fluid pressure value. It should be noted that the 5 mm expansion of the cone tip is necessary

so that the influences of the fluid compressibility and the dilatation of the hose on the measured cone tip resistances can be eliminated. Moreover, the jack, attached with the reaction beam, is not used in this step.

Step 3: The control valve is closed, and then the P-Cone is pushed into the ground by the jack, attached with the reaction beam, via the handle. During penetration, the cone tip resistance and the sleeve friction are measured by the pressure transducer and the strain gages, respectively. If the experiment of the P-Cone is performed in saturated soil, an additional pressure transducer is installed at the available holes of the jack to measure the pore pressure at the shoulder of the cone tip. The data of the measurements are recorded by the datalogger and computer. The test results obtained from the cone penetration test in this step are the cone tip resistance, the sleeve friction, and the pore pressure, the same as that of the conventional cone penetration test with measurement of pore pressure (CPTU).

Step 4: After the cone penetration testing has been completed, the bidirectional load test is started. The jack attached with the reaction beam is removed. Then, the telltales and the dial gauges are installed (Figures 3-19 and 3-23) to measure the downward and upward movements of the cone tip and the cone shaft, respectively, during the bidirectional load test. Next, the control valve is opened, and the loading is performed by the hand pump, via the handle.

After each successful load increment, the control valve is closed; before starting the next load increment, the control valve is opened. The process is repeated until the load test is completed. During testing, the cone tip and the shaft resistance are measured by the pressure transducer and strain gages, respectively, via the datalogger system. The test results obtained from the bidirectional load test at this period are those of the shear stress versus movement and the cone tip stress versus penetration.

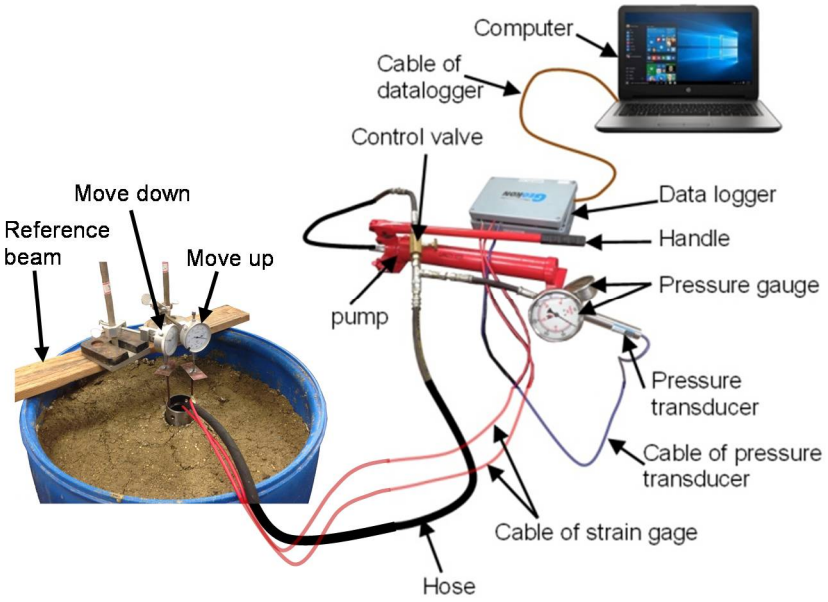

Figure 3-23 Bidirectional load test and measurements.

Step 5: The P-Cone can perform the in-situ consolidation compressive test for fine-gained soils by following Step 4. However, cone tips with a greater apex angle should be used to replace the cone tip with a 60^0 apex angle for the consolidation compressive tests. Since the consolidation compressive tests are often performed for the low-strength fine-gained soil, it is difficult to obtain the expected load increments while using the cone tip with a 60^0 apex angle. Furthermore, the vertical stress distribution below the cone tip is better with a great apex angle than with a small apex angle. In this study, a cone tip with a 120^0 apex angle and a 38 cm^2 base area was used to test consolidation. The test results obtained from the consolidation compressive tests of the P-Cone will be compared to the conventional consolidation compressive tests in the laboratory.

3.7 Summary

A novel cone penetration test device, the P-Cone, and the operating principle for the test cases have been presented. The main features of the P-Cone device are summarized as follows:

1) The cone penetration test: The measurement results obtained from the P-Cone are the same as those obtained from the conventional cone penetration test device, including the cone tip resistance, the sleeve friction, and the pore pressure.

2) The bidirectional load test: The measurement results gained from the P-Cone are the shear stress versus movements and the cone tip stress versus penetration of the soil at the desired depth. These engineering properties of soil play a vital role in determining the bearing capacity and settlement of a piled foundation for the short-term conditions, the long-term conditions, and the liquefaction conditions. To date, the conventional cone penetration test device has not provided such information.

3) The penetration depth improvement: The P-Cone, in combination with a hydraulic jack at the cone tip, allows improving the penetration depth by utilizing the pressure in a cell that uses the cone rods and surface anchors on the ground surface as a reaction to push the cone down.

4) The in-situ consolidation test: The P-Cone, in combination with a hydraulic jack at the cone tip, also allows performing the in-situ consolidation compressive test for the fine-grained soils. This feature of the P-Cone has not been found in the current cone penetration test devices.

It has become clear that the P-Cone device offers many advanced features in comparison with the current cone penetration devices; however, the first version of the P-Cone device has several limitations. First, the electric movement measurement instruments (the linear displacement transducers) were replaced by the mechanical

instruments (telltales and dial gauges) to save cost. Secondly, the porous element and the pressure transducer used to measure pore pressure at the shoulder of the cone tip have not been equipped yet. Finally, the load cell to tip resistance has not been yet been installed. It should be noted that these non-equipped instruments have not had any influence on the experiments of the P-Cone in the unsaturated soil chambers.

Chapter 4

Experimental Program

4.1 Introduction

Several important factors were considered before initiating the experimental program for the P-cone device in the laboratory. These included the effects of the boundary conditions, the lateral pressure components, the saturated or unsaturated status of the soil, the investigation of the work of the P-cone device, the investigation of the failure shape of the soil around the cone tip, and the availability of equipment in the laboratory.

After considering the above, clayey silt soil with high plasticity was selected to reduce the effects of the boundary conditions, and lateral pressure components were selected for the available chamber that had a 590-mm diameter and 900-mm height. The clayey silt soil was chosen because it makes the investigation of the work of the P-cone device and the failure shape of the soil around cone the tip easier. To accomplish this study's objective, unsaturated compacted soil was used for all of the P-cone device tests, except for the consolidation compressive test. Figure 4-1 shows the site location of the soil that was used for the laboratory testing.

The P-cone device is considered as a model pile; therefore, the experimental program consisted of penetration tests, conventional static load tests, bidirectional load tests, and end bearing tests in three compacted soil chambers, with different densities and water content. Another compacted soil chamber was saturated to perform the consolidation compressive tests. Details of the experimental program of the P-cone device are presented in the following.

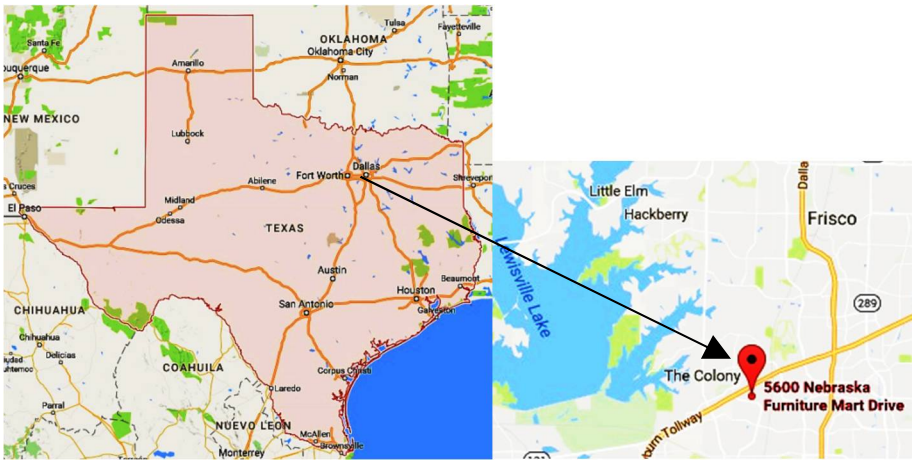

Figure 4-1 Site location of the soil used for the P-cone device test

4.2 Laboratory Test Program

4.2.1 Soil Preparation

The silty clay soil was collected at the site of the Nebraska Furniture Mart project (Figure 4-2a) located at 5600 Nebraska Furniture Mart Drive, The Colony, Texas, 75056. Approximately 1.0 $m^3$of soil was collected, which was enough for performing the P-cone device tests in the laboratory (Figure 4-2b).

a) b)

Figure 4-2 Soil collection: a) Soil at the site; b) Collected soil

The collected soil was dried (Figure 4-3a) and then crushed (Figure 4-3b). The soil was mixed to ensure the soil's homogeneousness for the compacted soil chambers (Figure 4-3b). After that, the mixed soil was sampled for the sieve analysis, Atterberg limit determination, specific gravity determination, and the Standard Proctor Test.

a) b)

Figure 4-3 Soil preparation: a) Dried soil, b) Soil mixing after crushing

4.2.2 Sieve Analysis

The sieve analysis was conducted according to ASTM Standard C117-03, "Materials Finer than 75-μm (No. 200) Sieve in Mineral Aggregates by Washing," and C136-01, "Sieve Analysis of Fine and Coarse Aggregates."

Three soil samples were taken from the mixed soil batch to perform the sieve analysis. The weight of each sample was 1000 g after drying at a temperature of 115^0C in the drying oven. After drying, the test samples were placed in the container, and sufficient water was added to cover them. Four days after being covered by water, the test samples were poured into the 75-μm (No. 200) sieve and washed until all of the finer grains adhering to larger particles had passed through the 75-μm (No. 200) sieve. All of the materials that remained on the 75-μm (No. 200) sieve were put into a pan for oven

drying at a temperature of 115^{0}C to a constant weight, and then the dry weights were recorded. The dry weights were used for the sieve analysis, following ASTM Standard C136-01, with sieve openings of 4.75 mm (No. 4), 2.00 mm (No. 10), 0.85 mm (No. 20), 0.60 mm (No. 30), 0.425 mm (No. 40), 0.25 mm (No. 60), 0.15 mm (No. 100), 0.075 mm (No. 200) and pan (Figure 4-4).

A set of used sieve openings

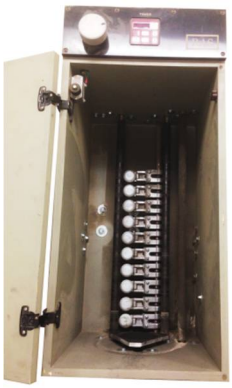
Electromechanical sieve shaker


2kg scale

Figure 4-4Tools used for the grain size analysis.

Hydrometer analysis was conducted according to ASTM Standard D422-63 (Reapproved 2007). Figure 4-5 shows the equipment used for the hydrometer analysis of the fine-grained soils. Three samples of the soil passing through the 75-μm (No. 200) sieve were taken from the mixed soil batch (Figure 4-2b) to perform sedimentation tests, using a hydrometer. The weight of each sample was 50 g after drying at a temperature of 115^{0}C to a constant weight. After drying and determining the mass, the soil samples were placed into 250 mL beakers and covered by 125 mL of sodium hexametaphosphate solution. The soil samples were stirred until the soil was thoroughly wetted, then soaked for 48 hours.

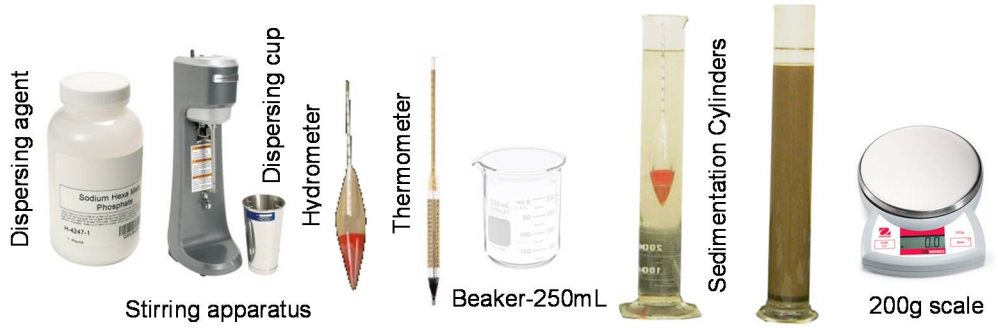

Figure 4-5 Apparatus to perform sedimentation test by use of a hydrometer.

The soil samples were dispersed further by using a stirring apparatus at the end of the soaking period. The soil-water slurry from the beaker was transferred into the dispersion cup and then stirred for a period of one minute. Immediately after dispersion, the soil-water slurry was given into the glass sedimentation cylinder, and the distilled water was added until the total volume reached 1000 mL. Then, a rubber stopper was inserted into in the open end of the cylinder, and the cylinder was continuously turned upside down, then right side up for a period of one minute. At the end of one minute, the cylinder was set in a convenient location, and hydrometer readings were taken at the following intervals of time: 0.25, 0.5, 1, 2, 4, 8, 15, 30, 60,120, 240, 480, 1440, and 2880 minutes.

Figure 4-6 presents the results of the sieve and hydrometer analyses for three soil samples, as well as the average particle-size distribution curve. The soil analysis indicated that the tested soil consisted of 0.1% gravel-size particles, 16.4% well-graded sand, 65.7% silt, and 17.8% clay-size particles.

The textural triangle of the United States Department of Agriculture (USDA) was used to determine the soil textural class from the determined fractions of 16.4% sand, 65.7% silt, and 17.8% clay, as shown in Figure 4-7.

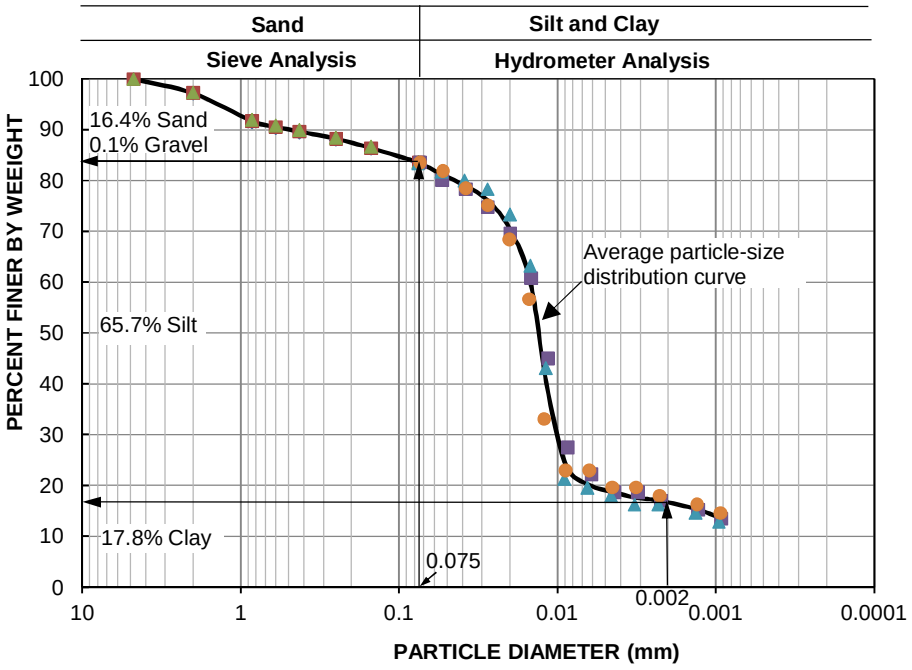

Figure 4-6 Particle-size distribution of the tested soil samples

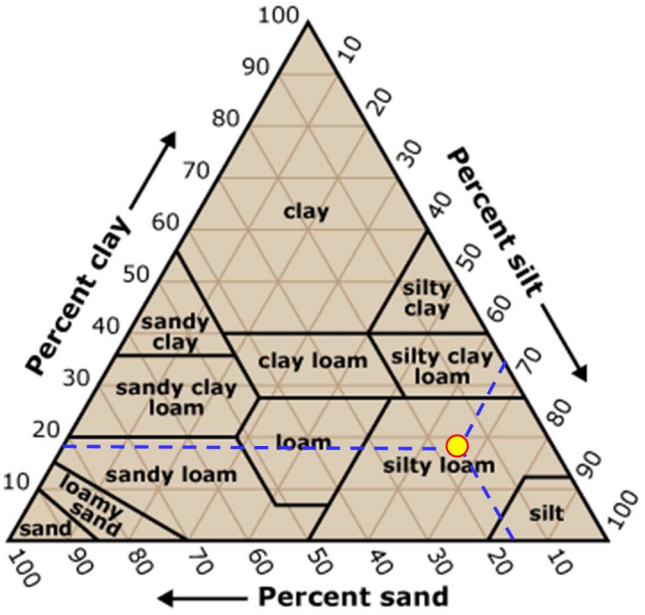

Figure 4-7 Soil classification following USDA textural triangle.

4.2.3 Consistency Limits

The soil consistency limit tests were carried out according to ASTM Standard D4318-05 to determine the liquid limit, plastic limit, and plastic index of the soils. Figure 4-8 shows the Casagrande tools used for the liquid limit test. The three soil samples passing through the 0.425 mm (No. 40) sieve were prepared for the liquid limit tests. The weight of each soil sample was about 200 g. The soil samples were mixed with distilled water in a mixing dish, using a spatula, and were tempered for 24 hours. (The wet preparation method was used for the tested soil samples.) The water content of the soil samples was adjusted to obtain a consistency of about 25 to 35 blows for the liquid-limit device to close the groove. (The multipoint liquid limit method was used for the tested soil samples.)

Before beginning the test, the prepared soil samples were remixed and placed into the cup of the liquid-limit device at the point in which the cup rests on the base. Then, the soil in the cup was squeezed down and spread into a 10 mm depth at its deepest point, then tapered to form an approximately horizontal surface.

Figure 4-8 Casagrande tools for liquid limit test.

Next, the grooving tool was used to cut an arc-shaped groove on the soil in the cup. The grooving tool was held perpendicular to the surface of the cup during cutting the groove. After that, the cup was lifted and dropped by means of turning the crank at a rate of 2.0 drops per second, until the two halves of the soil pat contacted with the groove bottom along a distance of 13 mm. The number of drops, N, was recorded. Following this, a slice of soil approximately the width of the spatula was taken, contained in a moisture can, and placed in the drying oven to determine the water content of the tested soil sample.

The process was repeated by returning the remaining soil inside the cup to the mixing dish and remixing whole soil specimen by supplementing the distilled water to increase the water content in the soil and reduce the number of blows required to close the groove. The cup and grooving tool were washed and dried before starting the next trial. The results of the liquid limit tests on the three representative soil samples are shown in Figure 4-9. Based on the flow curve obtained from the linear regression analysis of the test data, the liquid limit determined was about 60% at the blow number of 25.

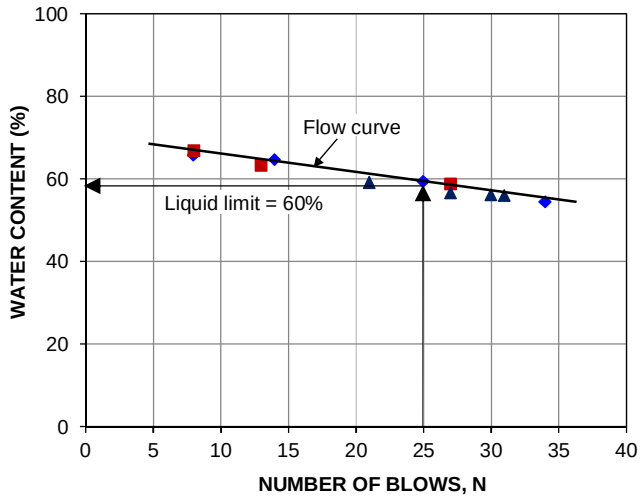

Figure 4-9 Liquid limit determination of three tested clayey silt soil samples

Figure 4-10 shows the tools for performing the plastic limit test. The plastic limit test tools consisted of a square plastic limit glass plate with a 0.3 m diameter, a 3 mm diameter steel rod, a mixing dish, a flexible spatula, a distilled water bottle, 200 g scale, and six moisture cans. The 20 g of soil needed for this test were taken from the soil prepared for the liquid limit test.

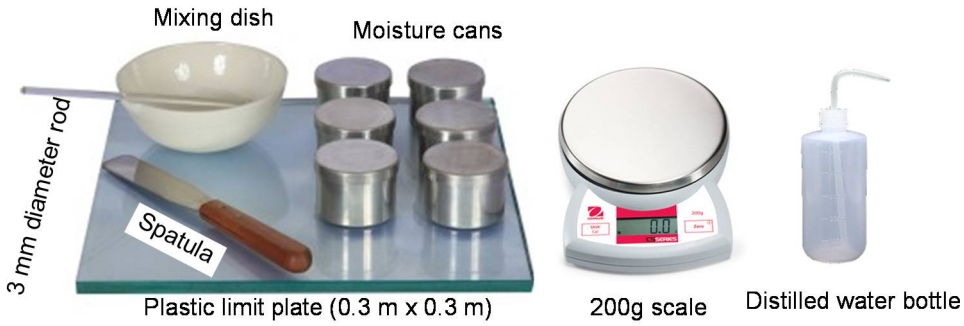

Figure 4-10 Tools for plastic limit test

The water content of the soil was reduced to a consistency where the soil could be rolled without sticking to the hands and then the soil was mixed continuously on the glass plate. The drying process of soil was increased by an electric fan, and a 2.0 g portion was selected to form an ellipsoidal mass. The mass was rolled by the palm with just enough pressure to roll it on the glass plate into a uniform diameter of about 3.2 mm. When the mass became a thread of 3.2 mm diameter, the thread was broken into several pieces and were squeezed together to form an ellipsoidal mass. Then, the mass was re-rolled to a thread of 3.2 mm diameter. This process was repeated until the thread crumbled under the pressure required to roll and the soil could no longer be rolled into a thread of 3.2 mm diameter. After that, the portions of the thread crumbled were gathered together and placed in a moisture can to put into the drying oven. The five other 2.0 g portions of soil from the plastic–limit specimen were tested similar to the above

procedure. The results of the six plastic limit tests showed an average plastic limit of 26%. Thus, the plastic index determined from the difference between the liquid limit and the plastic limit was about 34%. Based on the fine fraction of 83.5 % (65.7% silt and 17.8% clay), the liquid limit of 60% and the plastic index of 34%, the soil was classified as clayey silt with high plasticity (Figure 4-11).

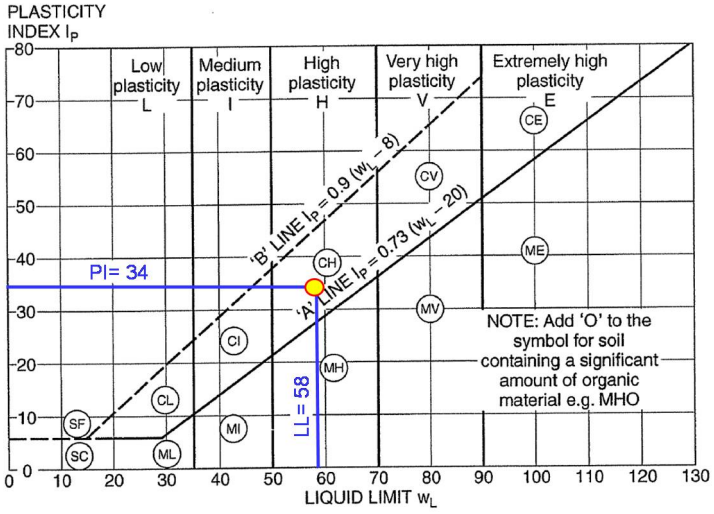

Figure 4-11 Plasticity chart (Head, 2006)

4.2.4 Specific Gravity

The specific gravity of the soil was determined according to ASTM Standard D854-14. Figure 4-12 shows the tools used for testing the specific gravity of the soil solids, using the Water Pycnometer Method. The tools used were a cylinder, distilled water bottle, dish, funnel, spoon, thermometer, 200g Scale and 500 mL pycnometers. (A 500 mL volumetric flask was used as a pycnometer.)

The five representative soil samples were taken from the mixed soil batch that passed through the 4.75-mm (No. 4) sieve and were dried. The weight of each soil sample after being dried was about 50 g. These soil samples were poured into the clean

and dry volumetric flasks, using a funnel and a spoon. It should be noted that the volumetric flasks were calibrated, and the mass was determined by following the instructions of ASTM Standard D854-14. Then, the volumetric flasks were filled to the calibration mark with de-aired water.

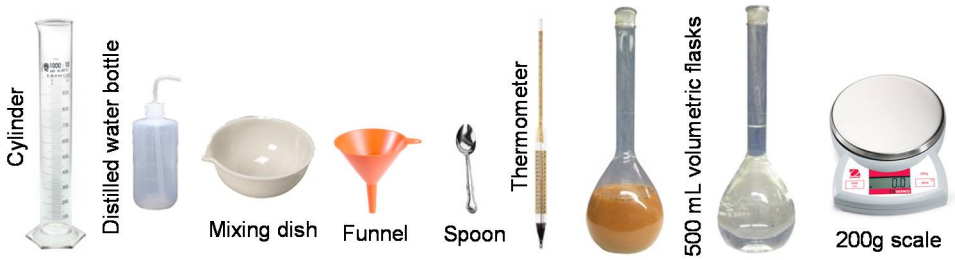

Figure 4-12 Tools used for testing specific gravity of soil

The water levels in the volumetric flasks were adjusted to the calibration mark before measuring and recording the mass of the volumetric flasks, water, and soil. The temperature of the water was measured by a thermometer and recorded to calculate the specific gravity of soil solids at 20°C. The specific gravity of the soil solids at the measured temperatures was determined as the ratio between masses of equal volume of soil solids and water. The specific gravity of the soil solids at 20°C was then calibrated according to ASTM Standard D854-14. The test results of the five tested soil samples indicated that the average specific gravity of the soil solids at 20°C was about 2.693.

4.2.5 Standard Proctor Test

Standard Proctor Tests were performed according to ASTM Standard D 698-07. Figure 4-13 shows the tools used for the tests: a 2.5 kg hammer, a mold with volume of 944 cm^3 and diameter of 101.6 mm, moisture cans, mixing bowl, trowel, scale, straight-edge blade, and water spray bottle. The 2.3 kg soil passing through the 4.75 mm (No. 4)

sieve was taken from the mixed soil batch to prepare the Standard Proctor Test. The mass of the mold and base plate were measured and recorded after the mold was affixed to the base plate. Then, the water-mixed soil was compacted into three layers by a hammer, after being placed into the mold and spread into a layer of uniform thickness.

Figure 4-13 Tools used for the Standard Proctor Test

Each soil layer was compacted with 25 blows; they were approximately equal in thickness after compaction. After the last layer compacted, the collar and base plate were removed from the mold, and the soil that extended above the top of the mold was trimmed carefully with a straight-edge blade. The mass of the specimen, mold, and base plate were measured and recorded to determine the moisture unit weight of compacted soil. The soil was removed from mold, and the representative soil portions of the soil layers were tested to determine the dry unit weight of the compacted soil and the water content of soil. The process was repeated with increased water contents of the soil by adding water from the water spray bottle. The dry unit weight determined from each soil compaction was plotted versus the corresponding moisture contents to gain the maximum dry unit weight of 15.3 kN/m^3 and the optimum moisture content of 21% for the tested soil, as shown in Figure 4-14.

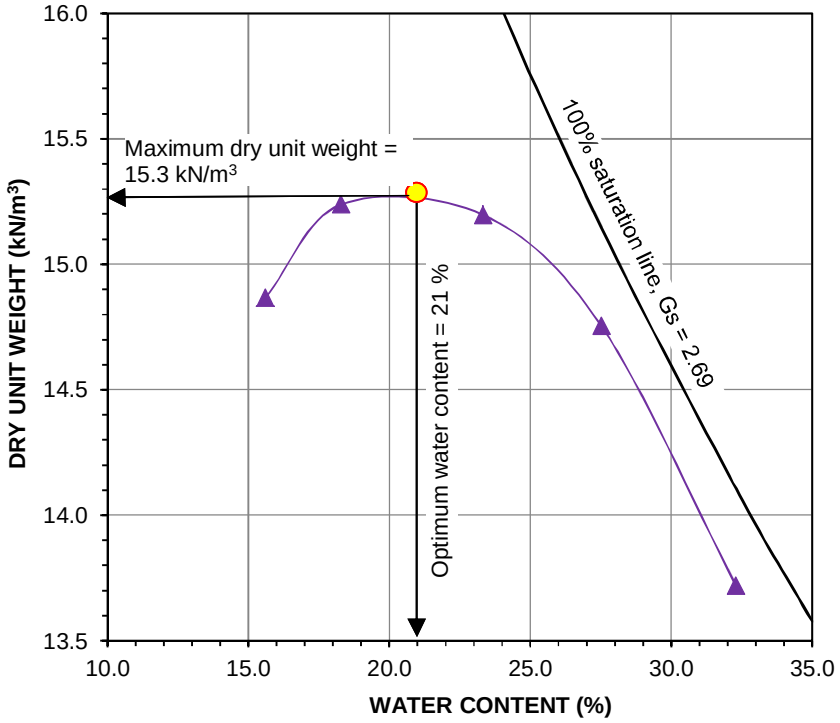

Figure 4-14 Standard Proctor compaction test results for the used clayey silt

4.2.6 Direct Shear Test

After the P-cone device tests, the compacted soil in the chamber was sampled at different depths to determine the density, water content, void ratio, degree of saturation, and the shear strength properties (Figure 4-15). A sampling ring with dimensions of 25.4 mm (1 inch) in height and in 63.5 mm (2.5 inches) in diameter was used.

The strain-controlled direct shear tests were performed on the compacted clay silt soil samples with a shear rate of 0.125 mm/minute. The strength of the soil obtained from shear tests at this shear rate is considered as the undrained strength and is reasonable for correlating with the quick load test results of the P-cone device. The

normal stresses applied to the direct shear tests ranged from 3.6 to 28.7 kPa (75 to 600 psf), which is suitable for considering the P-cone device tests in the shallow soil chamber.

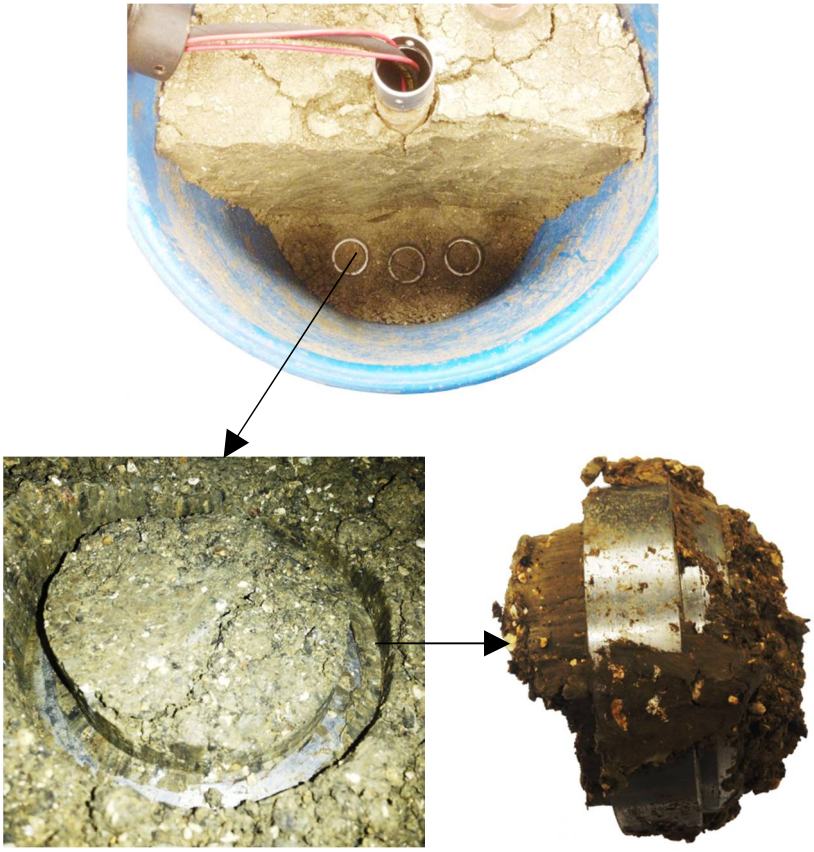

Figure 4-15 Soil sample extraction from the compacted soil chamber after the P-cone device tests

The advantage of using the direct shear test, in comparison with a simple shear test, is that it is possible to measure both the peak and residual shear strength when conducting the direct shear test. Moreover, it is performed directly on the soil samples extracted from the compacted soil chamber used for the P-cone device tests instead of using the triaxial compression equipment on soil samples that need to be prepared separately. Another advantage, in comparison with the triaxial compression equipment, is

the shear failure of the soil samples close to the shear failure of soil along the cone shaft. Figure 4-16 shows the direct shear device and the measurement system used for this study. The results from the direct shear test are given in Chapter 5.

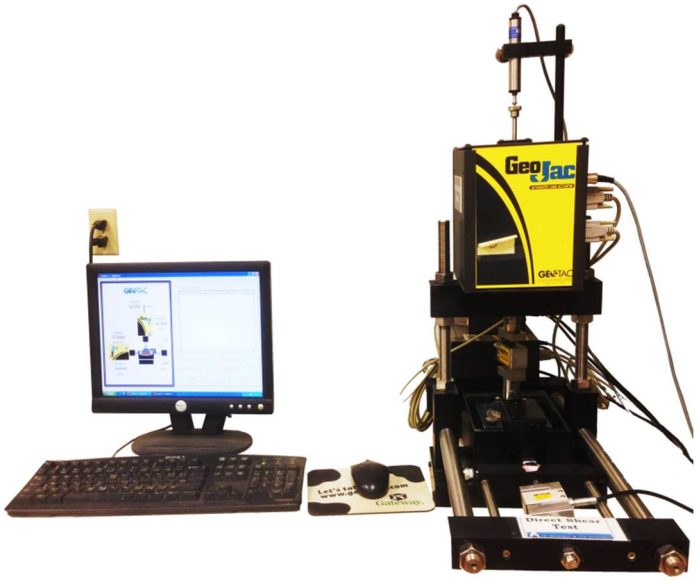

Figure 4-16 Direct shear test apparatus

4.2.7 One-Dimensional Consolidation Test

The one-dimensional consolidation test was conducted according to ASTM Standard D 2435-11 to determine the compression index, secondary compression, the rate of secondary compression, and the consolidation coefficient for saturated compacted clayey silt. For this test, a soil sample was confined laterally and loaded axially with the increments of the total stress. Each load increment was held until excess pore water pressures were essentially dissipated. The load-holding time for each load increment was equal to 24 hours. Because the instruments to measure the pore pressure dissipation was not equipped, the pore pressure was assumed to be dissipated based on the interpretation of the time-settlement curve obtained from constant total stress. The soil

samples are assumed to be 100% saturated after soaking in water for four days. Changes in the measurements of the soil specimen height were used to calculate the void ratio (or strain) and the effective axial stress. Readings of settlement versus time were taken throughout, and the consolidation rate was evaluated by the consolidation coefficient.

Figure 4-17 shows the apparatus used for the one-dimensional consolidation tests. The soil specimens prepared for the consolidation tests were sampled directly from the compacted soil chamber. After the soil specimens were placed in the consolidometer and the loading device, a seating load of 3 kPa was applied to keep the soil specimens from swelling.

Figure 4-17 Consolidation compressive test apparatus

The soil specimens were soaked for four days before starting the consolidation tests. The loading schedule consisted of a load increment ratio of one, which was gained by approximately doubling the total axial stress on the soil samples to get values of about

500, 1000, 2000, 4000, 8000, 16000, 32000 lb./ft^2 (24, 48, 96, 192, 383, 766, 1532 kPa). Readings of settlement versus time were taken on all applied loading levels and the successive load increments were applied after 100% primary consolidation was obtained. The results obtained from these one-dimensional consolidation tests were correlated with the consolidation test results obtained from the P-cone device, as presented in Chapter 5.

4.3 P-cone Device Test Program

The P-cone test device testing program was performed in three compaction-unsaturated-soil chambers to study the P-cone device as a small model pile foundation. Consolidation tests were also conducted in a compaction-saturated-soil chamber to study the potential application of the P-cone device for the in situ consolidation test.

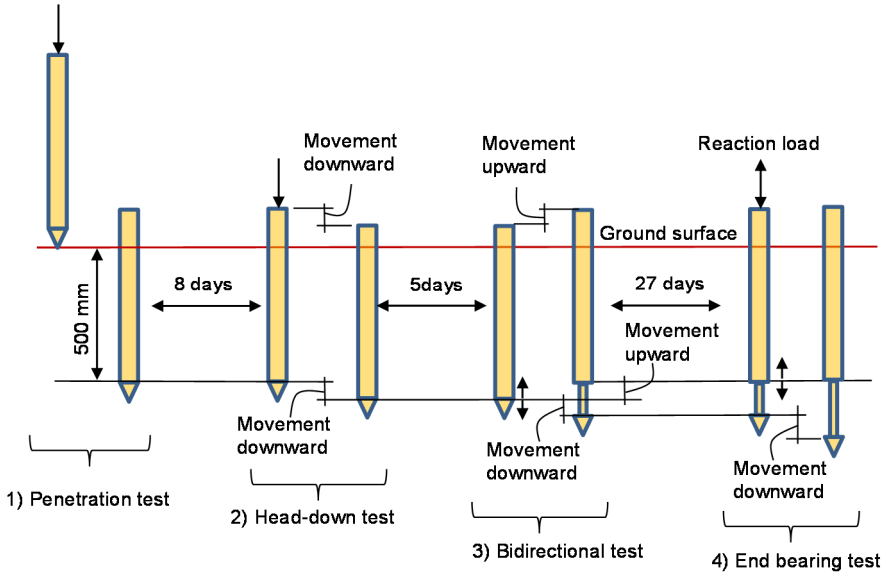

Figure 4-18 Test procedure of the P-cone performed

The P-cone device tests in the three compaction-unsaturated-soil chambers, with different densities and water contents, included the cone penetration tests, conventional

static load tests (head-down test), bidirectional tests, and the end bearing tests (Figure 4-18). The consolidation tests by the P-cone device in a compaction-saturated-soil chamber are presented in Section 3.3.5 below.

4.3.1 Setup of Soil Chamber and Loading System

A circular chamber with diameter and height of 590 mm and 889 mm, respectively, was used in the present research, as shown in Figure 4-19. The ratio of the chamber diameter to the cone diameter was about 9. Therefore, the effect of the chamber boundaries on the P-cone penetration test were considered in the interpretation of the test results (Ghionna and Jamiolkowski, 1991; Salgado et al., 1998).

Figure 4-19 also shows the tamper, mixer, and cement color used for the soil compaction. The weight and drop height of the tamper were about 0.06 kN and 0.5 m, respectively.

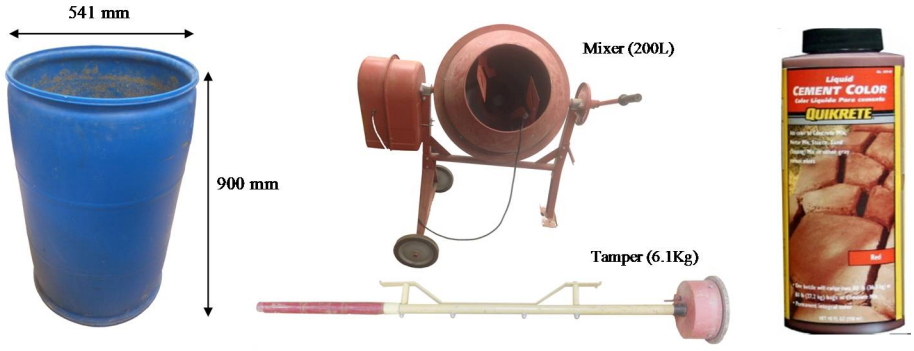

Figure 4-19 Soil box, portable mixer, tamper, and cement color used for soil compaction

After placing alternating layers of colored and non-colored soil into the chamber, the compaction was performed by using a tamper with a foot diameter of about 180 mm.

Each soil layer was subjected to 75 to 125 blows to produce a thickness of about 80 mm per lift after compaction. The total thickness of the soil in the chamber was comprised of about ten such compacted layers.

Figure 4-20 indicates the loading system setup for the testing. The loading system consisted of a steel frame, a 80-kN hydraulic jack with an opening of about 0.6 m, and a 100-kN hand pump. The cone penetration test was performed by increasing the fluid pressure inside the jack, via the pump handle, to push the cone into the chamber. The jack was also used for the conventional static load tests and the end bearing tests.

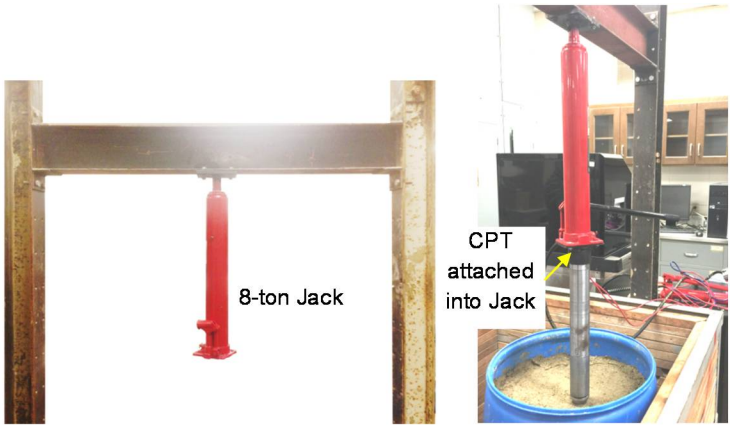

Figure 4-20 Jack attached to steel frame as reaction system

4.3.2 Cone Penetration Test

The cone penetration test was performed by pushing the cone 0.5 m below the ground surface with a penetration rate varying from 3 to 10 mm/s because datalogger system had low sample rate (sample rate of 1 per 10 seconds) (Figure 4-21). It should be noted that the standard penetration rate of 20 mm/s was not considered due to the penetration performed in the compaction-unsaturated soil and thus the influence of the penetration rate on the strength of soil obtained from penetration test was not significant. After connecting the hand pump to the jack and the reaction beam, the release valve of

the pump was closed and the control valve was opened to push the cone tip open about 5 mm (Figure 4-19). At this time, the fluid pressure value of the P-Cone was taken as the initial fluid pressure value. It should be noted that the 5 mm expansion of the cone tip was necessary so that the influences of the fluid compressibility and dilatation of hose on the measured cone tip resistances could be eliminated. After that, the control valve was closed, and the P-Cone was pushed into the ground by the jack, which was attached to the reaction beam via the handle. During penetration, the cone tip resistance and the sleeve friction were measured by a pressure transducer and the strain gages, respectively. The test results are reported in Chapter 5.

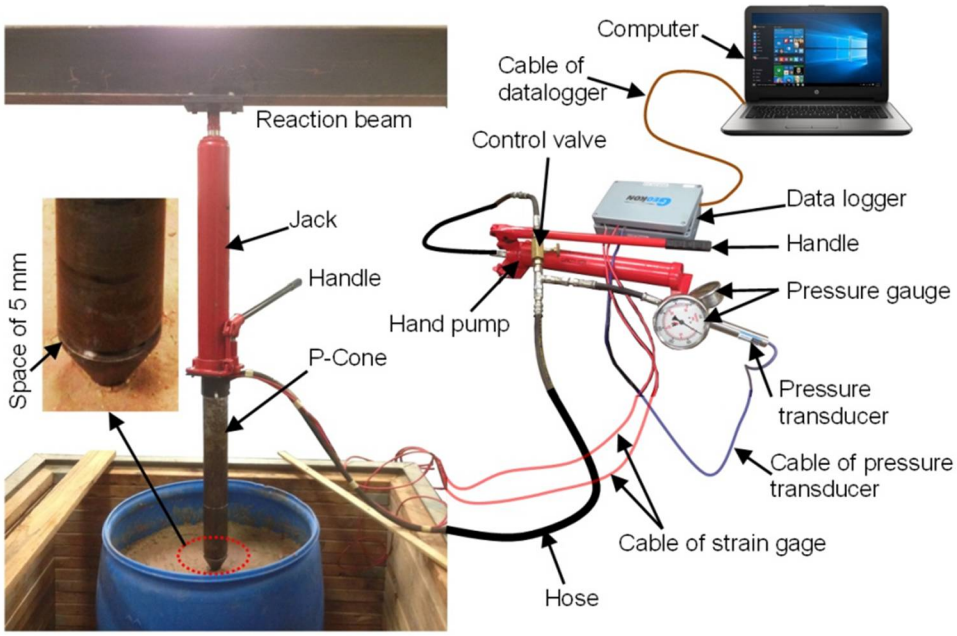

Figure 4-21 P-Cone penetration tests and measurements

4.3.3 Conventional Static Load test

The P-cone device, after being pushed into the ground, was considered as a small model pile. Therefore, the same conventional static load tests (head-down tests) on the P-cone device were performed as they were on the pile. Five to seven days after the cone penetration test, the conventional static load tests were conducted according to the quick loading method of ASTM Standard D1143-81. Figure 4-22 shows the setup for the head-down tests on the P-cone device. The loading was performed with the hydraulic jack placed at the top of the cone assembly, and the load imposed on the cone head was recorded by using a load cell (left side of Figure 4-22).

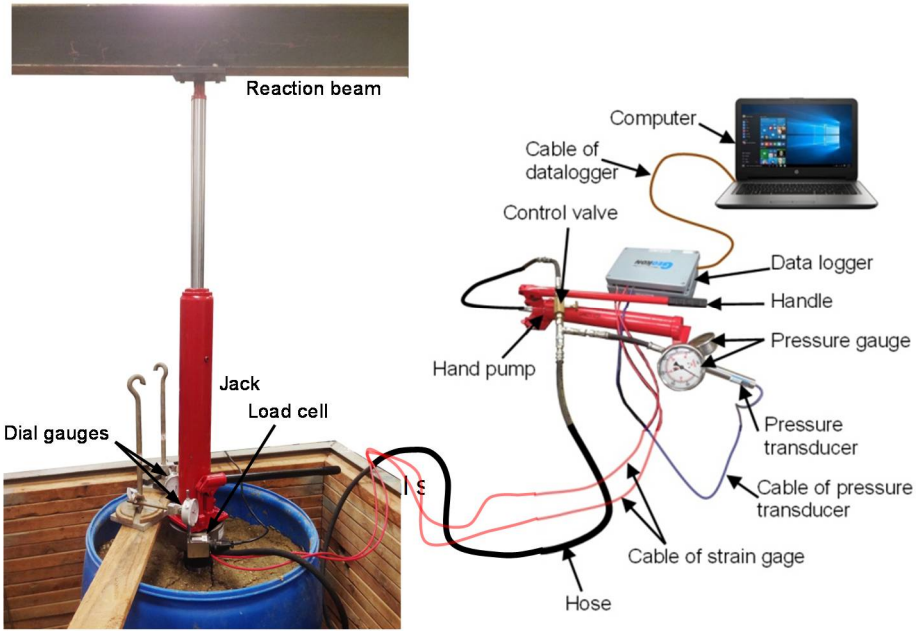

Figure 4-22 Conventional static load test and measurement

The movements were measured by dial gauges. During loading, the P-cone shaft and tip resistances were also measured and recorded by strain gages and the pressure transducer (right side of Figure 4-22). The head-down tests were performed in one cycle, with many small-load increments, until the bearing capacity of the model pile was

reached. Each of the 27 load increments was held constant for five minutes, and the unloading was performed in three steps. The head-down test results are presented in Chapter 5.

4.3.4 Bidirectional Load test

The bidirectional load tests were carried out five to ten days after the head-down test (Figure 4-23). The jack was removed, and the movement-measuring instruments were installed (Figure 4-23).

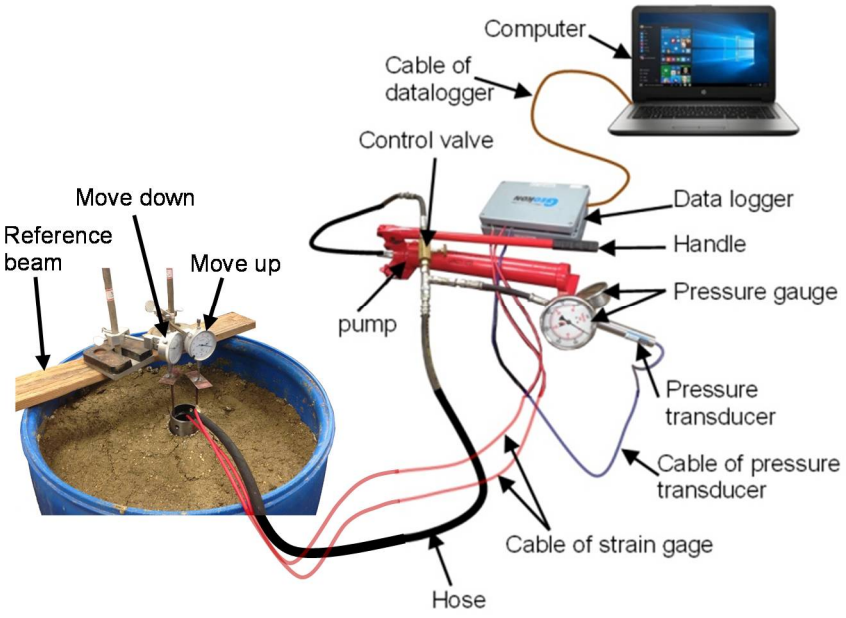

Figure 4-23 Bidirectional load test and measurement

The bidirectional load tests were performed according to the quick loading method of ASTM Standard D1143-81. The loading was carried out in many load increments, ranging from about 5 through 138 N, and the unloading was performed in

several steps. Each of the load increments was maintained from one to five minutes. The bidirectional load test results are presented in Chapter 5.

4.3.5 End Bearing Load Test

Normally, the bidirectional load tests fully mobilize one of the two resistance components of the pile, either the shaft resistance or the tip resistance, as explained earlier in Chapter 2. For the subject cases, the shaft resistance of the model pile was relatively small and not sufficient to fully mobilize the pile tip resistance due to the embedded pile length of 0.5 m. Therefore, the end bearing load tests were necessary to determine the ultimate bearing capacity of the pile tip for the purpose of re-evaluating the equivalent pile-head load-movement curve construction method. The end bearing load tests were performed by adding a reaction load at the pile head so that the shaft resistance plus the reaction load is enough to mobilize fully the pile tip resistance. Figure 4-24 shows set-up of the end bearing load test and the measurement.

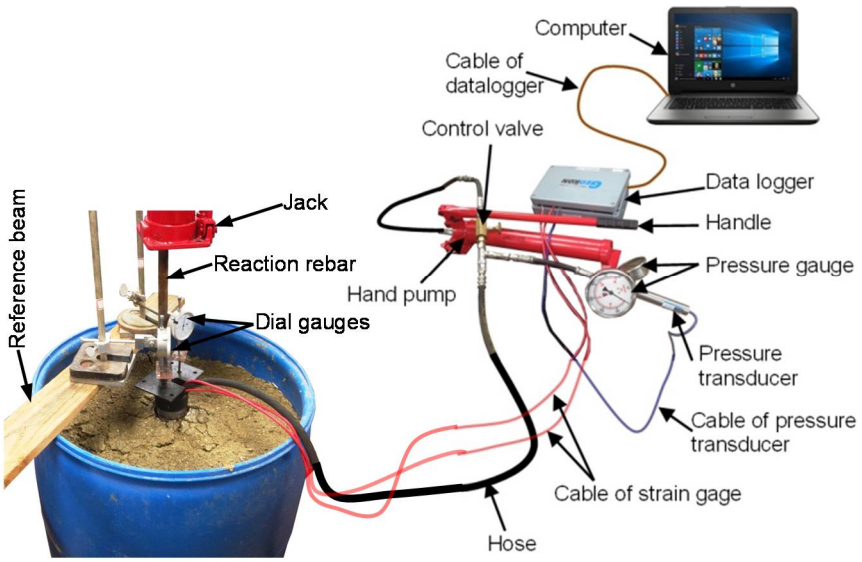

Figure 4-24 End bearing load test and measurement

The end bearing tests were conducted from five to twenty-seven days after the bidirectional tests. The load increments for the tests were performed in 9 to 44 increments, ranging from about 6 through 470 N, and the unloading was performed in several steps. All of the load levels were maintained from one to five minutes. It should be noted that the shaft resistance versus the movement upward was not measured during the end bearing load tests.

4.3.6 Consolidation Test by P-cone Device

Geotechnical engineers often face the challenges of predicting long-term settlement of piled foundations and earth structures. To obtain a more accurate prediction of the settlement, it is necessary to know the exact consolidation characteristics of the soil under an applied load. The consolidation characteristics of the soil obtained from the conventional one-dimensional consolidation tests are affected by many factors, such as the one-directional vertical drainage path, the laterally restrained soil specimen, the friction between the soil and the consolidation ring, partial saturation, sample size, disturbance, etc.

An attempt was made to carry out the consolidation tests on the P-cone device in the compaction-saturated soil chamber. A cone tip with an apex angle of 120^0 (Figure 3-5) was used to replace the 60^0 cone tip, and a compaction-saturated soil chamber was prepared for the consolidation tests. The saturation of the compacted soil chamber was performed according to the following steps:

Step 1: After preparing a compacted soil chamber, a borehole of 60 mm diameter, adjacent to the wall of the chamber, was drilled through the thickness of the soil layers and compacted in the chamber to shorten the saturation time. Then, the

compacted soil chamber was filled with water to about 15 cm above the ground surface, and was maintained for 45 days.

Step 2: After being soaked in the water for 45 days, the compacted soil chamber was dewatered to prepare for the installation of an open standpipe. The open standpipe, of 30-mm diameter and 1000-mm length, was made of PVC plastic and had 5-mm diameter holes drilled at the bottom so that the water from the soil could enter the open standpipe (Figure 4-25). The standpipe was about 150 mm long and was covered by geotextile and tied by plastic O-rings to prevent the soil particles from entering the standpipe.

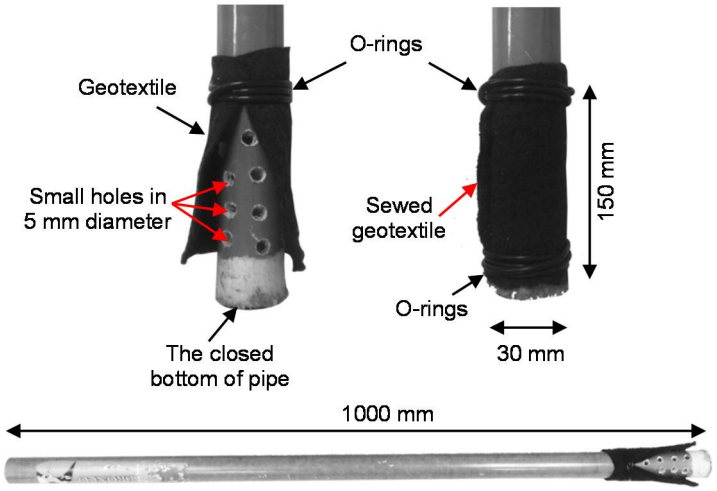

Figure 4-25 Open standpipe and filter at the bottom of the standpipe

The open standpipe was inserted into the compacted soil chamber via the available borehole. After that, the drilled hole was filled by bentonite-and-cement-water grout to prevent the surface water from entering the pipe (Figure 4-26a). The open standpipe, after installation, is shown in the right side of Figure 4-26b. After the open standpipe was installed, the compacted soil chamber was refilled with water to 150 mm above the ground surface, and was maintained for 30 days.

Step 3: The cone penetration test was performed 30 days after the compacted soil chamber was refilled with water, as shown in Figure 4-27. It remained saturated for 45 days.

Step 4: The first consolidation test was carried out 45 days after the cone penetration test was performed. Figure 4-28 shows the setup of the consolidation test of the P-cone device. The cone shaft resistance in this test case was relatively small and inadequate for pushing the cone tip down. Therefore, a rebar was added to the top of the P-cone, as a reaction load to push the cone tip down.

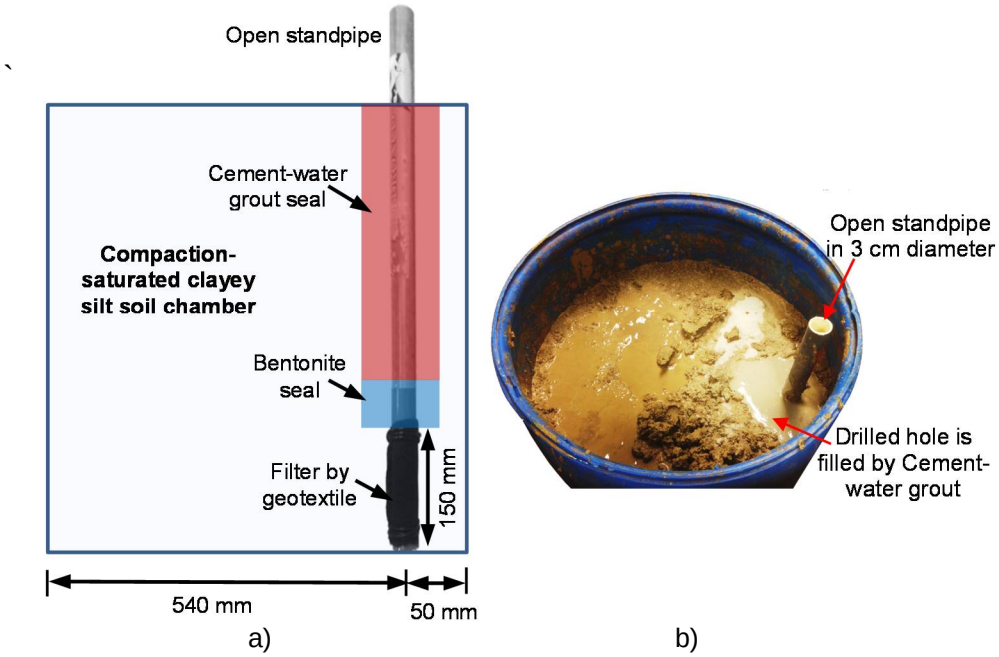

Figure 4-26 Open standpipe installation: a) Schematic of the standpipe after being installed in borehole; b) Standpipe after complete installation

The consolidation test by the P-cone device is illustrated in Figure 4-29. The loading procedure was performed with equal load increments of about 30 PSI. It should be noted that the load increment ratio of the ASTM Standard D 2435-11 cannot apply to

the consolidation test by the P-cone device because the bearing capacity of the soil below the cone tip is low. Moreover, the main reason the loading schedule of a one-dimensional consolidation test cannot apply to the equal load increments is because in doing so, the test results cannot provide the value of the pre-compression stress and the compression index (Leonard, 1962).

Figure 4-27 Cone penetration test performed 30 days after soil chamber was refilled with water

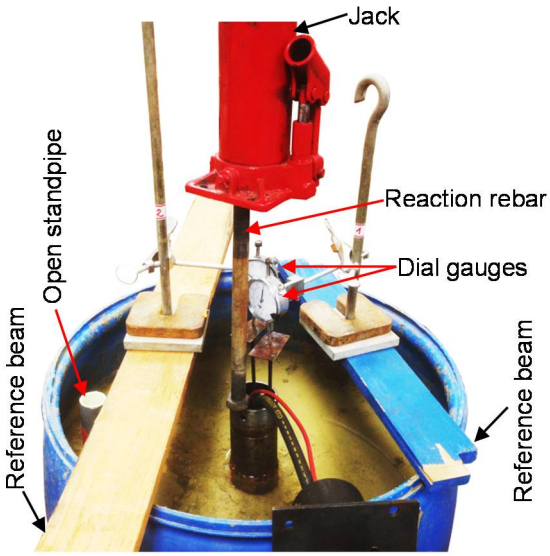

Figure 4-28 Setup of the consolidation test by the P-cone device

The experimental program of the P-cone device is summarized below. The basic laboratory tests of soil consisted of sieve size analysis, consistency limits, proctor tests, specific gravity, direct shear tests, and one-dimensional consolidation tests. The test results indicated that the soil was classified as clayey silt with 0.1% gravel, 16.4% sand, 65.7% silt, and 17.8 % clay. The liquid limit, plastic limit, and plastic index were about 58%, 26% and 34%, respectively. The average specific gravity was about 2.693, the maximum dry unit weight was about 15.3 kN/m^3, and the optimum moisture content was approximately 21%. The results of the direct shear tests and one-dimensional consolidation tests are presented in Chapter 5.

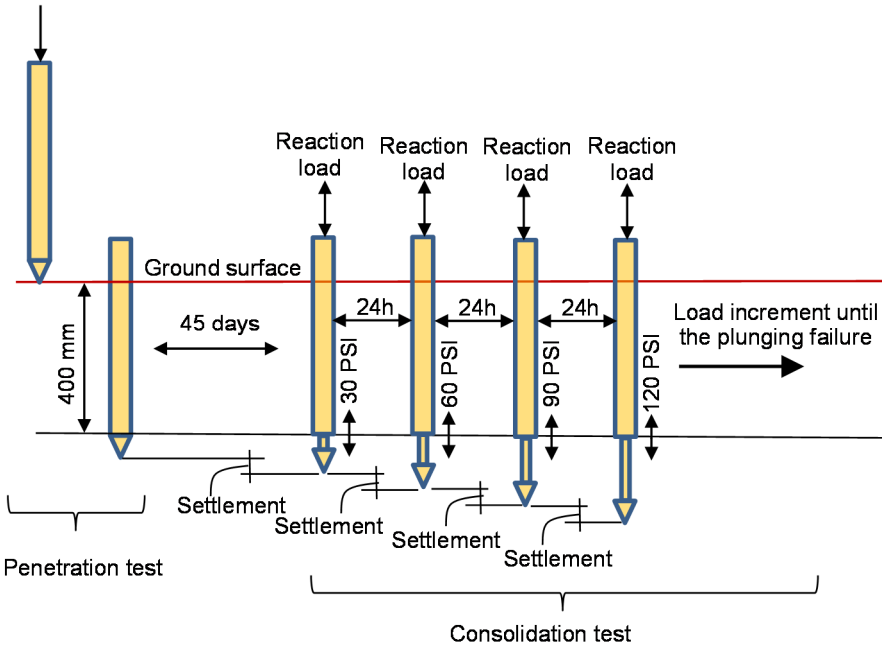

Figure 4-29 Loading procedure of the consolidation test by the P-cone

4.4 Summary

The P-cone device tests included cone penetration tests, head-down load tests, bidirectional load tests, end-bearing load tests, and consolidation tests. The P-cone device, after being pushed into the ground, was considered as a model pile. Therefore, the static load test results on the P-cone device allowed reconsidering the equivalent pile-head load-movement construction method. The consolidation test results by the P-cone device were compared with the one-dimensional consolidation test results. All of the P-cone device test results are presented in Chapter 5.

Chapter 5

Measurements and Analysis

5.1 Static Load Tests

5.1.1 Properties of Compacted Soils

5.1.1.1 Density and Water Content

After the P-cone device tests were performed, the compacted soil chambers were sampled at different depths to determine the density, water content, void ratio, degree of saturation, and shear strength properties. Three soil samples were taken from each layer to determine the water content of the soil, and three soil samples were taken by using the sampling ring to compute the soil density and to serve the direct shear tests. The soil test results if the three soil chambers are presented in Tables 1 through 3.

Table 5-1 presents test results of the first compacted soil chamber. For this soil chamber, four soil layers were sampled at depths of 113 through 607 mm. The soil test results showed that the average unit weight of the soil layers was about 19.0 kN/m^3 at moisture content of 25.0%. The average void ratio and degree of saturation calculated were about 0.736 and 95%, respectively.

Table 5-1 Densities and water contents of first soil chamber

Depth	Water Content (%)			Moisture Density (kN/m^3)		
Mm	1	2	3	1	2	3
113	24.3	24.6	25.0	19.0	19.1	18.8
300	25.6	23.5	25.3	18.9	18.9	19.4
497	25.0	25.6	25.1	19.3	18.5	18.8
607	26.5	25.6	24.7	19.0	19.1	19.5

Table 5-2 shows the test results of the second compacted soil chamber. For this soil chamber, ten soil layers were sampled at depths of 100 through 700 mm. The soil

test results showed that the average unit weight of the soil layers was about 19.5 kN/m^3 at moisture content of 25.7%. The average void ratio and degree of saturation calculated were about 0.704 and 98%, respectively.

Table 5-2 Densities and water contents of second soil chamber

Depth	Water Content (%)			Moisture Density (kN/m^3)		
mm	1	2	3	1	2	3
270	25.8	24.9	25.8	19.3	19.4	19.5
381	26.2	26.7	26.4	19.4	19.5	19.3
508	24.7	24.6	25.9	19.7	19.7	19.6
572	25.3	24.8	25.7	19.5	19.5	19.6
635	26.0	26.1	26.1	19.4	19.2	19.3

Table 5-3 presents the test results of the third compacted soil chamber. For this soil chamber, eight soil layers were sampled from depths of 100 through 700 mm. The soil test results showed that the average unit weight of the soil layers was about 18.7 kN/m^3 at moisture content of 29.4%. The average void ratio and degree of saturation calculated were about 0.826 and 96%, respectively.

Table 5-3 Densities and water contents of third soil chamber

Depth	Water Content (%)			Moisture Density (kN/m^3)		
Mm	1	2	3	1	2	3
100	30.0	30.1	30.3	18.7	18.5	18.9
180	29.0	29.1	28.1	18.3	18.7	19.1
270	30.2	29.4	29.2	18.7	18.5	19.1
350	29.7	29.0	28.7	18.7	18.4	18.9
430	29.7	29.3	29.8	18.6	18.1	18.9
500	31.0	28.9	29.3	18.7	18.5	18.9
600	29.2	29.6	29.6	18.7	18.6	19.2
700	29.3	28.4	29.0	18.8	18.6	19.1

5.1.1.2 Shear Strength Parameters

Strain-controlled direct shear tests were performed on the soil samples taken from the chambers with a shear rate of 0.125 mm/minute. For this shear rate, the strength of the soil obtained from the shear tests can be considered as the undrained strength, which is reasonable for correlating with the quick load test results of the P-cone device. The direct shear test results are presented in Figure 5-1.

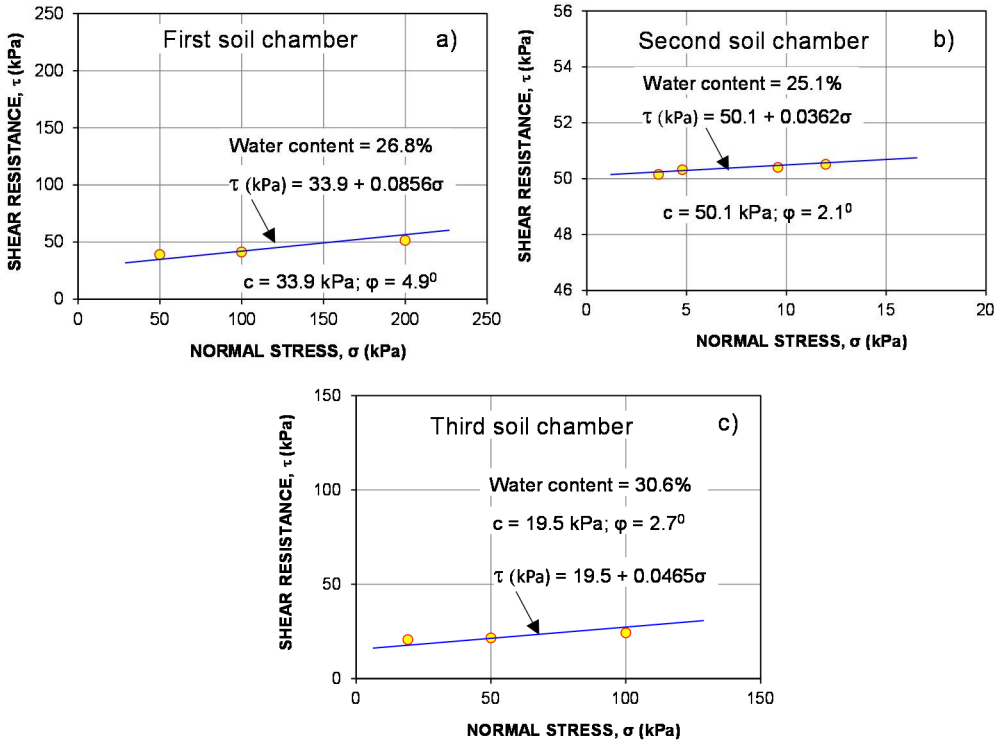

Figure 5-1 Direct shear strength of soil in three soil chambers: a) First soil chamber, b) Second soil chamber, and c) Third soil chamber

Figure 5-1a) presents the direct shear test results of the four soil samples taken from the first soil chamber. The normal stresses applied to these soil samples were relatively low, ranging from 3.6 through 12 kPa; however, these values are reasonable for

the actual conditions of the soil chamber. The results obtained from the direct shear tests showed a cohesion intercept, c, of 50.1 kPa and an angle of internal friction, ϕ, of 2.1°. Figure 5-1b) provides the direct shear test results of the three soil samples taken from the second soil chamber. The normal stresses applied to these soil samples ranged from 50 through 200 kPa. The results obtained from the direct shear tests showed a cohesion intercept, c, of 33.9 kPa and an angle of internal friction, ϕ, of 4.9°.

Figure 5-1c) depicts the direct shear test results of the three soil samples taken from the third soil chamber. The normal stresses applied to these soil samples ranged from 19 through 100 kPa. The results obtained from the direct shear tests showed a cohesion intercept, c, of 19.5 kPa and an angle of internal friction, ϕ, of 2.7°.

It should be noted that the tested soil samples were only partly saturated (degree of saturation around 95%); thus, when the total normal stress was increased, the strength of the soil was also increased because the total stress changes did not induce an equal increment of pore pressure. When the total stress imposed on a partly-saturated soil sample increased, both the pore pressure and the effective stress were slightly increased. This occurred because the mixture of water and air (the pore fluid) was compressible, and only a portion of the total stress added was carried by the pore fluid. The balance was carried by the skeleton of the soil grains, which led to an increase of the effective stress (Duncan and Wright, 2005). The movements necessary to obtain the peak values of the shear resistance on most of the tested soil samples were about 1.5 mm.

5.1.2 Penetration Tests

5.1.2.1 Penetration Resistance

The cone penetration tests were performed for three experimental soil chambers. The P-cone device was pushed 0.5 m below the ground surface with a penetration rate from 3 to 10 mm/s. The standard penetration rate of 20 mm/s was not considered due to the penetration performed in the compaction-unsaturated soil chambers. The penetration test results are presented in Figure 5-2 through 5-4.

Figure 5-2 shows the results of the cone penetration test in first soil chamber. As can be seen from the left diagram of Figure 5-2, the cone tip resistance increased linearly up to 200 mm of depth below the ground surface. At this depth, the cone tip resistance was measured at about 620 kPa. From 200 mm to 300 mm depth, the tip resistance reduced slightly and then decreased linearly to about 400 kPa at 500 mm depth. The right diagram of Figure 5-2 represents the cone shaft resistances up to 300 mm depth below the ground surface. The maximum shaft resistance measured was about 35 kPa at 100 mm depth. Below this depth, to 300 mm, the shaft resistance reduced gradually to about 12 kPa. The results of penetration indicated that the soil layers between 200 mm and 300 mm depths were more compacted.

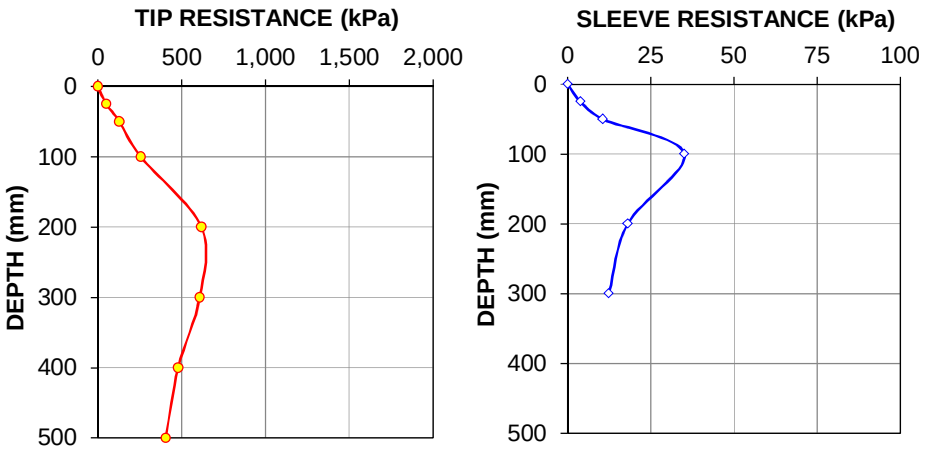

Figure 5-2 Shaft and tip resistance of cone penetration test in first soil chamber

Figure 5-3 shows the results of the cone penetration test in the second soil chamber. The left diagram of Figure 5-3 indicates that the cone tip resistance increased linearly to 1,618 kPa at 200 mm of depth. Below this depth, the cone tip resistance change was insignificant. The right diagram of Figure 5-3 represents the cone shaft resistances up to 300 mm of depth, below ground surface. The measured cone shaft resistance of 200 mm below ground surface was not significant. Below 200 mm depth, the average shaft resistance was about 28 kPa. The measurements indicate that the soil profile below 200 mm of depth was relatively homogeneous. The shaft resistances measured below 200 mm depth were significantly fluctuated. It is likely that the measurements were influenced by either the non-uniform penetration rate or the installation of strain gages, or both.

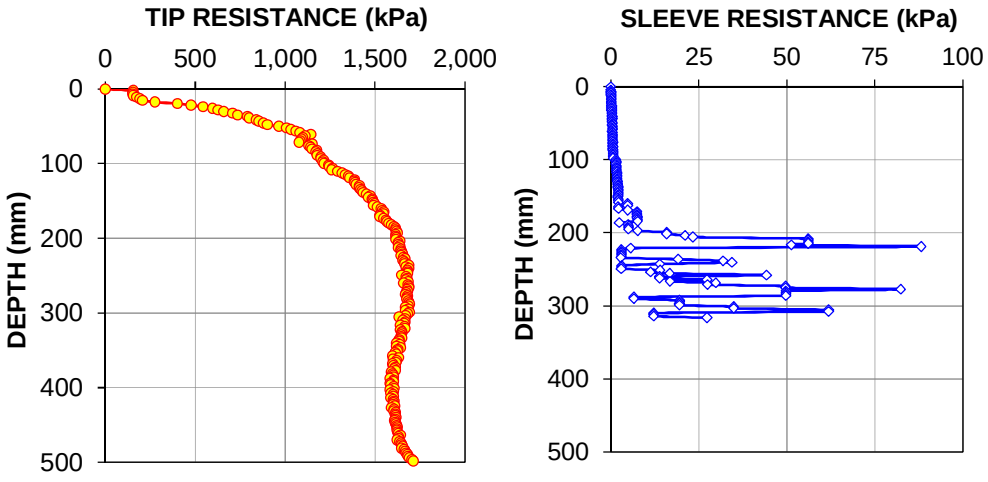

Figure 5-3 Shaft and tip resistance of penetration test in second soil chamber

Figure 5-4 shows the results of the cone penetration test in the third soil chamber. The left diagram of Figure 5-4 displays the cone tip resistance versus depth. It is interesting to see that the tip resistance was relatively steady throughout the penetrated depth, indicating that the soil compacted in the third chamber was relatively

homogeneous. The average tip resistance was about 576 kPa. The right diagram of Figure 5-4 represents the cone shaft resistances up to 300 mm below the ground surface. The average cone shaft resistance measured below 150 mm depth was about 21 kPa.

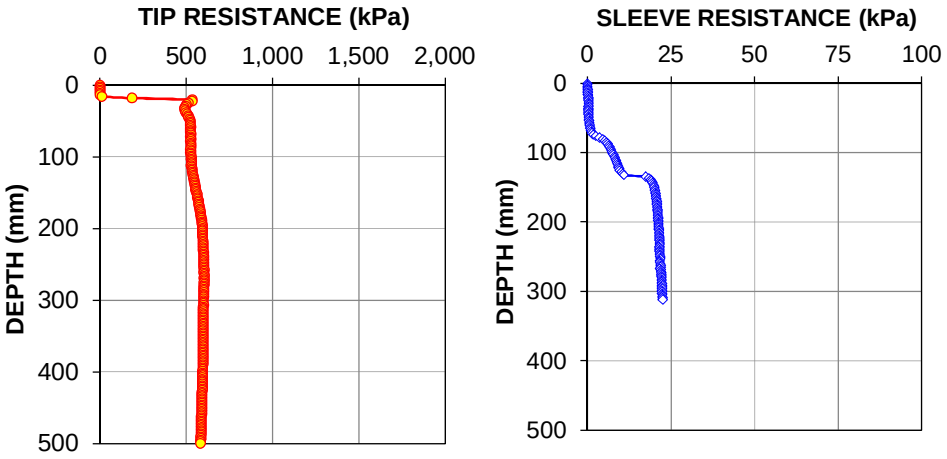

Figure 5-4 Shaft and tip resistance of penetration test in third soil chamber

5.1.2.2 Effects of Boundary Conditions

The ground surface cracks of the soil chambers, induced by the cone penetration tests, were measured to evaluate the effects of the boundary conditions. The ratio of chamber diameter to cone diameter was approximately 9, which is relatively small. Therefore, if the ground surface cracks expand into the boundary of the chamber, the effects of the cracks will be considered in the interpretation of the test results. if the ground surface cracks do not expand into the boundary of the chamber, such effects will be ignored. Figures 5-5 through 5-10 present the main ground surface cracks observed from the P-cone device tests in the three soil chambers.

Figures 5-5 provides the ground surface cracks observed from the P-cone device test in the first soil chamber. It can be clearly seen from Figure 5-5 that four main cracks

occurred around the cone. Details of the cracks are presented in Figures 5-6a through 5-6d.

The maximum width of the crack found at position no. 1 was about 5 mm at the cone wall. It gradually decreased to 0 mm at a distance of about 130 mm from the cone wall. According to the cone penetration test, the influence radius at this point was about twice the cone diameter. The influence radius of the cracks at the other positions varied from 80 through 130 mm (1.2 – 2.0 times the cone diameter), as can be seen clearly from Figures 5-6a through 5-6d.

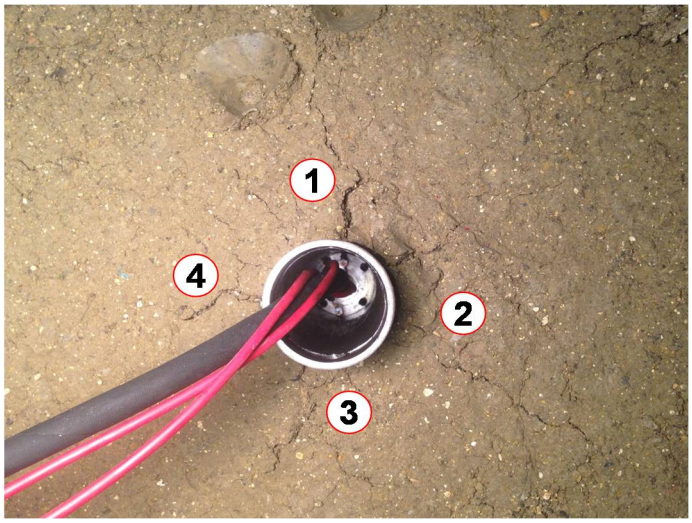

Figure 5-5 Effects of boundary conditions of cone penetration test in first soil chamber

Figure 5-7 depicts the ground surface cracks observed from the P-cone device test in the second soil chamber. Four main cracks took place around the cone. Details of the cracks are represented in Figures 5-8a through 5-8d. The maximum width of the crack found at position no. 2 was about 6 mm at the cone wall. It decreased gradually to 0 mm at a distance of about 130 mm. According to the cone penetration test, the influence radius at this point was about twice the cone diameter. The influence radius of

the cracks at the other positions varied from 60 through 100 mm (0.9 to 1.5 times the cone diameter).

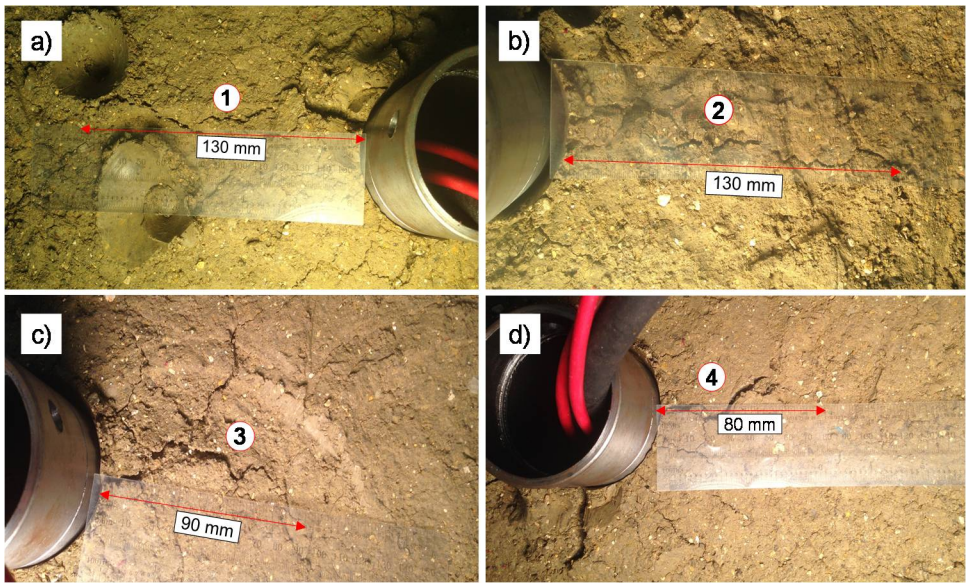

Figure 5-6 Details of four main cracks of cone penetration test in first soil chamber: a) Crack at position no.1, b) Crack at position no. 2, c) Crack at position no. 3, and d) Crack at position no.4

Figure 5-9 presents the ground surface cracks observed from the P-cone test in the third soil chamber. Four main cracks were found around the cone. Details of the cracks are presented in Figures 5-10a through 5-10d. The longest crack, about 100 mm (1.5 times the pile diameter), was found at position no. 2. The maximum width of this crack was about 3 mm at the cone wall. The influence radius at the other points was about 70 mm, which corresponded to 1.1 times the cone diameter. The observed cracks provided evidence that using the clayey silt with a chamber diameter of 590 mm was sufficient to eliminate the effects of the chamber boundaries on the cone test results of 65 mm diameter.

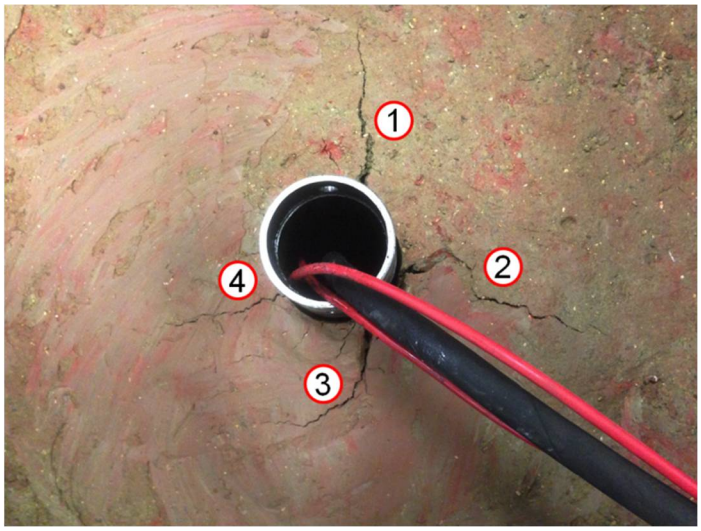

Figure 5-7 Effects of boundary conditions of cone penetration test in second soil chamber

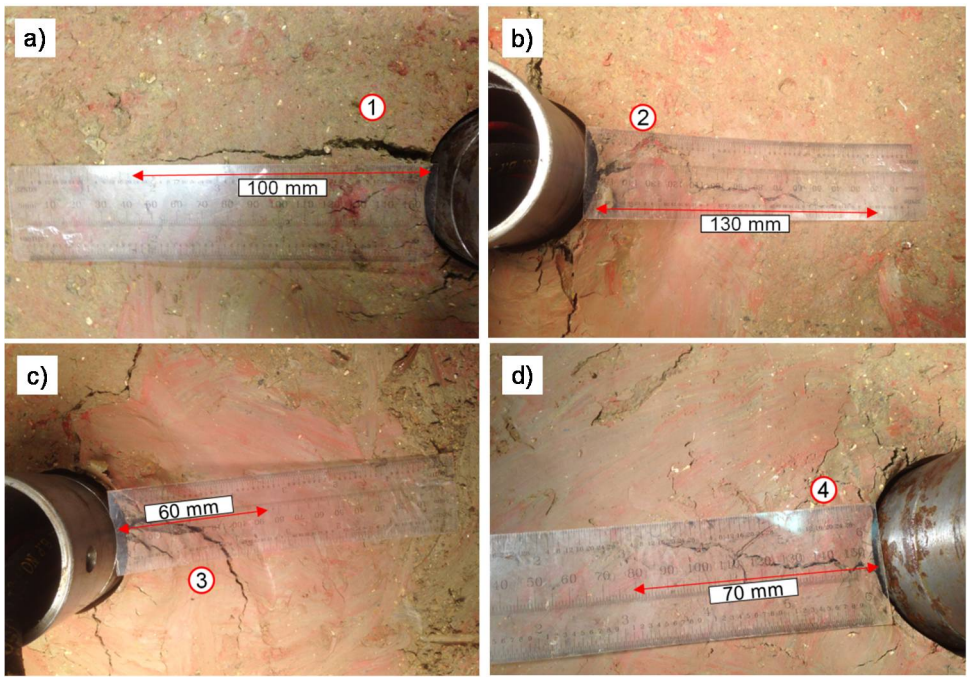

Figure 5-8 Details of four main cracks of cone penetration test in second soil chamber: a) Crack at position no.1, b) Crack at position no.2, c) Crack at position no.3, and d) Crack at position no.4

Figure 5-9 Effects of boundary conditions of cone penetration test in third soil chamber

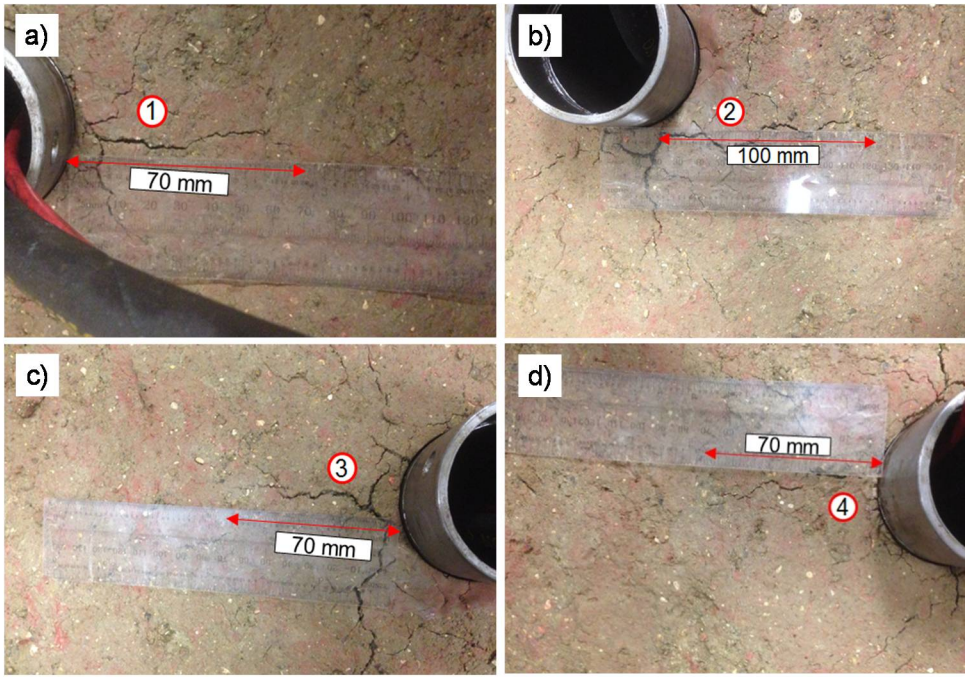

Figure 5-10 Details of four main cracks of cone penetration test in third soil chamber: a) Crack at position no.1, b) Crack at position no.2, c) Crack at position no.3, and d) Crack at position no.4

5.1.3 Results of Head-down Load Tests

The head-down load test results on the P-cone device in three soil chambers are presented in Figure 5-11. In the first soil chamber, only a head-down load test was performed. The test results are given in Figure 5-11a. In the second and third soil chambers, two head-down load tests were conducted for each soil chamber, as shown in Figure 5-11b and 5-11c, respectively. Six days after the first head-down load test, the second head-down load test was performed for the second soil chamber. Two days after the first head-down load test, the second head-down load test was performed for the third soil chamber.

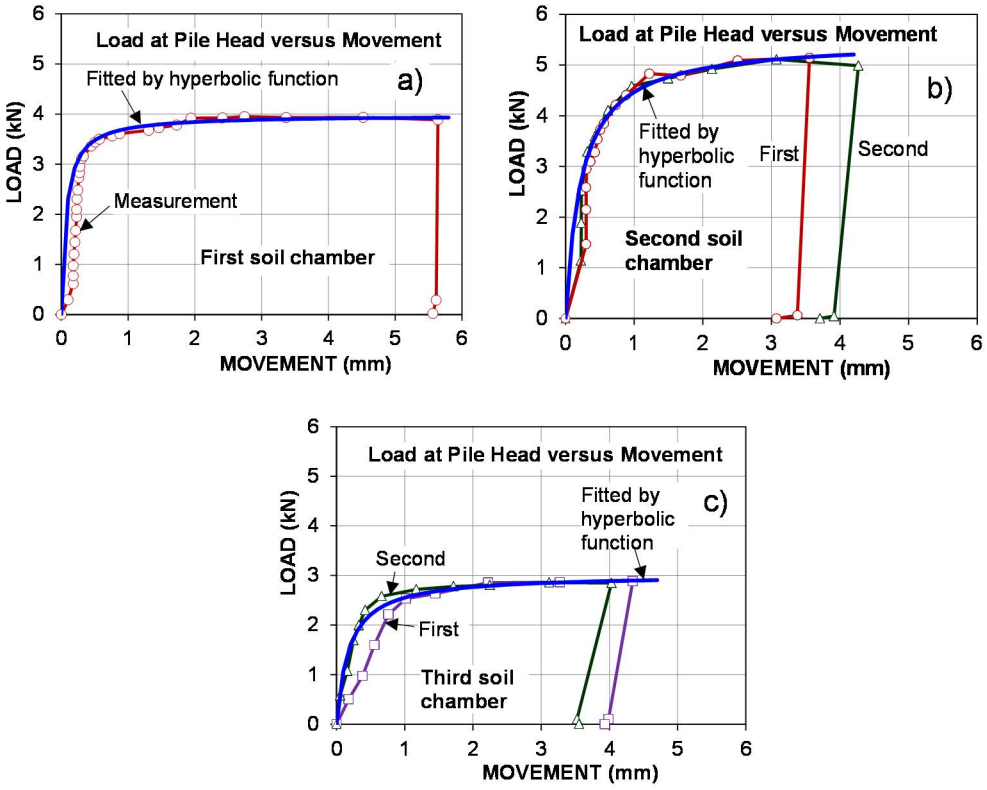

Figure 5-11 Load-movement curves of head-down load tests in three soil chambers: a) First soil chamber, b) Second soil chamber, and c) Third soil chamber.

All head-down load tests in the three soil chambers were performed until reaching plunging failure. The Quick Loading Method was applied for all tests. Each successful load increment was held constant for 2.5 minutes. The movements were recorded at the end of the 2.5-minutes for each load increment. The maximum loads obtained from the head-down load tests were about 3.95, 5.10, and 2.88 kN for first, second and third soil chambers, respectively. The maximum movements measured in the tests were approximately 3. 6 to 5.6 mm. It should be noted that the second tests performed in the second and third soil chambers were performed only six days and two days after the first tests; however, the test results were similar. It seems that the time effect is minimal for pile installed in unsaturated soil. To make calculations in the following sections simpler, the hyperbolic function was used to fit the test data, as can be seen in Figures 5-11a through 5-11c (the blue curves). The fitted curves show a good agreement with the load-movement curves measured from the head-down load tests in the three soil chambers. Therefore, using the fitted load-movement curves to estimate the pile capacities from the methods reported in Chapter 2 is considered reliable.

5.1.4 Results of Bidirectional Load Tests

The bidirectional load test results of the P-cone device in the three soil chambers are given in Figures 5-12 through 5-14. Figure 5-12 shows the three bidirectional load test results of the P-cone device in the first soil chamber. Five days after the head-down tests, the first bidirectional test was executed. Two days after the first bidirectional test, the second bidirectional tests were done. Thirty-one days after the first bidirectional test, the third bidirectional tests were performed. All load levels were maintained from two to five minutes. The maximum load for the three bidirectional load tests was about 1.35 kN.

The maximum downward and upward movements recorded were about 0.28 through 3.68 mm, 0.15 through 2.01 mm, and 0.19 through 3.25 mm, respectively.

It should be noted that the bidirectional load test reached the ultimate load in only one of the two resistance components. In the subject case, the cone shaft resistance reached an ultimate load of only about 1.35 kN (Figure 5-12a) because the cone penetration was not deep enough that the cone shaft resistance could be equal or greater than the cone tip resistance. However, in practice, the total cone shaft resistance is often greater than the cone tip resistance, fully mobilizing the cone tip resistance. Moreover, the second bidirectional test was performed only two days after the first bidirectional test, and the test results obtained were similar. It seems that the time effect of pile installed in unsaturated soil is not significant. To re-evaluate the equivalent pile head load-movement curve construction method, the hyperbolic function was used to fit the test data, as can be seen from the blue curve in Figure 5-12a.

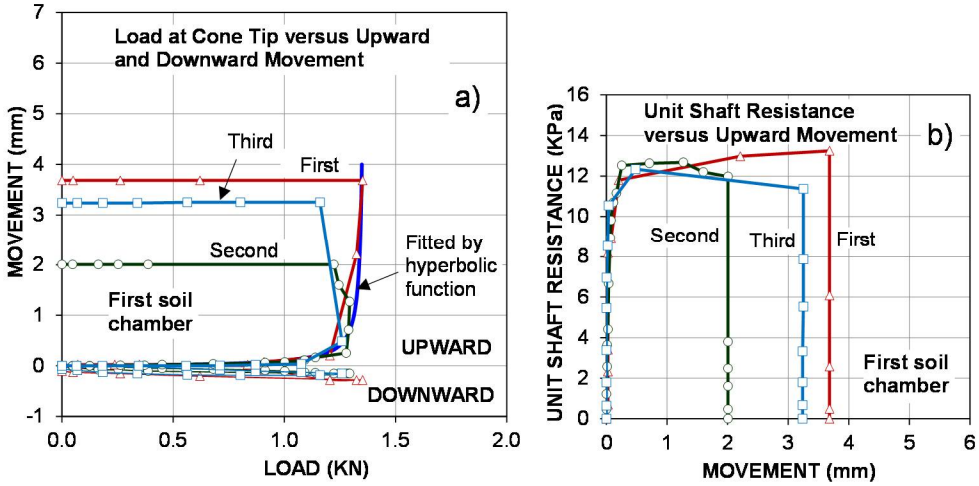

Figure 5-12 Load-movement curves and unit shaft resistance of bidirectional load test in the first soil chamber: a) Load-movement curves, and b) Unit shaft resistance versus movement

Figure 5-12b shows the unit cone shaft resistances versus movements. The unit cone shaft resistances were obtained by dividing the measured test load by the area of the cone shaft, then plotting them against movements. The maximum unit cone shaft resistance of the three bidirectional load tests was about 12 kPa. The movement necessary to fully mobilize the cone shaft resistance was relatively small, only about 0.5 mm (Figure 5-12b.)

Figure 5-13 presents the two bidirectional load test results of the P-cone device in the second soil chamber. The first bidirectional test was executed eleven days after the head-down tests. Seven days after the first bidirectional test, the second bidirectional test was conducted. Each of successful load increments and decrements were held for two to five minutes. The maximum load for the two bidirectional load tests was about 1.40 kN. The maximum downward and upward movements measured were about 0.05 through 5.61 mm and 0.03 through 5.11 mm, respectively.

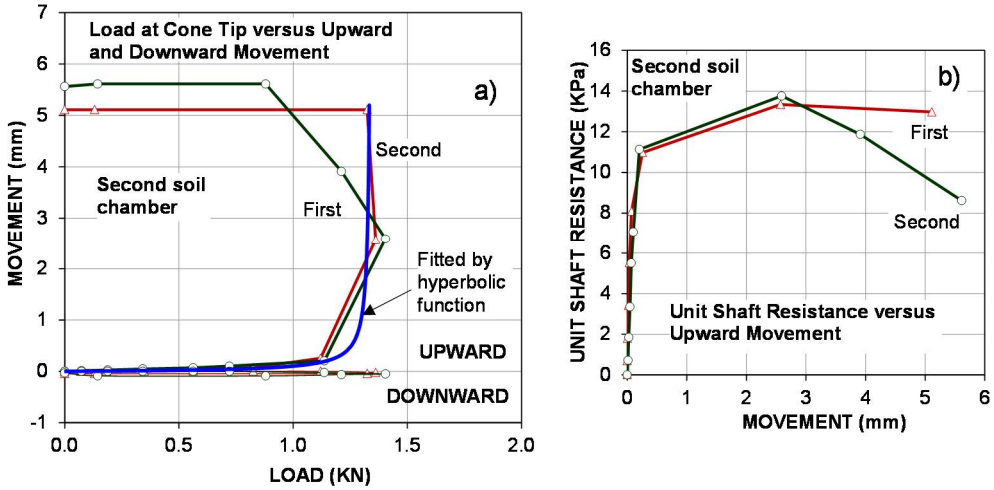

Figure 5-13 Load-movement curves and unit shaft resistance of bidirectional load test in the second soil chamber: a) Load-movement curves, b) Unit shaft resistance versus movement

Similar to the bidirectional tests in the first soil chamber, the cone shaft resistance was not enough large to fully mobilize the cone tip resistance. The hyperbolic function was also used to fit the test data, to serve the reconsideration of the equivalent pile-head load-curve construction method. (See the blue curve in Figure 5-13a.) Figure 5-13b shows the unit cone shaft resistances plotted against the movements. The maximum unit cone shaft resistance of the two bidirectional load tests was about 14 kPa, at a movement of about 2.6 mm.

Figure 5-14 depicts the results of the two bidirectional load test results in the third soil chamber. Nine days after the head-down tests, the first bidirectional test was performed. Four days after the first bidirectional test, the second bidirectional test was conducted. All load levels were maintained the same as for the above-mentioned bidirectional tests. The maximum load for the two bidirectional load tests was about 0.80 kN. The maximum downward and upward movements measured were about 0.14 through 2.89 mm and 0.14 through 4.45 mm, respectively.

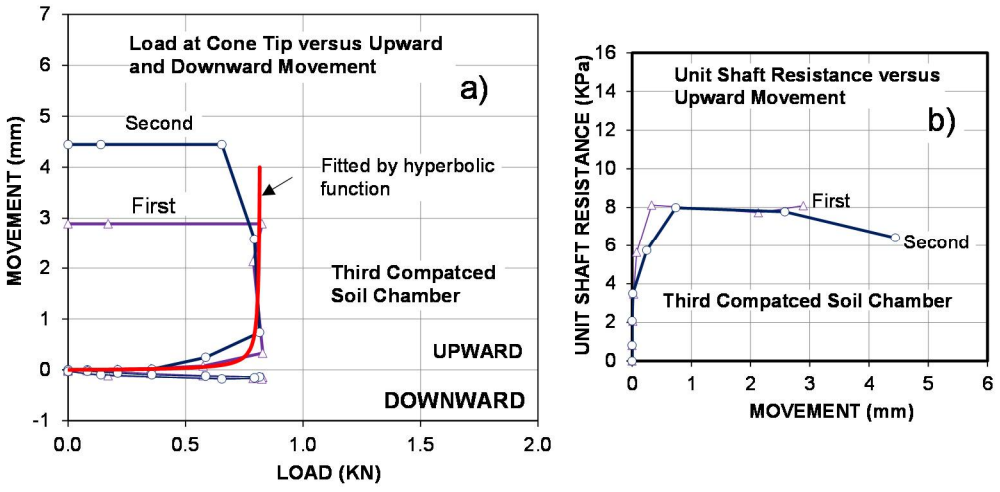

Figure 5-14 Load-movement curves and unit shaft resistance of bidirectional load test in the third soil chamber: a) Load-movement curves, and b) Unit shaft resistance versus movement

Similar to the above bidirectional tests, the cone shaft resistance was relatively small, only about 0.80 kN, and not large enough to fully mobilize the cone tip resistance. The hyperbolic function was fitted into the test data, as can be seen from the red curve in Figure 5-14a. Figure 5-13b presents the movement-unit cone shaft resistance curves of the two test results. The maximum unit cone shaft resistance of both tests was approximately 8.0 kPa at movement of about 0.5 mm.

5.1.5 End Bearing Tests

To reconsider the equivalent pile-head load-movement curve construction method, it is necessary to fully mobilize both resistance components of the test pile (shaft and tip resistance). The bidirectional load test results reported in section 5.1.4 above only mobilized the cone shaft resistance component. Therefore, the end bearing load tests were performed to mobilize fully the toe resistance component of the test pile. After each bidirectional load test was completed, the end bearing load tests were conducted immediately. Thus, the intervals between the end bearing load tests were similar to the bidirectional load test above. The measurements of the end bearing load tests are given in Figure 5-15.

Three-end bearing load tests were performed in the first soil chamber, while only two tests were conducted in the second and third soil chambers. For the three tests in the first soil chamber, five, three, and two loading cycles were applied for the first, second and third tests, respectively. The tests in the second and third soil chambers were carried out in one loading cycle. The maximum loads obtained from the tests in the first, second, and third soil chambers were about 2.4, 3.4 and 1.4 kN, respectively, as shown in Figures 5-15a through 5-15c, respectively. The maximum movements of all tests ranged from 2.69 through 5.84 mm. The load-movement curves measured were fitted by hyperbolic

function to serve the evaluation of the equivalent pile-head load-movement construction method.

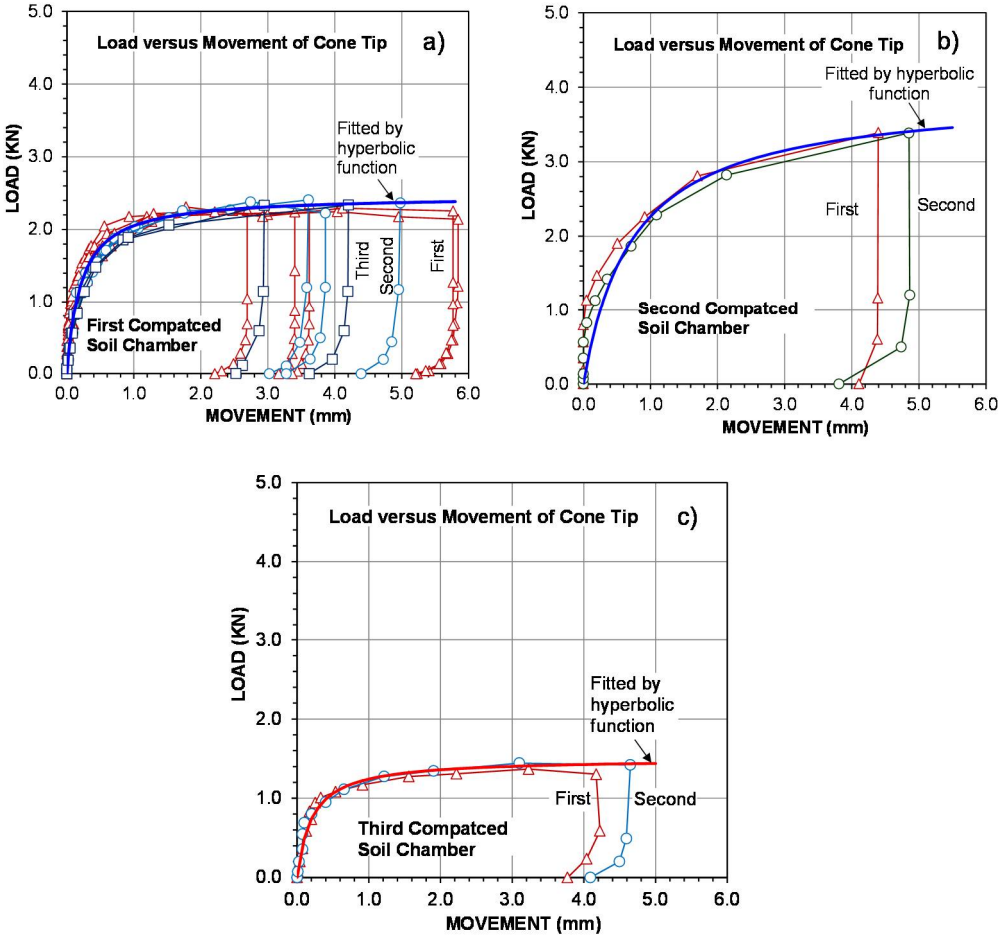

Figure 5-15 Load-movement curves of end bearing tests

It was surprising to see that the cyclic load test results in the first soil chamber showed a maximum load of about 2.4 kN. This implies that the cyclic load test had no influence on the capacity of the pile toe and that shear failure of soil did not take place below the toe. This problem will be investigated and discussed in section 5.4.

5.2 Re-evaluation of Equivalent Pile-Head Load-Movement Construction Method

As mentioned in Chapter 2, the equivalent pile-head load-movement construction method, based on the bidirectional load test results, was developed based on three assumptions (Osterberg, 1996): 1) The upward load-movement curve of the pile shaft in a bidirectional load test is similar to the downward load-movement curve of the pile shaft in a conventional load test, 2) The pile toe load-movement curve obtained from an bidirectional test is similar to the pile toe load-movement curve of the conventional head-down test, and 3) The pile is considered rigid.

To reconsider these assumptions, the results of the head-down load tests, bidirectional load tests, and end bearing load tests reported in sections 5.1.3 through 5.1.5, respectively, were used. It should be noted that there were no extrapolations for resistance components to build the equivalent pile-head load-movement curves in the subject cases. That is to say, the equivalent pile-head load-movement curves obtained from the test data were only based on the measurements, and they were enough reliable to re-evaluate the method proposed by Osterberg (1996).

As stated earlier, the P-cone device is regarded as a small model pile, with diameter and length of 0.065 m and 0.7 m, respectively, which corresponds to a ratio of length to diameter of 10.7. If ignoring the 0.2 m length of jack placed at the pile toe, the actual length of the steel pipe portion of this model pile was 0.5 m; therefore, the actual ratio of length to diameter was only about 7.7 m. For the steel pile thickness of 5 mm, it is reasonable to consider the model pile as rigid. In order words, elastic shortening of the pile material does not pertain to this model pile. Therefore, the third assumption is completely reasonable. Moreover, because of no elastic shortening of the pile material, the movement measured at the pile head was equal to the movement measured at the pile toe. Thus, the second assumption is also completely reasonable.

For the first assumption, the model pile, with a weight of about 5 Kg, was installed in the unsaturated soil chambers; hence, the effects of self-weight and buoyance were ignored. The important information to be gained from this assumption is the difference between the positive and negative shear resistances of soil along the pile shaft for the head-down and bidirectional load tests, respectively.

Figure 5-16 presents the equivalent pile-head load-movement construction from the results of the head-down load test, bidirectional load test, and end bearing test on the model pile performed in first soil chamber. Figure 5-16a shows the fitted load-movement curves of the bidirectional and end bearing load tests. These curves were divided into ten equal-movement points (from 1 to 10). At each similar movement point, the load on both curves was summed. By repeating this process, an equivalent pile head load-movement curve was obtained (dark red curve), as shown in Figure 5-16b.

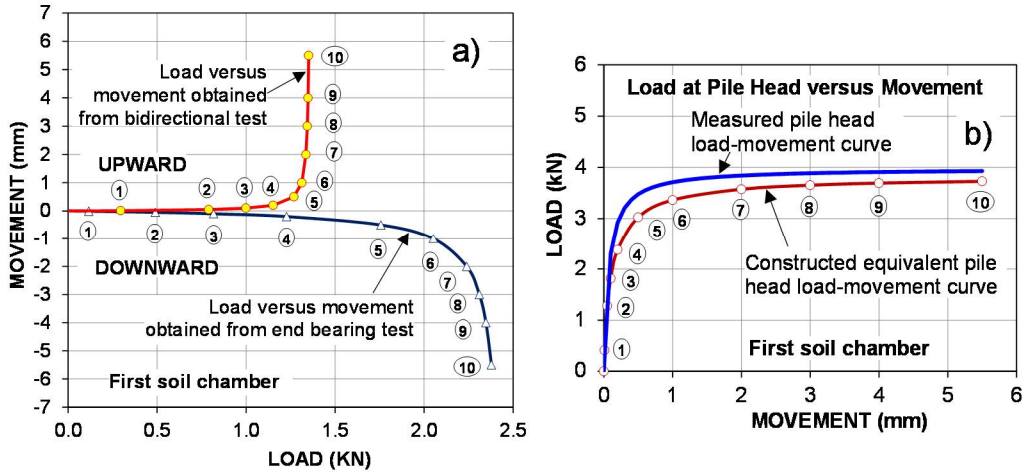

Figure 5-16 Equivalent pile-head load-movement construction from static load test results in the first soil chamber: a) Fitted load-movement curves of bidirectional and end bearing tests, and b) Measured and computed pile-head load-movement curves

Figure 5-16b also shows a measured pile head load-movement curve (blue curve) compared with the calculated pile head load-movement curve. It can be seen

clearly that the computed loads and the measurements are similar for points 1 to 3 and significantly different for points 4 through 10. Table 5-4 shows comparisons of the calculated and measured pile head loads at the equal-movement points. The average measured load was about 7.7 % greater than the average computed load.

Table 5-4 Comparison of the calculated and measured pile head loads in first soil chamber

Points	Movement	Load (kN)		Difference	
	(mm)	Calculated	Measured	(kN)	%
5	0.5	3.026	3.478	0.452	13.0
6	1	3.365	3.713	0.348	9.4
7	2	3.576	3.843	0.267	6.9
8	3	3.654	3.888	0.233	6.0
9	4	3.695	3.911	0.215	5.5
10	5.5	3.730	3.930	0.200	5.1
Average				0.286	7.7

Figure 5-17 presents the equivalent pile-head load-movement construction from the results of the head-down load test, bidirectional load test, and end bearing test on the model pile performed in the second soil chamber. Figure 5-17a) shows the fitted load-movement curves of the bidirectional and end bearing load tests. These curves were divided into nine equal-movement points (from 1 to 9). At each similar movement point, the load on both curves was summed. By repeating this process, an equivalent pile head load-movement curve was obtained (red curve), as shown in Figure 5-17b.

Figure 5-17b also shows a measured pile head load-movement curve (blue curve) that was added for the purpose of comparing it with the calculated pile head load-movement curve. It can clearly be seen that the computed loads and the measurements were similar for points 1 to 3 and significantly different for points 4 through 9. Table 5-5 shows comparisons between the calculated and measured pile head loads at the equal-

movement points. The average measured load was about 16% larger than the average computed load.

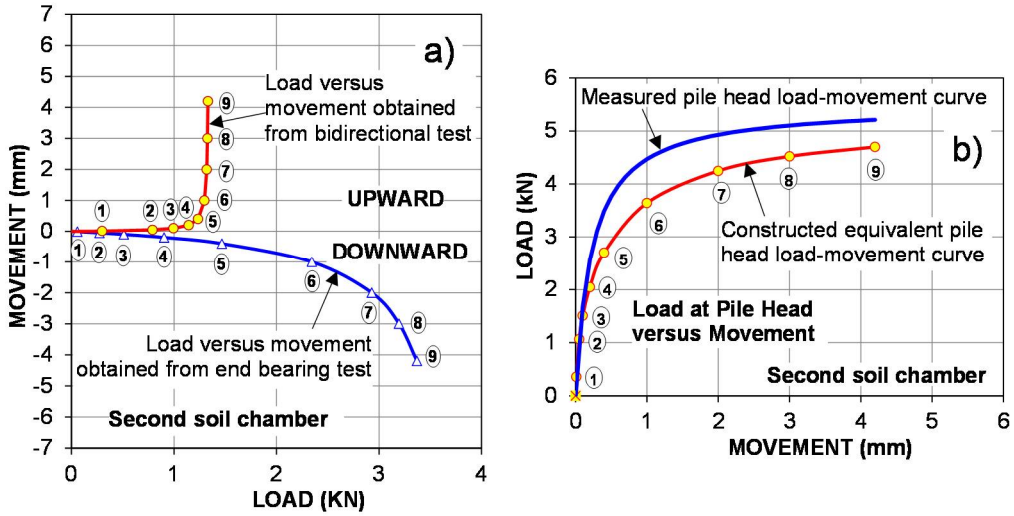

Figure 5-17 Equivalent pile-head load-movement construction from static load test results in the second soil chamber: a) Fitted load-movement curves of bidirectional and end bearing test, and b) Measured and computed pile-head load-movement curves

Table 5-5 Comparison of the calculated and measured pile head loads in second soil chamber

Points	Movement	Load (kN)		Difference	
	(mm)	Calculated	Measured	(kN)	%
4	0.2	2.047	2.558	0.511	20.0
5	0.4	2.702	3.491	0.788	22.6
6	1.0	3.643	4.469	0.826	18.5
7	2.0	4.249	4.929	0.680	13.8
8	3.0	4.522	5.104	0.582	11.4
9	4.2	4.700	5.210	0.509	9.8
Average				0.649	16.0

Figure 5-18 presents the equivalent pile-head load-movement construction from the results of the head-down load test, bidirectional load test, and end bearing test on the

model pile performed in the third soil chamber. Figure 5-18a shows the fitted load-movement curves of the bidirectional and end bearing load tests. These curves were divided into nine equal-movement points (from 1 to 9). At each similar movement point, the load of both curves was summed. By repeating this process, an equivalent pile head load-movement curve was obtained (green curve), as shown in Figure 5-18b. Figure 5-18b also shows a measured pile head load-movement curve (blue curve) that was added to compare it with the calculated pile head load-movement curve. It can be seen clearly that the calculated loads and the measurements were similar for points 1 to 4 and significantly different for points 5 through 9. Table 5-6 shows comparisons between the calculated and measured pile head loads at the equal-movement points. The average measured load was about 20.5% greater than the average computed load.

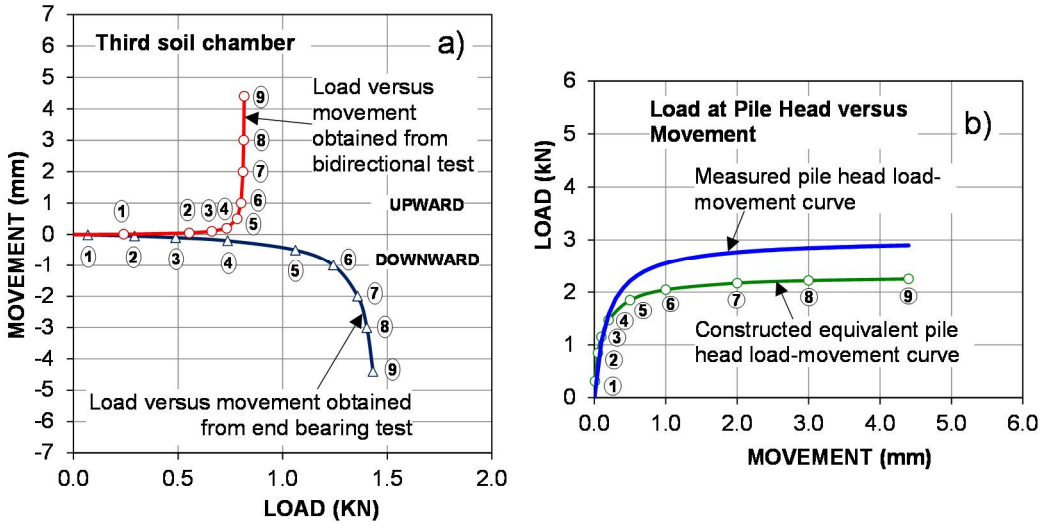

Figure 5-18 Equivalent pile-head load-movement construction from static load test results in the third soil chamber

The three results of the measurements and the equivalent pile-head load-movement curve constructions presented in Figures 16 through 18 and Tables 5-3

through 5-5 showed a major difference between the positive and negative shaft resistances of soil, when sheared. This meant that the first assumption (the upward load-movement curve of the pile shaft in bidirectional load test is similar to the downward load-movement curve of the pile shaft in conventional load test) of the equivalent pile-head load-movement curve construction method is not reasonable. Therefore, it was necessary to make an adjustment for this method.

Table 5-6 Comparison of the calculated and measured pile head loads in third soil chamber

Points	Movement	Load (kN)		Difference	
	(mm)	Calculated	Measured	(kN)	%
5	0.5	1.844	2.211	0.367	16.6
6	1.0	2.044	2.552	0.509	19.9
7	2.0	2.170	2.766	0.596	21.6
8	3.0	2.217	2.845	0.629	22.1
9	4.4	2.248	2.898	0.650	22.4
Average				0.550	20.5

Figure 5-19 shows the adjusted equivalent pile-head load-movement curves with coefficients of 1.07, 1.15, and 1.3 for the test results in the first, second, and third soil chambers, respectively. It can be clearly seen that the adjusted computation results of the first and third chambers showed a good agreement with the measured test results. For the test results in the second soil chamber, it was difficult to fit due to the difference of the curve shapes between the measurements and the calculations. However, the fitting coefficients for these test results only ranged from 1.1 through 1.2.

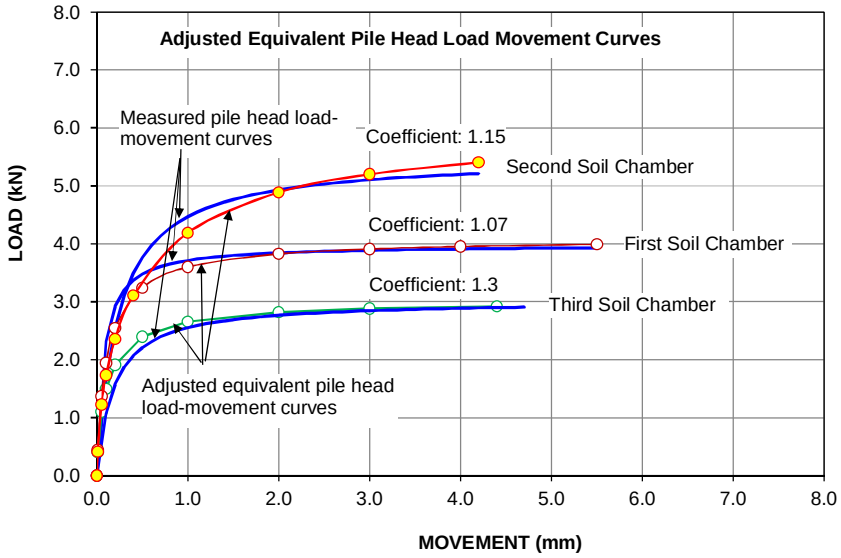

Figure 5-19 Adjustment of the equivalent pile-head load-movement curves

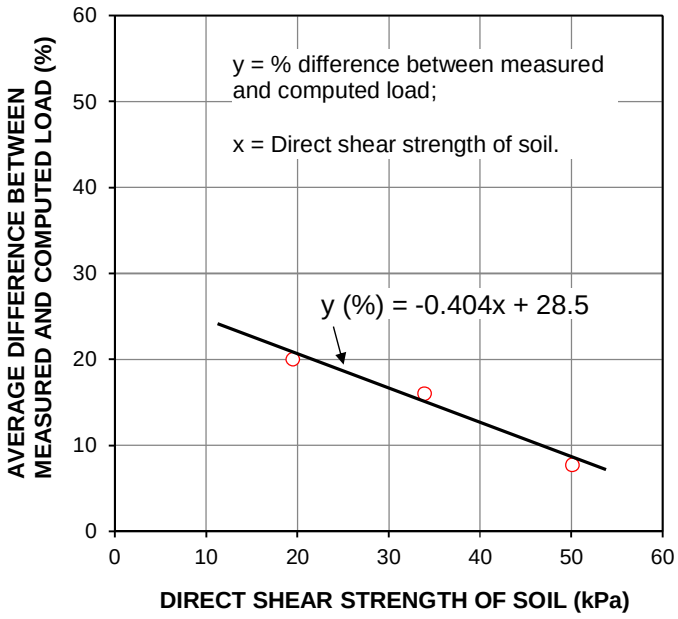

Figure 5-20 Correlation between the shear strength of soil and the difference of the measured and computed loads

It is interesting to note that the difference between the measured and computed loads depends on the shear strength of the soil. Figure 5-20 shows a correlation between the shear strength and the difference between the measured and computed loads. It is surprising to see that the difference of the positive and negative shear resistance of soil in this case decreased linearly with the increase of the direct shear strength of soil, as shown by equation of y = -0.404x + 28.5. Where, y is difference between the measured and computed load (%); x is the direct shear strength of soil. For this equation, the upper limit is at y equal to zero, and the lower limit is not necessary because the shear strength of soil is always greater than zero.

5.3 The Pile Capacity Analysis

5.3.1 Capacity of the Model Pile based on Static Load Test Results

The interpretation techniques of the conventional static load test results reported in Chapter 2 will be used to calculate the bearing capacity of the model pile (P-cone device) tested in the three soil chambers.

Figure 5-21 shows the evaluation of the pile capacity based on Vander Veen's method (1953). For various supposed values of P_{max}, the ultimate resistances Ln (1-P/P_{max}) were plotted against movements, as presented in Figures 5-31a, 5-31b, and 5-31c for the test results in the first, second, and third soil chambers, respectively. For values P_{max} of 3.95, 5.29, and 2.94 kPa, the curves appeared to transition to a straight line. Thus, these values were regarded as the pile capacities tested in first, second and third soil chambers, respectively.

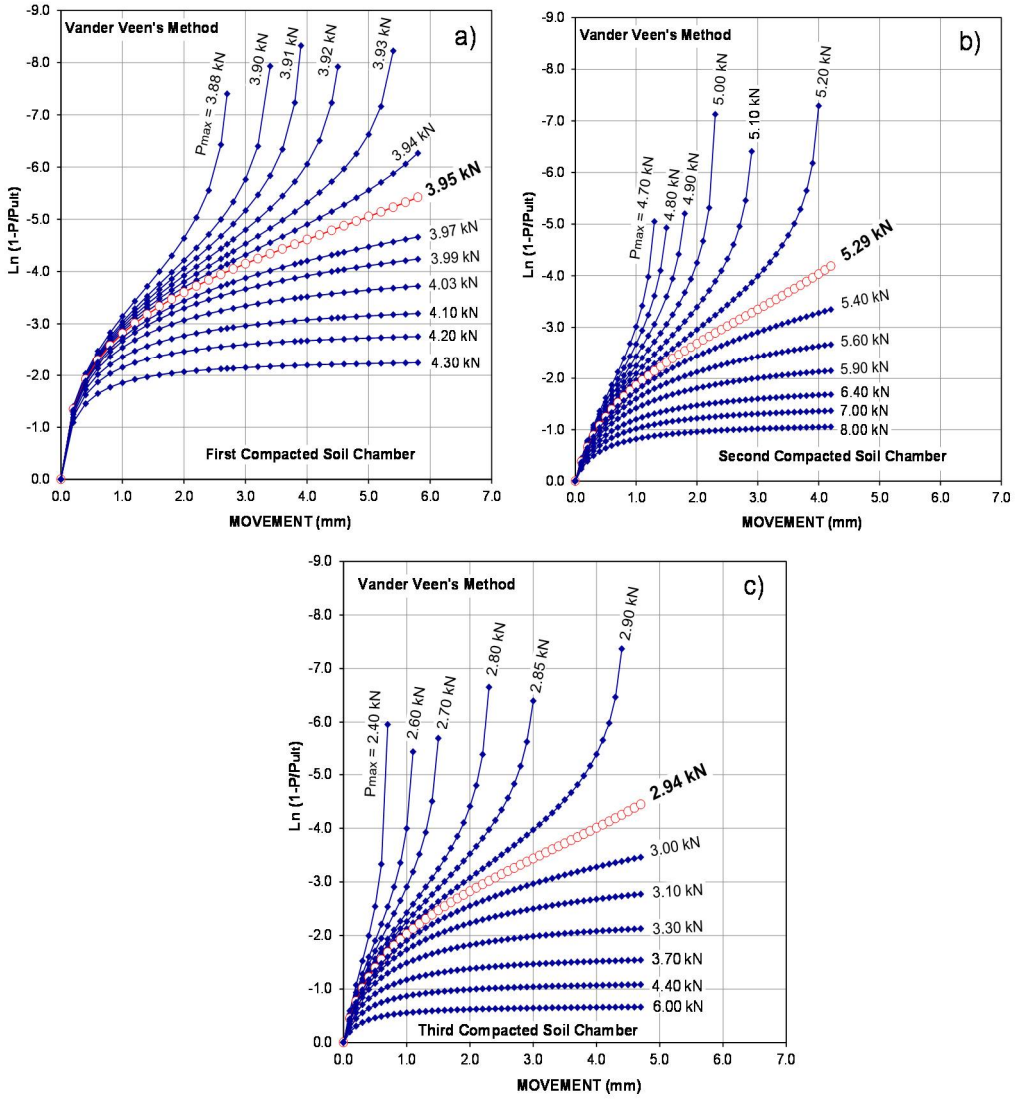

Figure 5-21 Pile capacities estimated from Vander Veen's method

Figure 5-22 shows the pile capacities predicted from Brinch Hansen's method (80% criterion). The test results were plotted by the square root of each displacement value divided by its load value versus the displacement. The 80% criterion defines the failure load as the load that is associated with four times displacement measured at the

pile head, as gained for 80% of the load (the $0.80Q_u/0.25\delta_u$ point lies on the curve). The estimated pile capacities are presented in Table 5-7.

Table 5-7 Pile capacities predicted from Brinch Hansen's method (80% criterion)

	C_1	C_2	δ_u	Q_u	$0.25\delta_u$	$0.8Q_u$
	Slope	Intercept	(mm)	(kN)	(mm)	(kN)
First soil chamber	0.0683	0.2301	3.369	3.988	0.842	**3.19**
Second soil chamber	0.0587	0.1650	2.811	5.081	0.703	**4.06**
Third soil chamber	0.0932	0.3204	3.334	2.893	0.834	**2.32**

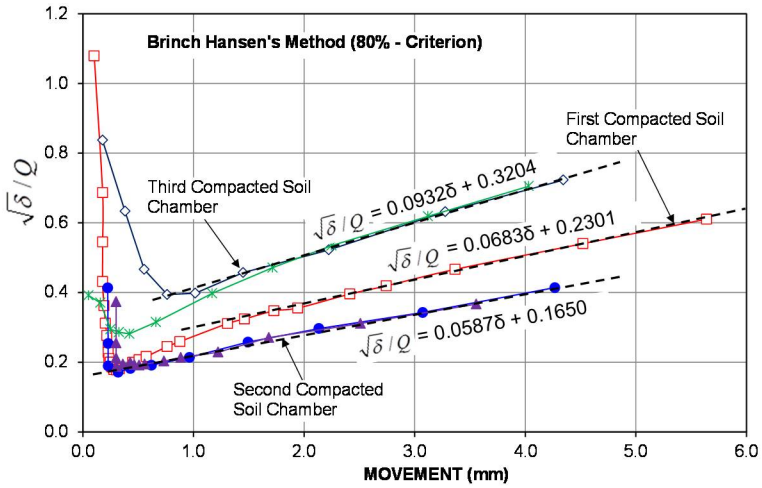

Figure 5-22 Pile capacities estimated from Brinch Hansen's method (80% criterion)

Figure 5-23 shows the pile capacities predicted from DeBeer's method. The static load test results from the three soil chambers were plotted in a double-logarithmic diagram, as presented in Figure 5-23. Two line approximations would appear if the ultimate load was reached. The intersection of the two lines is where a change occurred in the response of the piles to the imposed load. According to this approach, the pile

capacities were about 3.92, 5.09, and 2.85 kN for the static loading tests performed in the first, second, and third soil chambers, respectively, as shown in Figure 3-23.

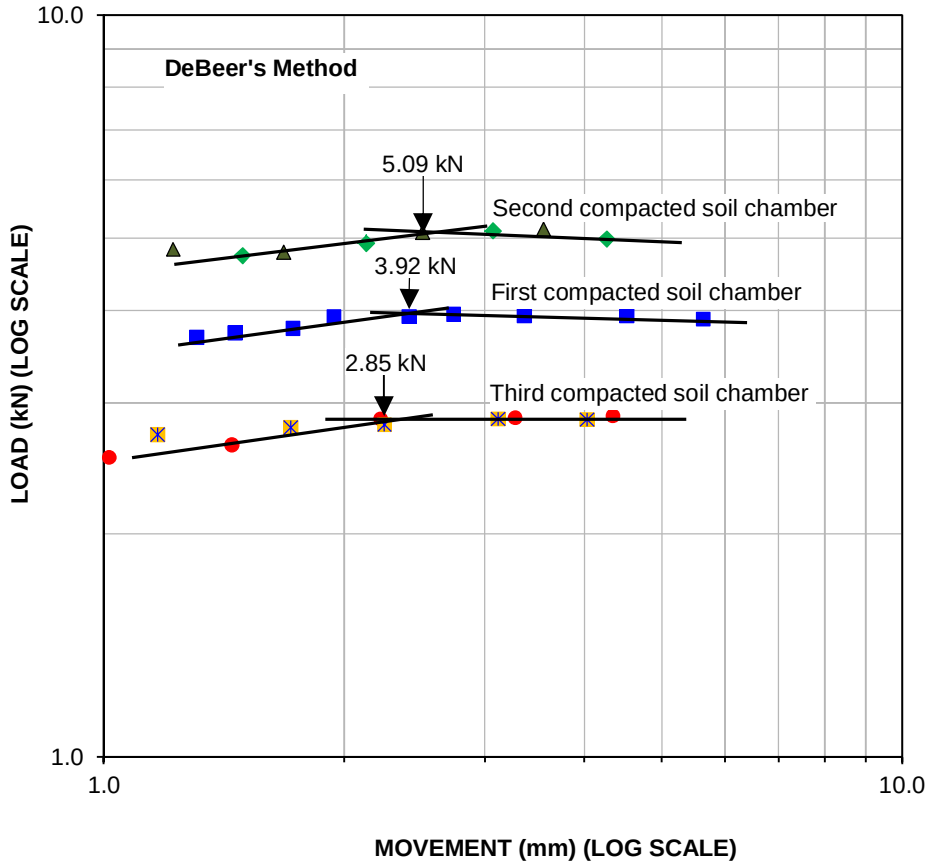

Figure 5-23 Pile capacities estimated from DeBeer's method

Figure 5-24 shows the pile capacities estimated from Chin-Konder's method. This method assumes that the load-movement relationship is hyperbolic, a plot of movement/load (δ/Q) versus movement (δ) is linear, and the inverse slope of this linear relationship is then the ultimate value of the load. The static load test results in the three soil chambers are displayed in Figure 5-34. The pile capacities estimated from this method are given in Table 5-8.

Table 5-8 Pile capacities predicted from Chin-Konder's method

	C_1 (Slope)	Q_u (kN)
First soil chamber	0.2577	3.88
Second soil chamber	0.1932	5.18
Third soil chamber	0.3432	2.91

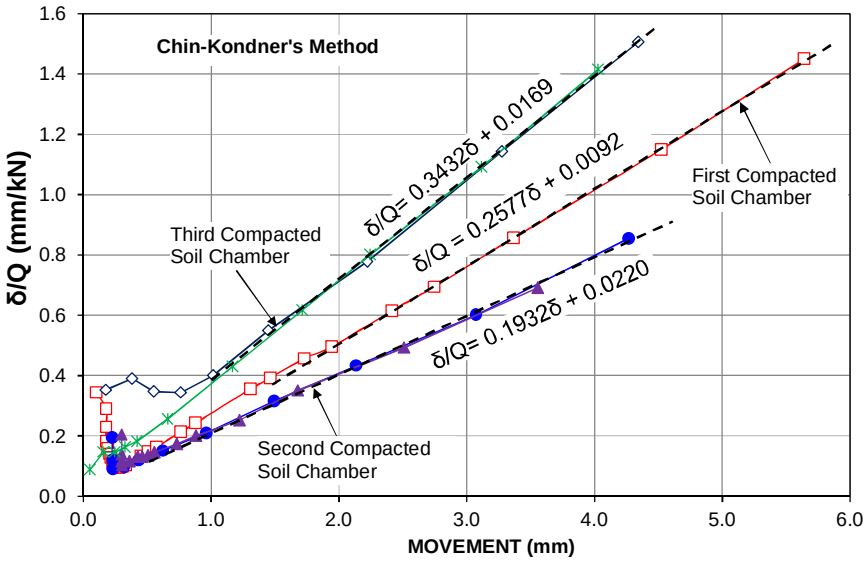

Figure 5-24 Pile capacities estimated from Chin-Konder's method.

Figure 5-25 shows the pile capacities estimated from Fuller and Hoy's method. The pile capacities were based on the maximum slopes of the load-settlement curve. The failure load can be defined as the load that results in a slope greater than 0.05 in. per ton, or 1.295 mm per kN the gross load-settlement curve. It is convenient to use the fitting curves of the static load test results of the three soil chambers to determine the ultimate bearing capacities of the pile. The pile capacities calculated from this method were about 3.58, 4.58, and 2.40 kN for the static load tests performed in first, second, and third soil chambers, respectively.

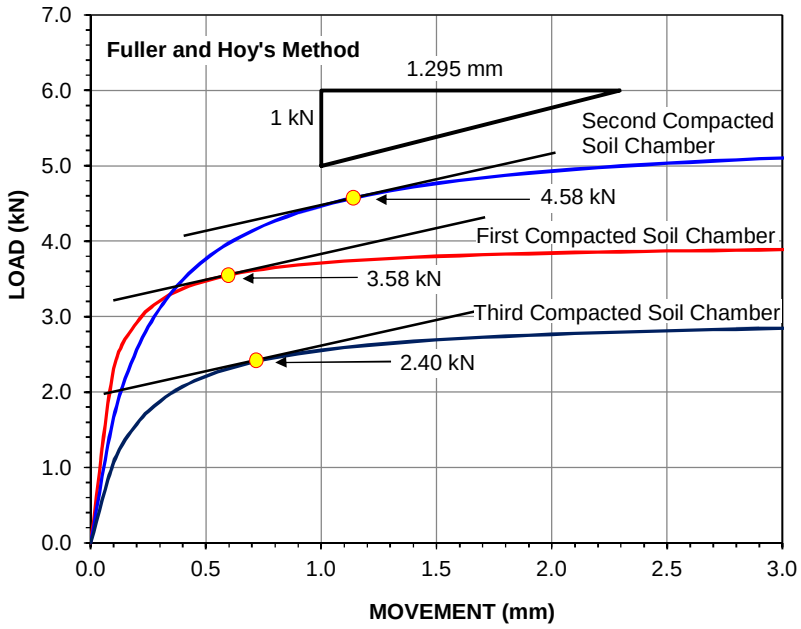

Figure 5-25 Pile capacities estimated from Fuller's and Hoy's method

Figure 5-26 provides the pile capacities estimated from Davisson's method. This method assumes that the pile capacity is reached at a certain small displacement of pile toe, and estimates that displacement by adjusting it to the pile stiffness, which is a function of diameter, length, and material. The load corresponds to the displacement that surpasses the elastic shortening of the pile about 4 mm, plus a coefficient equal to the pile diameter divided by 120. The diameter of the model test pile was 65 mm; thus, the offset value computed was 4.54 mm.

The elastic shortening of the pile material in the subject was zero, which led to the slope of line for determining the limit load, equal to zero. Moreover, the maximum movements of the test piles measured in the second and third soil chambers were less than 4.54 mm; thus, the fitting curves of these two test results were extrapolated into the limit load line, as shown in Figure 5-26. The pile capacities estimated from Davisson's

method were about 3.92, 5.20, and 2.90 kN for the tests carried out in the first, second, and third soil chambers, respectively (Figure 5-26).

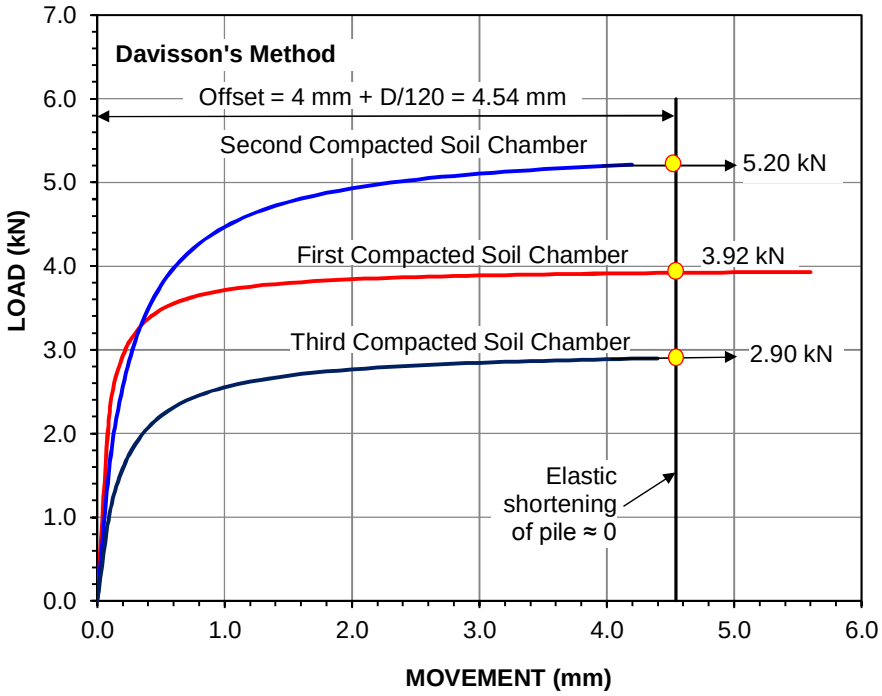

Figure 5-26 Pile capacities estimated from Davisson's method

Figure 5-27 shows the pile capacities estimated from Mazurkiewicz's method. A set of equal pile-head displacement lines were selected arbitrarily, and the corresponding load lines were built basing on the intersections of the displacement lines with the load-displacement curve. At the intersecting point between the load line and the load axis, a line of 45^0 was drawn to cut the next load line and these intersecting points fell nearly on a straight line. The intersection with the load axis was defined as the failure load. The pile capacities estimated from this method were about 3.86, 5.01, and 2.80 kN, as shown in Figures 5-27a, 5-27b and 5-27c, respectively.

Figure 5-28 shows the pile capacities estimated from Butler and Hoy's Method. For this method, the failure load was considered as the load at the intersection of the two tangent lines, with the first line drawn from the zero load point tangent to the initial flat portion of the load-displacement curve. The second line was drawn tangent to the steep portion of the load-displacement curve, with a slope 0.05 inch/ton or 1.295 mm per 1 kN of load for the tested piles. The pile capacities determined were about 2.22, 3.98, and 2.10 kN for the fitting load-movement curves obtained from the first, second, and third soil chambers, respectively.

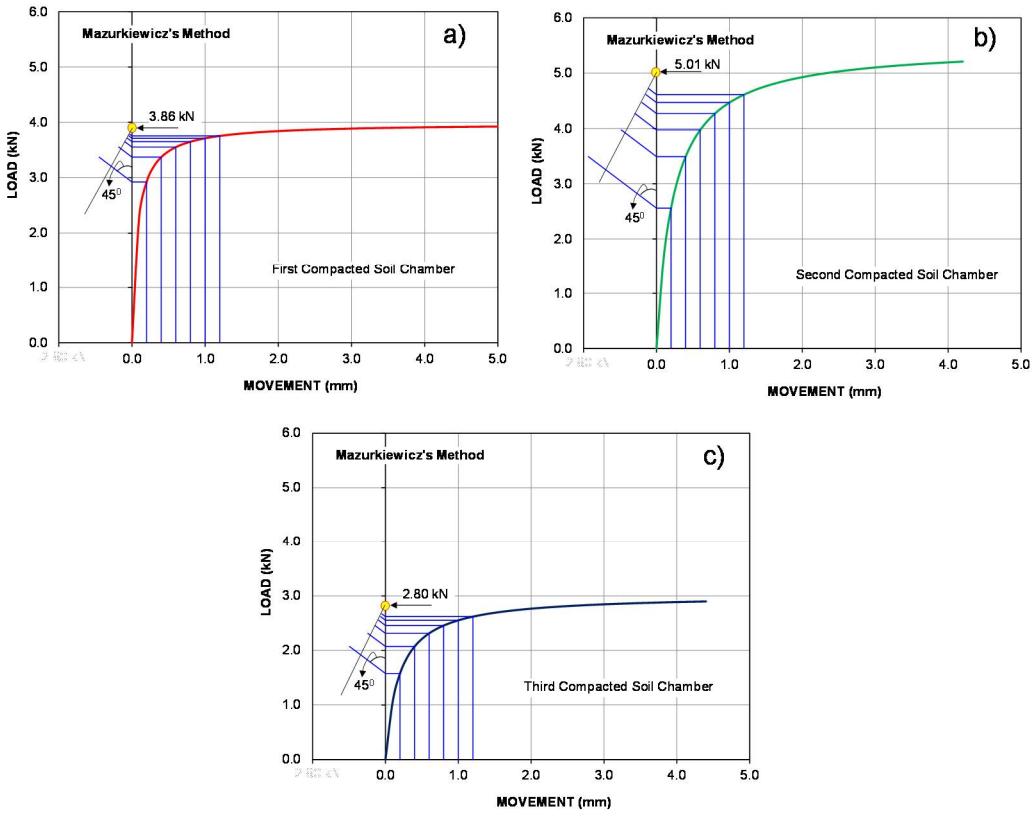

Figure 5-27 Pile capacities estimated from Mazurkiewicz's method

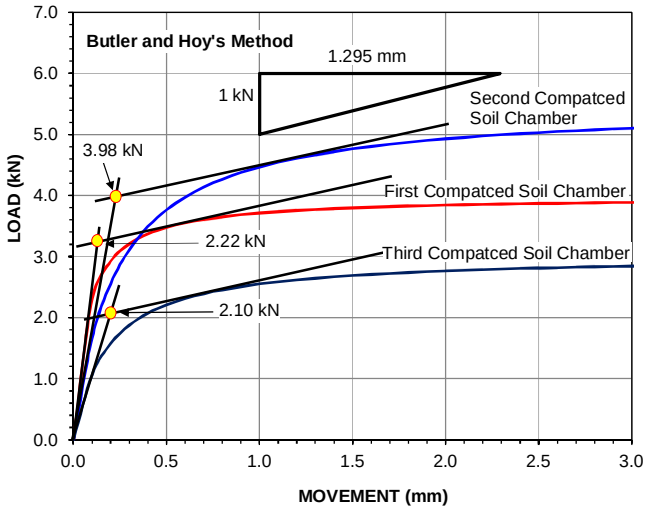

Figure 5-28 Pile capacities estimated from Butler and Hoy's Method

Figure 5-29 shows the pile capacities estimated from Decourt's method. From the load test results, the stiffness was computed and plotted versus the applied load. The failure load is considered as the load at zero stiffness. The pile capacities estimated from this method were about 3.83, 5.52, and 2.91 kN for the piles tested in the first, second, and third soil chambers, respectively, as can be seen in Figure 5-29.

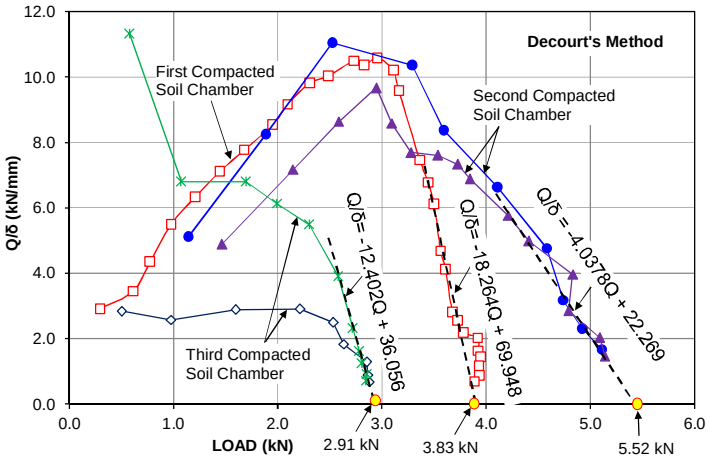

Figure 5-29 Pile capacities estimated from Decourt's method

Figures 5-30 through 32 show comparison of pile capacities estimated and measured in three experimental soil chambers. It can be seen clearly, from comparing the three static load test results, that the best prediction methods of pile capacity are DeBeer's and Davisson's, which differ only about 1%. The next best methods are Vander Veen's and Chin-Konder's, with a difference of only about 2%.

Mazurkiewicz's and Decourt's methods had a difference of only about 4%, and the methods of Fuller and Hoy, Brinch Hansen (80% criterion), and Butler and Hoy showed differences of 12, 19, and 31%, respectively.

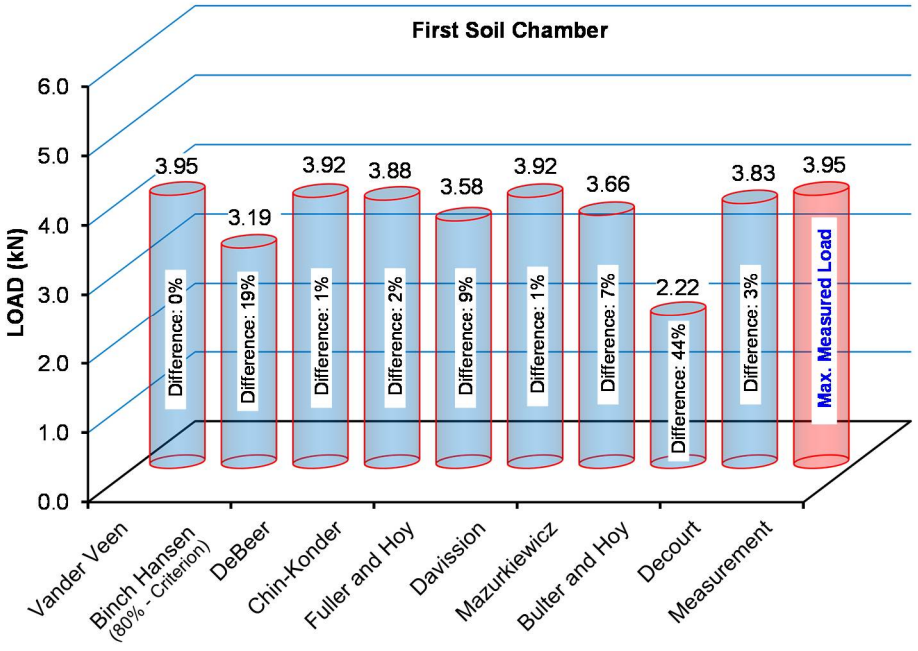

Figure 5-30 Comparison of pile capacities estimated from the static load results and measured in first soil chamber

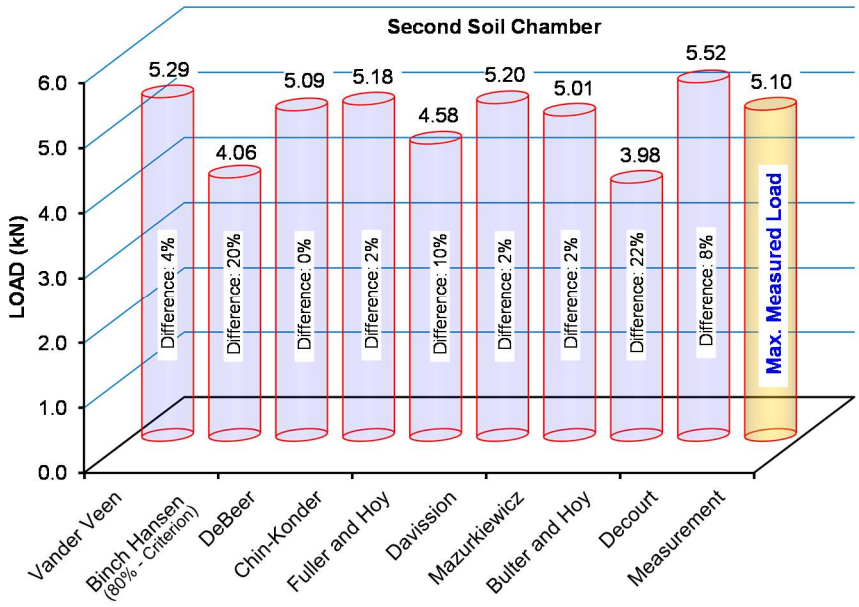

Figure 5-31 Comparison of pile capacities estimated from the static load results and measured in second soil chamber

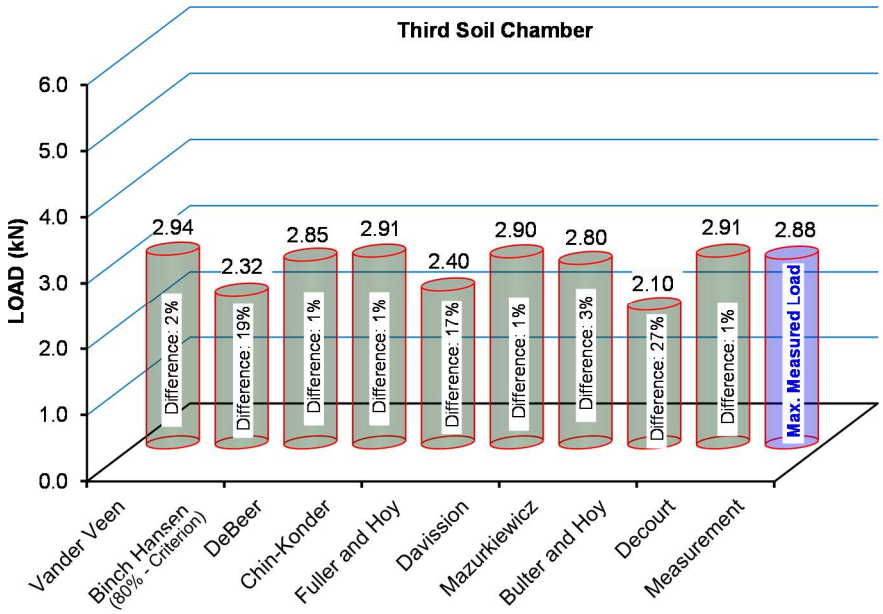

Figure 5-32 Comparison of pile capacities estimated from the static load results and measured in the third soil chamber

5.3.2 Capacity of the Model Pile based on Cone Penetration Test Results

The penetration test results of the three soil chambers were used to calculate the capacity of the model test pile. The direct CPT methods reported in Chapter 2 considered the cone as a model pile, in which the measured cone tip and sleeve resistances corresponded to the pile toe and shaft resistance. For this approach, the soil compressibility, rigidity, and mean effective stress influence the pile and the cone in a similar way. Thus it can eliminate the need to figure out the intermediate values, such as the bearing capacity coefficient, N_q, and the earth pressure factor, K_s. Within the scope of this study, the six direct methods mentioned in Chapter 2 were used to estimate the capacity of the P-cone device tested in the three soil chambers.

The P-cone device was used as a model test pile and installed only about 0.5 m below the ground surface. As a result, the penetration test data below the pile toes was not obtained, and it was not possible to take the average of the cone resistance over an influence zone from 8d above the pile toe and 0.7d to 4d below the pile toe (d is the P-cone device diameter). Thus, the average cone tip resistances over the installed length of the P-cone device were used to estimate the pile capacity. In addition, the effects of the pore pressure were not considered in the analysis because the penetration tests were performed in unsaturated soil. The analysis results of the pile capacities in the three soil chambers are presented in Table 5-9, and the comparison of the measured and calculated pile capacities is given in Figures 5-33 through 5-35.

Table 5-9 Capacity of Pile computed basing on Cone Penetration Test Data

	First Soil Chamber (kN)			Second Soil Chamber (kN)			Third Soil Chamber (kN)		
	R_t	R_s	**R**	R_t	R_s	R	R_t	R_s	**R**
Schmertmann and Nottingham	C = 0.5; K_f = 0.9 (Fellenius, 2017)								
	1.05	1.22	**2.27**	4.75	1.06	**5.81**	1.83	1.26	**3.08**
De Ruiter and Beringen	α = 0.5; Nc = 9; N_k = 20 (Lune et al., 1997; Fellenius, 2017)								
	0.95	0.81	**1.76**	4.28	3.67	**7.95**	1.64	1.41	**3.06**
Bustanmante and Gianselli	C_{LCPC} = 0.5; K_{LCPC} = 0.033 (Fellenius, 2017)								
	1.46	1.49	**2.95**	5.37	5.48	**10.86**	1.95	1.99	**3.94**
Mayerhof	C_1 = 1; C_2 = 0.77; K_f = 1 (Fellenius, 2017)								
	2.68	1.35	**4.03**	8.34	1.17	**9.51**	3.03	1.40	**4.43**
Tumay and Fakhroo	C = 0.5; K_f = 0.5 (Fellenius, 2017)								
	1.05	0.68	**1.73**	4.75	0.59	**5.34**	1.83	0.70	**2.53**
Eslami and Fellenius	C_t = 1; C_s = 0.025 (Fellenius, 2017)								
	2.10	0.81	**2.91**	9.50	3.67	**13.17**	3.65	1.41	**5.07**

R_t = Toe resistance; R_s = Shaft resistance; R = Total resistance

Figures 5-33 through 35 depict the comparison of pile capacities estimated and measured in three experimental soil chambers. The comparison shows that the differences between the measured and estimated pile capacities are significant. Schmertmann-Nottingham's and Tumay-Fakhroo's methods produced pile capacities close to the measurements, with differences of about 21 and 24%, respectively. The next most accurate methods were those of De Ruiter-Beringen and Mayerhof, with differences of about 39 and 47%, respectively. The most dramatic differences were yielded by the methods of Bustanmante-Gianselli and Eslami-Fellenius, with differences of about 58 and

87%, respectively. It is likely that taking the average of the cone tip resistances in the subject case, as well as the differences in cone sizes, led to such dramatic distinctions.

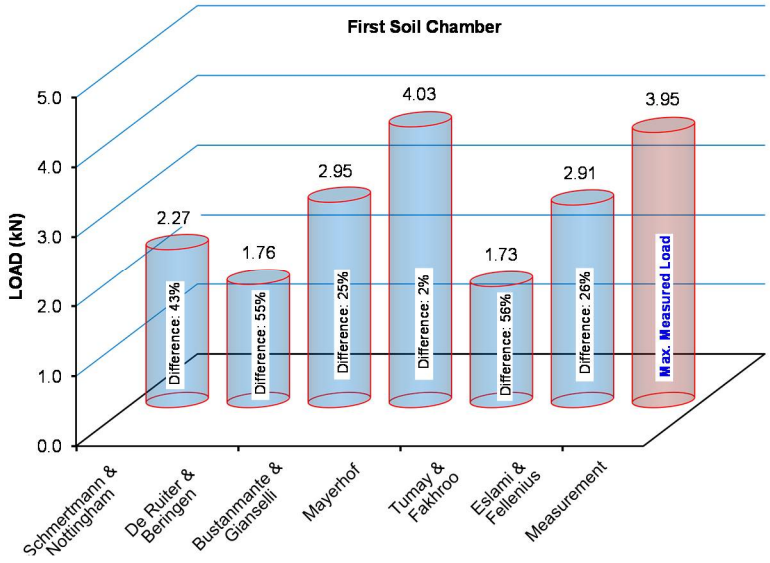

Figure 5-33 Comparison of pile capacities estimated from the penetration data and measured in third soil chamber

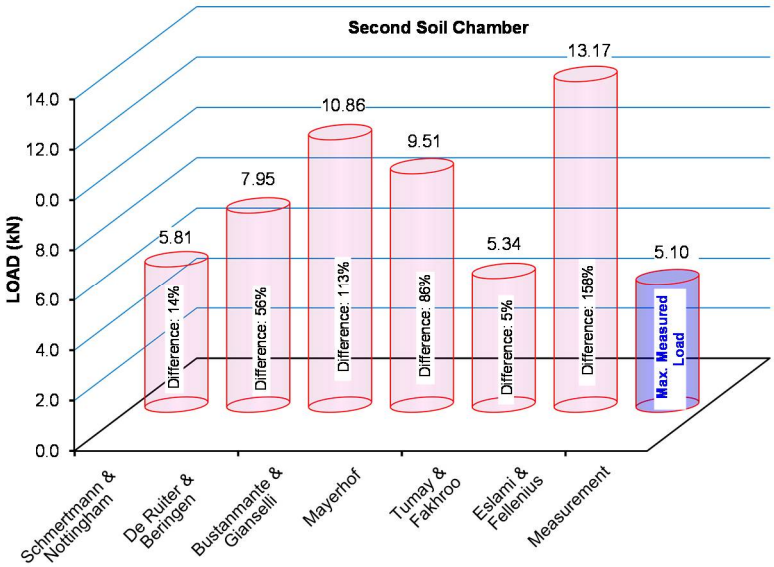

Figure 5-34 Comparison of pile capacities estimated from the penetration data and measured in third soil chamber

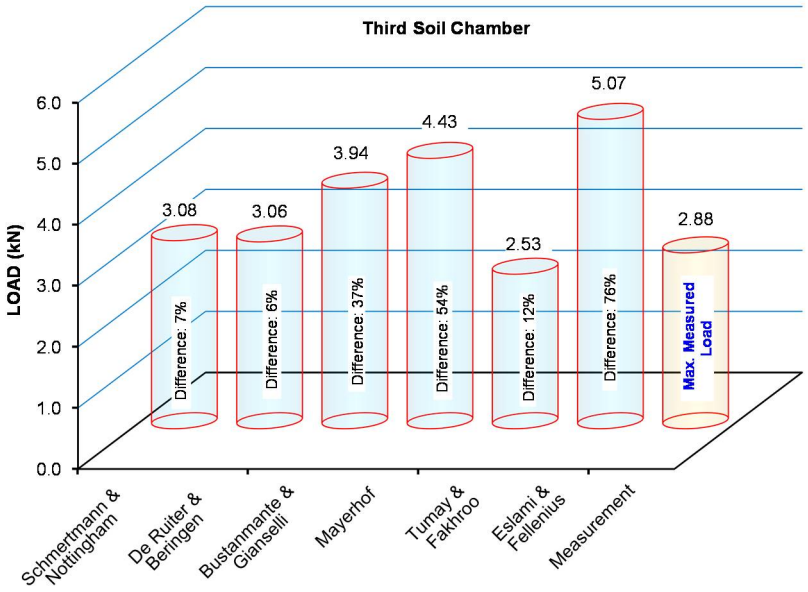

Figure 5-35 Comparison of pile capacities estimated from the penetration data and measured in third soil chamber

5.3.3 Capacity of the Model Pile Based on the Strength of Soil

Pile Toe Resistance

The bearing capacity of piles in cohesive soils is critical on a short-term basis because clay strength increases due to consolidation or strength regain of disturbed soils in the long term. Therefore, it is customary to compute the pile toe capacity in clay in terms of the undrained shear strength of the clay, c_u, and a bearing capacity factor, N_c. Thus the end-bearing pressure is

$$q_0 = c_u N_c \tag{5.1}$$

Bearing capacity factor, N_c, as shown in Figure 5-36, increases as the depth-to-pile-diameter ratio increases, until it reaches a value of 9 for $Df/B \geq 4$

(Skempton, 1951). For most pile foundations, the depth-to-diameter ratio *(Df/B)* is greater than 4; $N_c = 9$ may therefore be used for such cases.

Pile Shaft Resistance

The previous researchers showed that the shaft resistance mobilization is governed by the slenderness ratio of the pile and the over-consolidation ratio of the clay (Tomlinson, 1980). For the purposes of pile design, Randolph and Wroth (1982) proposed that the over-consolidation ratio should be represented by ratio of the undrained shear strength to the effective overburden stress (c_u/σ'_{v0}), which could be correlated with the adhesion factor, α. Basing on a large number of pile loading tests, Semple and Rigden (1984) established the correlation between the c_u/σ'_{v0} ratio and the adhesion factor (α) as shown in Figure 5-37a. To consider the slenderness ratio and flexibility of the pile, the values of α_p was reduced by a length coefficient, *F*, as presented in Figure 5-37b). Thus unit shaft resistance:

$$f_s = F\alpha_P c_u \tag{5.2}$$

Based on the shear strength parameters of soil reported in section 5.1, the equations of (5-1) and (5-2) were used to determine the pile capacities. The measured and computed pile capacities are presented in Table 5-10. It is obvious that the differences between the measured and calculated pile capacities were significant for all three tests. The average difference between the measurement and the calculation was about 29%.

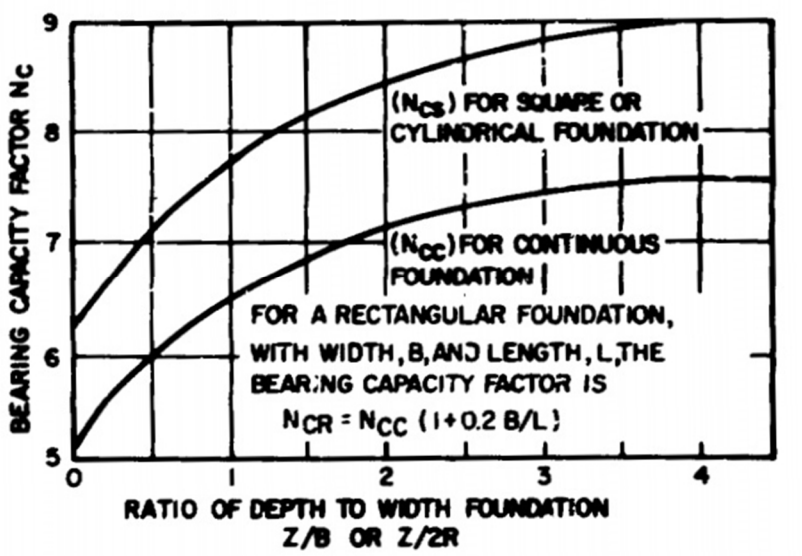

Figure 5-36 Values of N_c for various depth-to-pile diameter (D_f/B) ratios (NAVFAC, DM 1.2, 1982)

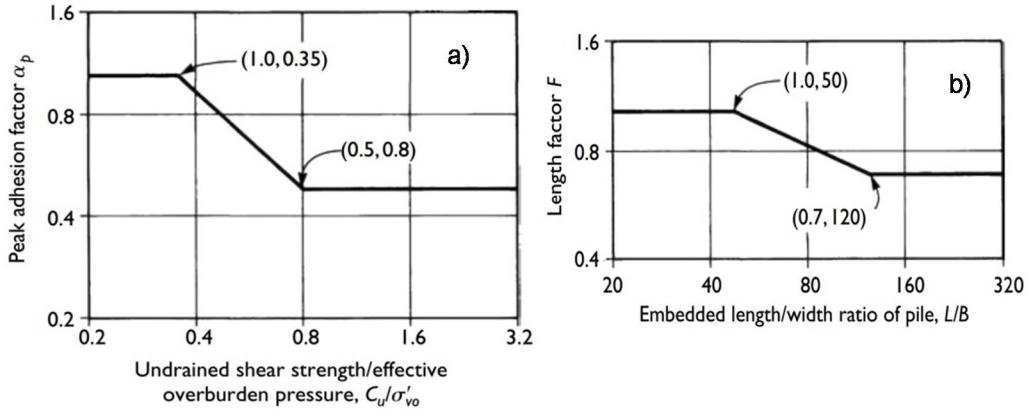

Figure 5-37 Adhesion factors for piles driven to deep penetration into clays: a) Peak adhesion factor versus shear strength/effective overburden pressure, and b) Length factor (Tomlinson M. and Woodward J., 2008)

Table 5-10 Pile Capacities computed from the shear strength of soil

	σ_v	C_u	N_c	α	F	R_t	R_s	R	Measured Load	Difference
	kN/m^2	kN/m^2	-	-	-	kN	kN	kN	kN	%
First soil Chamber	9.7	50.5	9	0.53	1.0	3.0	2.7	**5.7**	**3.95**	**44%**
Second soil chamber	9.9	34.8	9	0.53	1.0	2.1	1.9	**4.0**	**5.10**	**22%**
Third soil chamber	9.4	19.9	9	0.53	1.0	1.2	1.1	**2.3**	**2.88**	**20%**

R_t = Toe resistance; R_s = Shaft resistance; R = Total resistance.

5.4 Investigation of Soil Failure Surrounding Pile

In this section, discussion is focused on what are believed to be fundamental fallacies: 1) the bearing capacity concept of the pile toe; 2) the concept of the plunging failure load; and 3) the classical pile shaft resistance theory, as well as the shear strength theory of soil.

Before presenting the investigation results of the soil failures surrounding the P-cone device, it is necessary to review the previous assumed failure modes of soil below the pile toe and along the pile shaft.

5.4.1 Assumed Failure Patterns of Soil Surrounding Pile

Pile Toe Resistance

A pile toe is, in principle, a footing with a long stem. Therefore, the bearing capacity of a pile toe is treated in a manner similar to the treatment of a footing. This is recognized by the fact that people usually model the pile toe as a footing when determining pile toe bearing capacity.

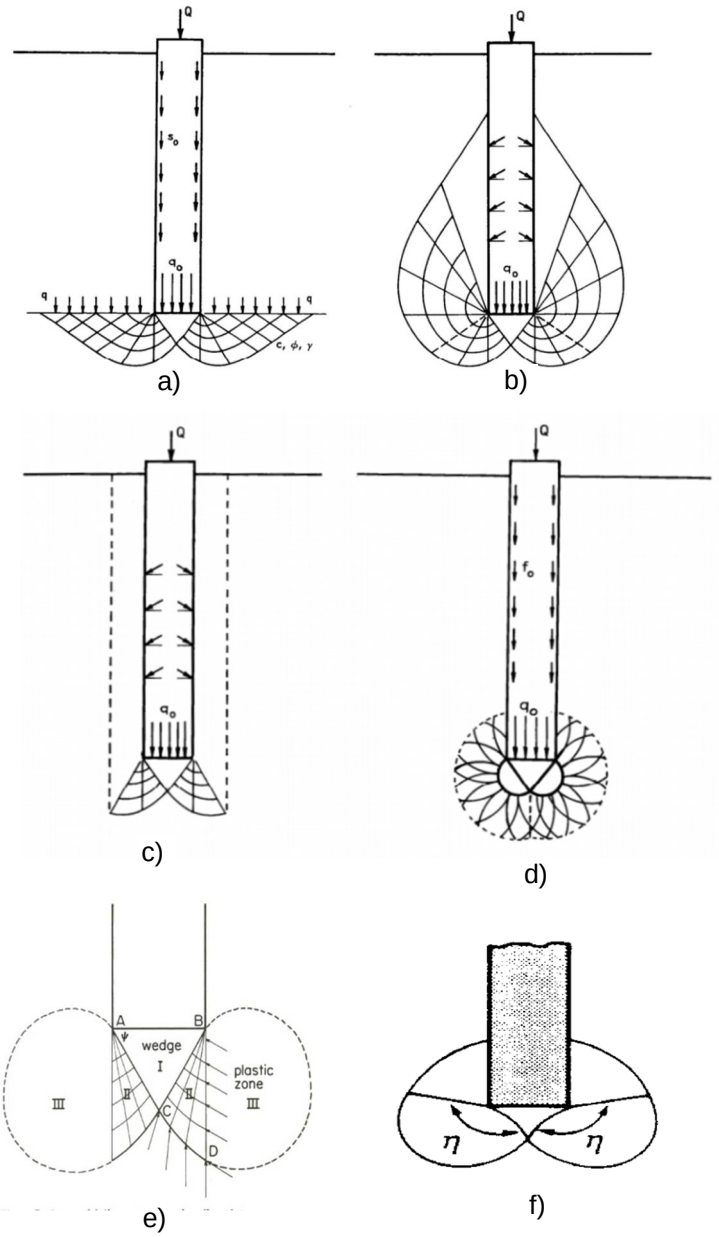

Figure 5-38 Different assumed failure patterns under deep foundation: a) Prandtl (1921), Reissner (1924), Caquot (1934), Buisman (1935), Terzaghi (1943); b) De Beer (1945), Jáky (1948), Meyerhof (1951); c) Berezantsev and Yaroshenko (1962), Vesic (1963), Salgado (1993); d) Bishop, Hill and Mott (1945), Skempton, Yassin and Gibson (1953); e) Vesic (1972), Yasufuku and Hyde (1995); f) Janbu (1976)

Different solutions for the problem of unit point resistance, q_0, are shown in Figure 5-38. A majority of these represent extensions of the classic work by Prandtl (1921) and Reissner (1924), whose solutions were first applied to the problem of bearing capacity of deep foundations by Caquot (1934) and Buisman (1935).

One of the solutions that somewhat differs in approach from all the others is that of Skempton, Yassin, and Gibson (1953), as shown in Figure 5-38d. Their analysis is based on the work by Bishop, Hill, and Mott (1945), who first presented the solution of a special case of expansion of a cavity inside a solid. The main feature of their approach is that the soil outside the plastic zone is assumed to behave as an ideal elastic, therefore compressible solid.

Solutions for q_0 are most frequently presented in the well-known form:

$$q_0 = cN_c\xi_c + \sigma'_{v0}N_q\xi_q \tag{5.3}$$

Where, σ'_{v0} is the effective vertical stress at the level of the pile toe, N_c and N_q are dimensionless bearing capacity factors; ξ_c and ξ_q are shape factors.

Pile Shaft Resistance

The conventionally theoretical approach for evaluation of unit skin resistance *(f_s)* is generally similar to that used to analyze the resistance to the sliding of a rigid body in contact with soil. It is assumed that f_s consists of two parts (Vesic, 1977): *adhesion (c_a),* which should be independent of the normal stress (σ_h) acting on the pile shaft; and *friction,* which should be proportional to that normal stress. Thus, in any particular stratum that is in contact with the foundation shaft:

$$f_s = c_a + K_s\sigma_h \tan\delta \tag{5.4}$$

Where, tanδ is the coefficient of friction between the soil and the pile shaft, which, according to experience with piles of normal roughness, can be taken as equal to tanϕ', the coefficient of friction of the remolded soil in terms of effective stresses; c_a is the adhesion between the soil and the pile shaft; σ_h is the normal stress acting on the pile shaft, which is conventionally related to the effective vertical stress at the corresponding level prior to placement of the pile by a coefficient of skin pressure *(K_s),* defined as σ_h / σ_v. The coefficient K_s depends mainly on the initial stress conditions of ground and the installation method of the pile; however, it is also affected by pile shape and length.

Figure 5-39 shows the deformation of the soil around the pile shaft, which is idealized as shearing of concentric cylinders. It should be noted that the maximum shear stress, τ_{max}, is induced at the pile wall.

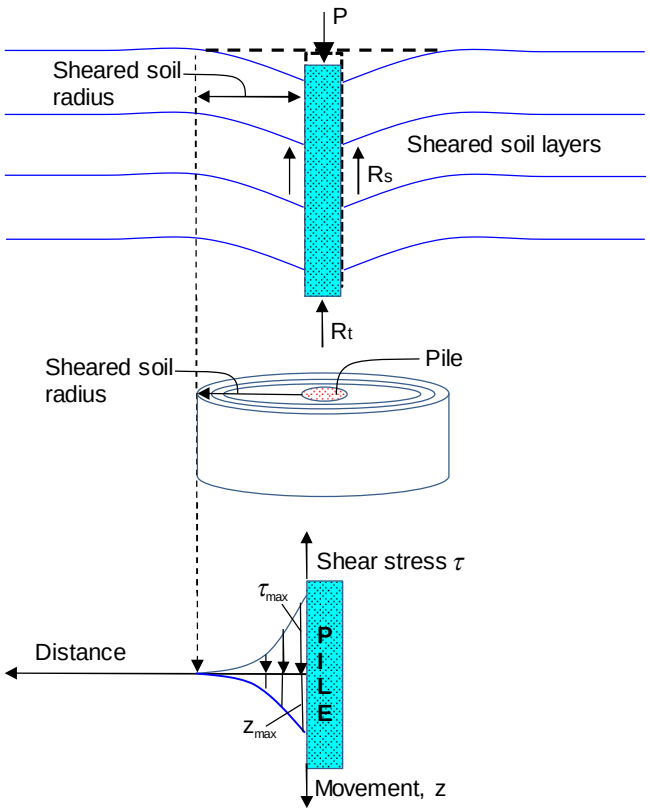

Figure 5-39 Shear stress and movement of soil surrounding axially loaded pile

5.4.2 Current Investigated Failure Patterns of Soil Surrounding P-cone device

After performing tests in three compacted soil chambers, the P-cone device was investigated to evaluate the failure patterns of soil surrounding the cone tip and along the cone shaft. The tensile area of the soil, if any, induced by the expansion of the jack, was also investigated to evaluate its effects on the results of the equivalent pile-head load-movement curve construction. The investigations were carried out by carefully excavating half of the compacted soil along the P-cone device. The results are presented in Figures 5-40 through 5-42.

Figure 5-40 shows the soil deformation surrounding the P-cone device in the first compacted soil chamber. The soil in this first chamber was not colored, making it difficult to see the soil deformation below the cone tip, along the cone shaft, and around the jack. The failure pattern below the cone tip was not formed through the bidirectional and end bearing tests that pushed the cone tip downward about 120 mm (185% diameter of cone). In other words, the horizontal stress build-up around the cone tip and shaft did not occur as in the conventional assumed failure modes of soil below pile toe, nor did the 120 mm opening of the jack create a tension of soil around the jack.

The compacted soils in the second and third chambers were colored, as shown in Figures 5-41 and 5-42, respectively, to improve the quality of the investigation of the soil deformation surrounding the P-cone device. As can be seen clearly from Figures 5-41a and 42a, the failure of the soil below the cone tips did not take place though the movements of the cone tip measured were about 100 to 120% diameter of the cone tip. When the cone tip penetrated into a deeper stratum, the soil surrounding the cone wall and below the cone tip became denser because the volume of the cone reduced the volume of the soil mass. An example of this physical phenomenon of soil is the placement of a solid mass into a water bottle, where the increase of the water volume

inside the bottle is equal to the volume of the placed solid mass. However, a distinction between the water and soil is that the soil possesses a skeleton of solid grains with voids, a type of discontinued material. Therefore, the total reduced volume of soil surrounding the pile must be equal to the volume of the installed pile. This means that the denser soil is, the larger is the influence area surrounding the pile. Consequently, the shaft and tip resistances have to be increased by the soil surrounding the denser compacted pile.

a) b)

Figure 5-40 Deformation of soil around cone after static load tests performed in first compacted chamber: a) Deformation of soil below cone tip, and b) Shear deformation of soil along cone shaft

Although the openings for the jack were about 100 to 120% diameter of the cone tip, no tension areas of soil around the jack were found; nor did the surrounding soil enter the gap created by the jack. In practice, if the cone test is performed in saturated soil, it is likely that water and soil would enter the gap created by the jack. To solve this problem,

the P-cone device needs to be filled with water for the bidirectional load test. If the water level in the P-cone device is higher than the groundwater table, it will prevent the soil surrounding the jack from entering the gap.

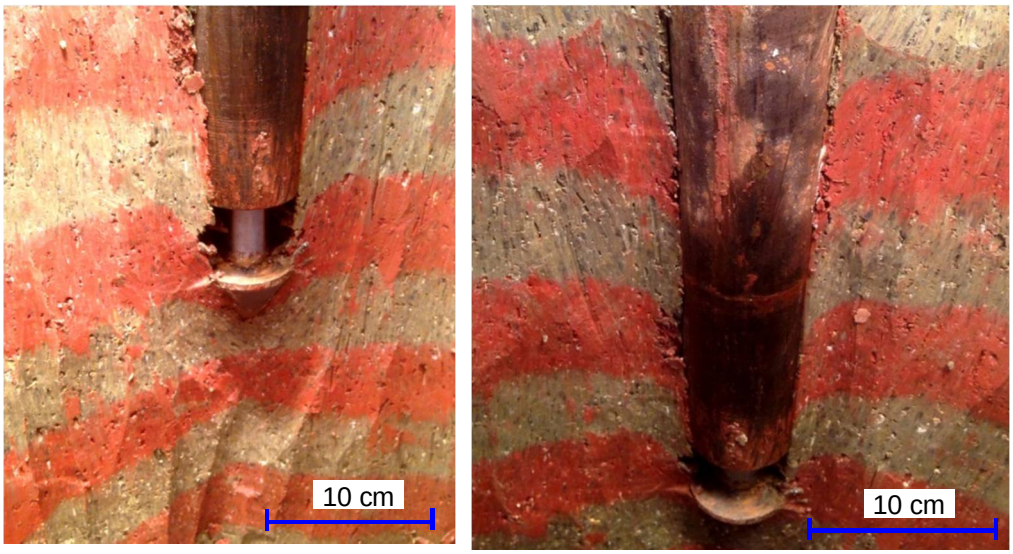

a) b)

Figure 5-41 Deformation of soil around cone after static load tests performed in second compacted chamber: a) Deformation of soil below cone tip, and b) Shear deformation of soil along cone shaft

Figures 5-41b and 5-42b show the soil deformation surrounding the cone shaft. The sheared soil areas surrounding the cone shaft were about 1.5 times or less the cone diameter. Shear failure only occurred at the interface between the pile and soil, and very small movements of approximately 2 mm were necessary to fully mobilize the shaft resistances. Therefore, the assumed shear failure of soil along the cone shaft was reasonable.

a) b)

Figure 5-42 Deformation of soil around cone after static load tests performed in third compacted chamber: a) Deformation of soil below cone tip, and b) Shear deformation of soil along cone shaft

5.4.3 Discussion

Discussion on the Bearing Capacity of the Pile Toe

There is nothing unusual about the assumptions of the soil failure below the pile toe in section 5.4.1 deviating from reality. When major consequences of theories are in agreement with observations, it is reasonable to retain and use them. However, if there is not enough evidence that at least the major consequences of a theory agree with experience, such a theory must be reconsidered and improved or rejected.

The experimental observations from the model pile tests of previous researchers (Rourk, 1961; Jumikis, 1962; Vesic, 1963; Robinsky and Morrison, 1964; Szechy, 1968;

Allersma, 1982; Yasufuku et al., 2001; Kuwajima et al., 2009; Manandhar and Yasufuku, 2011) and in this dissertation provide compelling evidence that the assumed soil failure modes below the pile toe are not in agreement with reality. The conventional bearing capacity theories assume that failure types of foundations result from the underlying soil being sheared and displaced laterally. However, unfortunately, the bearing capacity failures of deep foundations are rarely found in practice unless an earthquake temporarily liquefies a sandy soil where the pile toe is placed. The number of full-scale tests on both shallow and deep foundations did not satisfy the classical bearing capacity theories (Fellenius, 1999, 2011, 2016; Nguyen et al. 2013, 2014, 2016, 2017).

To prove the fallacy of the ultimate bearing capacity concept for the pile toe and the plunging failure load, an additional test was performed on a footing with a long stem, as shown in Figure 5-43. It is worth noting that a pile toe is, in principle, a footing with a long stem. The diameters of the footing and stem were 65 and 55 mm, respectively (left photo of Figure 5-43).

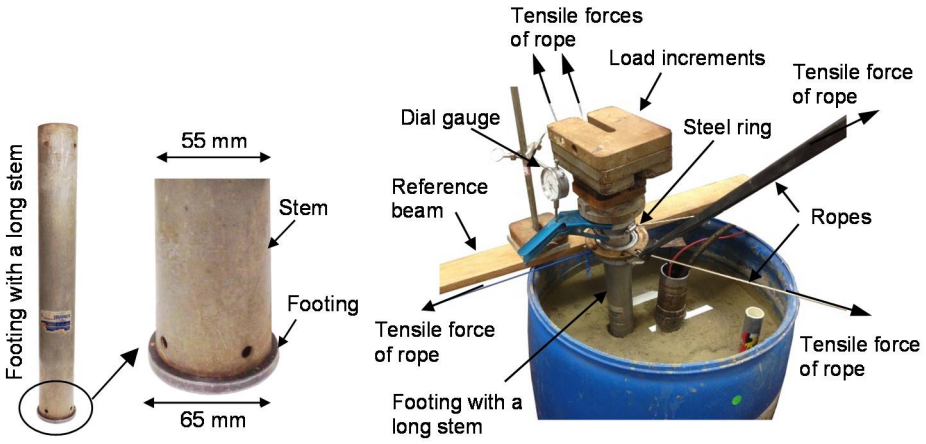

Figure 5-43 Set-up of static load test system for footing with a long stem

The difference between the footing and the stem diameter was 10 mm, which was enough to eliminate the shaft resistance of the stem, if any, when the footing moved

downward because of load increments. The footing was placed directly on the ground surface, which had been saturated for five months before the pile test was performed, in the compaction-saturated-soil chamber.

To simulate the actual condition of a pile toe, a steel ring was affixed by ropes (right photo of Figures 5-43 and 5-44) and was used to stabilize the footing during loading. The loading was performed in seven increments by placing the steel plates directly on the stem head. It should be noted that jacks were not used for this footing test, because using a jack system in the conventional static load tests has the effect of hiding details, rather than revealing them. The unloading was done in three decrements. Each of load increments was held for about 24h, and each of load decrements was held for 5 minutes. The test results are presented in Figure 5-45.

The left diagram of Figure 5-45 shows the measured stress-settlement of the footing. The right diagram presents stress against relative settlement for the similar data (The relative settlement is the measured settlement divided by the footing's diameter). It can be seen clearly from Figure 5.45 that the curves showed no break or other indication of failure in spite of relative settlements of about 78% footing diameter.

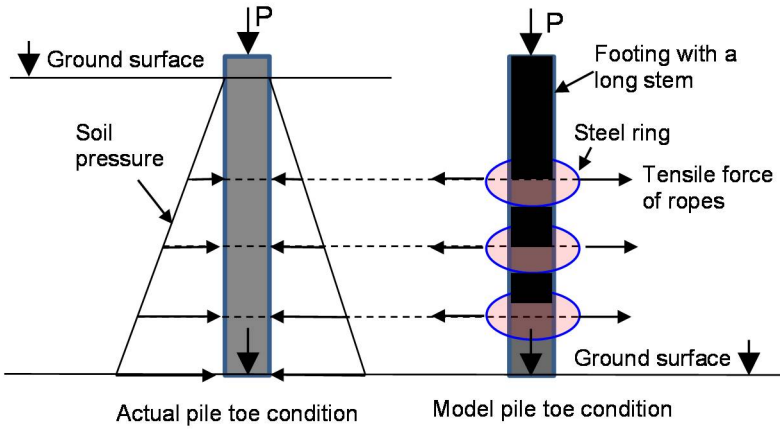

Figure 5-44 Comparison between the actual and model pile toe condition

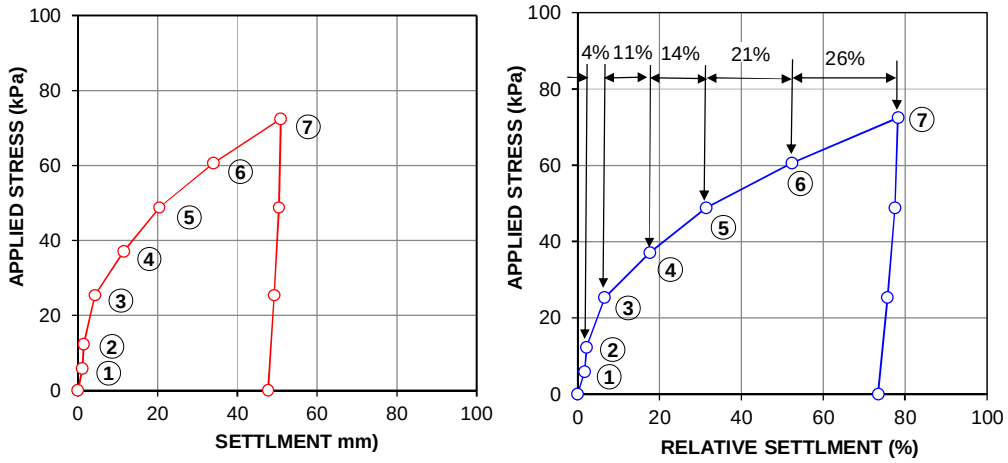

Figure 5-45 Stress versus settlement and stress versus relative settlement

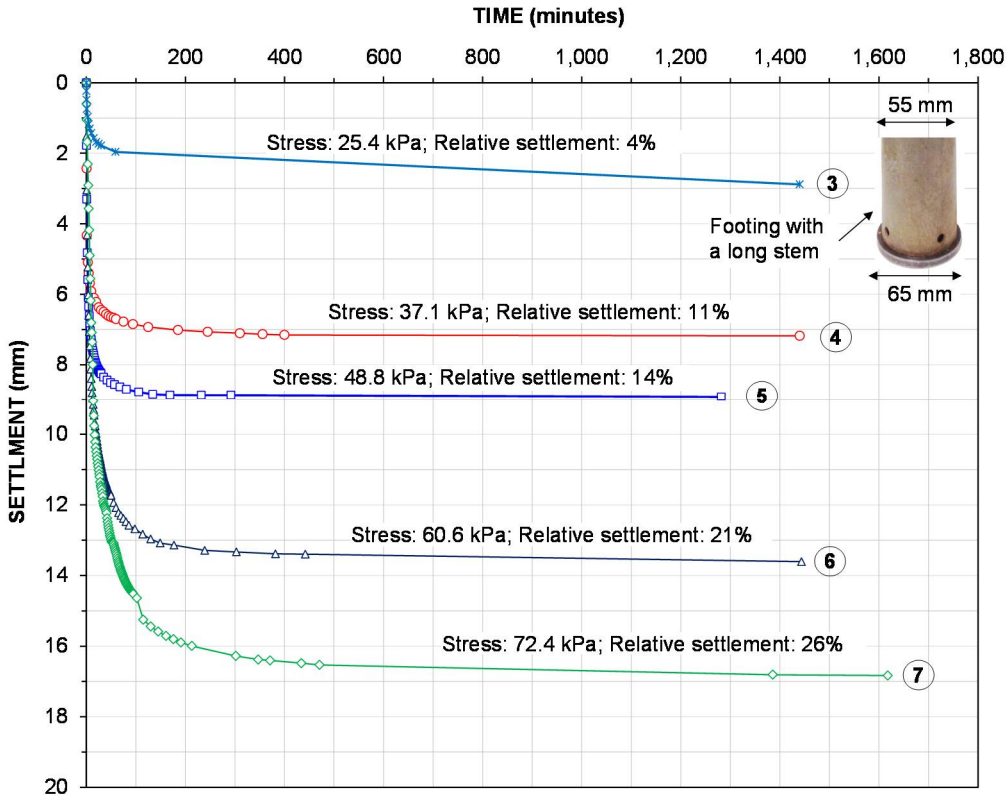

Figure 5-46 Settlement versus time of last five load increments

It has become clearly that when a deep foundation or a piled foundation is overloaded, it remains stable under the support of the lateral soil pressure (Figure 5-44) until a new stable position is found in the deeper stratum (Figure 5-46). This suggests that the ability of the soil to support a foundation depends, in part, on the depth of the foundation. Thus, it can be said the deeper the foundation, the greater the stability.

Therefore, the behavior of overloaded foundations (both deep and shallow foundations) is similar to a boat. It sinks deeper until it finds its stable depth. This can be seen clearly in Figure 5-45 and 5-46. After increasing load into 25.4 kPa, 37.1 kPa, 48.8 kPa, 60.6 kPa, and 72.4 kPa (load increments no.3 through no.7), the footing settled rapidly at the beginning and slowly after some elapsed minutes. After 100 elapsed minutes, the footing stabilized, after finding the new balance positions at the deeper strata. The consolidated settlements versus time were then continued; however, they were insignificant compared to the total settlement of each load increment.

The primary distinction between the foundation and a boat is that soils are much denser than water and possess shear strength. Therefore, eccentric loading and variations in shear strength inevitably cause the structure to tilt one way or the other. As a result, the soil is sheared and weakens through remolding. However, if central loading is applied and the strength of soil is homogenous, the soil below the foundation will consolidate and become stronger instead of shearing and becoming weaker.

Unfortunately, the central loading and homogeneousness of soil strength are impossible to obtain in practice, thus the shear failure of soil for the design of shallow foundations needs to be considered. However, using this approach for the pile toe is absolutely wrong because the pile toe is normally placed in deep soil and is supported by the lateral pressure of the soil; therefore, shear failure will not take place as found in shallow foundations. The investigative results of soil failures surrounding the model piles

presented in this dissertation are strong evidence that the ultimate bearing capacity concept for the pile toe is a fallacy.

Discussion on the so-called Plunging Failure Load

To give an explanation of the so-called plunging failure load concept in the conventional static load test, using a hydraulic jack system, it is necessary to reconsider the end bearing load test results in the second soil chamber, as shown in Figure 5-47.

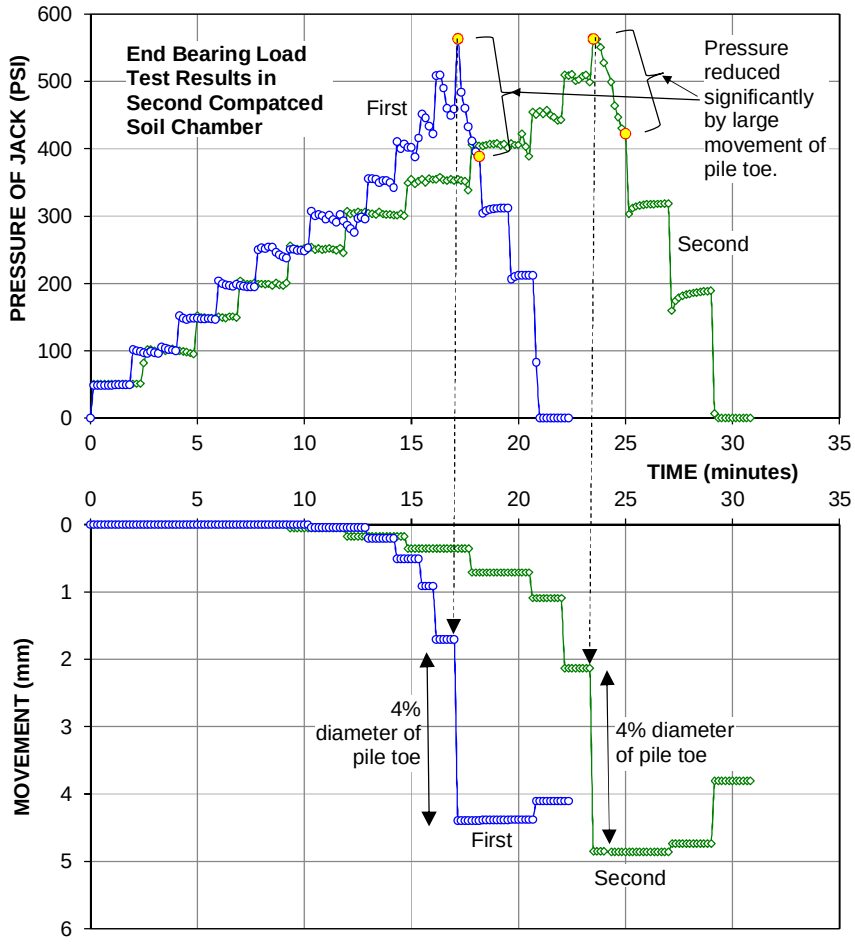

Figure 5-47 Loading schedule and movement versus time of end bearing load tests in second soil chamber

It can be seen clearly that when the jack was pressurized to about 560 psi, the movement of the pile toe increased quickly to about 4% of the diameter of the pile toe. As a result of this large movement, the pressure inside the jack was reduced continuously to around 400 psi pressure (the upper diagram of Figure 5-47), and it was nearly impossible to maintain the pressure level of 560 psi. This physical phenomenon was explained as a so-called plunging failure load. However, this explanation is not absolutely correct because the movement of the 4% pile toe diameter was only equal to the movement of the load increment from no. 2 to 3 and much less than the subsequent load increments in the footing test result shown in the right diagram of Figure 5-45 and Figure 5-46. It is obvious that the so-called plunging failure load in the conventional static load test, using a hydraulic jack system, did not reflect the actual failure of soil. It only reflected the failure of the hydraulic jack system to remain a stable pressure for the large movement of the test pile.

5.5 Consolidation Compression Tests

Soil engineering problems are of two basic types. The first type is when there is danger of the shearing stresses exceeding the shearing strength of the soils. The problems of this type have been discussed in the above sections. The second type is where there is no possibility of the stresses being sufficiently large to overcome the strength of soil in shear, but where the strains lead to what may be serious magnitudes of settlements of the soil mass. Problems of this type will be addressed in this section.

In practice, the weights of buildings cause compressions in the underground, which at shallow depths are definitely three-dimensional, but which, in deeply buried strata, are essentially one-dimensional. If a constant thickness of fill is placed over a very large area of ground surface, below which there is no horizontal variation in the soil,

compressions below the central portions of the area approach a truly one-dimensional case. Therefore, the concepts of the one-dimensional analysis have important practical applications.

For truly one-dimensional consolidation, two requirements must be satisfied. First, strains must occur in the vertical direction only. If the surface of the compressible stratum is an appreciable distance below ground, it is generally recognized that very little lateral movement can occur in the clay during its compression; thus this requirement is essentially satisfied. Second, all pore water that escapes must be along vertical seepage paths. A considerable variation from this assumed condition takes place in nature, and this is one of the major reasons that it is so difficult to accurately predict time for the analyses.

The assumption that a one-dimensional case exists in nature is used because any other case would at present be too difficult a solution. The consolidation test in the laboratory is conducted in such a way that it essentially follows one-dimensional conditions. However, this method has a lot of limitations because of the effects of sample sizes, sample disturbances, state of stresses, sample storage, friction rings, sample swells, porous stones, partial saturation, load-increment ratios, temperature, and others (Taylor, 1942; Olson, 1986; Crawford, 1986). These effects can lead to responses that deviate widely from predictions made using Terzaghi's original theory.

This dissertation is based on research performed by administering consolidation compression tests, using the P-cone device in the compaction-saturated soil chamber, to correlate the results with those of the one-dimensional consolidation tests. During preparation of the compacted soil chamber, the soil layers were sampled to serve the one-dimensional consolidation test in the laboratory. Table 5-11 shows the properties of the soils prepared for the consolidation test by the P-cone device. The average water

content was about 25%, the average density was about 19.2 kN/m^3, and the void ratio calculated was about 0.721.

Table 5-11 Densities and water contents of compacted soil of third experiment

Depth	Water Content (%)			Moisture Density (kN/m^3)		
mm	1	2	3	1	2	3
300	24.2	23.6	25.0	19.5	19.2	-
400	25.8	24.8	25.2	19.2	19.3	-
500	23.4	23.6	25.2	19.2	19.4	-
600	27.4	28.4	26.2	18.9	18.7	-

The penetration test by the P-cone device was performed after the compacted soil chamber had been saturated for three months, and the test results are presented in Figure 5-48. At the consolidation test time, the groundwater levels in the open standpipe and in the P-cone device were about 160 mm below the ground surface.

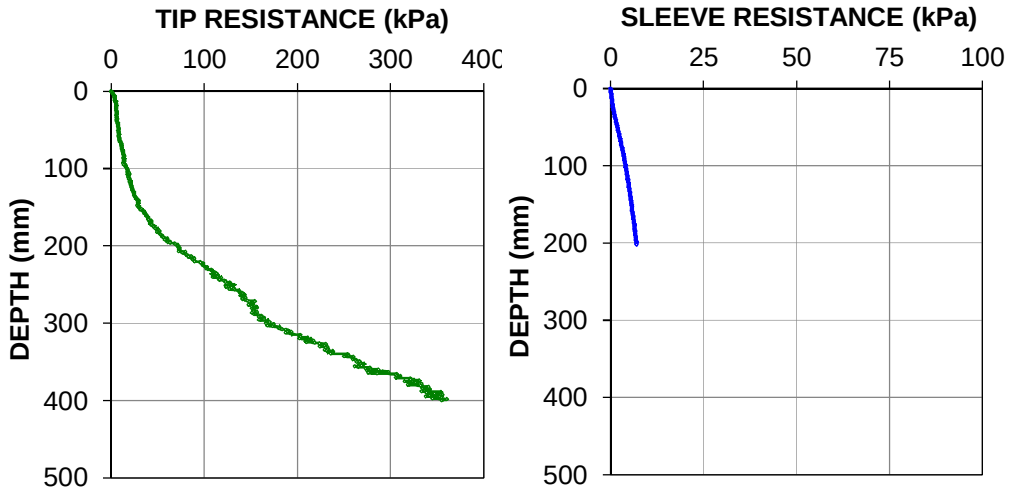

Figure 5-48 Cone shaft and tip resistance measured in the saturated soil chamber

5.5.1 Results of One-Dimensional Consolidation Tests in the Laboratory

One-dimensional consolidation tests were performed on the soil samples extracted from four different depths of the saturated soil chamber. Before carrying out the consolidation tests, the soil samples were saturated for four days. The loading procedures were performed according to Standard ASTM D 2435-11. The consolidation test results are presented in Figure 5-49.

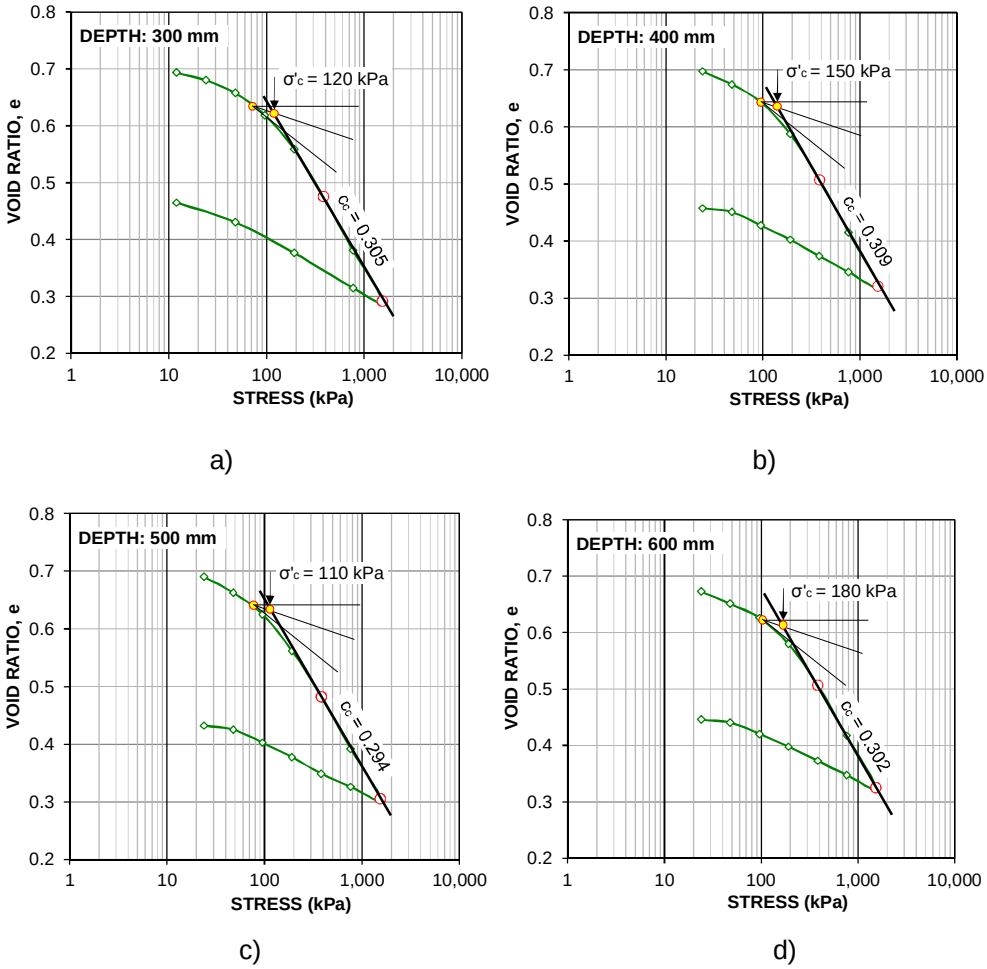

Figure 5-49 One-dimensional consolidation test results of four soil samples at different depths

The compression index (C_c) determined was about 0.305, 0.309, 0.294 and 0.302 for 300, 400, 500 and 600 mm depths below ground surface, respectively. The precompression stresses determined, based on Casagrande's method, were about 120, 150, 110 and 180 kPa, as shown in Figures 5-49a through 5-49d, respectively.

To correlate the consolidation test data of the oedometer device with the consolidation test data of the P-cone device, it was necessary to convert the compression indexes obtained for the one-dimensional consolidation into the modulus numbers (m) of Janbu's method (1967) as:

$$m = \ln 10 \frac{1+e_0}{C_c} = 2.3 \frac{1+e_0}{C_c} \tag{5.5}$$

The calculation results of the modulus numbers, based on the compression indexes and void ratios, are presented in Table 5-12.

Table 5-12 Modulus numbers determined from the compression index and void ratio

Depth	e_0	C_c	m
300 mm	0.699	0.305	12.8
400 mm	0.706	0.309	12.7
500 mm	0.700	0.294	13.3
600 mm	0.681	0.302	12.8

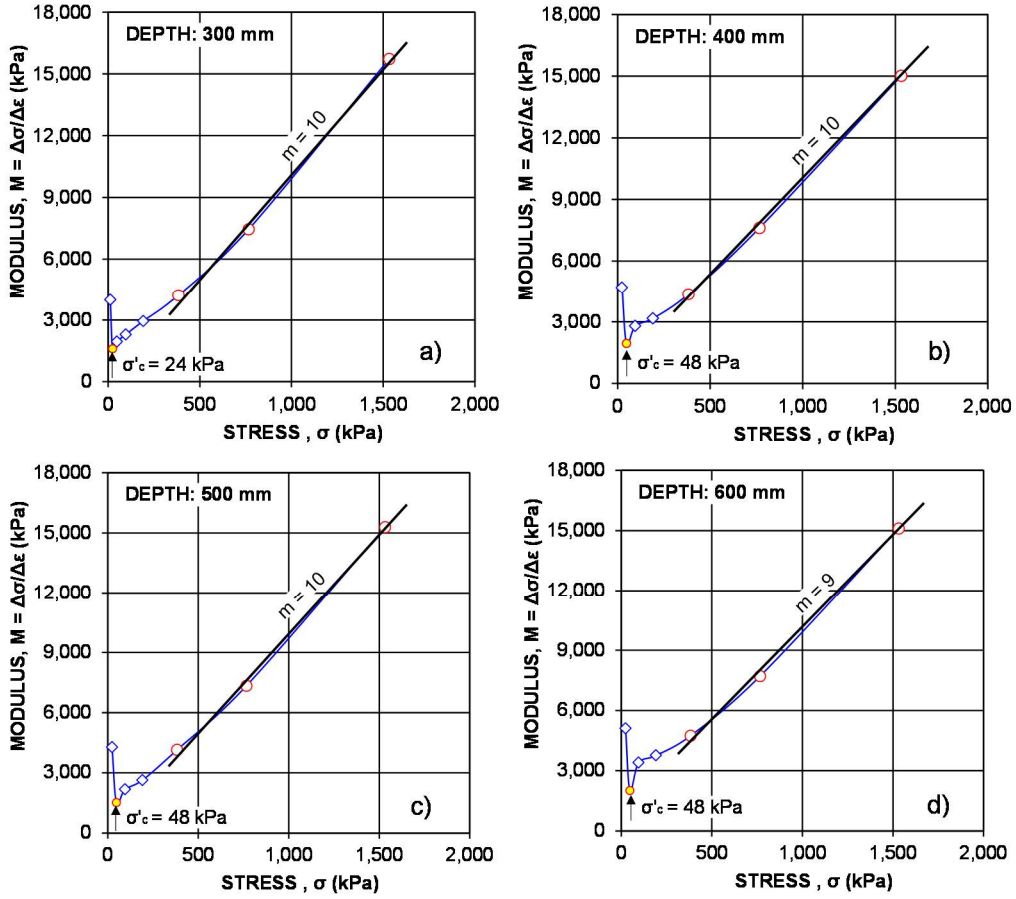

Figure 5-50 Determination, using Janbu's method (1967), of modulus number and preconsolidation stresses

It is often difficult to obtain an exact value of the preconsolidation stress based on Casagrande's method, even from oedometer tests on high quality specimens. Therefore, Janbu's method was also used to evaluate the preconsoldation stress from the consolidation test data, as shown in Figure 5-50. The analysis of the four tested soil samples showed an average modulus number, m, of about 10 and an average preconsoldation stress of about 42 kPa.

5.5.2 Results of Consolidation Tests by P-cone Device

Two consolidation compression tests were performed by the P-cone device in the saturated soil chamber. The first consolidation compression test was conducted five months after saturation. Seven days after the first consolidation test, the second consolidation test was performed. It should be noted that most of load increments were only held for 1h because the current P-cone device has not yet been equipped with an automatic pressure control system, which makes it difficult to maintain a stable pressure stable during the load-holding time. As indicated in the consolidation test results of the footing (Figure 5-46), the settlements measured from 1h through 24h were relatively small. This means that the 1h holding time had an insignificant influence on the consolidation test results by the P-cone device.

To calculate the modulus numbers, based on the consolidation compression test data from the P-cone device, the following equation was used (Fellenius, 2017):

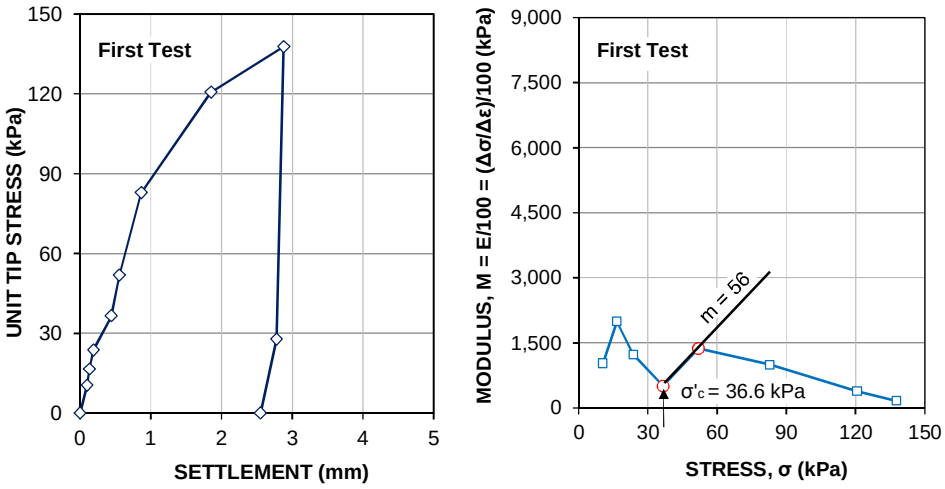

Figure 5-51 Load versus settlement and modulus number obtained from first consolidation test by the P-cone device.

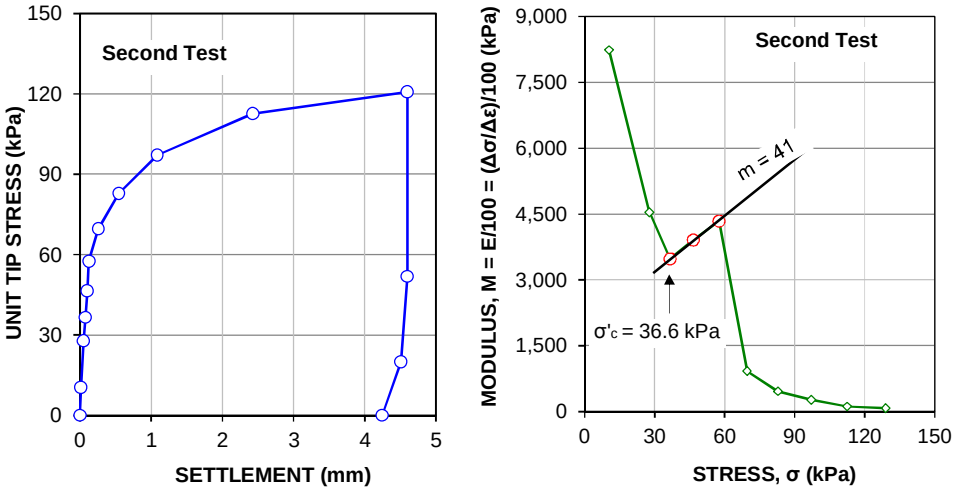

Figure 5-52 Load versus settlement and modulus number obtained from second consolidation test by the P-cone device.

$$m = \frac{E}{100} = \frac{\Delta\sigma / \Delta\varepsilon}{100} \tag{5-6}$$

Where, m is modulus number, E is modulus of soil in units of kPa, Δσ is the applied stress and Δε is the measured strain.

The consolidation test and analysis results are presented in Figures 5-51 through 5-52. The load-settlement data measured by the consolidation tests are provided in the left diagrams of Figure 5-51 and 5-52.

5.5.3 Discussion

Table 5-14 shows a comparison of pre-consolidation stress and the modulus number obtained from the oedometer and P-cone test device. It can be seen clearly that the modulus numbers were significantly different: about 80% for Janbu's method and 73% for Casagrande's, while the difference in pre-consolidation stresses was about 15% for Janbu's method and 283% for Casagrande's.

Table 5-13 Preconsolidation stress and modulus number obtained from Oedometer and P-cone device

	Oedometer		P-cone	Difference	
	Casagrande	Janbu	Janbu	Casagrande	Janbu
Average preconsolidation stress, σ'c (kPa)	140	42	36.6	283%	15%
Average modulus number, m	13	10	49	73%	80%

5.6 Summary

The important findings obtained from the measurements and analyses of the P-cone device tests (penetration test, head-down test, bidirectional test, end bearing test, and consolidation test) are summarized below.

1. The P-cone device penetration tests and measurements were performed successfully in three soil chambers with different densities and water contents. The maximum length of the ground surface cracks induced by the cone penetration tests was about twice the diameter of the cones, indicating that the ratio of chamber diameter to cone diameter of 9 is enough to eliminate the effects of the boundary conditions.
2. The head-down test results showed that the pile capacities were about 3.95, 5.10, and 2.88 kN for the pile tests performed in the first, second, and third soil chambers, respectively. The bidirectional load tests indicated that the unit shaft resistances were about 12, 14, and 8 kPa for the tests conducted in the first, second, and third soil chambers, respectively. The end bearing load

test measurements showed that the pile toe capacities were about 2.4, 3.4, and 1.4 kN for the tests done in the first, second and third soil chambers, respectively.

3. The re-evaluation of the Equivalent Pile-Head Load-Movement Curve Construction shows a significant difference between the positive and negative shaft resistance of soil when it is being sheared. The average differences were about 8%, 16%, and 21% for the test results performed in the first, second, and third soil chambers, respectively. An adjustment was proposed for the constructed equivalent pile-head load-movement curves. The adjustment coefficients were about 1.07, 1.15, and 1.3 for the tests performed in the first, second and third soil chambers, respectively.
4. The estimations of the pile capacity were conducted based on the head-down load test results. The comparison of the measured and estimated pile capacities showed that the best prediction methods were those of DeBeer and Davisson, with a difference of only about 1%. The next most accurate methods were those of Vander Veen and Chin-Konder, with a difference of only about 2%. Mazurkiewicz and Decourt's method had a difference of only about 4%, Fuller and Hoy's, Brinch Hansen's (80% criterion), and Bulter and Hoy's showed differences of 12, 19, and 31%, respectively.
5. The estimations of the pile capacity were performed based on the cone penetration test results. The comparison of the estimated and measured pile capacities showed considerable differences. The methods that produced pile capacities closest to the measurements were those of Schmertmann-Nottingham and Tumay-Fakhroo, with differences of about 21 and 24%, respectively. The next accurate methods are those of De Ruiter-Beringen

and Mayerhof, with differences of about 39 and 47%, respectively. The methods that gave the most dramatic differences were Bustanmante-Gianselli's and Eslami-Fellenius's, with differences of about 58 and 87%, respectively. It is likely that taking the average of the cone tip resistances in the subject cases, as well as the differences in cone sizes, led to such dramatic distinctions.

6. Based on the shear strength parameters of the soil, the pile capacities computed were about 5.7, 4.0, and 2.3 kN for the test piles installed in the first, second and third soil chambers, respectively. The differences between the computed and measured pile capacities were about 44, 22 and 20%, respectively. The average difference of the tests performed in the three soil chambers was about 29%.
7. The investigation of soil failures along the cone shaft and below the cone tips showed that the sheared soil areas surrounding the cone shaft were twice the diameters of the cone, and the shear failures took place at the interface of the cone wall and soil. Shear failures did not occur below the cone tip although the movements of the cone tip ranged from 100 through 185% of the cone diameter. In order words, there was no build-up of horizontal stress around the cone tip and shaft, as there was for the conventional assumed-failure modes below the pile toe. The investigation of soil deformation around the jack indicated that the expansion of the jack did not create tension areas for any of the tests. Thus, the effects of the tension areas created by the jack expansion can be ignored for the equivalent pile-head load-movement curve construction from the bidirectional load test results.

8. The consolidation test results performed by the P-cone device were correlated with the oedometer test data. The correlation modulus numbers obtained from the oedemeter and P-cone test device were significantly different, at about 80% for Janbu's method and 73% for Casagrande's. The difference of the pre-consolidation stresses was about 15% for Janbu's method and 283% for Casagrande's.

Chapter 6

Modeling of Static Load Tests on P-cone Device

6.1 Introduction

Engineering is basically related to modelling and finding solutions to the real problems. Therefore, it is necessary to see the essence of the problem and identify the key features to be modelled; that is, those features need to be considered and included in the design. One aspect of engineering judgment is to identify those features which are believed to be safe to ignore. The finite element modeling seems to be the most common procedure employed in geotechnical engineering. For deep foundations, conventional methods to calculate deformations and bearing capacities cannot generally account for the factors such as stresses and disturbances caused by driving, in situ stress and its spatial variation, variations in strength of soils and interfaces, size and length of embedment, geometrical changes, consolidation and negative skin friction, group and interaction effects, cyclic loading, and physical phenomenon like arching. The finite element method has shown significant promise in handling many of these factors.

The PLAXIS 3D Foundation Version 2.0 was used to model the P-cone tests conducted in the three soil chambers. The embedded pile approach was used to model the axial static compression load test, and the standard finite element approach was used to model bidirectional load test because the embedded pile approach in PLAXIS 3D Foundation did not allow the modelling of the bidirectional load test. The purpose of the modelling was to consider the influence area of the soil surrounding the P-cone device for selecting the reasonable chamber dimension in the future, especially for small strains and stresses which could not be observed visually, during investigation of soil failure surrounding the P-cone device.

6.2 Geometry of Model Piles

To model the tested P-cone device (small model pile) using PLAXIS 3D FOUNDATION, a working area of 2 m x 2 m was used (Figure 6-1) instead of the actual area of the soil chambers. The analysis was done to model the penetration behavior and hence the boundary conditions are not included in the modeling predictions.

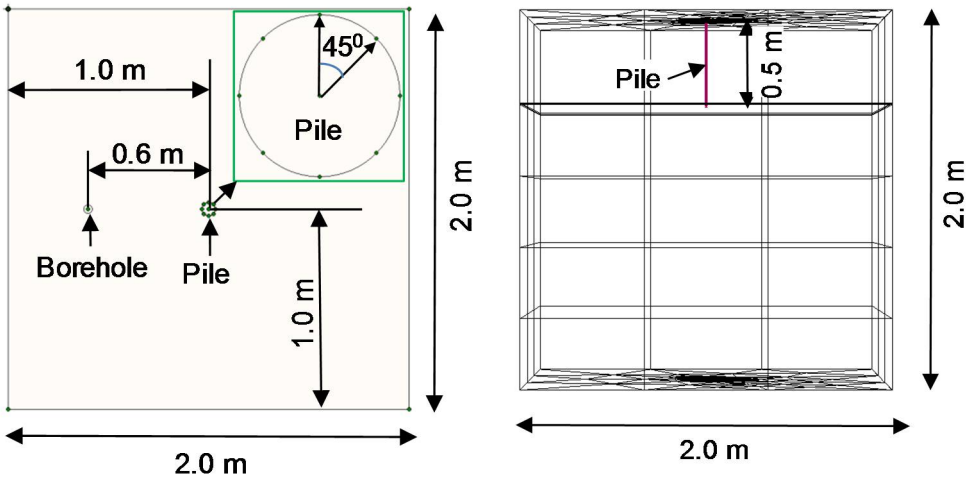

Figure 6-1 Working area and location of borehole and modeled pile

The P-cone device was modelled as a solid pile, using volume elements in the center of the mesh. The dimensions of the modeled piles are shown in Figure 6-2. The soil consisted of a single layer of compacted clayey silt soil with properties as provided in Table 6-1. The load was modelled as a distributed load at the pile head and the position of the jack (Figure 6-2).

The generation of a 3D finite element model started with the creation of a geometry model, which was a composition of a borehole (Figure 6-1) and horizontal work planes (Figure 6-2). The borehole was used to determine the local stratigraphy (vertical soil layer position) and ground surface level. The work planes were used to define

geometry lines, piles, and loads. During the definition of the borehole, a data set of model parameters for the clayey silt soil layer and pile was created and assigned to the borehole and the pile, respectively.

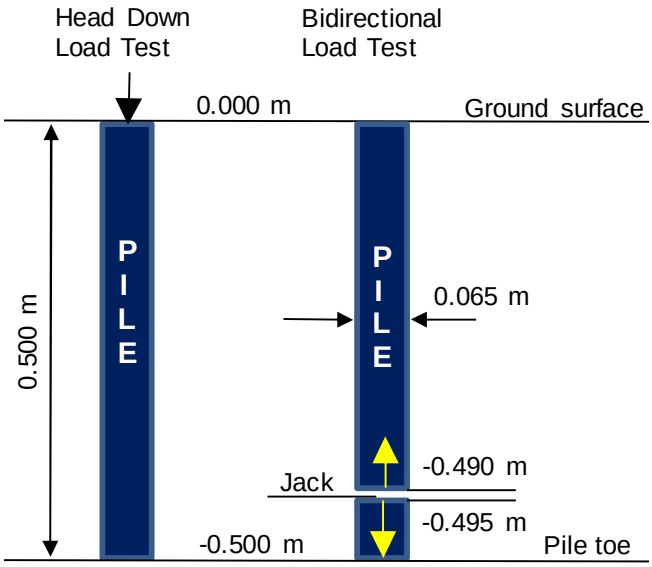

Figure 6-2 Dimensions and work planes of modeled piles for head-down and bidirectional load tests

From the geometric model, a 2D mesh was generated and optimized by global and local refinement, after which an extension into the *y* direction (the third dimension) was made. PLAXIS program generated automatically this 3D mesh, considering the information from the boreholes and work planes.

6.3 Material Properties of Soils and Pile

The required soil parameters were determined based on the laboratory tests conducted. The Mohr-Coulomb model was used for the soil behavior surrounding the model piles. This model consisted of five parameters: Elastic modulus *E*, Poisson's ratio

v, the cohesion *c*, the friction angle ϕ, and the dilatancy angle ψ. Undrained total strength and stiffness parameters are considered and used in the analysis.

The first two parameters governed the characteristics of the load-movement curve of the modelled piles, while the remaining parameters governed the bearing capacity of the modeled piles. It should be noted that the bearing capacity of the pile is also an input parameter for the embedded pile approach, and it was thus used in the modelling. As opposed to the embedded pile approach, the standard finite element approach showed that the capacity of pile was governed by the shear strength parameters of soil; hence it is likely that the capacities of pile obtained from modelling will differ from the measured capacities of pile.

The elastic modulus of soil, E_s, may be estimated from empirical correlations (USACE EM 1110-1-1904) as follows:

$$E_s = K_c C_u \tag{6-1}$$

Where, E_s is Elastic modulus of soil, K_c is correlation factor and C_u is undrained shear strength of soil. The K_c factor is a function of the overconsolidation ratio and plasticity index PI, which was determined from field measurements (Figure 6-3).

However, the modulus of soil is not a constant; it tends to increase with confining pressures. Moreover, it also depends on the loading paths. The stiffness is much higher for reloading than for primary loading. As stated earlier, this parameter governs the characteristics of the load-movement curve; therefore, the values of the soil modulus were adjusted to match the load-displacement curves obtained from modelling with those of the conventionally axial static compression and bidirectional load tests. The plasticity index of soil used for the P-cone tests was about 34, and thus the coefficient K_c,

estimated from the diagram in Figure 6.3, was about 500 for the assumed overconsolidation ratio of unit.

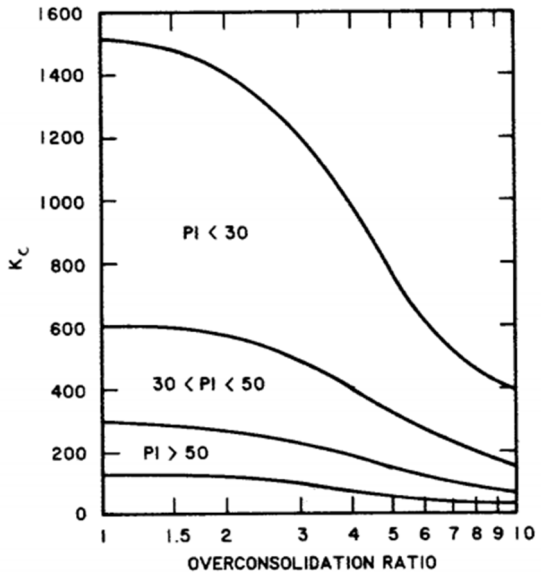

Figure 6-3 Chart for estimating constant Kc to determine the elastic modulus from the undrained shear strength.

Poisson's ratio (v) of soil material was evaluated by matching the lateral earth pressure coefficient (K_0), following the equation of $v = K_0/(1+ K_0)$. The lateral earth pressure coefficient (K_0) was determined based on the effective friction angle of soil according to equation of, $K_0 = 1 - \sin\phi'$. Because the drained direct shear tests of soil were not performed, the effective friction angle of soil was estimated based on the correlation with the plasticity index. For the soil plasticity index of 34, the effective peak friction angle of soil is about 28^0 (Ameratunga et al., 2016). Therefore, the coefficient (K_0) and Poisson's ratio (v) estimated were about 0.55 and 0.35, respectively. This value of Poisson's ratio is compatible with recommendations in the Manual of Plaxis 3D Foundation for undrained behavior of soil (For undrained behavior of soil, Poisson's ratio should range from 0.30 to 0.35).

The unit weights of compacted soils were applied to both saturated and unsaturated soil weights in the Mohr-Coulomb model. The soil strength was modelled by setting the cohesion parameters equal to the undrained shear strength, combined with undrained friction angles (ϕ) of the direct shear tests.

In addition to the soil properties, the data set also contained parameters for deriving interface properties from the soil model parameters. The main parameter of interface is the factor of strength reduction R_{inter}, which was assigned as Rigid (which corresponds to R_{inter} = 1.0) for materials of both of soil and pile.

The real interface thickness δ_{inter}, is a parameter that represents the real thickness of a sheared zone between the pile and the soil. The δ_{inter} is only of importance when the hardening soil model is used and combined with the interfaces. Therefore, it was not considered for analysis. The values of the Mohr-Coulomb model parameters are shown in Table 6-1.

The pile material was modelled as a non-porous linear elastic material with three parameters: Elastic modulus *E*, Poisson ratio v and unit weight of pile γ. The elastic modulus of pile was used from the tension test results of the steel tubes, which was about $2.25*10^8$ kPa (Lan et al., 2016). The Poisson ratio (v) was set as zero, because the elastic shortenings of the pile material obtained from the static load test were not significant. The unit weight of the pile material was about 76.5 kN/m^3. Tables 6-2 and 6-3 show the input parameters for the piles modelled by the standard finite element and embedded pile approaches for the axial static compression and bidirectional load tests, respectively.

Table 6-1 Material properties of the clayey silt and its interface

Parameter	Soil chamber			Unit
	First	Second	Third	
Material model	M-C	M-C	M-C	-
Type of material behavior	Undrained	Undrained	Undrained	-
Soil weight, ($\gamma_{unsat,}$ γ_{sat})	19	19.5	18.7	kN/m^3
Young's modulus ($E = 500*C_u$)	16,950	25,050	9,750	kN/m^2
Poisson's ratio (v)	0.35	0.35	0.35	-
Cohesion (c_u)	33.9	50.1	19.5	kN/m^2
Friction angle (ϕ)	4.9	2.1	2.7	^{0}
Dilatancy angle (ψ	0.0	0.0	0.0	^{0}
Interface strength (R_{inter})	1.0	1.0	1.0	-
Lateral pressure coefficient (K_0)	0.55	0.55	0.55	-

Table 6-2 Input parameters of pile for modelling bidirectional load test

Parameter		Value	Unit
Material model	Model	Linear elastic	-
Type of material behavior	Type	Non-porous	-
Unit weight	γ	76.5	kN/m^3
Young's modulus	E	$2.25*10^8$	kN/m^2
Poisson's ratio	v	0.0	-
Interface strength	R_{inter}	1.0	-

Table 6-3 Input parameters of embedded pile for modelling head-down load test

Parameter	Soil chamber			Unit
	First	Second	Third	
Unit pile weight, (γ)	76.5	76.5	76.5	kN/m^3
Young's modulus (E)	$2.25*10^8$	$2.25*10^8$	$2.25*10^8$	kN/m^2
Diameter (d)	0.065	0.065	0.065	m
Skin resistance at pile top ($T_{top,max}$)	11	12	9	kN/m^2
Skin resistance at pile bottom ($T_{bot,max}$)	11	12	9	kN/m^2
Base resistance (F_{base})	2.4	3.4	1.4	kN

6.4 Mesh Generation

To carry out the finite element analysis, the geometry has to be divided into elements and the combination of finite elements is called the finite element mesh. The 2D mesh of work planes was generated after the geometry model has been generated and the material properties were assigned to all soil layers and the pile. For this research, the 2D mesh was made fully satisfactory before proceeding to the 3D mesh generation. After the 2D mesh was deemed satisfactory, the 3D mesh generation was performed. It should be noted that the PLAXIS 3D FOUNDATION program generated automatically the 2D and 3D finite element meshes.

To reduce the calculation time, the coarse and very coarse 2D meshes were generated for test piles modelled by the embedded pile and standard finite element. However, the meshes were enough fine to gain accurate numerical results because the dimensions of the modeled piles were relatively small (pile diameter of 0.065 m and the

embedded pile length of 0.5 m), as shown in Figure 6-4. The elements of the modelled axial compression and bidirectional load test piles were 630 and 11,942, respectively.

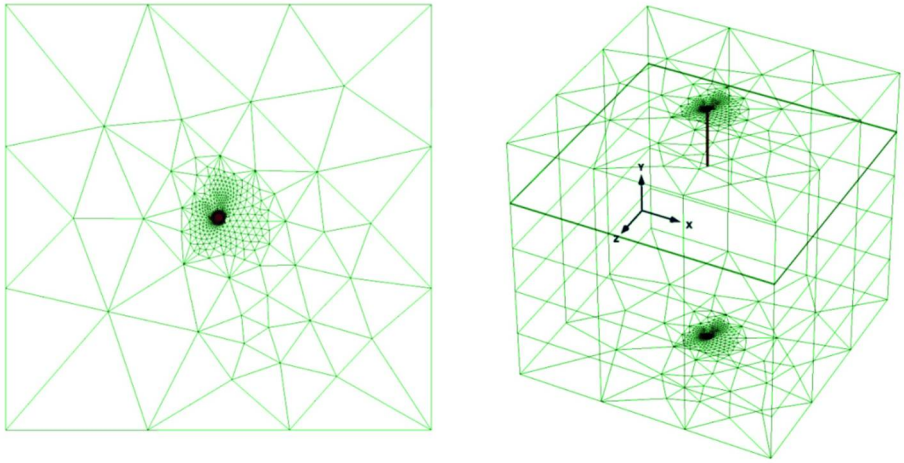

Figure 6-4 2D and 3D meshes for modelled bidirectional test piles

6.5 Calculation Stages

Defining calculation phases

The initial stress state (initial phase) is computed by the real calculation of finite element, where the weight of soil can be applied by gravity loading or the K_0 procedure. Gravity loading and the K_0 procedure are only available for the initial phase. Gravity loading is a type of plastic calculation, where the initial stress state is generated by the weight of the soil. The K_0 procedure can be used to determine the initial stresses of the model if the lateral earth pressure is known. This procedure was used for modeling the tested piles of this study with the lateral earth pressure K_0 of 0.55. The initial phase is the beginning point to consider further calculations; nevertheless, displacements computed from the initial phase are not considered for the following calculations. Thus, these movements are reset to zero at the starting for the following calculation phase.

To begin a new calculation phase after the Initial phase, the definition starts with the selection of the calculation types as plastic, consolidation, and phi/c reduction. The

plastic calculation is used to perform the analysis of the elastic-plastic deformation following the theory of the small deformation. The stiffness matrix in a plastic calculation is based on the original un-deformed geometry. This calculation type is suitable for the practical geotechnical applications, and it was used for the analysis of the test piles.

The consolidation analysis is often performed for the saturated clay-type soils. However, this case was not considered since the piles were tested in the compaction-unsaturated soil chambers. The analysis of phi-c reduction in PLAXIS 3D FOUNDATION can be performed by decreasing the strength parameters of the soil. This process is termed “phi-c deduction” and it is available for calculation as a separate type. Phi-c deduction is only chosen when it is desired to compute a global safety factor for the situation at hand. Thus, it was not considered for this study.

Load Stepping Procedures

The program of PLAXIS 3D FOUNDATION sets up an automatic load stepping procedure as a solution for non-linear plasticity problems. The procedure is controlled by several calculation control parameters. Therefore, the default setting for the automatic load stepping procedure was applied in all analyses of the test piles modelled in this dissertation. Table 6-4 shows the loading steps of the modelled test piles.

Table 6-4 Loading procedures of the modelling piles tested in three soil chambers

Loading Steps	Head-down Load Test	Bidirectional Load Test	
	(kN)	(kN)	(kPa)
Initial Phase	K_0 Procedure	K_0 Procedure	K_0 Procedure
Pile Installation (Plasticity)	Self-weight	Self-weight	Self-weight
Loading step 1 (Plasticity)	1.0	0.5	151
Loading step 2 (Plasticity)	2.0	1.0	302
Loading step 3 (Plasticity)	2.5	1.5	452
Loading step 4 (Plasticity)	3.0	2.0	603
Loading step 5 (Plasticity)	3.5	2.5	754
Loading step 6 (Plasticity)	4.0	3.0	905
Loading step 7 (Plasticity)	4.5	3.5	1,055
Loading step 10 (Plasticity)	4.7	4.0	1,206

6.6 Modelling Results

6.6.1 Pile Installation

The modelling of the pile installation phase evaluates the effects of the boundary conditions during P-cone penetration in the soil chambers. In Figure 6-5, the standard finite element approach shows the soil deformation surrounding the pile, in the pile installation phase in the first soil chambers. The embedded pile approach does not take into account the installation effects of piles. It can be seen clearly from Figure 6-5a) and 6-5b) that the influence radius of the P-cone penetration at the ground surface was about 0.3 m, which is equal to four times the diameter of the P-cone. The influence zone of the P-cone penetration reduced gradually versus depth. The influence zone at the elevation of the P-cone tip was estimated at about half of the ground surface elevation.

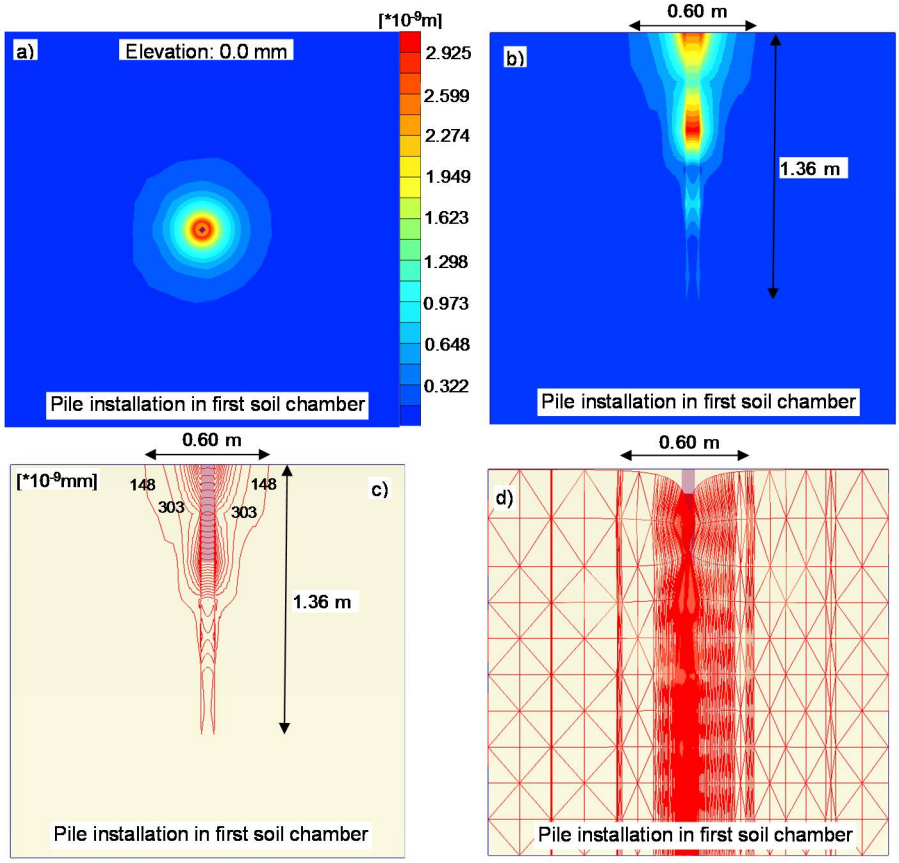

Figure 6-5 Pile installation in first soil chamber: a) Deformation soil at elevation 0.0 mm, b) deformation soil along pile, c) contour lines of soil deformation along pile, d) plane deformation of soil around pile

The influence zone below the P-cone tip was about 0.86 m, which was equal to 13 times the diameter of P-cone. The outermost boundary soil strain of the influence zone was about $148*10^{-9}$ mm. It is apparent that this small strain value could not be observed by eye-balling, so the numerical tools were very useful for evaluating the small strains of soil. It should be noted that the cracks observed from the experiments showed that the influence zones at the ground surface were only about twice the diameter of the P-cone device, which was observed by eye-balling. The small strain of soil around the P-

cone device during penetration was not measured for comparison with the results of numerical modelling because it was not pertinent to this dissertation.

The results of modelling the installed P-cone showed that the actual dimensions of the soil chamber used for the P-cone tests were not large enough to eliminate completely the effects of the boundary conditions. However, the soil strains of the modelling were so small that it was not necessary to consider an adjustment from the test results of the P-cone device. Modelling of P-cone penetrations in three soil chambers was performed; however, only the results of modelling for the first soil chamber were presented because the results from all three chambers were relatively similar.

6.6.2 Axial static compression load test

Figures 6-6 through 6-8 present deformations and shear stresses of soil surrounding pile modeled by the standard finite element approach for an axial compression load test in the first soil chamber at a load increment of 1206 kPa (4 kN). It should be noted that the embedded pile approach in Plaxis 3D FOUNDATION did not take into account the effects of the pile installations or the deformation of soil surrounding the pile under the applied loads.

Deformation of Soil Surrounding P-cone

Figure 6-6 shows deformation of the .soil surrounding the modelled pile for loading of 1206 kPa (4 kN). For this loading level, the influence zone of soil surrounding the P-cone device at the ground surface elevation was expanded to twice the influence zone in the pile installation phase (Figures 6-6c through 6-6d). The expansion of the influence zone below the P-cone tip was not significant, at about 0.14 m. The uttermost

deformation contour of soil was relatively small, at about $10*10^{-3}$ mm, as shown in Figure 6-6c).

Mobilized Shear Strength and Relative Shear Stress of Soil around P-cone

Figures 6-7 and 6-8 show the mobilized shear strength and relative shear stress of soil around the P-cone modeled in the first soil chamber. It can be seen clearly from Figures 6-7c and 6-7d that the working area of the modeled pile was not large enough to eliminate the effects of the boundary conditions.

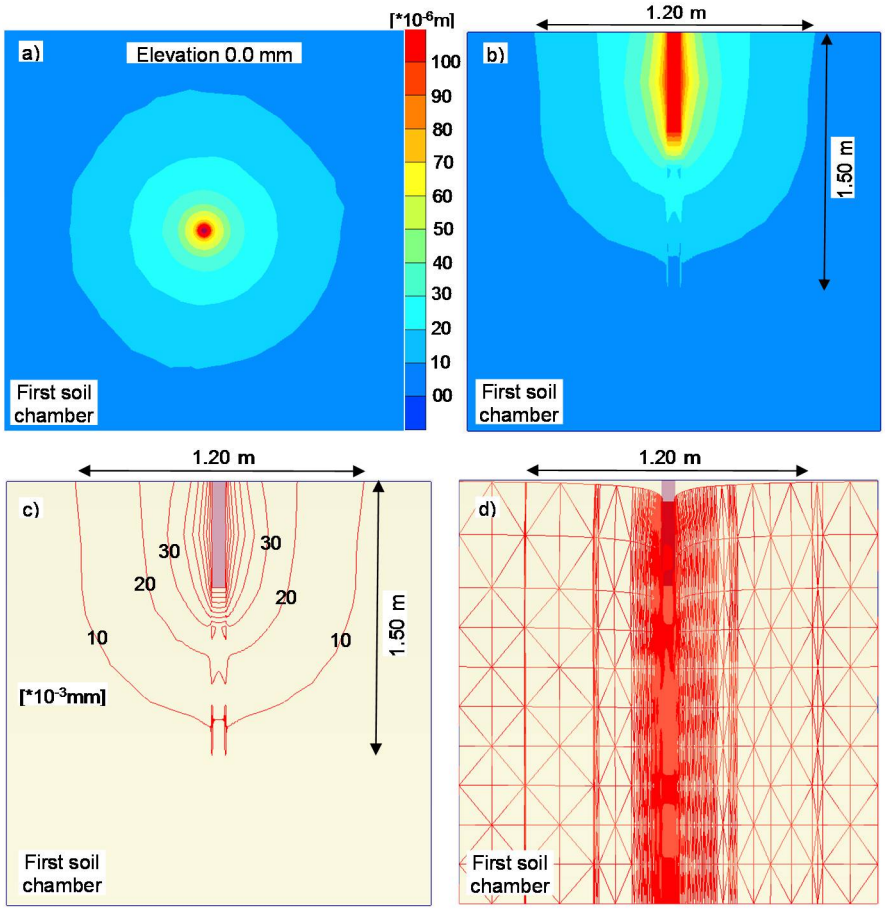

Figure 6-6 Deformation of soil surrounding pile tested in first soil chamber for loading of 1206 kPa (4 kN): a) Deformation soil at elevation 0.0 mm, b) deformation soil along pile, c) contour lines of soil deformation along pile, d) plane deformation of soil around pile

It should be noted that the investigation of the soil failure around the P-cone device in Chapter 5 showed that the effects of the boundary conditions were only twice the diameter of P-cone. The shear stresses of soil surrounding the P-cone device were not measured to compare with the numerical modelling results because it was not relative to the research objective of this dissertation. The outermost mobilized shear strength of soil was about 2 kPa, which is equal to about 5% relative shear stress (Figure 6-8d). It seems that this shear stress did not cause the strain of soil as shown in Figure 6-6. Maximum mobilized shear strength of soil was 37 kPa, which was about 8% greater than the undrained cohesion of soil.

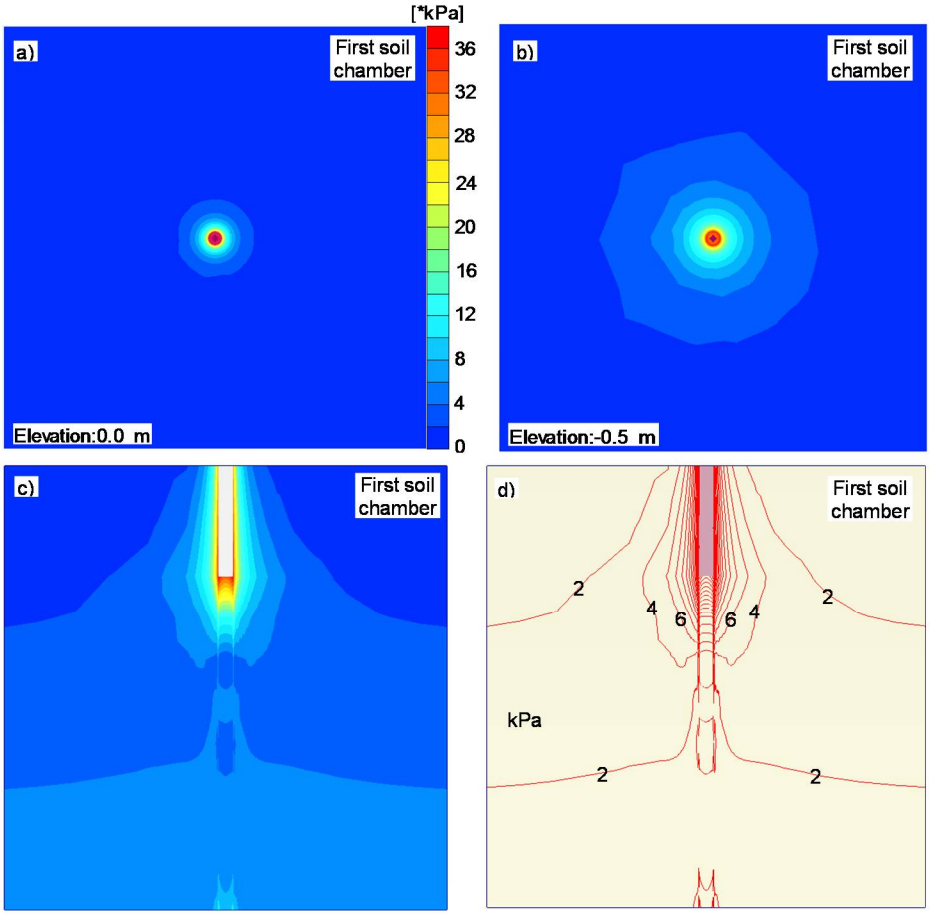

Figure 6-7 Mobilized shear strength of soil around P-cone for loading of 4 kN

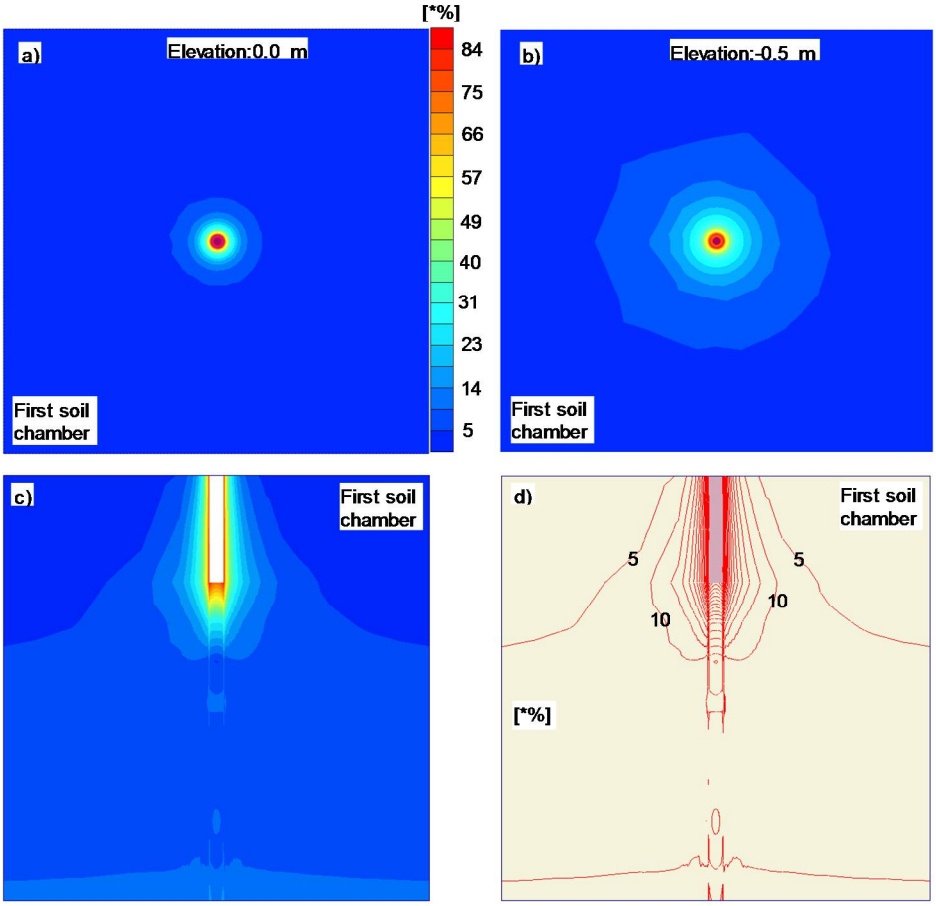

Figure 6-8 Relative shear stress of soil around P-cone for loading of 1206 kPa (4 kN)

Load-Movement Curves

Figure 6-9 shows the load-movement curves of modelling the axial static compression load tests in three soil chambers by the embedded pile approach in PLAXIS 3D FOUNDATION. For the values of the elastic modulus, E, estimated from Figure 6.3 (E = 500*Cu), the maximum load and movement obtained from modelling were about 4.0 KN and 7.55 mm for first soil chamber, 4.7 kN and 3.94 mm for second soil chamber, and 2.5 kN and 25.57 mm for third soil chamber, respectively (Figure 6.9a). The load-movement curves were approximately linear to loading of 2.5 kN, 3.5 and 1.0 kN for first,

second, and third soil chambers, respectively. After these loadings, the slopes of the load-movement curves reduced significantly until reaching the failure loads.

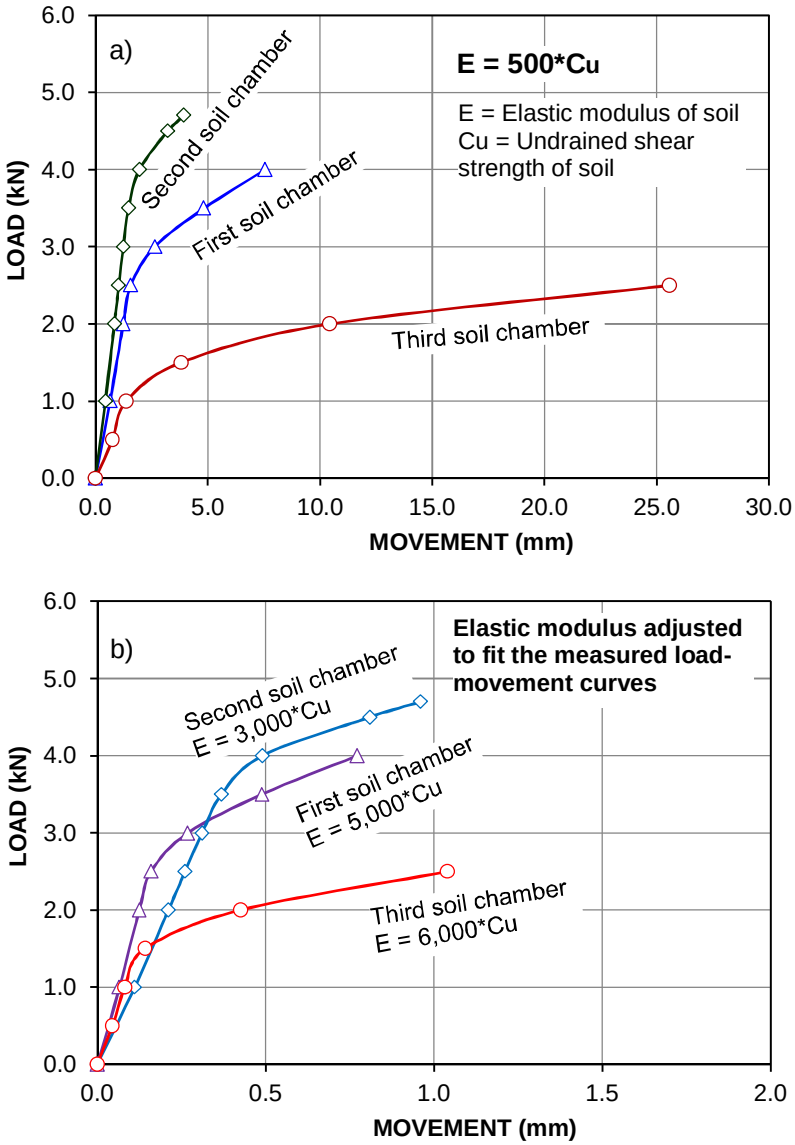

Figure 6-9 Load-movement curves of modelling the axial static compression load tests in three soil chambers: a) Elastic modulus of soil obtained from Figure 6.3 (E = 500*Cu) and b) Elastic modulus of soil adjusted to fit the measured load-movement curves.

To fit the measured load-movement curves of the modelling with the measurements, the adjustments of the elastic modulus were performed with the coefficients K_c of 5,000, 3,000, and 6,000 for the first, second, and third soil chambers, respectively. For the adjusted values of the elastic modulus, the maximum movements obtained from modelling were about 0.77, 0.96, and 1.04 mm for the first, second, and third soil chambers, respectively (Figure 6.9b).

6.6.3 Bidirectional Load Test

Deformation of soil surrounding pile

Figures 6-10 and 6-11 show deformations of soil surrounding the P-cone device for loading of 452 kPa (1.5 kN) of bidirectional load test in the first soil chamber. For the piles modelled in the second and third soil chambers, the deformations recorded were similar to the pile modelled in first soil chamber; therefore, they are not presented.

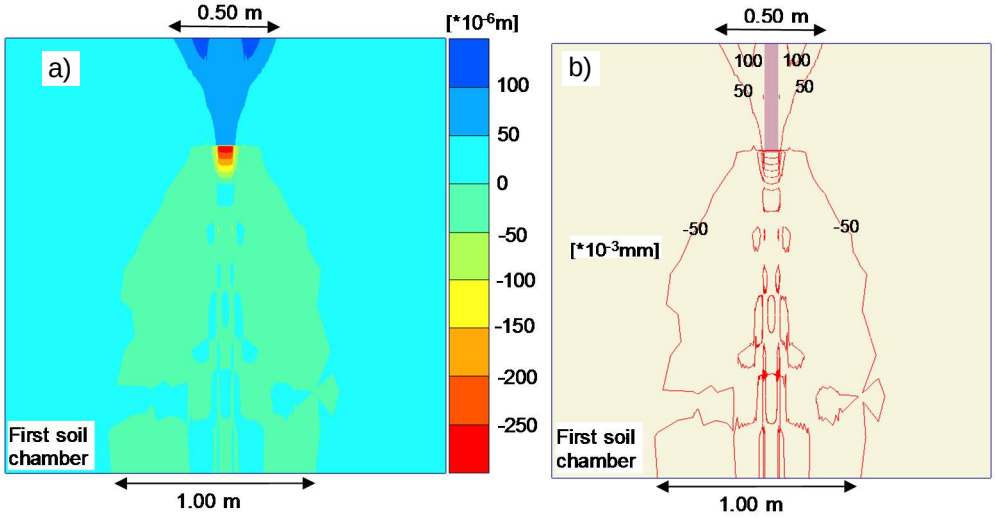

Figure 6-10 Deformation of soil along depth of pile: a) Shades of soil deformation and b) contours of soil deformation

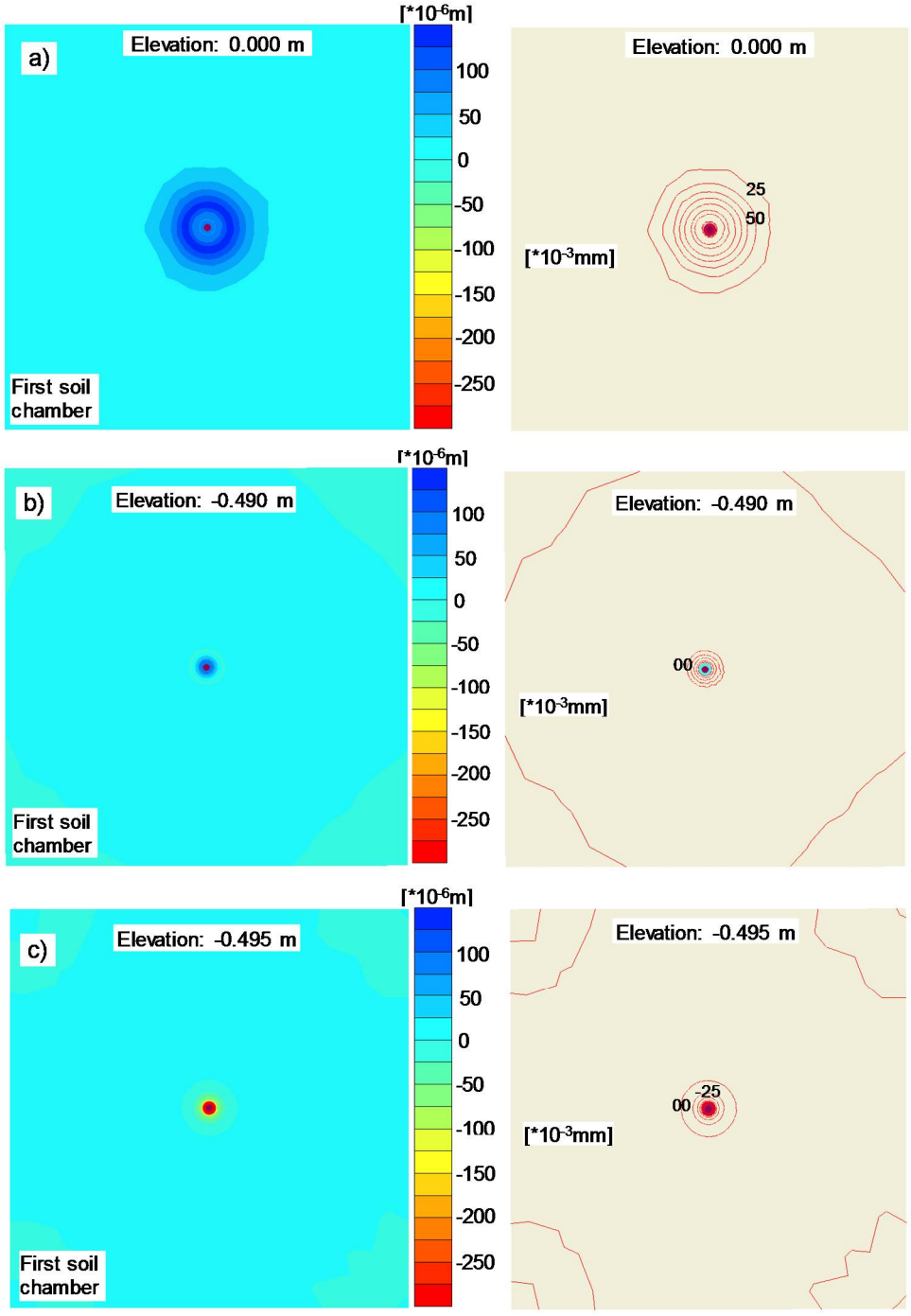

Figure 6-11 Deformation of soil at the different depths of pile: a) Elevation 0.000 m, b) elevation 0.490 m, and c) elevation 0.495 m

It can be seen clearly from Figure 6-9 that the deformation zones of soil at the elevation of the jack were not significant. The most dramatic deformation zones occurred at the upper and lower boundaries of the modelled soil chamber. The diameter of the influence zones was about 0.5 and 1.0 m for the upper and lower boundaries (Figure 6-10). It was noted that the shear failure of soil occurred below the P-cone tip instead of along the P-cone shaft, as measured from experiments (Figure 6-10a).

The differences between measurements and modelling could be due to the input data of soil, the simulation of the bidirectional load test, and the modelled P-cone tip shape. Although the modelled P-cone tip was flat, its area was only half of the actual P-cone tip area (66 cm^2). Figures 6-10d and 6-10e also show the influence depth below the P-cone tip of about 0.8 m (12 times the diameter of the P-cone tip). The maximum upward and downward movements at the position of the jack for loading of 452kPa (1.5 kN) were 0.0915 and 0.2954 mm, respectively. It was noted that the soil surrounding the modeled pile was collapsed for loading of 603 kPa, and thus the loading of 452 kPa is regarded as the maximum load obtained from modelling of pile tested in the first soil chamber.

For the piles modelled in the second and third soil chambers, the maximum upward and downward movements at the position of the jack for loading of 603 kPa (2.0 kN) and 302 kPa (1.0 kN) were 0.1454 through 0.0474 mm and 0.4366 through 0.3220 mm, respectively. Similar to pile modeled in the soil chamber, the soil surrounding the pile modeled in the second and third soil chambers was collapsed for loading of 754 and 452 kPa.

Mobilized Shear Strength and Relative Shear Stress of Soil around P-cone

Figures 6-12 and 6-13 show the mobilized shear strength and relative shear stress of soil around the P-cone modeled in the first soil chamber. It can be seen clearly

from Figures 6-13c and 6-13d that the working area of the modeled pile was not large enough to eliminate the effect of the boundary conditions for the shear stress. The outermost mobilized shear strength of soil was about 10 kPa, which was equal to about 8% relative shear stress. It appears that the relative shear stress of 5% did not cause the strain of soil, as shown in Figure 6-9. The maximum mobilized shear strength of soil was 121 kPa, which is 2.4 times greater than the undrained cohesion of soil.

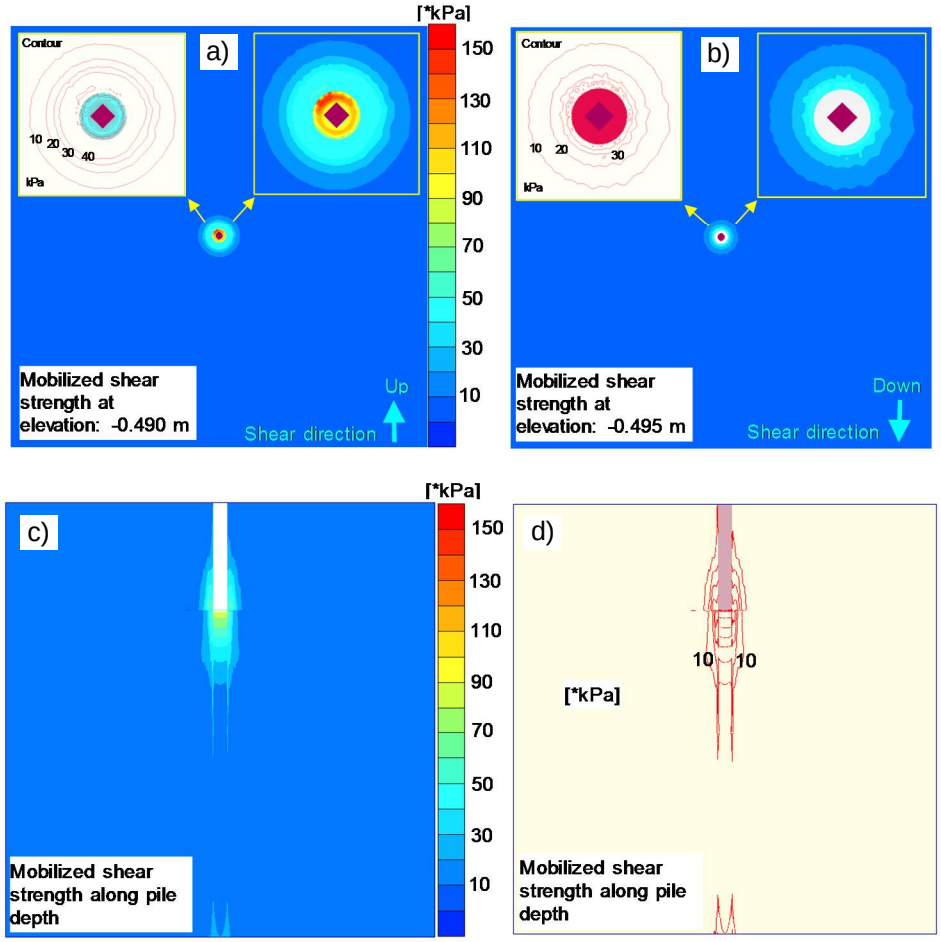

Figure 6-12 Mobilized shear strength of soil around P-cone for loading of 452 kPa (1.5 kN) in first soil chamber

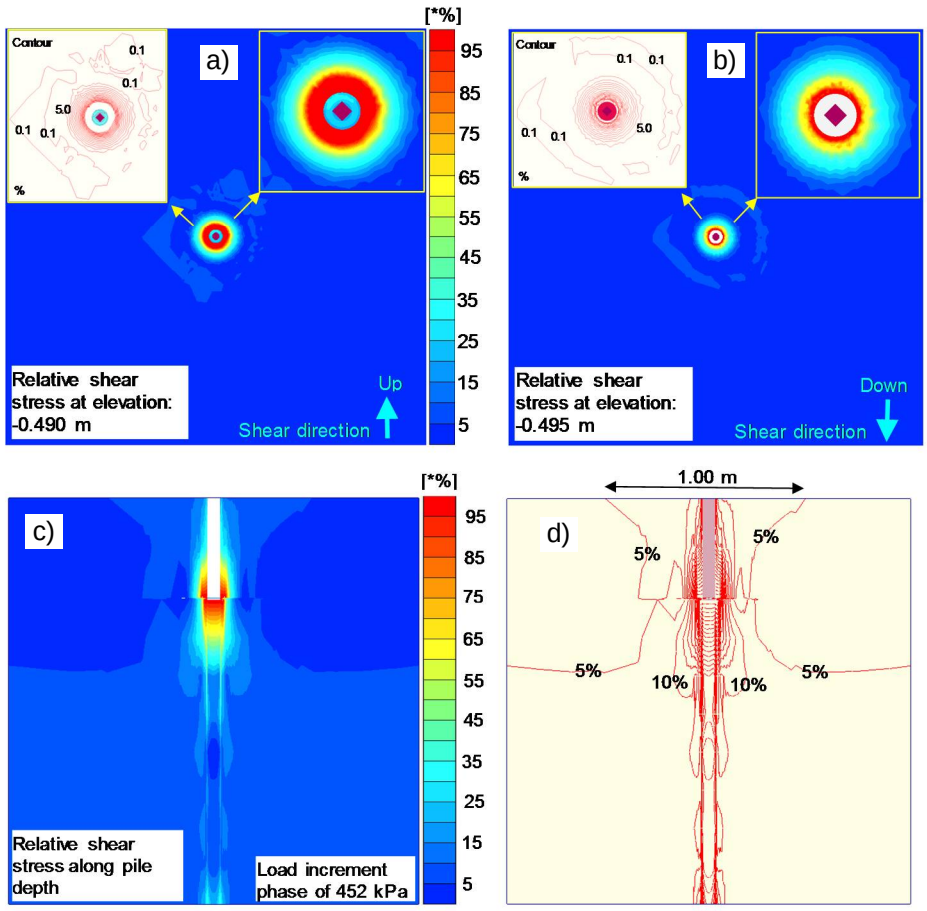

Figure 6-13 Relative shear stress of soil around P-cone for loading of 452 kPa (1.5 kN) in first soil chamber

Load-Movement Curves

Figure 6-14 shows the load-movement curves of modelling the bidirectional load tests in three soil chambers by the standard finite element approach in PLAXIS 3D FOUNDATION. For the values of the elastic modulus, E, estimated from Figure 6.3 (E = 500*Cu), the upward maximum loads obtained from modelling were about 2.5, 3.0, and 2.0 kN for first, second, and third soil chambers, respectively. The maximum upward movements were about 1.10, 0.98, and 1.71 mm for first, second, and third soil

chambers, respectively (Figure 6.9a). The maximum downward movements were about 1.68, 1.39, and 2.89 mm for first, second, and third soil chambers, respectively.

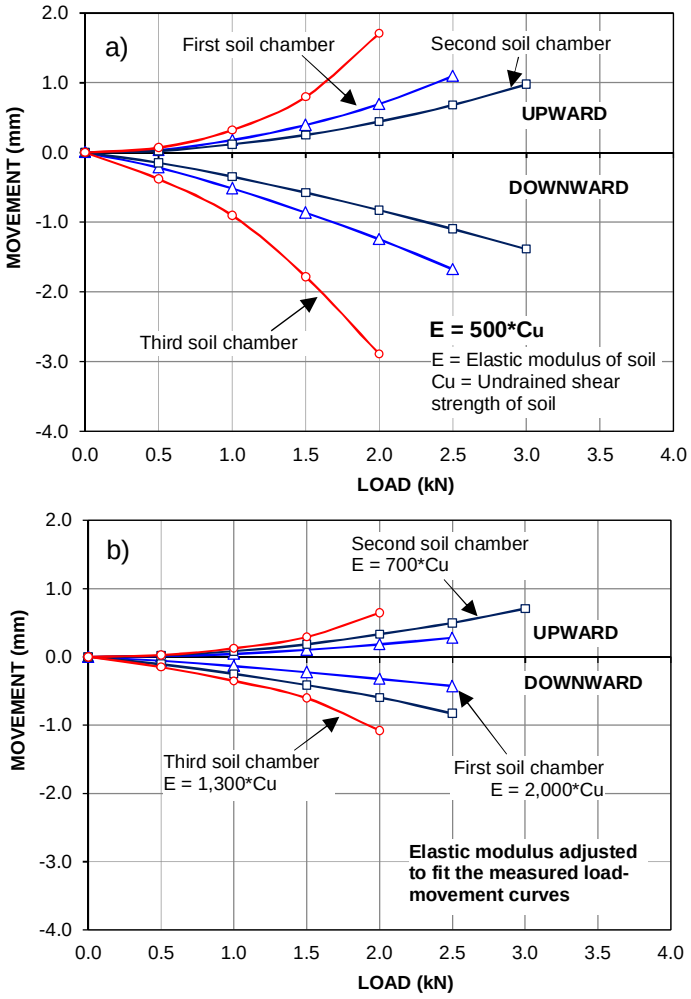

Figure 6-14 Load-movement curves of modelling the bidirectional load tests in three soil chambers: a) Elastic modulus of soil obtained from Figure 6.3 (E = 500*Cu), and b) Elastic modulus of soil adjusted to fit the measured load-movement curves

To fit the load-movement curves of the modelling with the measurements, the adjustments of the elastic modulus were performed with the coefficients K_c of 2,000, 700,

and 1,300 for the first, second, and third soil chambers, respectively. For the adjusted values of the elastic modulus, the maximum upward movements were about 0.28, 0.71, and 0.65 mm, and the maximum downward movements were about 0.43, 0.83, and 1.08 mm for the load increments of 2.5, 3.0, and 2.0 kN in the first, second, and third soil chambers, respectively (Figure 6.9b).

6.7 Comparison with Measurements

To validate the accuracy of the PLAXIS approach, the load-movement curves measured from axial static compression and bidirectional load tests were compared with those of the modelling, as shown in Figures 6-15 through 6-20.

Figures 6-15, 6-16, and 6-17 present the comparisons between the load-movement curves obtained from modelling the axial static compression load tests with measurements in the first, second, and third soil chambers.

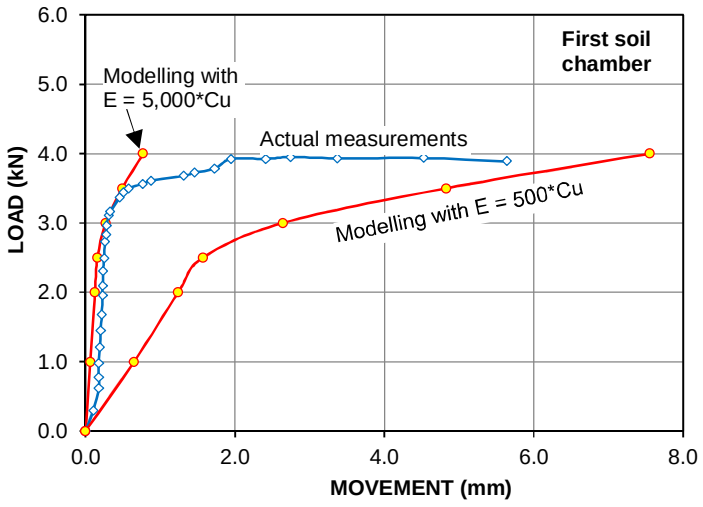

Figure 6-15 Load-movement curves of modelling and measurement obtained from axial compression load test in first soil chamber

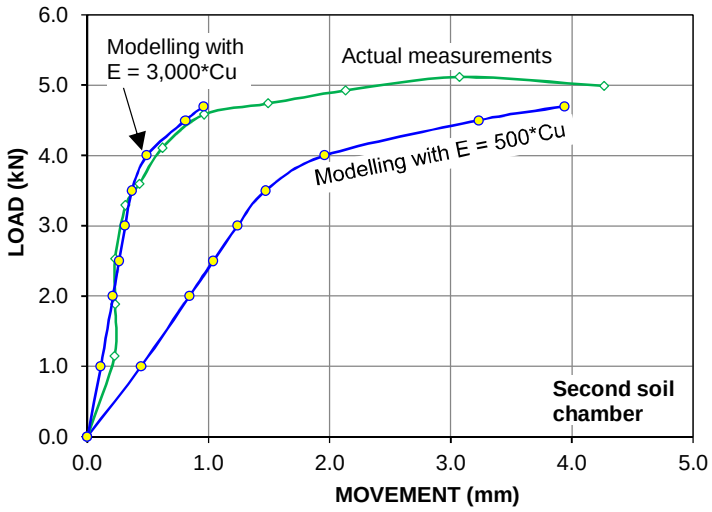

Figure 6-16 Load-movement curves of modelling and measurements obtained from axial compression load test in second soil chamber

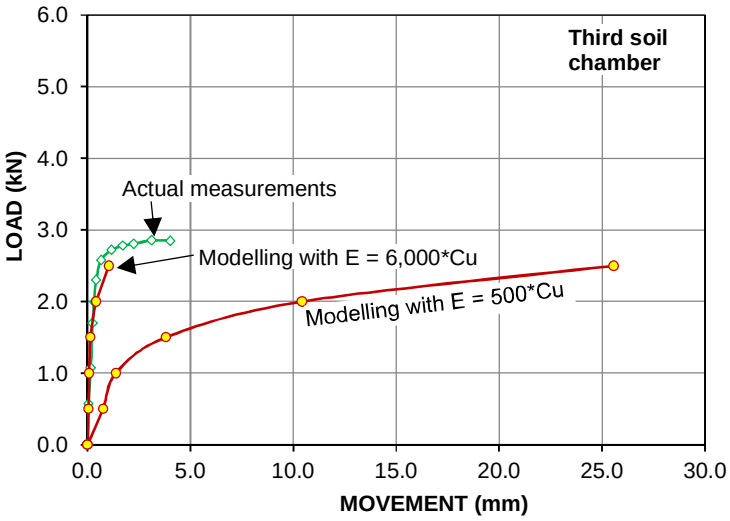

Figure 6-17 Load-movement curves of modelling and measurements obtained from axial compression load test in third soil chamber

It can be seen clearly that the differences between the measurements and the modellings are significant for the values of elastic modulus estimated from Figure 6.3 (E

= 500*Cu). The results obtained from modelling showed a good agreement with the measurements for the adjusted values of the elastic modulus. The average load difference of the axial static compression load tests for the three modelled cases was about 7% for the equivalent movements. It has become clear that the modulus of soil plays a vital role in determining the settlement of piled foundation in practice, as well as in modelling. The P-cone device, in combination with a jack at the cone tip, allows evaluating the modulus of the in-situ soil at depths where the pile toe elevation will be installed.

Figures 6-18, 6-19, and 6-20 display the comparisons between the load-movement curves obtained from modelling the bidirectional load tests and measurements in the first, second, and third soil chambers. It should be noted that the load-movement curves measured from bidirectional and end bearing load tests were combined for comparison with those of modelling.

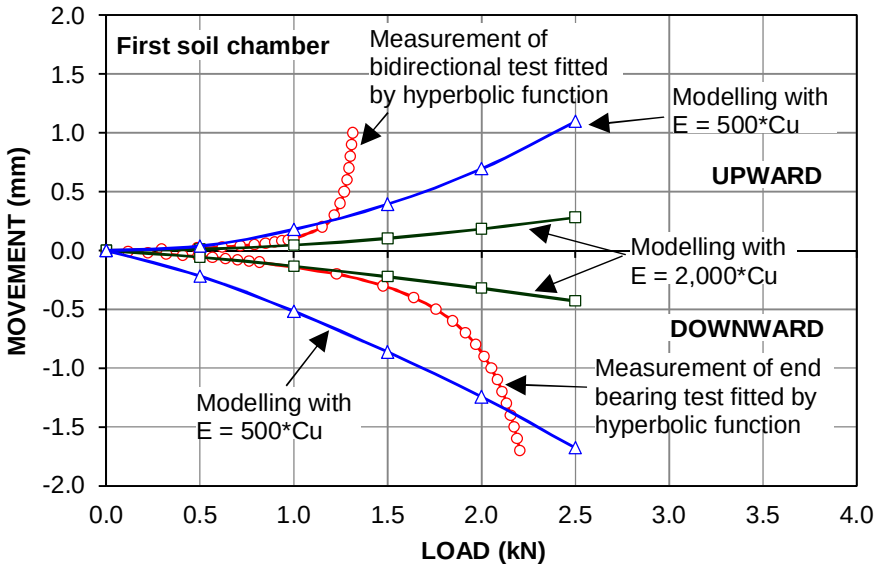

Figure 6-18 Load-movement curves of modelling and measurements obtained from bidirectional load test in first soil chamber

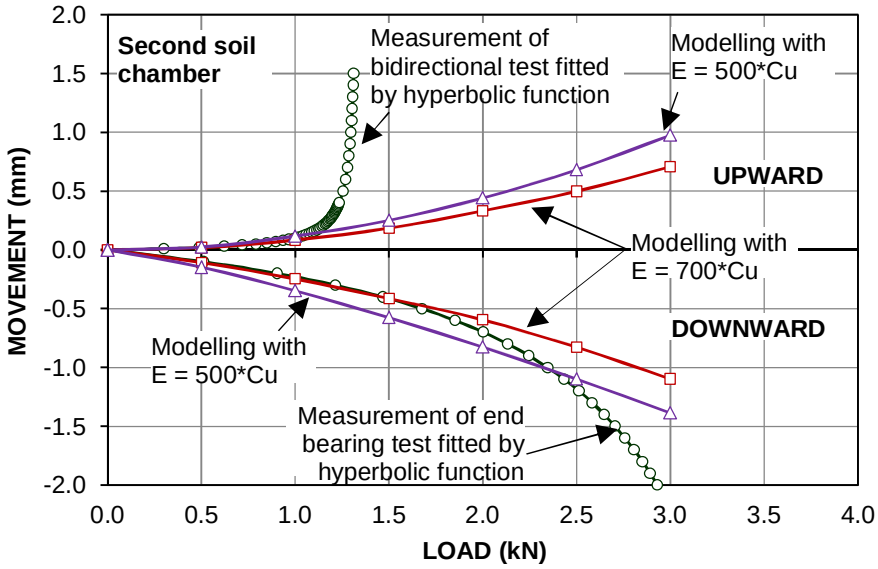

Figure 6-19 Load-movement curves of modelling and measurements obtained from bidirectional load test in second soil chamber

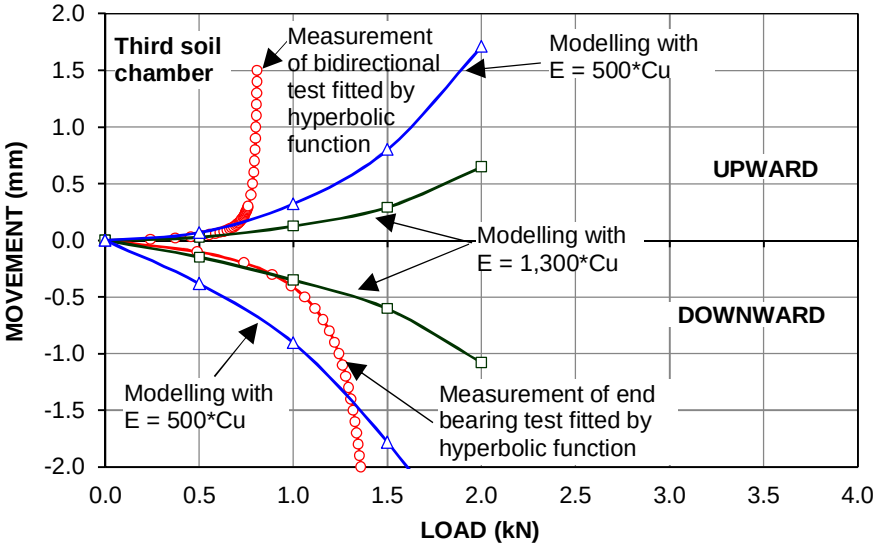

Figure 6-20 Load-movement curves of modelling and measurements obtained from bidirectional load test in third soil chamber

Similar to the modelling of the axial static compression load tests, the differences between measurements and modellings of bidirectional load tests were relatively significant for the values of elastic modulus estimated from Figure 6.3 (E = 500*Cu). For the adjusted values of elastic modulus, the results obtained from modelling showed a good agreement with the measurements for the load increments less than 1.0 and 1.5 kN, for the upward and downward load-movement curves. After the load increments, the differences between the measurements and the modeling with the adjusted values of soil modulus were considerable.

6.8 Summary

The axial static compression and bidirectional load tests on the P-cone installed in three soil chambers were modelled, using the embedded pile and standard finite element approach, respectively. The results obtained showed that the influence zones surrounding the P-cone shaft and below the P-cone tip, caused by the P-cone installation, were about four and thirteen times the diameter of the P-cone, respectively. This means that the actual dimensions of the soil chamber used for the P-cone tests were not large enough to eliminate completely the effect of the boundary conditions. In addition, the soil strains obtained from modelling were too small ($148*10^{-9}$ mm); therefore, adjustments of the test results obtained from the P-cone device were not considered.

The load-movement curves obtained from modelling the axial static compression and bidirectional load tests with the elastic soil modulus of E = 500*Cu showed a significant difference from the measurements. The modelling of the axial static compression load tests by the embedded pile approach with the adjusted values of elastic soil modulus showed a good agreement with the measurements for all three soil chambers. The modelling of the bidirectional load tests by the standard finite element approach showed a good agreement with the measurements of the load increments of

less than 1.0 and 1.5 kN for the upward and downward load-movement curves, respectively.

It has become clear that the standard finite element approach in PLAXIS 3D FOUNDATION is useful for considering the effects of the pile installation. The embedded pile approach is a powerful tool for fitting the load-movement curves measured from axial static compression load tests because it considers the measured capacities of pile as an input parameter.

Chapter 7 Summary, Conclusions, and Recommendations

7.1 P-Cone: A Novel Cone Penetration Test Device

A novel cone penetration test device, the P-Cone, and the operating principles for the test cases have been presented. The main features of the P-Cone device are summarized as follows:

1. The measurements obtained from the P-Cone are the same as those obtained from the conventional cone penetration test device, including the cone tip resistance, the sleeve friction, and the pore pressure.
2. The P-Cone measures the shear stress versus movement and the cone tip stress versus penetration of the soil at the desired depth.
3. The P-Cone, in combination with a hydraulic jack at the cone tip, allows improving the penetration depth by utilizing the pressure in a cell that uses the cone rods and surface anchors on the ground surface as a reaction to push the cone down.
4. The P-Cone, in combination with a hydraulic jack at the cone tip, also allows performing the in-situ consolidation compressive test for the fine-grained soils.

It has become clear that the P-Cone device offers many more advanced features than the current cone penetration devices. The in situ soil test results obtained from the P-cone device play an important role in designing deep foundations, especially for considering the bearing capacity and settlement of a piled foundation in the short-term conditions, the long-term conditions, and the liquefaction conditions.

7.2 Conclusions

P-cone Penetration test Results

The P-cone penetration tests and measurements were performed successfully for the experimental soil chambers. The ratio of the chamber diameter to the cone diameter was approximately 9. The P-cone device was pushed 0.5 m below the ground surface with a penetration rate from 3 to 10 mm/s. (The standard penetration rate of 20 mm/s was not considered due to the penetration performed in the compaction-unsaturated soil chambers.) The ground surface cracks of the soil chambers, induced by the cone penetration tests, were about twice the diameter of the cones, indicating that the ratio of the chamber diameter to the cone diameter of 9 is enough to eliminate the effects of the boundary conditions.

Static Load Tests on P-cone Device

The static load tests (the head-down load tests, bidirectional load tests, and end bearing load tests) were performed successfully in three soil chambers. In the first soil chamber, the maximum test loads of head-down, bidirectional, and end bearing tests were about 3.95, 1.35 and 2.4 kN, respectively; while the loads were about 5.10, 1.40, and 3.4 kN for the second soil chamber, respectively. For the third soil chamber, the maximum test loads were about 2.88, 0.80, and 1.4 kN for head-down, bidirectional, and end bearing tests, respectively.

The estimations of the pile capacity, based on the head-down load test results, showed that the best prediction methods were those of DeBeer and Davisson, followed by those of Vander Veen, Chin-Konder, Mazurkiewicz and Decourt. The pile capacity estimation from the methods of Fuller and Hoy, Brinch Hansen (80% criterion), and Bulter and Hoy showed significant differences.

The estimations of the pile capacity, based on the cone penetration test results, differed considerably from the measurements. The methods that produced pile capacities closest to the measurements were those of Schmertmann-Nottingham and Tumay-Fakhroo, followed by those of De Ruiter-Beringen and Mayerhof. The methods that gave the most dramatic differences were Bustanmante-Gianselli's and Eslami-Fellenius's. It is likely that taking the average of the cone tip resistances in the subject cases, as well as the differences in cone sizes, led to such dramatic distinctions.

The estimations of the pile capacity, based on the shear strength parameters of the soil, were about 5.7, 4.0, and 2.3 kN for the test piles installed in the first, second, and third soil chambers, respectively. The differences between the computed and measured pile capacities were about 44, 22, and 20%, respectively. The average difference of the tests performed in the three soil chambers was about 29%.

Re-evaluation of Equivalent Pile-Head Load-Movement Curve Construction

The comparison of the measurements and the equivalent pile-head load-movement curve constructions shows a significant difference between the positive and negative shaft resistance of soil when it is being sheared. The average differences were about 8%, 16%, and 21% for the test results performed in the first, second, and third soil chambers, respectively. An adjustment was proposed for the constructed equivalent pile-head load-movement curves. The adjustment coefficients were about 1.07, 1.15, and 1.3 for the tests performed in the first, second, and third soil chambers, respectively.

Investigation of Soil Failures surrounding P-cone Device

The investigation of soil failures along the cone shaft and below the cone tips showed that the sheared soil areas surrounding the cone shaft were twice the diameters of the cone, and the shear failures took place at the interface of the cone wall and soil.

Shear failures did not occur below the cone tip, although the movements of the cone tip ranged from 100 through 185% of the cone diameter.

The investigation of soil deformation around the jack indicated that the expansion of the jack did not create tension areas for any of the tests. Thus, the effects of the tension areas created by the jack expansion can be ignored for the equivalent pile-head load-movement curve construction from the bidirectional load test results.

The investigation also provided compelling evidence that the assumed soil failure modes below the pile toe are not in agreement with reality. A load testing platform on a footing with a long stem provided a better understanding of the behavior of the pile toe. The test results confirmed that the ultimate bearing capacity concept for the pile toe is a fallacy. The settlement measurement at each load increment of the platform load test on footing also provided evidence that the plunging failure load concept is totally wrong. The fact is that the so-called plunging failure load is a failure of the jack system; it is not a failure of the test pile.

Consolidation Compression Test by P-cone Device

The consolidation tests performed by the P-cone device were correlated with the oedometer test data. The correlation modulus numbers obtained from the oedometer and P-cone test device were significantly different, at about 80% for Janbu's method and 73% for Casagrande's. The difference of the pre-consolidation stresses was about 15% for Janbu's method and 283% for Casagrande's.

Modelling of Static Load Tests on P-cone Device

Modelling was performed, by the embedded pile and standard finite element approach, of the axial compression and bidirectional load tests on P-cones installed in

three soil chambers. The results obtained from the modelling showed that the influence zones surrounding the P-cone shaft and below the P-cone tip, caused by the P-cone installation, were about four and thirteen times the diameter of the P-cone, respectively. It seems that the actual dimensions of the soil chamber used for the P-cone tests were not large enough to eliminate completely the effects of the boundary conditions. However, the soil strains obtained from modelling were too small ($148*10^{-9}$ mm); therefore, adjustments of the test results obtained from the P-cone device were not considered.

The load-movement curves obtained from modelling axial static compression and bidirectional load tests with the elastic soil modulus of E = 500*Cu showed a significant difference from the measurements. The modelling of the axial static compression load tests by the embedded pile approach with the adjusted values of elastic soil modulus showed a good agreement with the measurements for all three soil chambers. The modelling of the bidirectional load test by the standard finite element approach showed a good agreement with the measurements of the load increments less than 1.0 and 1.5 kN for the upward and downward load-movement curves, respectively.

It has become clear that the standard finite element approach in PLAXIS 3D FOUNDATION is useful for considering the effects of the pile installation. The embedded pile approach is a powerful tool for fitting the load-movement curves measured from axial static compression load tests because it considers the measured capacities of pile as an input parameter.

7.3 Limitations of Research

The first version of the P-Cone device manufactured and tested has several limitations, as follows:

1. The electric movement measurement instruments (the linear displacement transducers) were replaced by the mechanical instruments (telltales and dial gauges).
2. The porous element and the pressure transducer used to measure pore pressure at the shoulder of the cone tip have not been equipped yet.
3. The load cell has not been yet been installed. It should be noted that these non-equipped instruments did not influence the experiments of the P-Cone in the unsaturated soil chambers.
4. The loading system was operated by hand; therefore, it was hard to control the penetration rate of the P-cone.
5. The datalogger system had a low sample rate (sample rate of 1 per 10 seconds); thus, the penetration rate of P-cone was limited.
6. The automatic pressure control system was not equipped; hence it was difficult to maintain a stable pressure during the consolidation and static load tests.
7. The dimensions of the chamber used for tests were relatively small, and it is likely that some effects of the boundary conditions could not be observed visually.

7.4 Recommendations for Future Research

The first version of the P-Cone device for deep foundation design was developed, and the experimental program was performed in compaction-unsaturated soil. Recommendations for improving the P-Cone device in the future are as follows:

1. Linear displacement transducers to measure movement and a datalogger system with high sample rates should be utilized.
2. Automatic pressure control system should be installed to maintain constant pressure during testing.
3. Porous element and the pressure transducer should be installed to measure pore pressure at the shoulder of the P-cone tip during penetration.
4. Load cell should be attached to measure the P-cone tip resistance parallel with the pressure transducer.
5. P-Cone device program should be performed in sand or saturated clay soil.

Appendix A

Calibration Report of Pressure Transducer and Strain Gages

GEOKON 48 Spencer St. Lebanon, NH 03766 USA

Vibrating Wire Pressure Transducer Calibration Report

Model Number: 4500HH-5 MPa

Serial Number: 1529383

Calibration Instruction: VW Pressure Transducers

Cable Length: 5 meters

Date of Calibration: September 02, 2015

This calibration has been verified/validated as of 09/10/2015

Temperature: 23.10 °C

Barometric Pressure: 995 mbar

Technician:

Applied Pressure (MPa)	Gage Reading 1st Cycle	Gage Reading 2nd Cycle	Average Gage Reading	Calculated Pressure (Linear)	Error Linear (%FS)	Calculated Pressure (Polynomial)	Error Polynomial (%FS)
0.0	9063	9062	9063	0.009	0.17	-0.001	-0.03
1.0	8308	8305	8307	1.001	0.01	1.003	0.06
2.0	7554	7552	7553	1.990	-0.21	1.998	-0.04
3.0	6791	6788	6790	2.992	-0.17	3.000	0.00
4.0	6024	6023	6024	3.997	-0.06	4.000	-0.01
5.0	5253	5250	5252	5.010	0.20	5.000	0.01

(MPa) Linear Gage Factor (G): -0.001312 (MPa/ digit)

Polynomial Gage factors: A: -5.246E-09 B: -0.001237 C:

Thermal Factor (K): 0.001043 (MPa/ °C)

Calculate C by setting P=0 and R_1 = initial field zero reading into the polynomial equation

(psi) Linear Gage Factor (G): -0.1904 (psi/ digit)

Polynomial Gage Factors: A: -7.609E-07 B: -0.1795 C:

Thermal Factor (K): 0.1513 (psi/ °C)

Calculate C by setting P=0 and R_1 = initial field zero reading into the polynomial equation

Calculated Pressures:

Linear, $P = G(R_1 - R_0) + K(T_1 - T_0) - (S_1 - S_0)$*

Polynomial, $P = AR_1^2 + BR_1 + C + K(T_1 - T_0) - (S_1 - S_0)$*

*Barometric pressures expressed in MPa or psi. Barometric compensation is not required with vented transducers.

Factory Zero Reading: 9053 Temperature: 21.9 °C Barometer: 1001.4 mbar

The above instrument was found to be in tolerance in all operating ranges.
The above named instrument has been calibrated by comparison with standards traceable to the NIST, in compliance with ANSI Z540-1.

GEOKON 48 Spencer St. Lebanon, NH 03766 USA

Vibrating Wire Strain Gage Batch Calibrations

Revision Date: May 13, 2015

Strain Gage Type	Nominal Batch Factor (B)
Model 4000	0.96
Model 4100 / 4150 / 4151 / 4202	0.91
Model 4200	0.97

Please Note: To calculate changes of strain use the formula $\Delta\mu = (R1-R0)G \times B$ where G is the gage factor for that particular model of strain gage.

This applies only to dataloggers

Where the strains are read using GK403 or GK404 readout boxes on the appropriate channels C, D or E, the displayed readings already include the gage factor ,G, so that with portable readout boxes the change of strain is simply (R1-R0) x B microstrain

Gage Model	G
4000	4.062
4100/4150/4202	0.391
4200	3.304

Model:	4200	4202	4204	4210	4212	4214
Gage Factor:	3.304	0.391	1.422	0.3568	0.3624	0.3665
Start Frequency (P28):	4 (450 Hz)	14 (1400 Hz)	8 (800 Hz)	14 (1400 Hz)	14 (1400 Hz)	14 (1400 Hz)
End Frequency (P28):	12 (1200 Hz)	35 (3500 Hz)	16 (1600 Hz)	35 (3500 Hz)	35 (3500 Hz)	35 (3500 Hz)

The above factor is derived by averaging the gage factors of controlled samples of all gages produced. The data from calibration of the above instrument samples was collected using standards traceable to the NIST and in compliance with NCSL/ANSI Z540-1.

References

Allersma, H.G.B., 1982. Photoelastic investigation of the stress distribution during penetration. Proc. ESOPT2, Amsterdam (May 1982) A.A. Balkema, Rotterdam, Vol.2, pp.79-83.

Ameratunga J, Sivakugan N, Das BM (2016) Correlations of soil and rock properties in geotechnical engineering. Developments in geotechnical engineering. Springer, New Delhi.

American Society for Testing and Materials (ASTM D136). (2001). Standard test method for sieve analysis of fine and coarse aggregates.

ASTM-D422-63 (2007). Standard test method for particle size analysis of soils.

ASTM-D4318-05. Standard test methods for liquid limit, plastic limit, and plasticity index of soils.

ASTM-D854-14 Standard test methods for specific gravity of soil solids by water pycnometer.

ASTM-D698-12. Standard test methods for compaction characteristics of soil using standard effort.

ASTM D1143-81, Standard method of testing piles under static axial compressive load. Vol. 04.08, Philadelphia, 1989, pp. 179-189.

ASTM D2435/D2435M – 11 Standard test methods for one-dimensional consolidation properties of soils using incremental loading.

Amir J.M., 1981. Experience with rock piles in Israel. Seminar on Engineering Geology of Dolomite Areas, Pretoria, pp. 381-383.

Amir, J.M., 1983. Interpretation of load tests on piles in rock. Proc. of the 7th Asian Regional Conference on Soil Mechanics and Foundation Engineering, Haifa, August 14-19, pp. 235-238.

Bach V. H. L., Nguyen M. H., Puppala A. J. and Nguyen C. M., 2016. Comparing the response of static loading tests on two model pile groups in soft clay. Proceedings of the 69th Canadian Geotechnical Conference, Vancouver, October 2-5, paper No. 3678, 8 p.

Baligh, M.M., Vivatrat, V., and Ladd, C.C., 1978. Exploration and evaluation of engineering properties for foundation design of offshore structures. Research Report R78-40, No. 607, Department of Civil Engineering, MIT, Cambridge, Mass., 268p.

Baligh, M.M., Vivatrat, V., and Ladd, C.C., 1980. Cone penetration in soil profiling. Journal of the Geotechnical Engineering, ASCE, Vol. 106, No.4, 447-461.

Baligh, M.M., Azzouz, A.S., Wissa, A.Z.E., Martin, R.T., Morrison, M 1981. The piezocone penetrometer. *Cone penetration testing and experience*, (Proc. ASCE National Convention, St. Louis), American Society of Civil Engineers, Reston, Virginia, pp. 247-263.

Barentsen, P., 1936. Short description of field testing method with cone shaped sounding apparatus. In Proceedings 1st International Conference on Soil Mechanics and Foundation Engineering, Cam- bridge, Mass, 1, B/3:6-10.

Begemann, H.K.S., 1953. Improved method of determining resistance to adhesion by sounding through a loose sleeve placed behind the cone. Proc. 3rd ICSMFE, Vol. I, pp. 213-217.

Begemann H.K.S., 1963. The use of the static penetrometer in Holland. New Zealand Engineering 18(2): p. 41.

Begemann, H.K.S., 1965. The friction jacket cone as an aid in determining the soil profile. Proceedings 6th International Conference on Soil Mechanics and Foundation Engineering, Montreal, Vol. 1, pp. 17 – 20.

Berezantsev, V. G., 1961. Load bearing capacity and deformation of piled foundations. Proceedings of the Fifth International Conference on Soil Mechanics and Foundation Engineering. Paris, Vol. II, pp. 11-12.

Bishop, R.F., Hill, R., and Mott, NF. 1945. The theory of indentation and hardness tests. Proceedings of the Physical Society **57**: 147-159.

Bjerrum L. and Simons N.E., 1960. Comparison of shear strength characteristics of normally consolidated clays. In: Proceedings of research conference on the shear strength of cohesive soils, ASCE, Boulder, Colorado, pp 711–726.

Bozozuk, M., 1976. Tower silo foundations. *Canadian Building Digests, CBD*-177, Institute for Research in Construction, National Research Council Canada, 4p.

Briaud, J.L., and Tucker, L., 1984. Piles in sand: A method including residual stresses. Journal of Geotechnical Engineering, ASCE, 110: 1666–1680.

Brinch Hansen, J., 1963. Discussion, Hyperbolic Stress-Strain response, Cohesive Soil. Journal of Soil Mechanics and Foundation Engineering Division, ASCE, 89(SM4), 241-242.

Broms, B.B., 1974. General Report on "Penetration Testing in Scandinavia". *Proc. European Symp. Penetration Testing,* Stockholm, 2.1: 14-23.

Broms, B.B. and Flodin, N., 1988. History of soil penetration testing. International symposium on penetration testing, ISOPT 1, Orlando, March 1988. Proceedings, Vol. 1, pp. 157-220.

Burland, J.B., Jamiolkowsky, M. and Viggiani, C., 1998. Stabilizing the leaning tower of Pisa*. Bulletin of Engineering Geology and the Environment* 57, 91-99*.*

Bustamante, M. and Gianeeselli, L., 1982. Pile bearing capacity predictions by means of static penetrometer CPT. Proceedings of the Second European Symposium on Penetration Testing (ESOPT II), Amsterdam, A. A. Balkema, Vol. 2, pp. 493 - 500.

Butler, H.D. and Hoy, H.E., 1977. Users Manual for the Texas Quick-Load Method for Foundation Load Testing. Federal Highway Administration, Office of Development, Washington, pp. 59.

Campanella, R.G., Robertson P.K., and Gillespie, D., 1986. Seismic cone penetration test. *Use of In-Situ Tests in Geotechnical Engineering* (GSP 6), ASCE, Reston, Virginia, pp. 116-130.

Chin, F.V., 1970. Estimation of the ultimate load of piles not carried to failure. Proceedings of 2nd Southeast Asian conference on Soil Engineering, pp. 81 - 90.

Cooke, R.W., and Price, G., 1973. Strains and displacements around friction piles. Proceedings of the 8th International Conference on Soil Mechanics and Foundation Engineering, Moscow, Vol. 2.1, pp. 53–60.

Cooke, R.W., 1979. Influence of residual installation forces on the stress transfer and settlement under working loads of jacked and bored piles in cohesive soils. Behaviour of deep foundations. Edited by R. Lundgren. American Society for Testing and Materials, Special Technical Publication STP 670, pp. 231–249.

Dahlberg, R., 1974. Penetration testing in Sweden: State-of-the-art report. *Proc. European Symp. Penetration Testing,* Stockholm, 1: 115-131.

Davie, J.R. and Lewis, M.R., 1988. Settlement of two tall chimney foundations. Proceedings of the 2nd International Conference on Case Histories in Geotechnical Engineering, Rolla, MO, pp 1309-1313.

Davisson, M.T., 1972. High capacity piles. Proceedings, Lecture Series, Innovation in Foundation Construction, ASCE, Illinois Section, pp. 52.

Decourt, L., 1999. Behavior of foundations under working load conditions. Proc. of 11th Pan-American Conference on Soil Mechanics and Geotechnical Engineering, Foz DoIguassu, Brazil, August 1999, Vol. 4, pp. 453-488.

Decourt, L., 2008. Loading tests: interpretation and prediction of their results. ASCE GeoInstitute GeoCongress New Orleans, March 9-12, Honoring John Schmertmann—From Research to Practice in Geotechnical Engineering, Geotechnical Special Publication, GSP 180, Edited by J.E. Laier, D.K. Crapps, and M.H. Hussein, pp. 452-488.

Delft Laboratory of Soil Mechanics, 1936. The predetermination of the required length and the prediction of the toe resistance of piles. *Proc. 1st Int. Conf. on Soil Mech. and Foundation Eng.*, Cambridge: 181–184.

DeRuiter J. and Beringen F.L., 1979. Pile foundations for large North Sea structures. Mar Geotechnol 3(3):267–314.

DeRuiter, J., 1981. Current penetrometer practice. *Cone Penetration Testing and Experience*, (Proc. ASCE National Convention, St. Louis), American Society of Civil Engineers, Reston, Virginia, pp. 1-48.

Duncan J.M. and Wright S.G., 2005. Soil strength and slope stability. John Wiley & Son, New Jersey, 297p.

Eslami, A. and Fellenius, B.H., 1995. Toe bearing capacity of piles from cone penetration test (CPT) data. Proc. of the International Symposium on Cone Penetration Testing, CPT 95, Linköping, Sweden, October 4 - 5, Swedish Geotechnical Institute, SGI, Report 3:95, Vol. 2, pp. 453 - 460.

Eslami, A., 1996. Bearing capacity of piles from cone penetrometer test data. Ph. D. Thesis, University of Ottawa, Department of Civil Engineering, 516 p.

Eslami, A. and Fellenius, B.H., 1996. Pile shaft capacity determined by piezocone (CPTU) data. Proc. of 49th Canadian Geotechnical Conference, September 21 - 25, St. John's, Newfoundland, Vol. 2, pp. 859 - 867.

Eslami, A. and Fellenius, B.H., 1997. Pile capacity by direct CPT and CPTu methods applied to 102 case histories. *Canadian Geotechnical Journal*, Vol. 34, No. 6, pp. 880-898.

Fellenius B.H., 1975b. Test loading of piles. Methods, interpretation, and new proof testing procedure. ASCE Journal of Geotechnical Engineering Division, 101(GT9) 855-869.

Fellenius, B.H., 1980. The analysis of results from routine pile loading tests. Ground Engineering, London, 13(6) 19-31.

Fellenius, B.H., 1984a. Negative skin friction and settlement of piles. Proc. of the Second International Seminar, Pile Foundations, Nanyang Technological Institute, Singapore, 18 p.

Fellenius, B.H., 1998. Recent advances in the design of piles for axial loads, dragloads, downdrag, and settlement. Proc. of a Seminar by ASCE and Port of New York and New Jersey, April 1998, 19 p.

Fellenius, B.H., 1999. Bearing capacity of footings and piles—A delusion? Proc. of the Deep Foundation Institute Annual Meeting, October 14 - 16, Dearborn, 17 p.

Fellenius, B.H., Brusey, W. G., and Pepe, F., 2000. Soil set-up, variable concrete modulus, and residual load for tapered instrumented piles in sand. ASCE Specialty Conference on Performance Confirmation of Constructed Geotechnical Facilities, University of Massachusetts, Amherst, April 9 - 12, 2000, Special Geotechnical Publications, GSP94, pp. 98 - 114.

Fellenius, B.H., 2002a. Determining the resistance distribution in piles. Part 1: Notes on shift of no-load reading and residual load. Part 2: Method for determining the residual load. Geotechnical News Magazine. Geotechnical News Magazine, 20(2 35-38), and 20(3 25-29).

Fellenius, B.H., 2006. Results from long-term measurement in piles of drag load and downdrag. Canadian Geotechnical Journal 43(4) 409-430.

Fellenius, B.H. and Siegel, T.C., 2008. Pile design consideration in a liquefaction event. ASCE Journal of Geotechnical and Environmental Engineering, 132(9) 1312-1416.

Fellenius, B.H., Kim, S.R., and Chung, S.G., 2009. Long-term monitoring of strain in instrumented piles. ASCE Journal of Geotechnical and Geoenvironmental Engineering, 135(11) 1583-1595.

Fellenius, B.H. and Nguyen, M.H., 2013. Large diameter long bored piles in the Mekong delta. International Journal of Case Histories 2(3) 196-207.

Fellenius, B.H. and Nguyen, M.H., 2013. Wick drains and piling for Cai Map Container Port, Vietnam. Honoring Robert D. Holtz—Sound Geotechnical Research to Practice. ASCE Geotechnical Special Publication, GSP 230, Edited by A.W. Stuedlein and B.R. Christopher. pp. 444-461.

Fellenius, B.H., 2015. Analysis of results of an instrumented bidirectional-cell test. Geotechnical Engineering Journal of the SEAGS & AGSSEA 46(2) 64-67.

Fellenius, B.H., 2015b. Static tests on instrumented piles affected by residual load. Journal of the Deep Foundation Institute, 9(1) 11-20.

Fellenius, B.H., 2016. The unified design of piled foundations. The Sven Hansbo Lecture. Geotechnics for Sustainable Infrastructure Development – Geotec Hanoi 2016, edited by Phung Duc Long, Hanoi, November 23-25, pp. 3-28.

Fellenius, B.H., 2016. Fallacies in piled foundation design. Geotechnics for Sustainable Infrastructure Development– Geotec Hanoi 2016, edited by Phung Duc Long, Hanoi, November 23-25, pp. 41-46.

Fellenius, B.H., 2017. Basics of foundation design. Electronic Edition. www.Fellenius.net, 464 p.

Fleming, W.G.K., Weltman, A.J., Randolph, M.F., and Elson, W.K., 1992. Piling engineering. 2nd ed., Blackie/Halsted Press, John Wiley and Sons, NY, 390 p.

Flodin, N. and Broms, B., 1981. Historical development of civil *engineering* in *soft clay*. In *Soft Clay Engineering*, Edited by Brand E. W. and Brenner R. P., Elsevier, Ch.l, 27-156.

Fuller, F. M. and Hoy, H. E., 1970. Pile load tests including quick-load test method, conventional methods and interpretations. HRB 333, pp. 74-86.

Gary A.J., Dirk, V.Z., and Eben, R., 1981. Mine tailings characterization by piezometer cone. *Cone Penetration Testing and Experience*, (Proc. ASCE National Convention, St. Louis), American Society of Civil Engineers, Reston, Virginia, pp. 303-324.

Gibson, G.L. and Devenny, D.W., 1973. Concrete to bedrock testing by jacking from the bottom of a borehole. Canadian Geotechnical Journal 10(2) 304-306.

Gregersen, O.S., Aas, G., and DiBiagio, E., 1973. Load tests on friction piles in loose sand. Proceedings of the 8th International Conference on Soil Mechanics and Foundation Engineering, Moscow, Vol. 2.1, pp. 109–117.

Head, K.H., 2006. Manual of Soil Laboratory Testing—Volume 1: Soil Classification and Compaction Tests, 3rd edition, Whittles Publishing, Caithness, UK, 405p.

Holloway, D.M., Clough, G.W., and Vesic, A.S., 1978. The effects of residual driving stress on piles performance under axial loads. Proceedings of the Offshore Technology Conference, Houston, OTC 3306, pp. 2225–2236.

Horvath, R.G., Kenney, T.C., and Kozicki, P., 1983. Methods of improving the performance of drilled piers in weak rock. Canadian Geotechnical Journal 20(4) 758-772.

Hunley, A., 1915. Concrete Pile Standards. Published by Hunley Abbott, New York, 59p.

Hunter, A.H. and Davisson, M.T., 1969. Measurement of pile load transfer. *In* Performance of deep foundation. American Society for Testing and Materials, Special Technical Publication STP 444, pp. 106–117.

Ishihara, K. and Yoshimine, M., (1992). Evaluation of settlements in sand deposits following liquefaction during earthquakes. *J. Soil Mech., Found. Engng*, 118(32), 173-188.

Janbu, N., 1967. Settlement calculations based on the tangent modulus concept. University of Trondheim, Norwegian Institute of Technology, Geotechnical Institution, Bulletin 2, 57 p.

Janbu, N. and Senneset, K., 1974. Effective stress interpretation of in situ static penetration tests. Proceedings of the European Symposium on Penetration Testing, ESOPT, Stockholm, 2.2, 181-193.

Janbu, N. 1976. Static bearing capacity of friction piles. *In* Proceedings of the 6th European Conference on Soil Mechanics and Foundation Engineering, Vienna, Austria. Vol. 1.2, pp. 479–488.

Jumikis, A.R. (1956) Rupture surfaces in sand under oblique loads. Journal of Soil Mechanics and Foundation Design, ASCE, Vol.82, Issue 3, pp. 1155-1159.

Kantey B. A., 1951. Significant developments in subsurface exploration for piled foundations. Transaction South Africa Institution of Civil Engineering, Vol.1, No. 6, pp. 159-185.

Kondner, R. L., 1963. Hyperbolic stress-strain response: Cohesive soil. Journal of Soil Mechanics and Foundation Engineering Division, ASCE, 189(SM1), 1 15 - 143.

Kuwajima, K., Hyodo, M., & Hyde, A. F. L., 2009. Pile bearing capacity factors and soil crushability. Journal of Geotechnical and Geoenvironmental Engineering 135, No. 7, 901–913.

Leonards, G.A. and Darrag, A.A., 1987. Analysis of residual stress effects in piles. Discussion. Journal of Geotechnical Engineering, ASCE, 113: 589–593.

Loadtest International Pte. Ltd., 2013. Reports on Barrette Pile Testing, Exim Bank Tower, HCMC, Vietnam, 13813I-1, 178 p.

Lunne, T., Robertson, P.K., Powell, J.J.M., 1997. Cone penetration testing in geotechnical practice. Blackie Academic/London, Routledge, NY, 312 p.

Maiorano, R.M.S., Viggiani, C., and Randolph, M.F., 1996. Residual stress system arising from different methods of pile installation. Proceedings of the 5th International Conference on the Application of Stress-Wave Theory to Piles, Orlando, Vol. 1.pp. 518–528.

Manandhar, S. and Yasufuku, N., 2011a. End bearing capacity of tapered piles in sands using cavity expansion theory. Mem. Fac. Eng. Kyushu Univ., 71 (4) (2011), pp. 77–99.

Massarsch, K.R., 2014. Cone penetration testing - A historic perspective. Proceedings, Proceedings of 3rd International Symposium of Cone Penetration Testing, CPT14. Edited by P.K. Robertson and K.L. Cabal, May 13-14, 2014, Las Vegas, Nevada, USA. Printed by Omnipress; ISBN: 978-0-615-98835-1, Paper # KN-4, pp. 97-134.

Mazurkiewicz, B. K., 1972. Test Loading of Piles According to Polish Regulations. Royal Swedish Academy of Engineering Sciences Commission on Pile Research. Report No. 35, Stockholm, 20p.

Meyerhof, G.G., 1951. The bearing capacity of foundations. Geotechnique 2(4) 301-332.

Meyerhof, G.G., 1963. Some recent research on bearing capacity of foundations. Canadian Geotechnical Journal 1(1) 16-26.

Meyerhof, G.G., 1976. Bearing capacity and settlement of pile foundations. The Eleventh Terzaghi Lecture, November 5, 1975. ASCE Journal of Geotechnical Engineering 102(GT3) 195-228.

Mohan, D., Jain, G. S., and Jain, M. P., 1967. A new approach 10 load tests. Geotechnique, Vol.17, pp. 274-283.

Muromachi, T., 1981. Cone penetration testing in Japan. *Cone Penetration Testing and Experience*, (Proc. ASCE National Convention, St. Louis), American Society of Civil Engineers, Reston, Virginia, pp. 49-75.

NAVFAC DM7-02 (1982) Foundations and Earth Structures.

New York State Department of Transportation, Static Load Test Manual, N.Y. DOT Soil Mechanics Bureau, Soil Control Procedure SCP4/74, 1974, 35 pp.

Nguyen M.H., Nguyen K.T., Bouassida M., Madhira M.R., Indraratna B., and Fellenius B. H. (Editors). Proceedings of the First International Conference on Foundation and Soft Ground Engineering Challenges in Mekong Delta. Binh Duong, Vietnam, June 5-6, 2013.

Nguyen M.H., Nguyen K.T., Phung D.L., and Pham V.N., 2013. Analysis of floating pile capacity in improved ground for Thi Vai Port, Vietnam. The 18th International Conference on Soil Mechanics and Geotechnical Engineering, Paris, France, September 2-6, 2013, pp. 2485-2488.

Nguyen M.H. and Do H.D., 2013. Non-conventional pile loading tests in Vietnam. The 18th International Conference on Soil Mechanics and Geotechnical Engineering, Paris, France, September 2-6, 2013, pp. 2747-2750.

Nguyen M.H., Do, H.D., and Nguyen, T.T., 2013. Analysis by Menard direct method of O-cell instrumented pile load tests. A Parallel Session on Pressuremeters ISP-6, the

18th International Conference on Soil Mechanics and Geotechnical Engineering, Paris, France, September 4, 2013, pp. 40-45.

Nguyen M.H. and Fellenius, B.H., 2013. Analysis of piled-raft foundation for Cai Mep Container Port, Vietnam. 7th International Conference on Case Histories in Geotechnical Engineering and Symposium in Honor of Clyde Baker**,** The Westin Chicago North Shore**,** Wheeling (Chicago) Illinois, April 29 - May 4, 2013, Paper No. 2.12, 6p.

Nguyen M.H. and Fellenius, B.H., 2013. Failure of embankment on soil-cement columns for Thi Vai Port, Vietnam. 7th International Conference on Case Histories in Geotechnical Engineering and Symposium in Honor of Clyde Baker**,** The Westin Chicago North Shore**,** Wheeling (Chicago) Illinois, April 29 - May 4, 2013 Paper No. 3.08, 11p.

Nguyen M.H., 2013. Analysis of bidirectional test for Red River Bridge, Vietnam. The 3th International Conference on Geotechnical Engineering, Hammamet, Tunisia, February 21 - 23, 2013, pp. 495-504.

Nguyen M.H., Than, V.D., Tran, T.Q., Le, H.V., Phuong, N. T., and Pham, V.N, 2013. Back-analysis of head-down tests on two instrumented bored piles. The first International Conference on Foundation and Soft Ground Engineering Challenges in Mekong Delta, Binh Duong, Vietnam, June 5-6, 2013, pp. 153-158.

Nguyen, M.H. and Fellenius, B.H., 2014. O-cell tests on two 70-m long bored piles in Vietnam. ASCE Geotechnical. Special Publication, GSP 233, Ed. by M. Iskander, J. Garlanger, M. Hussein. pp. 482-496.

Nguyen, M.H. and Fellenius, B.H., 2015. Bidirectional cell tests on not-grouted and grouted large-diameter bored piles. Journal of GeoEngineering Sciences, IOS Press, 2(3-4) 105-117.

Nguyen M. H., Fellenius, B.H., Puppala, A. J., Nguyen, C. O., and Bheemasetti, V.T., 2016. Results of static loading tests on single piles and on pile-supported LPG tanks. Proceedings of the 69th Canadian Geotechnical Conference, Vancouver, October 2-5, paper No. 3673, 10 p.

Nguyen M. H., Puppala, A. J., Patil, D. U., and Bach, V.H.L., 2016. Problems of cycled head-down pile load tests in soft soil region. Proceedings of the Third International Conference on Geotechnics for Sustainable Infrastructure Development, Geotec Ha Noi 2016, Vietnam, November 24-25, 2016, pp. 109-114.

Nguyen M. H., Puppala, A. J., and Patil, D. U., 2016. Multi-level O-cell tests on The Phu My Bridge, Vietnam. Proceedings of the Second National Conference on Transport Infrastructure with Sustainable Development, Da Nang, Vietnam, September 17-18, 2016, pp. 281-288.

Nguyen H. M., Puppala, A. J., Patil, U. D., Mosadegh, L., and Banerjee, A., 2017. Multi-level O-cell tests on the instrumented bored piles in Mekong Delta. ASCE GeoInstitute, Geo-Frontiers, Florida, February 23-26, 2014, 10p.

Niazi, F.S. and Mayne, P.W., 2013. *Cone penetration test based direct methods for evaluating static axial capacity of single piles*: A State-of-the-Art Review. Geotechnical and Geological Engineering, (31), 979–1009.

Nottingham L.C., 1975. Use of quasi-static friction cone penetrometer data to predict load capacity of displacement piles. PhD Thesis, University of Florida, 553P.

Osterberg, J.O., 1986. Device for testing the load-bearing capacity of concrete-filled earthen shafts. Patent US4614110 A, September 30, 13p.

Osterberg, J.O., 1996. Method and apparatus for subterranean load-cell testing. Patent US 5576494 A, November 19, 7p.

Osterberg, J.O., 1998. The Osterberg load test method for drilled shaft and driven piles. The first ten years. Deep Foundation Institute, Seventh International Conference and Exhibition on Piling and Deep Foundations, Vienna, Austria, June 15 - 17, 1998, 17 p.

Platema, G., 1948. Construction and method of operating a new deep sounding apparatus. Proceedings of the 2nd Int. Conference on Soil Mechanics and Foundation Engineering, Rotterdam, Vol. 1, pp. 277-279.

Prakash, *S*. and Sharma, H.D. *Pile Foundations in Engineering Practice*. John Wiley & Sons, Inc., New York, *1990*, 729p.

Randolph, M.F. and Wroth, C P., 1982. Recent developments in understanding the axial capacity of piles in clay. Ground Engineering, V15, N7, pp. 17–25.

Raymond Concrete Pile. The Raymond Concrete Pile Company, New York and Chicago, 1926, 64p.

Robinsky, E.I. and Morrison, C.F., 1964. Sand displacement and compaction around model friction piles. Canadian Geotechnical Journal 1(2): 81-93.

Rourk, T.L., 1961. Model studies of a pile failure surface in a cohesive soil. Master's thesis, Georgia Institute of Technology, Atlanta (1961).

Salgado R., 1993. Analysis of penetration resistance in sands. Ph.D. Thesis, University of California, Berkeley, 297p.

Sanglerat, G., 1972. The penetrometer and soil exploration. Elsevier, Amsterdam, 464 pp.

Schmertmann, J.H., 1978. Guidelines for cone penetration test, performance and design. U.S. Department of Transportation, Washington, DC, Report No. FHWA-TS-78-209, 145 p.

Schmertmann, H.J. and Hayes, A.J., 1997. The Osterberg cell and bored pile testing - A symbiosis. Proceedings of the 3rd International Geotechnical Engineering Conference, Cairo University, Cairo, Egypt, pp. 3-12.

Semple, R.M. and Rigden, W.J., 1984. Shaft capacity of driven pipe piles in clay. Proc. of the symposium on analysis and design of deep foundations, San Francisco, USA: 59-79.

Senneset, K., 1974. *Penetration testing in Norway*. Proceedings of the European Symposium on Penetration Testing, ESOPT, Stockholm, Sweden, pp. 85-95.

Skempton, A. W., 1951. The bearing capacity of clays. Proceedings, Building Research Congress, London, pp. 180-189.

Terzaghi, K., 1942. Discussion of the progress report of the Committee on the Bearing Capacity of Pile Foundations. ASCE Proc. 68(2) 311-323.

The Pedestal Pile. The Mac Arthur Concrete Pile and Foundation Company, New York, 1910, 61p.

Tokimatsu, K. and Seed, H.B., 1987. Evaluation of settlements in sands due to earthquake shaking. *J. Geotech. Engng*, 113(8), 861-879.

Tomlinson, M.J., 1980. Foundation design and construction, Fourth Edition. Pitman Publishing Inc., London, 793 p.

Torstensson, B.A., 1975. Pore pressure sounding instrument. Proceedings ASCE Specialty Conference on In-Situ Measurement of Soil Properties. Vol. 2. Raleigh, pp. 48 – 54.

Tumay, M.T., and Fakhroo, M., 1981. Pile capacity in soft clays using electric QCPT data. *Cone Penetration Testing and Experience*, (Proc. ASCE National Convention, St. Louis), American Society of Civil Engineers, Reston, Virginia, pp. 434-455.

Tumay, M.T., Boggess, R.L., and Acar, Y., 1981. Subsurface investigations with piezocone penetrometers. *Cone Penetration Testing and Experience*, (Proc. ASCE National Convention, St. Louis), American Society of Civil Engineers, Reston, Virginia, pp. 325-342.

Vermeiden, J., 1948. Improved sounding apparatus as developed in Holland since 1936. *Proc. Int. Conf. SoilMech. Found. Eng., 2nd, Rotterdam,* 1: 280 - 287.

Vesic, A. S., 1963. Bearing capacity of deep foundations in sand, Highway Research Record, 39, National Academy of Sciences, National Research Council, pp.112-153.

Vesić, A.S., 1967. Ultimate load and settlement of deep foundations in sand. *In* Proceedings of the Symposium on Bearing Capacity and Settlement of Foundations, Durham, N.C., 5–6 April 1965. *Edited by* A.S. Vesić. Duke University, Durham, N.C. pp. 53–68.

Vesić, A.S., 1972. Expansion of cavities in infinite soil mass. *Journal of the Soil Mechanics and Foundations Division*, ASCE, Vol. 98, Issue 3, pp. 265-290.

Vesic, A.S., *1977*. *Design* of *Pile Foundations*. National. Cooperative Research Program, *Synthesis* of *Highway*. *Practice No*. *42*, Transportation Research Board, Washington, DC., 68p.

Villet C.B.W. and Mitchell, J.K., 1981. Cone resistance, relative density and friction Angle. *cone penetration testing and experience*, (Proc. ASCE National Convention, St. Louis), American Society of Civil Engineers, Reston, Virginia, pp. 178-207.

Whitaker, T., 1976. The Design of Piled Foundations. (Second edition). Pergamon Press, Oxford, 218 p.

Wissa, A.E.Z., Martin, R.T., and Garlanger, J.E., 1975. The piezometer probe. In Proceedings of ASCE Specialty Conference on In-Situ Measurement of Soil Properties. Raleigh, N.C., Vol.1, pp. 536-545.

Yasufuku, N. and Hyde, A. F. L., 1995. Pile end-bearing capacity in crushable sands. Géotechnique, Volume 45 Issue 4, pp. 663-676.

Zuidberg, H., 1974. Use of static cone penetrometer testing in the North Sea. Proceedings of the European Symposium on Penetration Testing (ESOPT), Vol. 2.2, Stockholm, 1974, pp. 433-436.

Zuidberg, H., Schaap, L., and Beringer, F., 1982. A penetrometer for cone resistance and dynamic pore pressure. Proceedings of the Second European Symposium on Penetration Testing, Amsterdam, Vol. 2, 963-970.

Biographical Information

Hai Minh Nguyen was born and grew up in Mekong Data of Vietnam. He completed a Bachelor of Engineering degree in Civil Engineering in the year 2003 from Water Resources University in Vietnam, after which he worked as geotechnical engineer for five years at the Hydropower Project Management Unit No.6, Electricity of Vietnam at the Dai Ninh Hydropower Project.

He was a technical manager for three years at the Adcom South Joint Stock Company, working on piled foundation projects, such as the Tan Son Nhat-Binh Loi Outer Ring Road project, the Sunrise City Central Tower project, the Ca Mau Fertilizer Plant Project, etc. During this period, he attended Ho Chi Minh City University of Technology to pursue a master's degree. He received his Master of Engineering in Civil Engineering in April, 2011.

Upon completion of his master's degree, Hai Minh Nguyen worked as geotechnical/structural design engineer for two years at the Japan Port Consultants Company, at the Cai Mep and Thi Vai International Container Port Project.

In the Spring of 2014, he enrolled in the University of Texas at Arlington's Ph.D. program. He worked under the guidance of Dr. Anand J Puppala on the development of a novel cone test device for deep foundation design. He successfully defended his dissertation in April 2017. During his course of study, he submitted six technical papers for geotechnical conferences and journals.